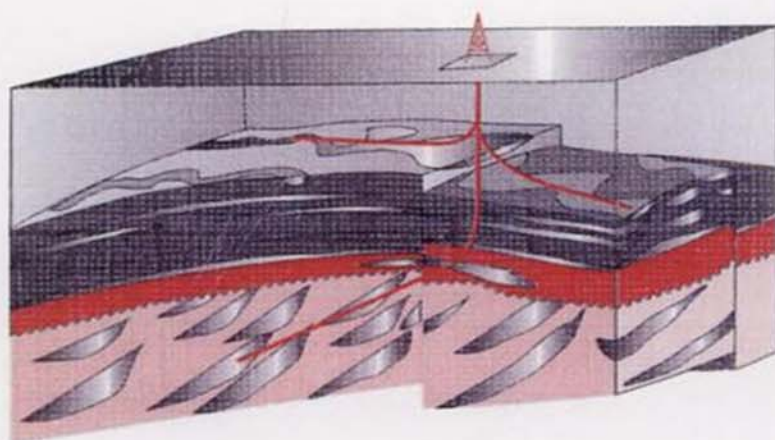


G. BOURDAROT

WELL TESTING: INTERPRETATION METHODS

pdfelement



ÉDITIONS TECHNIP



WELL TESTING: INTERPRETATION METHODS



FROM THE SAME PUBLISHER

- Basics of Reservoir Engineering
R. COSSÉ
- Drilling
J.P. NGUYEN
- Drilling Data Handbook
G. GABOLDE, J.P. NGUYEN
- Progressing Cavity Pumps
H. CHOLET
- Cement Evaluation Logging Handbook
D. ROUILLAC
- Cementing Technology and Procedures
Edited by J. LECOURTIER and M.V. CARTALOS
- Log Data Acquisition and Quality Control
Ph. THEYS
- Dictionnaire du forage et des puits
Dictionary of Drilling and Boreholes
anglais-français, français-anglais
M. MOUREAU, G. BRACE



GILLES BOURDAROT

Engineer, Elf Aquitaine

WELL TESTING: INTERPRETATION METHODS

Translated from the French by Barbara Brown Balvet

Center for
PETROLEUM
ENGINEERING
AND PROJECT
DEVELOPMENT

1998

ÉDITIONS
TECHNIP

27 rue Ginoux
75737 Paris Cedex 15



ÉCOLE DU PÉTROLE
ET DES MOTEURS
IFP ■ SCHOOL

Translation of
Essais de puits : méthodes d'interprétation, G. Bourdarot
© 1996. Éditions Technip and Institut français du pétrole
ISBN 2-7108-0697-5

© 1998. Éditions Technip, Paris
and Institut français du pétrole, Rueil-Malmaison

ISBN 2-7108-0738-6

ISSN 1271-9048

All rights reserved. No part of this publication may be reproduced or transmitted in any form or by any means, electronic or mechanical, including photocopy, recording, or any information storage and retrieval system, without the prior written permission of the publisher.

Contents

Symbols and abbreviations	11
PRINCIPLE	17
Chapter 1 Principles of well testing	19
1.1 Introduction	19
1.2 Darcy's law	20
1.3 Compressibility	21
1.4 Diffusion equation	23
1.5 Solving the diffusivity equation	25
1.6 Compressible zone	26
1.7 Radius of investigation	28
1.8 Flow regimes	30
1.9 Principle of superposition	31
Chapter 2 Wellbore storage	33
2.1 Definition	33
2.2 Naturally eruptive wells.....	34
2.3 Pumping wells	35
2.4 Orders of magnitude	35
2.5 Pressure variations	35
2.6 Bottomhole flow	37
2.7 End of the wellbore storage effect	37
Chapter 3 Skin	39
3.1 Definition	39
3.2 Infinitesimal skin.....	39
G. BOURDAROT	5

CONTENTS

3.3	Finite thickness skin	40
3.4	Effective radius	41
3.5	Generalization of the skin concept	43
INTERPRETATION METHODS		45
Introduction		47
Chapter 4 Conventional interpretation methods		51
4.1	Drawdown test	52
4.2	Pressure buildup: Horner's method	54
4.3	Pressure buildup: MDH method	58
4.4	After varying flow rates	60
4.5	Simplification of the flow rate history	63
4.6	Buildup radius of investigation	66
Chapter 5 Type curves		67
5.1	Introduction	67
5.2	Gringarten type curves	67
5.3	Interpretation method	70
5.4	Using type curves during buildup	75
Chapter 6 The derivative		79
6.1	Representation	79
6.2	Properties of the derivative	80
6.3	The derivative as diagnostic tool	81
6.4	Analysis with type curves	82
6.5	Direct interpretation by means of the derivative	88
6.6	Conclusion	89
RESERVOIR BOUNDARIES		91
Introduction		93
Chapter 7 Linear sealing faults		95
7.1	Description	95
7.2	The method of images	96

CONTENTS

7.3	Conventional interpretation method	97
7.4	Type curves: the derivative	100
Chapter 8 Channels		103
8.1	Description of flows	103
8.2	Linear flow	104
8.3	Conventional interpretation	105
8.4	Bounded channels	106
8.5	Pressure buildup with varying flow rates	109
8.6	Pressure derivative, type curves	110
Chapter 9 Intersecting faults		113
9.1	Conventional analysis	113
9.2	Type curves; pressure derivative	114
Chapter 10 Constant pressure boundary		117
10.1	Conventional interpretation method	118
10.2	Type curves; derivative	121
Chapter 11 Closed reservoir		123
11.1	Producing well, pseudosteady-state regime	123
11.2	Shut-in well, average pressure	131
Chapter 12 Productivity index		141
12.1	Definition	141
12.2	Productivity index during the infinite-acting period	141
12.3	Productivity index during the pseudosteady-state flow	142
12.4	Real and theoretical PI	143
RESERVOIR ASPECTS		145
Chapter 13 Naturally fractured reservoirs		147
13.1	Geometry	147
13.2	Porosity	149
13.3	Capacity	150
13.4	Permeability	152
13.5	Matrix-fracture exchange: λ	153

CONTENTS

13.6	Analysis of flows	153
13.7	Choosing between the pseudosteady-state and the transient interporosity flow models	162
13.8	Type curve analysis	163
13.9	Type curves derivatives	171
13.10	Two examples of interpretation in a fractured reservoir	175
Chapter 14 Two-layer reservoirs		181
14.1	Introduction	181
14.2	Description of a two-layer reservoir	181
14.3	The Bourdet model	182
14.4	Testing a two-layer reservoir	184
WELL ASPECTS		191
Chapter 15 Partial penetration wells		193
15.1	Introduction	193
15.2	Flow around a partial penetration well	195
15.3	Radial flow at the perforations	196
15.4	Spherical flow	197
15.5	Radial flow over the whole net thickness	199
15.6	Extrapolated pressure, average pressure	203
15.7	Pressure derivative	203
15.8	Ambiguous interpretation	205
15.9	Comparison with core samples	206
15.10	Partial perforation and fractured reservoirs	206
Chapter 16 Slanted wells		209
16.1	Introduction	209
16.2	Flows and skin factor for slanted wells	210
16.3	Influence of permeability anisotropy	211
Chapter 17 Artificially fractured wells		213
17.1	Description of the fracture	213
17.2	Flows around an artificially fractured well. Conventional interpretation methods	214
17.3	Type curves, the derivative	222
17.4	Type curves	228
17.5	Conclusion	231

CONTENTS

Chapter 18 Horizontal wells	233
18.1 Description of a horizontal well	233
18.2 Flows around a horizontal well. Conventional interpretation methods	233
18.3 Type curves, the derivative	239
Chapter 19 Injection wells	241
19.1 Description of an injection well	241
19.2 Description of flows	242
19.3 Type curves and derivative	246
19.4 The objectives of testing an injection well	248
FLUID ASPECTS	251
Chapter 20 Gas wells	253
20.1 Pseudopressure	253
20.2 Deviation from Darcy's law	257
20.3 Interpretation of a gas well test	259
20.4 Presentation of absolute open-flow potential tests	263
20.5 Conventional AOFP tests	263
20.6 Interpretation of AOFP tests: Houpeurt's method	266
20.7 Interpretation of absolute open-flow potential tests: empirical method	271
20.8 Other test procedures	274
Chapter 21 Multiphase flows	281
21.1 Introduction	281
21.2 Perrine method hypotheses	282
21.3 Perrine's method	283
21.4 Productivity index of an oil well producing under the bubble point; Vogel's equation	287
INTERFERENCES	291
Chapter 22 Interference tests	293
22.1 Presentation, particulars	293
22.2 Interpretation methods in a homogeneous reservoir	294

CONTENTS

22.3	Interference tests in fractured reservoirs	299
22.4	Influence of flow rate history	303
22.5	Skin and wellbore storage effect	305
22.6	Objective of interference tests, two examples	306
Chapter 23 Pulse tests		313
23.1	Presentation	313
23.2	Interpreting pulse tests: the Kamal and Brigham method	315
Practical units		325
References		327
Index		333



Symbols and abbreviations

A	drainage area of the well
a	distance from the well to the end of the channel
AOFP	absolute open flow potential
B	volume factor
B_g	gas volume factor
B_o	oil volume factor
B_w	water volume factor
c	compressibility
C	wellbore storage
C_A	drainage area shape factor
C_D	dimensionless wellbore storage
C_{Df}	dimensionless wellbore storage of the fractures
C_{Df+m}	dimensionless wellbore storage of the fractured reservoir
C_{Dm}	dimensionless wellbore storage of the matrix
C_{Dxf}	dimensionless wellbore storage versus a fracture
c_e	equivalent compressibility
C_f	fracture capacity
C_{f+m}	capacity of the fractured reservoir
c_g	gas compressibility
C_m	capacity of the matrix
c_o	oil compressibility
c_p	pore compressibility
c_{pf}	compressibility of the voids located in the fractures
c_{pm}	matrix pore compressibility
C_r	relative conductivity of the fracture
c_t	total compressibility
c_{tf}	total compressibility of the fractures

LISTE DES NOTATIONS

c_{tm}	total compressibility of the matrix
c_{tw}	total compressibility in the water zone
c_w	water compressibility
D	coefficient of deviation from Darcy's law
d	distance from the well to a boundary
e	eccentricity of the well in the channel
F	ratio of the pulse length to the total cycle length during a pulse test
g	gravity acceleration
h	thickness of a layer
h_D	dimensionless thickness in an anisotropic reservoir (see deviated wells)
h_e	thickness of a screen in a two-layer reservoir
h_p	perforated thickness
K	hydraulic diffusivity
k	permeability
k_f	fracture permeability
k_g	permeability to gas
k_h	horizontal permeability
k_m	matrix permeability
k_{min}, k_{max}	principal directions of the permeability tensor
k_o	permeability to oil
k_s	skin permeability
k_s	spherical permeability
k_v	vertical permeability
k_{ve}	vertical permeability of a screen
k_w	permeability to water
k_x, k_y, k_{xy}	permeability tensor component
l	width of the channel
L	length of a horizontal drainhole
M	molecular weight of the gas
m	slope of the semi-log straight line
m_l	slope of the straight line on the linear flow plot
m_o	slope of the semi-log straight line in the oil zone
m_s	slope of the straight line on the spherical flow plot
m_w	slope of the semi-log straight line in the water zone
n	characteristic dimension of a matrix bloc
p	pressure
p'	pressure derivative
p'_{st}	value of the derivative corresponding to a stabilized derivative
p_{1h}	pressure read for $\Delta t = 1h$ on the semi-log straight line
\bar{p}	average pressure

LISTE DES NOTATIONS

p_D	dimensionless pressure
p_{DMDH}	Miller-Dyes-Hutchinson dimensionless pressure
p^*	extrapolated pressure
p_l^*	extrapolated pressure on the straight line characteristic of linear flow
p_s^*	extrapolated pressure on the straight line characteristic of spherical flow
PI	productivity index
p_i	initial pressure
p_{sc}	standard pressure
p_{wf}	flowing bottomhole well pressure
p_{ws}	shut-in bottomhole well pressure
q	wellhead flow rate
q_f	bottomhole flow rate
q_g	wellhead flow rate of gas
q_{max}	maximum multiphase well flow rate
q_{sc}	wellhead flow rate of gas in standard conditions
q_{tf}	total bottomhole flow rate
q_w	wellhead flow rate of water
R	ideal gas constant
r	distance from a point to the well
r_D	dimensionless distance ($r_D = r/r_w$)
r_{Dl}	dimensionless distance from the well to the end of the channel ($r_{Dl} = a/l$)
r_i	radius of investigation
r_j	injection radius
R_m	water-oil mobility ratio
r_m	characteristic length of a matrix bloc
R_s	oil dissolution ratio
r_S	real skin radius
r_s	radius of the equivalent spherical source
r_w	well radius
S	geometrical skin
S, S'	skin
S_a	skin due to anisotropy in a horizontal well
S_f	geometrical skin due to the fracture
S_g	gas saturation
S_i	skin due to well inclination
S_o	oil saturation
S_p	plugging skin in a horizontal well
S_{pp}	partial penetration skin
S_w	water saturation

LISTE DES NOTATIONS

S_{wi}	irreducible water saturation
t	time
T	temperature
t_D	dimensionless time
t_{DA}	dimensionless time versus drainage area
t_{Df}	dimensionless time corresponding to the beginning of pseudoradial flow around a fracture
t_{Di}	dimensionless time corresponding to t_i
t_{DL}	dimensionless time with L as a reference length (horizontal wells)
t_{Dl}	dimensionless time with l as a reference length (channel)
t_{Dxf}	dimensionless time with x_f as a reference length
t_{DXl}	dimensionless time of the intersection of the straight lines m/l and $2m/l$
t_i	time corresponding to the intersection of the semi-log straight lines with slope m and $2m$
t_L	time lag during a pulse test
t_{LD}	dimensionless time versus t_L
t_p	dimensionless production time versus the drainage area
t_{pDA}	constant flow rate production time
t_{pe}	equivalent production time
T_{sc}	standard temperature
\vec{v}	velocity
V	volume
V_f	relative volume of the fractures compared to that of the sample
V_i	porous volume drained by the well
V_I	volume of injected water
V_m	relative volume of the matrix
VP	pore volume
V_u	volume of the well per unit of length
V_w	volume of the well
w	width of a fracture
w_S	width of the skin around a fracture
x_f	fracture half length
Z	gas compressibility factor
\bar{Z}	average gas compressibility factor
z_w	distance between the horizontal well and the floor of the reservoir
α	characteristic coefficient of matrix bloc geometry
β, β'	characteristic dimensionless parameter of transition for transient flows in a fractured reservoir
Δp	pressure difference
Δp_s	pressure drop due to skin
Δt	time interval

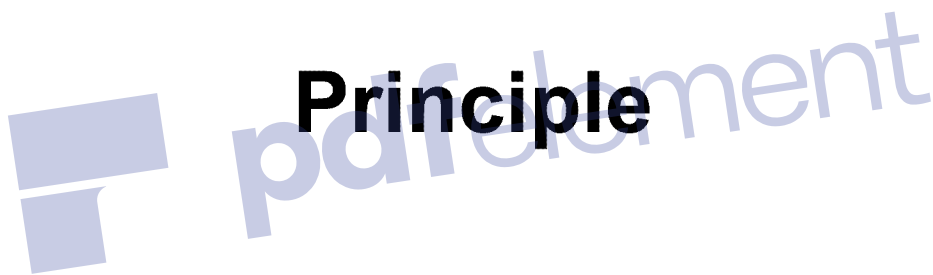
LISTE DES NOTATIONS

Δt_c	duration of a cycle during a pulse test
Δt_e	Agarwal equivalent time
Δt_p	duration of a pulse during a pulse test
$\Delta p'$	pressure derivative
η	ratio between the diffusivity inside the fracture and that of the reservoir
κ	transmissivity contrast between two layers in a multilayer reservoir
λ	exchange parameter between matrix and fractures or between two layers in a two-layer reservoir
μ	viscosity
$\bar{\mu}$	average gas viscosity
$\bar{\mu}_o$	oil viscosity
μ_w	water viscosity
ω	capacity contrast between the matrix and fractures or between two layers in a two-layer reservoir
Ψ	pseudopressure function
$\bar{\Psi}$	average pseudopressure function
$\bar{\Psi}_{wf}$	flowing pseudopressure function
ρ	density
σ	factor characterizing well eccentricity
θ	angle: between two intersecting faults, of the deviated well in a reservoir
ϕ	porosity
ϕ_f	fracture porosity
ϕ_m	matrix porosity.

Functions

div	divergence
$Ei(-x)$	exponential integral function
$\exp(x)$	exponential function
$g(Cr)$	conductivity function of the fracture
grad	gradient
ln	Neperian logarithm
log	decimal logarithm.





Principle



Chapter 1

Principles of well testing

The principles that are discussed in this chapter and the methods that are dealt with in later chapters consider one-phase flow of oil in a reservoir.

Chapters 20 and 21 show how the principles and methods differ when the fluid is a gas or when it is multiphase.

1.1 INTRODUCTION

Generally speaking, the aim of well testing is to get information about a well and about a reservoir.

To get this information, the well flow rate is varied and the variation disturbs the existing pressure in the reservoir.

Measuring the variations in pressure versus time and interpreting them gives data on the reservoir and the well.

The pressure can be measured:

- in the well where the flow rate has been changed: this is the method used in most tests;
- or in another well: this is the aim of interference tests.

The variations in pressure are interpreted using a number of laws of fluid mechanics.

This chapter will introduce the major ones that are used and their consequences.

1.2 DARCY'S LAW

Darcy's law is used to describe fluid flow in a porous medium. Let us look at its area of application and its consequences on a well test.

- **Presentation of the law:**

According to Darcy's law, the flow rate of a fluid flowing through a rock sample is proportional to:

- the pressure gradient applied to the rock sample;
- the sample's cross-section, S ;
- the mobility of the fluid, k/μ .

Darcy's law is valid within a time interval when the flow rate and other parameters are constant.

It does not depend on the porosity of the medium, or on the compressibility of either the fluids or the rock.

- **Vectorial expression:**

The vectorial expression of Darcy's law is as follows:

$$\vec{q} = -\frac{k}{\mu} S \vec{\text{grad}} p \quad (1.1)$$

A well test studies the variations in pressure that occur after a flow rate variation. Since the flow rate has varied, Darcy's law can not be applied macroscopically to describe the flow around the well.

Darcy's law can also be expressed as a function of the fluid's filtration rate:

$$\vec{V} = \frac{\vec{q}}{S} \quad (1.2)$$

$$\vec{V} = -\frac{k}{\mu} \overrightarrow{\text{grad } p} \quad (1.3)$$

(The filtration rate is different from the apparent rate in the porous medium $\frac{\vec{V}}{\phi S_o}$.)

- **Expression in radial flow:**

Darcy's law in radial flow is expressed by:

$$q = \frac{k}{\mu} 2\pi r h \frac{\partial p}{\partial r} \quad (1.4)$$

It can be integrated between two values of distance from the well, r_w and r_e (Fig. 1.1):

$$q = \frac{2\pi k h}{\mu} \frac{p_w - p_e}{\ln \frac{r_w}{r_e}} \quad (1.5)$$

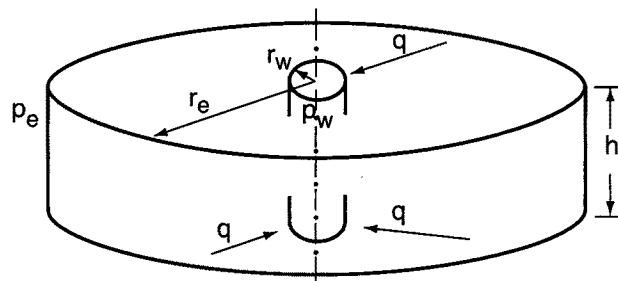


Fig. 1.1

1.3 COMPRESSIBILITY

All the information from a well test is obtained because the rock and the fluids are compressible.

The compressibility of any material is defined by the relative change in the material's volume per unit of pressure variation at constant temperature:

$$c = -\frac{1}{V} \left(\frac{\partial V}{\partial p} \right)_T \quad (1.6)$$

It can also be expressed in terms of density:

$$c_e = \frac{1}{\rho} \left(\frac{\partial \rho}{\partial p} \right)_T \quad (1.7)$$

• **Total compressibility of an oil reservoir:**

In an oil reservoir several components are compressible:

- the oil;
- the water, even at irreducible saturation;
- the pore volume itself.

When decompression occurs, the fluid is produced:

- by expansion of the fluids:

$$\text{oil: } \Delta V_o = -c_o S_o V_p \Delta p \quad (1.8)$$

$$\text{water: } \Delta V_w = -c_w S_w V_p \Delta p \quad (1.9)$$

- by a decrease in the pore volume V_p .

The pore volume is balanced between the influence of the fluid pressure and the lithostatic pressure.

When decompression occurs, the fluid pressure decreases while the lithostatic pressure remains constant. The pore volume decreases, thereby causing general fluid production:

$$\Delta V_p = -c_p V_p \Delta p \quad (1.10)$$

In contrast, the compressibility of the material itself is negligible in comparison.

The overall compressibility of a pore volume unit is due to the sum of all its compressible components:

$$c_t = c_o S_o + c_w S_w + c_p$$

The compressible capacity of a unit volume of the porous medium is equal to ϕc_t .

- **Equivalent compressibility:**

The reservoir is modeled by:

- an incompressible porous rock with a porosity of ϕS_o ;
- and a fluid of equivalent compressibility:

$$c_e = \frac{c_o S_o + c_w S_w + c_p}{S_o} \quad (1.11)$$

- **Order of magnitude:**

The order of magnitude for compressibility is as follows:

- for oil: $3 \text{ to } 10 \cdot 10^{-6} \text{ psi}^{-1}$
- for water: $3 \cdot 10^{-6} \text{ psi}^{-1}$
- for pore spaces : $3 \text{ to } 100 \cdot 10^{-6} \text{ psi}^{-1}$.

1.4 DIFFUSION EQUATION

The diffusivity equation governs the variations in pressure in the reservoir versus time. It is based on two laws and one equation of state:

- **Fluid flow equation:**

It is assumed that Darcy's law governs fluid flow.

Darcy's law is not applicable macroscopically over the whole duration of the test: the flow rate has just varied, the fluid can not be considered incompressible.

However, it is applied microscopically during the time interval when the various parameters and the flow rate can be considered constant.

The expression used is the same as equation (1.3):

$$\vec{V} = -\frac{k}{\mu} \text{grad } p \quad (1.3)$$

In this expression, gravitational forces are disregarded. This is the hypothesis that is made in most well test interpretations.

• **Material balance:**

The variation in the mass of fluid contained in the reservoir volume unit is equal to the difference between the amount of fluid input and output during the time interval:

$$\operatorname{div} \rho \vec{V} + \frac{\partial (\rho \phi S_o)}{\partial t} = 0 \quad (1.12)$$

Equation of state:

The gravity of the fluid varies with pressure and the variation is shown by the equivalent compressibility of the flowing fluid:

$$c_e = \frac{1}{\rho} \left(\frac{\partial \rho}{\partial p} \right)_T \quad (1.7)$$

Diffusion equation:

Let us consider the material balance equation (1.12) and express filtration rate and density versus pressure using Darcy's law (1.3) and the equation of state (1.7).

We will get the following pressure expression:

$$\Delta p + c_e (\operatorname{grad} p)^2 - \frac{\phi \mu c_t}{k} \frac{\partial p}{\partial t} = 0 \quad (1.13)$$

Providing two assumptions:

- fluid c is low and constant: this is the case for a liquid not for a gas;
- pressure gradients are low: this is the case in reservoirs where flow rates are small;

$c_e (\operatorname{grad} p)^2$ is small compared to the two other terms of equation (1.13). The equation is reduced to an ordinary diffusivity equation:

$$\Delta p - \frac{1}{K} \frac{\partial p}{\partial t} = 0 \quad (1.14)$$

$K = \frac{k}{\phi \mu c_t}$ is called **the hydraulic diffusivity of the porous medium.**

It is the ratio between the mobility of the fluids k/μ and the compressible capacity of the reservoir ϕc_t .

The diffusivity equation is written as follows in radial flow:

$$\frac{\partial^2 p}{\partial r^2} + \frac{1}{r} \frac{\partial p}{\partial r} - \frac{1}{K} \frac{\partial p}{\partial t} = 0 \quad (1.15)$$

1.5 SOLVING THE DIFFUSIVITY EQUATION

• Boundary conditions:

The equation that describes the variations in pressure in the reservoir versus time and the distance from the well is obtained by solving the diffusivity equation with three boundary conditions. These conditions describe:

- the pressure at the beginning of the test;
- the reservoir boundaries;
- the well.

• Infinite homogeneous reservoir solution:

The assumption that is usually made is to suppose that the reservoir is homogeneous, isotropic, with constant thickness and limited by impermeable boundaries. The well penetrates the total reservoir thickness. The fluid compressibility and viscosity are constant and uniform using the following boundary conditions:

- uniform initial pressure: p_i ;
- infinite reservoir;
- constant flow rate in the well that is considered to have an infinitesimal radius.

The variations in pressure versus time and the distance from the well verify the equation:

$$p_i - p(r, t) = - \frac{qB\mu}{4\pi kh} \text{Ei} \left(\frac{-r^2}{4Kt} \right) \quad (1.16)$$

where $\text{Ei}(x)$ is the exponential integral function defined by:

$$- \text{Ei}(-x) = \int_x^\infty \frac{\exp(-u)}{u} du$$

The way to solve the diffusivity equation is indicated with various sets of boundary conditions in the book by F. Daviau [Ref. 1].

The equation is written as follows:

$$p_D = -\frac{1}{2} \text{Ei} \left[-\frac{r_D^2}{4t_D} \right]$$

using the following dimensionless factors:

Pressure: $p_D = \frac{2\pi kh}{qB\mu} \Delta p$ (in SI units)

$$p_D = \frac{kh}{141.2 qB\mu} \Delta p$$
 (in practical US units)

$$p_D = \frac{kh}{18.66 qB\mu} \Delta p$$
 (in practical metric units)

Length: $r_D = \frac{r}{r_w}$

Time: $t_D = \frac{k \Delta t}{\phi \mu c_t r_w^2}$ (in SI units)

$$t_D = \frac{0.000264 k \Delta t}{\phi \mu c_t r_w^2}$$
 (in practical US units)

$$t_D = \frac{0.00036 k \Delta t}{\phi \mu c_t r_w^2}$$
 (in practical metric units)

1.6 COMPRESSIBLE ZONE

The flow at a distance r from the well at time t can be determined based on the microscopic Darcy's law expressed in radial flow (1.4) and based on equation (1.16) which describes the pressure variation:

$$q(r, t) = qB \exp\left(-\frac{r^2}{4Kt}\right) \quad (1.17)$$

where:

- q is the wellhead flow rate;
- q_B is the bottomhole flow rate.

Figure 1.2 shows the flow profile at time t versus the distance from the well.

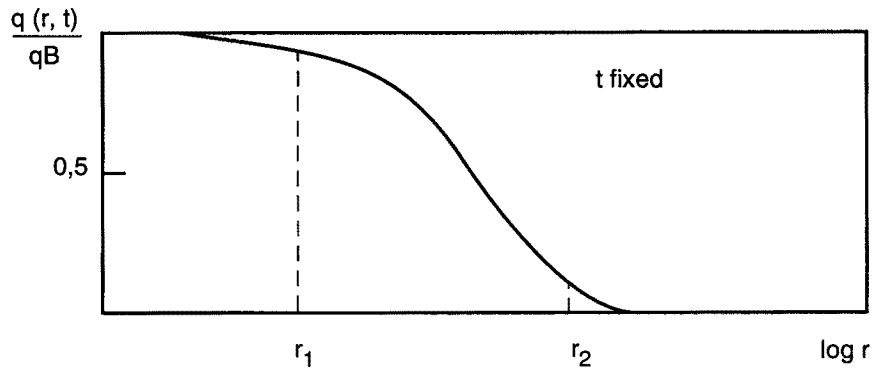


Fig. 1.2 Flow profile

On the flow profile it can be seen that between the wellbore and r_1 the flow rate has almost the same value as near the wellbore. Darcy's law is applicable macroscopically in these areas.

There is a negligible flow through the areas located beyond r_2 . The pressure drop between r_2 and an infinite distance is negligible.

Let us look at the variations in the flow profile between two times t and t' (Fig. 1.3).

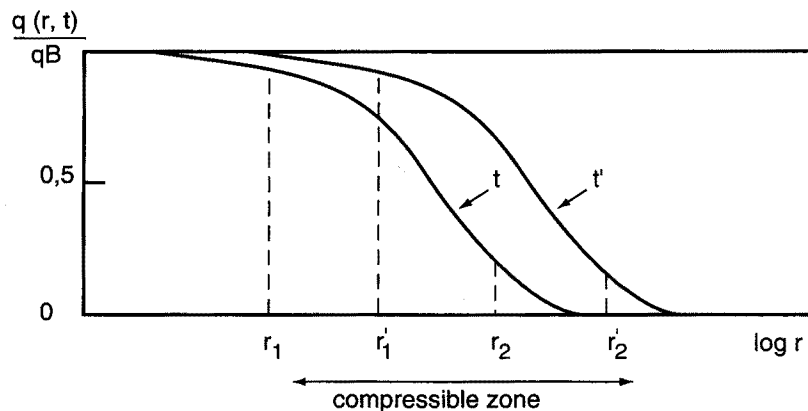


Fig. 1.3

Through the area located between the well and r_1 there is a flow close to q_B . From t to t' the pressure drop between the well and r_1 is small.

The area located beyond r_2' is not yet involved in the flow. The pressure drop between r_2' and an infinite distance remains negligible.

Between t and t' the pressure drop between an infinite distance and the well is therefore mainly due to what is occurring between r_1 and r_2' .

It is in this area that the reservoir's compressibility, allowing the flow to go from 0 to qB , comes into play. This area is called **the compressible zone**.

The pressure drop at the well since the initial pressure is equal to the pressure drop between an infinite distance and the well.

The pressure drop in the well mainly reflects the reservoir properties in the compressible zone.

At the beginning of the test the pressure drop reflects the reservoir properties in the vicinity of the well. Later on the test reaches areas that are farther away.

This is what enables a well test to:

- characterize the average properties far way from the well, permeability for example;
- detect facies heterogeneities;
- identify permeability barriers.

Nota bene:

The concept of compressible zone is used to locate the reservoir area that is affected by the flow perturbation in a practical way. This is despite the fact that equation (1.16) shows that the whole reservoir is affected as soon as the well is opened.

It would be inaccurate to treat the pressure perturbation in terms of propagation and define a propagation velocity. In fact, the perturbation is diffused rather than propagated in the medium. Equation (1.14) is a diffusion equation. A propagation equation would involve a second order differential equation versus time.

1.7 RADIUS OF INVESTIGATION

The pressure variations at the well give an indication of the properties of the part of the reservoir involved in the compressible zone. It is important to locate the compressible zone and this is what is involved in the concept of a test's radius of investigation.

Oil industry literature offers a large number of different definitions of the radius of investigation. The article by H.K. Van Poolen [Ref. 3] provides a good summary of the definitions. Among them, the following can be found:

• **Jones's definition:**

The radius of investigation is the point in the reservoir where the pressure variations represent 1% of the variations observed at the well:

$$r_i = 4 \sqrt{\frac{kt}{\phi\mu c_t}} \quad (\text{in SI units}) \quad (1.18)$$

• **Poettmann's definition:**

The radius of investigation is the point in the reservoir where the flow is equal to 1% of the well flow rate:

$$r_i = 4.29 \sqrt{\frac{kt}{\phi\mu c_t}} \quad (\text{in SI units}) \quad (1.19)$$

• **J. Lee [Ref. 3] and Muskat's [Ref. 2] definition:**

The radius of investigation is the point where the pressure variations are the fastest.

The variations are given by the equation below (1.16):

$$p_i - p(r, t) = -\frac{qB\mu}{4\pi kh} \text{Ei}\left(\frac{-r^2}{4Kt}\right)$$

The pressure variations are equal to:

$$\frac{dp}{dt} = \frac{qB\mu}{4\pi kh} \frac{\exp(-r^2)}{4Kt} \quad (1.20)$$

The variation is at a maximum for $\frac{d^2 p}{dt^2} = 0$, i.e. for $\frac{r^2}{4Kt} = 1$.

In other terms:
$$r_i = 2 \sqrt{\frac{kt}{\phi\mu c_t}} \quad (\text{in SI units}) \quad (1.21)$$

Simulations performed with a grid-type well simulator show that an event (a fault for example) is perceived in the well pressure variations at a time close to that computed with the last formula mentioned above. It seems to be the most suitable one to use in locating a well test's radius of investigation range.

In practical units it is expressed as follows:

$$r_i = 0.032 \sqrt{\frac{kt}{\phi\mu c_t}} \quad (\text{in practical US units}) \quad (1.22)$$

$$r_i = 0.038 \sqrt{\frac{kt}{\phi\mu c_t}} \quad (\text{in practical metric units}) \quad (1.23)$$

1.8 FLOW REGIMES

- **Transient flow:**

Until the compressible zone reaches the boundaries of the reservoir or comes under the influence of another well, the reservoir behaves as if it was infinite for testing purposes.

During this period the flow regime is called **transient**.

- **Pseudosteady-state flow:**

When the compressible zone reaches a series of no-flow boundaries, the flow regime becomes **pseudosteady-state**. This is the type of flow in a producing reservoir with no flow boundaries.

- **Steady-state flow:**

When the compressible zone is affected by some constant pressure outer boundaries, the flow becomes **steady-state**. This is the type of flow in a reservoir producing under gas-cap or water drive conditions when the mobility of the water is high compared to that of the oil.

A well test is almost always performed in a transient flow regime even though some boundaries are reached.

1.9 PRINCIPLE OF SUPERPOSITION

In section 1.5, equation (1.16) reflects the pressure variations when the well is opened.

How can the pressure be described in the reservoir when several flow rate variations occur?

The usual way of dealing with this problem is to use the fact that the pressure variation equations are linear versus flow rate.

The pressure variations due to several flow rates are equal to the sum of the pressure drops due to each of the different flow rates. This property is called superposition.

- **Two flow rates:**

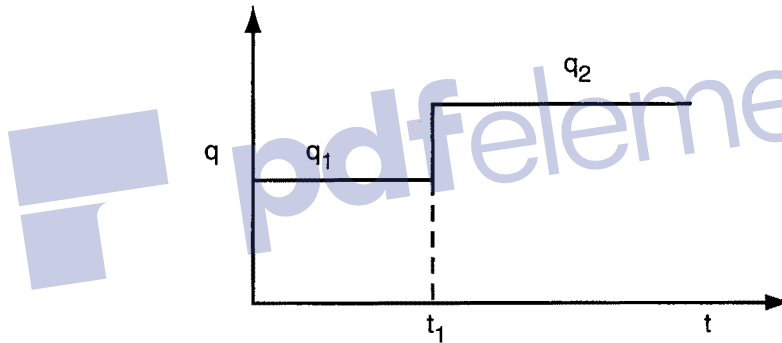


Fig. 1.4 Diagram for two flow rates

If $p_i - p(t) = \frac{qB\mu}{2\pi kh} p_D(t)$ the pressure drop due to a flow rate, q , beginning at time, $t = 0$.

The diagram shown in Figure 1.4 can be considered as the sum of:

- a production at flow rate q_1 since $t = 0$, and;
- a production at flow rate $(q_2 - q_1)$ since $t = t_1$.

The pressure variation due to the two rates is equal to:

$$p_i - p(t) = \frac{q_1 B \mu}{2\pi kh} p_D(t) + \frac{(q_2 - q_1) B \mu}{2\pi kh} p_D(t - t_1) \quad (1.24)$$

- **Pressure buildup:**

One case is of particular interest: when q_2 is zero. This is case for the great majority of tests (see Fig. 1.5).

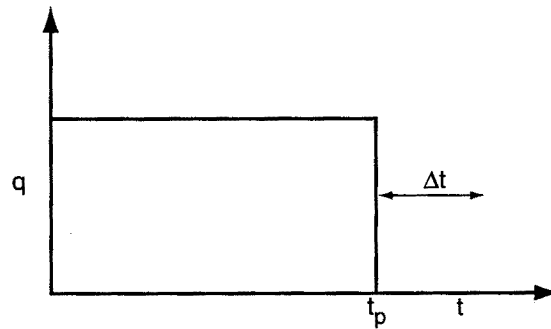


Fig. 1.5 Shut-in test

Equation (1.24) becomes:

$$p_i - p(t) = \frac{qB\mu}{2\pi kh} [p_D(t_p + \Delta t) - p_D(\Delta t)] \quad (1.25)$$

- **Multirate testing:**

For multirate testing (Fig. 1.6):

$$p_i - p(t) = \frac{B\mu}{2\pi kh} \sum_{i=1}^n (q_i - q_{i-1}) p_D(t - t_{i-1}) \quad (1.26)$$

with $q_0 = 0$ and $t_0 = 0$.

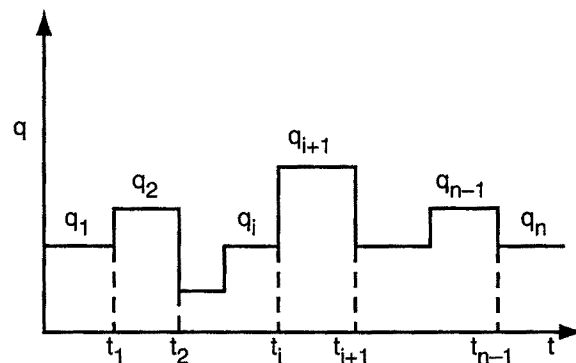


Fig. 1.6 Multirate testing

Chapter 2

Wellbore storage

2.1 DEFINITION

A well test begins with a sudden variation in the well flow rate. The variation occurs in the well, at the wellhead usually, or closer to the formation in a DST or with a bottomhole shut-in.

The flow out of the formation undergoes a gradual variation because of the compressibility of the fluid column in the tubing between the bottom of the hole and the shut-in point.

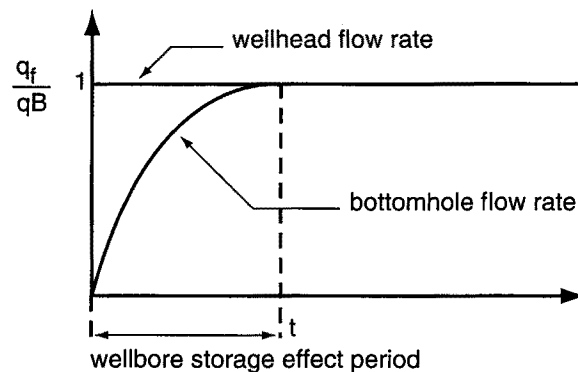


Fig. 2.1

The surface flow rate when the well is opened is assumed to go at once from 0 to q , but the bottomhole flow rate does not increase instantly from 0 to q_B . The bottom of the well begins producing gradually (Fig. 2.1).

The period when the bottomhole flow varies is called the wellbore storage effect period.

Wellbore storage is defined by:

$$C = - \frac{\Delta V}{\Delta p} \quad (2.1)$$

where:

ΔV is the volume variation of fluid in the well under well conditions;

Δp is the variation in pressure applied to the well.

Wellbore storage is homogeneous with the product of a volume by a compressibility.

A dimensionless factor is related to wellbore storage defined by:

$$C_D = \frac{C}{2\pi\phi c_t h r_w^2} \quad (\text{in SI and practical metric units}) \quad (2.2)$$

$$C_D = \frac{0.89 C}{\phi c_t h r_w^2} \quad (\text{in practical US units}) \quad (2.3)$$

2.2 NATURALLY ERUPTIVE WELLS

In a naturally eruptive well, the variation in fluid volume depends on the compressibility of the fluid in the well:

$$\Delta V = - c V_w \Delta p$$

$$\text{therefore: } C = c V_w \quad (2.4)$$

where:

V_w is the volume of the wellbore;

c is the compressibility of the fluid.

The compressibility of the fluid in the wellbore is very often much greater than that of the oil in reservoir conditions because the oil releases gas.

The presence of gas causes wellbore storage to vary during testing, quite a lot in the beginning and less afterwards.

2.3 PUMPING WELLS

In a pumping well the variation in liquid volume is due to the changing liquid level in the well:

$$\Delta V = V_u \Delta h$$

where:

V_u is the volume of the wellbore per unit of length (V_u is homogeneous with a surface);

Δh is the variation in fluid level;

$\Delta p = \Delta \rho g \Delta h$;

$\Delta \rho$ is the difference in gravity of the fluids contained in the wellbore (generally speaking oil and gas);

therefore:

$$C = \frac{V_u}{\Delta \rho g} \quad (2.5)$$

Wellbore storage of pumping wells is considerably greater than wellbore storage of eruptive wells.

A pressure buildup in a pumping well can be considered as never leaving the wellbore storage effect period: when the flow goes to zero at the bottom of the hole, the pressure buildup is finished.

2.4 ORDERS OF MAGNITUDE

By way of comparison, here are a few wellbore storage orders of magnitude:

DST:	0.0001	to	0.001	m ³ /bar
Eruptive well:	0.01	to	0.1	m ³ /bar
Pumping well:	0.1	to	1	m ³ /bar.

Shutting in the well at the bottom of the hole considerably reduces wellbore storage.

2.5 PRESSURE VARIATIONS

Just after the well has been opened, the bottomhole pressure is mainly affected by the wellbore storage effect.

$$\Delta p = \frac{qBt}{24C} \quad (\text{in practical metric and US units}) \quad (2.6)$$

$$p_D = \frac{t_D}{C_D} \quad (\text{in dimensionless factors}) \quad (2.7)$$

If well storage is constant, the bottomhole pressure varies linearly versus time as long as wellbore storage has a dominating effect.

The slope of the straight line, when bottomhole pressure drop is plotted versus time, is used to compute C (Fig. 2.2):

$$C = \frac{qB}{24 \times \text{slope}} \quad (\text{in practical US and metric units}) \quad (2.8)$$

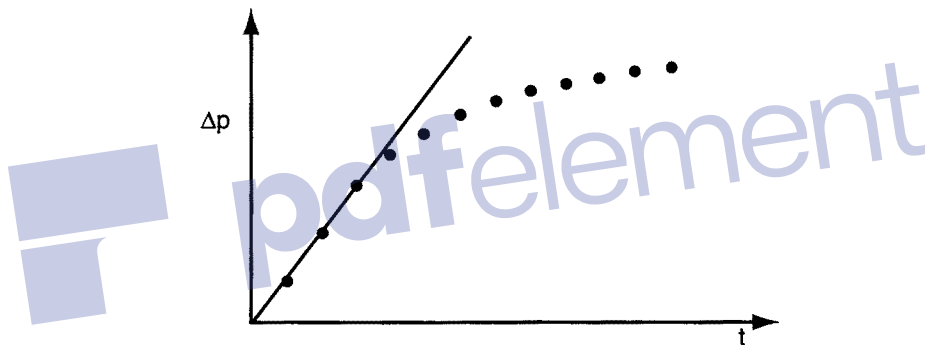


Fig. 2.2

The straight line should go through the origin of the coordinate axes. Several reasons may explain why this is not the case:

- a shut-in pressure error;
- a shut-in time error.

If such errors are plausible, the value of the offset at the origin can be used to correct the data.

The correction should, however, be made with caution since other causes may explain the offset:

- too much time elapsed between measurements: the wellbore storage effect period is ending when the second measurement is made;
- variable wellbore storage due to gas;
- fluid segregation in the wellbore.

2.6 BOTTOMHOLE FLOW

When the well is opened, the wellbore storage effect delays bottomhole production.

Bottomhole flow under standard conditions is given by:

$$q_f = q + \frac{24C}{B} \frac{dp}{dt} \quad (2.9)$$

$$q_f = q \left(1 - C_D \frac{dp_D}{dt_D} \right) \quad (2.10)$$

2.7 END OF THE WELLBORE STORAGE EFFECT

Three criteria are proposed in oil industry literature to determine the end of the wellbore storage effect:

- **Ramey's criterion:**

$$t_D = (60 + 3.5 S) C_D \quad (2.11)$$

i.e. approximately:

$$t = \frac{(200\,000 + 12\,000 S) C}{kh/\mu} \quad (\text{in practical US units}) \quad (2.12)$$

where S is the skin of the well (see Chapter 3).

- **Chen and Brigham's criterion:**

$$t_D = 50 C_D \exp(0.14 S) \quad (2.13)$$

i.e. approximately:

$$t = \frac{170\,000 C \exp(0.14 S)}{kh/\mu} \quad (\text{in practical US units}) \quad (2.14)$$

- **Rule of thumb:**

This criterion can be applied to the representation used for type curves (Chapter 6). This representation shows pressure variations versus time on a log-log graph.

The period when the well storage effect prevails is represented by a straight line with a slope of 1.

The rule of thumb locates the end of the well storage effect at the intersection of the measurement point curve and the line parallel to the slope 1 line translated by 1.5 cycles (Fig. 2.3).

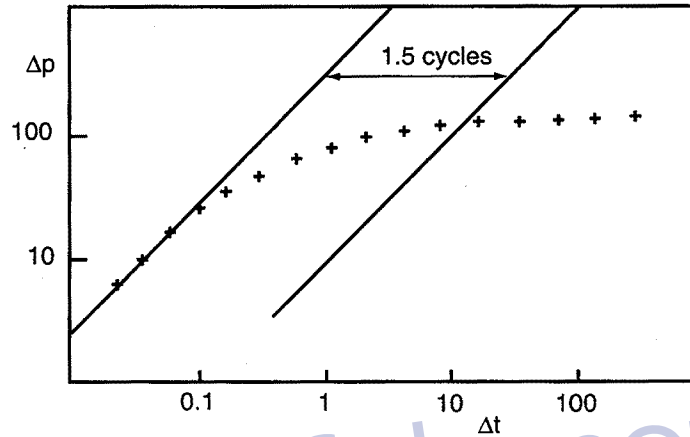


Fig. 2.3

Chapter 3

Skin

3.1 DEFINITION

The vicinity of the wellbore has characteristics that are different from those in the reservoir as a result of drilling and well treatment operations.

The skin effect reflects the difference in pressure drop that exists in the vicinity of the well between:

- the reservoir as it is, and
- as it would be if its characteristics (especially permeability) were uniform right up to the wellbore.

The skin effect reflects the connection between the reservoir and the well. The difference in pressure drop in the vicinity of the wellbore can be interpreted in several ways:

- by using infinitesimal skin;
- skin of a finite thickness;
- or the effective radius method.

3.2 INFINITESIMAL SKIN

The additional pressure drop due to the skin effect is defined by:

$$\Delta p_s = \frac{\alpha q B \mu}{k h} S \quad (3.1)$$

with:

$$\begin{aligned}\alpha &= 1/2\pi && \text{(in SI units)} \\ \alpha &= 141.2 && \text{(in practical US units)} \\ \alpha &= 18.66 && \text{(in practical metric units).}\end{aligned}$$

In Hurst and Van Everdingen's approach [Ref. 5], the pressure drop due to the skin effect is located in an infinitely thin film around the wellbore (Fig. 3.1).

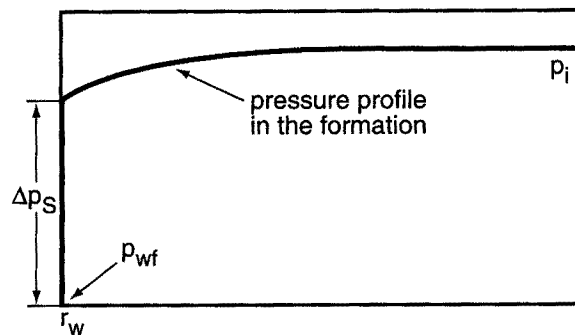


Fig. 3.1

The skin effect, S , is homogeneous with a dimensionless pressure drop.

3.3 FINITE THICKNESS SKIN

Another representation consists in assuming the pressure drop is located in an area with a radius r_s and permeability k_s around the well (Fig. 3.2).

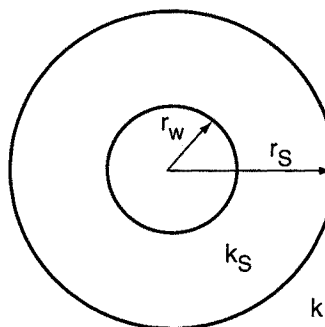


Fig. 3.2

When the compressible zone leaves this area, the flow can be considered pseudosteady-state and is governed by Darcy's law.

The difference in pressure drop between the real reservoir and a reservoir uniform right up to the wellbore is expressed as follows with Darcy's law:

$$\Delta p_S = \frac{qB\mu}{2\pi k_S h} \ln \frac{r_S}{r_w} - \frac{qB\mu}{2\pi kh} \ln \frac{r_S}{r_w}$$

By expressing Δp_S with equation (3.1) we get:

$$S = \left(\frac{k}{k_S} - 1 \right) \ln \frac{r_S}{r_w} \quad (3.2)$$

Nota bene:

Equation (3.2) shows that a **damage** ($k_S < k$) corresponds to a **positive skin**. When the vicinity of the wellbore is plugged the skin can have very large values. The more permeable the medium and the greater the damage, the higher the values.

Well treatments, such as acidizing for example, are performed to improve the near-well permeability and thereby reduce the skin value.

Equation (3.2) shows that an **improved permeability** corresponds to a **negative skin**. What value can negative skin reach?

Let us imagine a sufficiently effective treatment so that k/k_S is small compared to 1 on a radius r_S of 2 m around the wellbore. Considering a wellbore with a radius of 10 cm, equation (3.2) shows that under these conditions the skin is -3 .

Improved permeability distributed homogeneously and involving a radius of over 2 m around the well would not be very probable.

An improvement in permeability in the vicinity of the wellbore can correspond to a contribution of between 0 and -3 to the skin. A smaller skin value must be explained by other phenomena, e.g. fractures, fissures.

3.4 EFFECTIVE RADIUS

The effective radius method consists in replacing the real well with a radius r_w and skin S by a fictitious well with a radius r'_w and zero skin (Fig. 3.3).

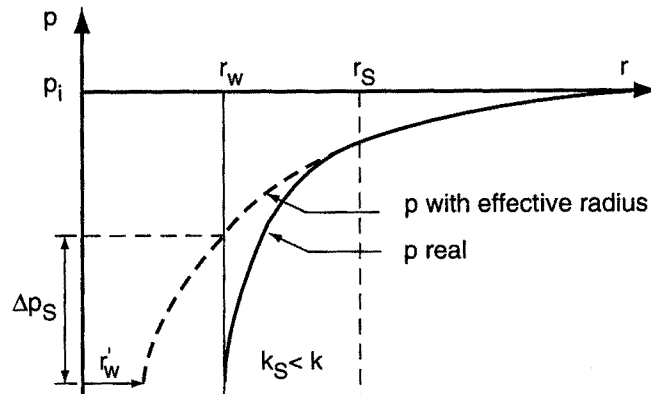


Fig. 3.3

Radius r'_w is determined to have a pressure drop between r_s and r'_w in the fictitious well equal to the pressure drop between r_s and r_w in the real well:

$$\Delta p(r'_w, S = 0) = \Delta p(r_w, S)$$

Expressing the pressure drop with Darcy's law:

$$\frac{qB\mu}{2\pi kh} \ln \frac{r_s}{r'_w} = \frac{qB\mu}{2\pi kh} \left(\ln \frac{r_s}{r_w} + S \right)$$

we get:

$$\boxed{r'_w = r_w \exp(-S)} \quad (3.3)$$

Nota bene:

The effective radius method is used to represent the skin analytically in all possible cases, including when the skin is negative.

It expresses the effect of well treatments.

This can be illustrated by the case of a gravel pack. The effective radius of the well should normally fall between the screen radius and the underreaming radius. An effective radius that is less than the liner radius would mean that the gravel pack is particularly ineffective.

The skin reflects the connection between the borehole and the reservoir. This is why it is recommended to use the inner radius of the borehole as radius r_w to

compute the skin: the inner casing radius when there are perforations and the inner radius of the liners when there is a gravel pack.

3.5 GENERALIZATION OF THE SKIN CONCEPT

The skin represents an additional pressure drop located in the vicinity of the wellbore.

In the preceding sections, the additional pressure drop was due to variations in permeability in the near-well formation.

The skin concept can be generalized to any additional pressure drop situated in the area near the well.

The skin can be used to account for:

- **Perforations:**

The skin due to perforations includes several phenomena:

- the flow restriction due to the perforation hole: a positive skin;
- the punctured reservoir due to the perforating operation itself: a negative skin (minifracture);
- the fact that only some of the perforations are active: a positive skin.

These different phenomena are generally not dissociated from the damage effect.

- **Inclined wells** (see Chapter 16):

The inclination of a well improves flow in the vicinity of the wellbore and contributes to negative skin.

- **Partially perforating the reservoir** (see Chapter 15):

Perforating only part of the thickness of the reservoir causes a restriction in the stream lines near the wellbore and contributes to positive skin.

- **Hydraulic fracturing** (see Chapter 17):

Hydraulic fracturing considerably improves the flow around the wellbore. It produces a negative skin.

- **A horizontal well** (see Chapter 18):

A horizontal well can under certain conditions be treated as a vertical well with negative skin due to the improvement to flow brought about by the well.

- **Gas well: deviation from Darcy's law** (see Chapter 20):

The fluid velocity in the vicinity of a gas well is often high. Flow does not follow Darcy's law near the well.

Positive skin, depending on the flow rate, shows the additional pressure drop due to the deviation from Darcy's law.

- **Injection skin** (see Chapter 19):

Injection of fluid (water, polymers, etc.) into the reservoir creates a zone of different mobility in the vicinity of the wellbore. It causes additional pressure drop that can also be considered as a skin when the compressible zone is beyond the fluid injection radius.

- **Geological skin:**

A well in a low-input lens can be reflected by a skin:

- the reservoir has the characteristics of the distant regions that supply the lens;
- the skin reflects the characteristics of the lens.

In all cases the additional pressure drop in the vicinity of the wellbore can be treated like a skin provided that the flow in the skin can be considered steady-state. For this to be true the compressible zone must have reached beyond the skin zone.

The concept of the vicinity of the wellbore may cover a number of very different things in actual fact:

- When acidizing has been performed, the additional pressure drop involves a distance of less than 2 m around the well.
- When hydraulic fracturing has been done, the test needs to have started affecting regions located several tens of meters from the well before the fracture can be considered in terms of skin.

Interpretation methods



A lot of different methods can be used to analyze a well test, they can be classified into two main groups:

- methods using type curves;
- conventional methods.

Inside each of the two groups the methods depend on the type of well, reservoir and reservoir boundaries.

This introduction deals with the features that are common to the methods in each group.

In the following chapters we will consider the flow in the reservoir as a one-phase flow of oil.

The first three chapters will introduce interpretation methods in the simplest case, i.e. a vertical well in an infinite homogeneous reservoir.

Then we will discuss bounded reservoirs and more complicated reservoir-well configurations. Gas and multiphase reservoirs will be covered in Chapters 20 and 21.

First of all let us look at what the methods in each group have in common with each other.

- **Type curve matching:**

These methods began to be used in the seventies, but only became developed and widespread in the eighties.

They first appeared in the form of sets of curves using dimensionless parameters.

The curves undergo simplifying hypotheses to be easily presented that often severely limit their conditions of use.

Their popularity is directly related to the enormous progress made in computer science, i.e. the considerable reduction in CPU time on increasingly powerful computers.

This means that the pressure variations expected throughout the well test can be simulated according to the chosen reservoir-well configuration by means of an analytic model with a minimum amount of simplification.

Type curves produced by a well model on a PC have eliminated most of the method's limitations.

From 1983 on, type curve methods were greatly improved as they were used in conjunction with the pressure derivative. What type curve methods have in common is that they take into account at the same time all the pressure variations recorded during the well test.

This allows the determination of the different flows occurring during the test and then a diagnosis of the well and the reservoirs.

The different flow periods allow the application of conventional interpretation methods corresponding to the determination of each flow.

• Conventional methods:

Conventional methods were developed in the thirties and were the only ones available until the seventies.

They consist in identifying the different periods of characteristic flow in succession on the pressure recording.

During a characteristic flow (radial, linear, etc.) the pressure variation is represented by a time scale adapted to have a straight line for the particular flow.

Using only conventional methods to analyze a test leads to several drawbacks:

- It is sometimes difficult to diagnose a flow. The flow corresponds to a straight line on the pressure versus $f(t)$ graph. The straight line exists only if the different flows are separated, otherwise there is no straight line. No conventional interpretation is possible.

- Interpretation takes only the points located on the straight line into account. The points corresponding to the transition between two flows are not used. Because of this, it often happens that only a small proportion of the data is used a conventional analysis.
- It is sometimes difficult to draw the proper straight line. In many interpretations several straight lines may seem to appear. It is often difficult to determine which straight line corresponds to the relevant analysis. Some straight lines only correspond to the tangent to a curve with a slight camber.

- **Interpretation procedure:**

Since type curves have been integrated in analysis, the procedure has been considerably modified.

The process now in use is as follows:

Diagnosis: Diagnosis allows the determination of the sequence of flows appearing during the test. Identifying the flows determines which reservoir-well configuration will then be used for the interpretation.

The diagnosis is made mainly on the basis of the pressure derivative.

Analysis: Analysis aims to quantify the parameters of the reservoir-well configuration. It is performed with type curves, the pressure derivative and conventional methods.

Validation: Analysis is validated by generating a type curve simulating the data and its derivative as closely as possible by means of an analytic model adapted to the reservoir-well configuration and to the recorded flow rates.

The initial parameters in the model are determined during the analysis phase.

A final adjustment of parameters is usually necessary to fit the data better, especially for transitions between the different flow regimes.



Chapter 4

Conventional interpretation methods

During a well test on an infinite homogeneous reservoir two flows can be seen if the test lasts long enough:

- flow that is related to wellbore storage;
- radial flow over the whole reservoir thickness.

Analysis methods will be presented for this configuration—the simplest one that can be found—then developed in later chapters with more complex reservoir-well configurations.

The flow related to wellbore storage and its analysis were dealt with in Chapter 2.

In Chapter 4 the effect of wellbore storage is considered to be over and the methods covered are used to study radial flow around a well that has been perforated over the whole reservoir thickness.

Three flow rate conditions are examined:

- the drawdown test.
- the buildup test, with pressure buildup preceded by one constant flow rate.
- the test following any number and type of previous flow rates.

4.1 DRAWDOWN TEST

The equation that describes pressure variations versus time and distance from the well after opening the well at a constant flow rate, q , was established in section 1.5:

$$p_i - p(r, t) = - \frac{qB\mu}{4\pi kh} \operatorname{Ei} \left(\frac{-r^2}{4Kt} \right) \quad (4.1)$$

with $K = k/\phi\mu c_t$ hydraulic diffusivity.

When the pressure is measured in the well where the flow rate disturbance is located, $r = r_w$.

As soon as $\frac{r_w^2}{4Kt} < 10^{-2}$, which usually occurs before the wellbore storage effect is over, the Ei function can be replaced by its logarithmic approximation:

$$p_i - p_{wf}(t) = \frac{qB\mu}{4\pi kh} \left(\ln \frac{Kt}{r_w^2} + 0.81 \right) \quad (4.2)$$

Taking pressure drops in the skin into account, this expression becomes:

$$p_i - p_{wf}(t) = \frac{qB\mu}{4\pi kh} \left(\ln \frac{Kt}{r_w^2} + 0.81 + 2 S \right) \quad (4.3)$$

It can also be written in other equivalent forms:

– in practical US units:

$$p_i - p_{wf} = \frac{162.6 qB\mu}{kh} \left(\log t + \log \frac{k}{\phi\mu c_t r_w^2} - 3.23 + 0.87 S \right) \quad (4.4)$$

– in practical metric units:

$$p_i - p_{wf} = \frac{21.5 qB\mu}{kh} \left(\log t + \log \frac{k}{\phi\mu c_t r_w^2} - 3.10 + 0.87 S \right) \quad (4.5)$$

– as a dimensionless equation:

$$p_D = \frac{1}{2} \left(\ln t_D + 0.81 + 2 S \right) \quad (4.6)$$

• **Interpretation:**

Equations (4.2) to (4.6) show that bottomhole pressure varies logarithmically versus time.

If the pressure measured at the bottom of the hole is plotted on a graph versus the logarithm of time, a straight line with a slope of m can be observed once the wellbore storage effect has ended:

$$m = \frac{162.6 qB\mu}{kh} \quad (\text{in practical US units}) \quad (4.7)$$

$$m = \frac{21.5 qB\mu}{kh} \quad (\text{in practical metric units}) \quad (4.8)$$

The slope, m , is used to determine the reservoir's kh :

$$kh = \frac{2.303 qB\mu}{4\pi m} \quad (\text{in SI units}) \quad (4.9)$$

$$kh = \frac{162.6 qB\mu}{m} \quad (\text{in practical US units}) \quad (4.10)$$

$$kh = \frac{21.5 qB\mu}{m} \quad (\text{in practical metric units}) \quad (4.11)$$

The **skin** value is usually computed using the pressure measurement at 1 hour **on the semi-log straight line**; for this point $\log t = 0$.

$$S = 1.15 \left(\frac{p_i - p_{1h}}{m} - \log \frac{k}{\phi\mu c_t r_w^2} + 3.23 \right) \quad (\text{in practical US units}) \quad (4.12)$$

$$S = 1.15 \left(\frac{p_i - p_{1h}}{m} - \log \frac{k}{\phi\mu c_t r_w^2} + 3.10 \right) \quad (\text{in practical metric units}) \quad (4.13)$$

Care must be taken to read the pressure at 1 hour on the semi-log straight line and not by interpolating among the measurement points. After one hour the data may still be affected by the wellbore storage effect (Fig. 4.1). In this case, they do not verify the semi-log straight line equation.

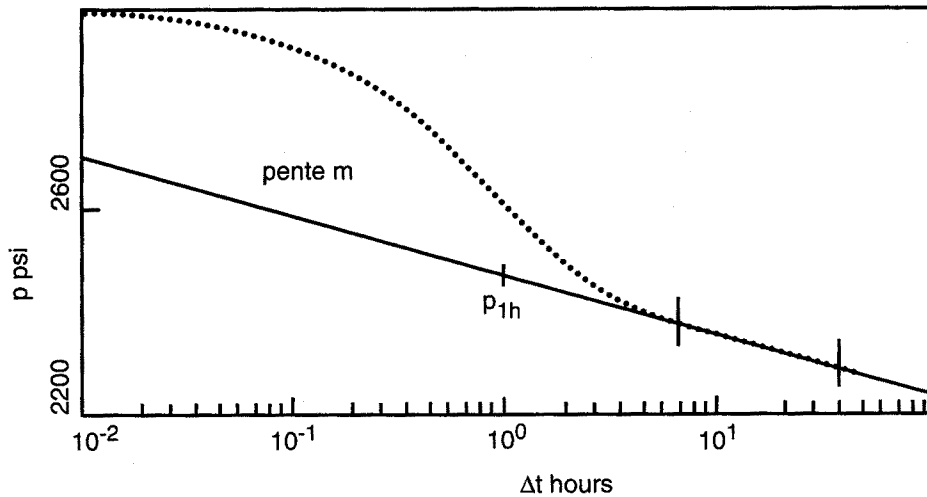


Fig. 4.1

4.2 PRESSURE BUILDUP: HORNER'S METHOD

Most of the information from a well test comes from interpreting the pressure buildups.

Interpreting a drawdown test is limited by the flow rate fluctuations inherent to production. The fluctuations cause pressure variations that are greater near the end of the test than the pressure variation due to the initial change in flow rate.

The zero flow rate that corresponds to pressure buildups does not cause this type of problem.

The symbols used are presented in Figure 4.2:

$p_{wf}(t)$ is the flowing pressure; time is counted from when the well is opened.

$p_{ws}(\Delta t)$ is the pressure during the buildup phase; time is counted from when the well is shut in, t_p :

$$p_{ws}(\Delta t = 0) = p_{wf}(t_p)$$

Pressure buildup is analyzed using the flow rate superposition principle mentioned in section 1.9:

$$p_i - p_{ws}(\Delta t) = [p_i - p_{wf}(t_p + \Delta t)] - [p_i - p_{wf}(\Delta t)] \quad (4.14)$$

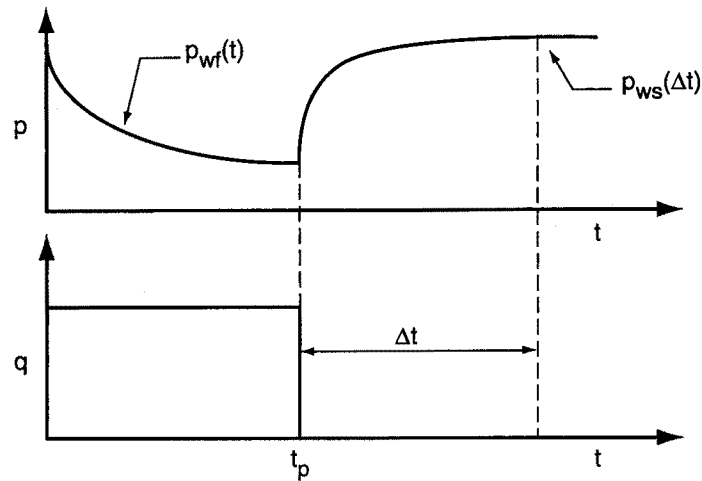


Fig. 4.2

The variations in flowing pressure are given by equation (4.3) once the wellbore storage effect has ended. Replacing the two right-hand terms of equation (4.14) by the semi-logarithmic expression of radial flow (equation 4.3) gives:

$$p_i - p_{ws}(\Delta t) = \frac{qB\mu}{4\pi kh} \ln \frac{t_p + \Delta t}{\Delta t} \quad (4.15)$$

which is written:

– in practical US units:

$$p_i - p_{ws}(\Delta t) = \frac{162.6 qB\mu}{kh} \log \frac{t_p + \Delta t}{\Delta t} \quad (4.16)$$

– in practical metric units:

$$p_i - p_{ws}(\Delta t) = \frac{21.5 qB\mu}{kh} \log \frac{t_p + \Delta t}{\Delta t} \quad (4.17)$$

• **Analysis:**

The equations and analysis method were presented by Horner in 1951 [Ref. 6].

Equations (4.15) to (4.17) show that the bottomhole pressure varies linearly versus $\log \frac{t_p + \Delta t}{\Delta t}$.

If the value of the pressure measured at the bottom of the hole is plotted versus the logarithm of $\frac{t_p + \Delta t}{\Delta t}$, on a graph, once the wellbore storage effect has ended a straight line with a slope of m can be observed:

$$m = \frac{162.6 qB\mu}{kh} \quad (\text{in practical US units}) \quad (4.18)$$

$$m = \frac{21.5 qB\mu}{kh} \quad (\text{in practical metric units}) \quad (4.19)$$

• **Reservoir kh:**

As with drawdown, the value of slope m is used to compute the reservoir's kh:

$$kh = \frac{162.6 qB\mu}{m} \quad (\text{in practical US units}) \quad (4.20)$$

$$kh = \frac{21.5 qB\mu}{m} \quad (\text{in practical metric units}) \quad (4.21)$$

• **Skin:**

The skin value is computed from the difference between:

– the value of the pressure recorded after 1 hour of buildup **on the semi-log straight line** (Fig. 4.3):

$$p_i - p(1 \text{ h}) = \frac{162.6 qB\mu}{kh} \log(t_p + 1)$$

– and the value of the pressure at shut-in time:

$$p_i - p_{wf}(t_p) = \frac{162.6 qB\mu}{kh} \left(\log t_p + \log \frac{k}{\phi\mu c_t r_w^2} - 3.23 + 0.87 S \right)$$

Subtracting the two expressions term by term, the skin can be deduced:

$$S = 1.15 \left(\frac{p_{1h} - p_{wf}(t_p)}{m} + \log \frac{t_p + 1}{t_p} - \log \frac{k}{\phi\mu c_t r_w^2} + 3.23 \right) \quad (\text{US}) \quad (4.22)$$

$$S = 1.15 \left(\frac{p_{1h} - p_{wf}(t_p)}{m} + \log \frac{t_p + 1}{t_p} - \log \frac{k}{\phi\mu c_t r_w^2} + 3.10 \right) \quad (\text{metric}) \quad (4.23)$$

The term $\log \frac{t_p + 1}{t_p}$ is usually negligible compared to the other terms.

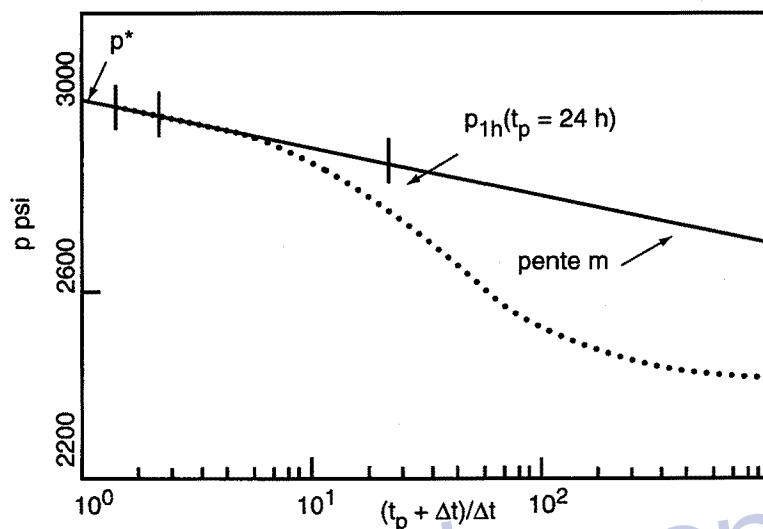


Fig. 4.3

- **Extrapolated pressure:**

During initial tests the amount of fluid produced before shut-in is usually negligible compared with the amount of oil in place.

If the pressure buildup was to continue indefinitely, the bottomhole pressure would be equal to the initial reservoir pressure.

The initial reservoir pressure can be read on the pressure buildup for

$$\Delta t = \infty, \text{ i.e. } \frac{t_p + \Delta t}{\Delta t} = 1 \text{ (Fig. 4.3).}$$

This pressure value is called the extrapolated pressure and is written p^* .

It is equal to the initial reservoir pressure in most initial tests.

It is used to compute the average pressure when production is not negligible compared to the amount of oil in place. The method used to determine average pressure by means of p^* is covered in Chapter 11.

4.3 PRESSURE BUILDUP: MDH METHOD

The preceding section showed that in buildup the pressure varies linearly versus the logarithm of $(t_p + \Delta t)/\Delta t$.

This expression can be written in a simplified form whenever production time t_p is large compared to the pressure buildup time Δt .

If t_p is large compared to Δt :

$$t_p + \Delta t \approx t_p$$

Equation (4.15) becomes:

$$p_i - p_{wf} = -\frac{qB\mu}{4\pi kh} (\ln \Delta t - \ln t_p)$$

The bottomhole pressure varies linearly versus pressure buildup time.

This means that during buildup the pressure drop due to previous production is disregarded.

Figure 4.4 illustrates this interpretation method developed by Miller Dyes and Hutchinson [Ref. 8], i.e. the MDH method:

- the real pressure buildup is Δp ;
- the pressure buildup dealt with by the MDH is Δp_{MDH} .

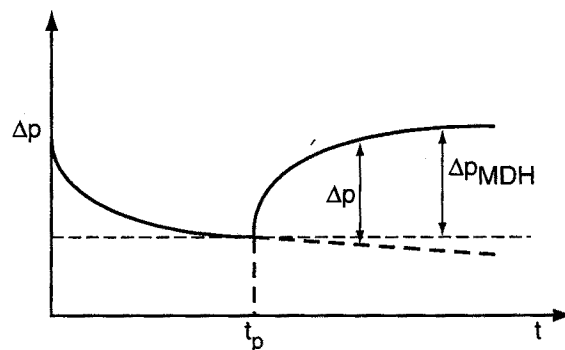


Fig. 4.4

The difference between Δp and Δp_{MDH} is negligible when Δt is small compared to t_p , i.e.:

- at the beginning of buildup;
- after a long period at constant flow rate.

• Interpretation method:

The pressure varies linearly versus the logarithm of time. By plotting Δp_{MDH} versus Δt , a semi-log straight line with a slope of m (Fig. 4.5) can be seen once the wellbore storage effect has ended:

$$m = \frac{162.6 qB\mu}{kh} \quad (\text{in practical US units}) \quad (4.24)$$

$$m = \frac{21.5 qB\mu}{kh} \quad (\text{in practical metric units}) \quad (4.25)$$

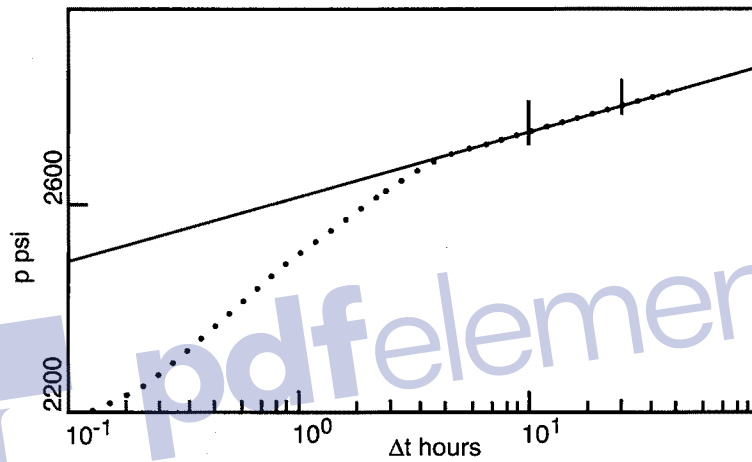


Fig. 4.5

The slope is used to compute the reservoir's kh :

$$kh = \frac{162.6 qB\mu}{m} \quad (\text{in practical US units}) \quad (4.26)$$

$$kh = \frac{21.5 qB\mu}{m} \quad (\text{in practical metric units}) \quad (4.27)$$

The skin is computed the same way as in the Horner method:

$$S = 1.15 \left(\frac{p_{1h} - p_{wf}(t_p)}{m} - \log \frac{k}{\phi\mu c_t r_w^2} + 3.23 \right) \quad (\text{US}) \quad (4.28)$$

$$S = 1.15 \left(\frac{p_{1h} - p_{wf}(t_p)}{m} - \log \frac{k}{\phi\mu c_t r_w^2} + 3.10 \right) \quad (\text{metric}) \quad (4.29)$$

The advantage of this method is that it is very simple, however it has two major drawbacks:

- it can not be used to find the extrapolated pressure;
- it can be used only for values of Δt that are small compared to t_p .

When production time is short or close to Δt (initial tests on a well), the last buildup points are located under the theoretical semi-log straight line in the MDH representation (Fig. 4.6).

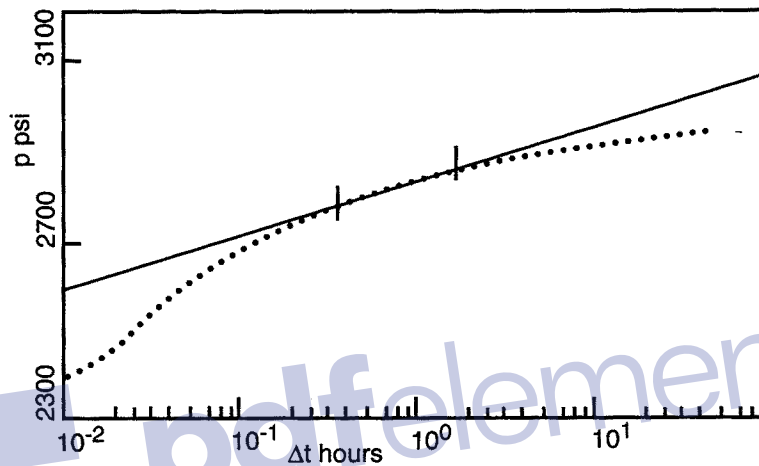


Fig. 4.6

4.4 AFTER VARYING FLOW RATES

A test after varying flow rates is interpreted using the flow rate superposition principle discussed in section 1.9:

$$p_i - p_{wf}(t) = \frac{B\mu}{2\pi kh} \sum_{i=1}^n (q_i - q_{i-1}) p_D(t - t_{i-1}) \quad (4.30)$$

Once the wellbore storage effect has ended, the pressure variations are given by equation (4.3). Equation (4.30) then becomes:

$$p_i - p_{wf}(t) = \frac{B\mu}{4\pi kh} \sum_{i=1}^n (q_i - q_{i-1}) \left(\ln \frac{K(t - t_{i-1})}{r_w^2} + 0.81 + 2S \right) \quad (4.31)$$

The interpreter is interested in the pressure variations since the last change in flow rate, t_{n-1} . The pressure variation at the time when the change took place is:

$$p_i - p_{wf}(t_{n-1}) = \frac{B\mu}{4\pi kh} \sum_{i=1}^{n-1} (q_i - q_{i-1}) \left\{ \ln \frac{K(t_{n-1} - t_i)}{r_w^2} + 0.81 + 2 S \right\}$$

The pressure buildup since the time when the well was shut in is expressed by:

$$p_{ws}(\Delta t) - p_{wf}(t_{n-1}) = \frac{B\mu}{4\pi kh} \left\{ \sum_{i=1}^{n-1} (q_i - q_{i-1}) \ln \frac{t_{n-1} - t_{i-1}}{t_{n-1} - t_{i-1} + \Delta t} - (q_n - q_{n-1}) \left(\ln \frac{K \Delta t}{r_w^2} + 0.81 + 2 S \right) \right\} \quad (4.32)$$

Δt is the time elapsed since the last change in flow rate.

It can be written as follows:

$$p_{ws}(\Delta t) - p_{wf}(t_{n-1}) = \frac{162.6 B\mu}{kh} \left\{ \sum_{i=1}^{n-1} (q_i - q_{i-1}) \log \frac{t_{n-1} - t_{i-1}}{t_{n-1} - t_{i-1} + \Delta t} - (q_n - q_{n-1}) \left(\log \Delta t + \log \frac{k}{\phi \mu c_t r_w^2} - 3.23 + 0.87 S \right) \right\} \quad (\text{in practical US units}) \quad (4.33)$$

$$p_{ws}(\Delta t) - p_{wf}(t_{n-1}) = \frac{21.5 B\mu}{kh} \left\{ \sum_{i=1}^{n-1} (q_i - q_{i-1}) \log \frac{t_{n-1} - t_{i-1}}{t_{n-1} - t_{i-1} + \Delta t} - (q_n - q_{n-1}) \left(\log \Delta t + \log \frac{k}{\phi \mu c_t r_w^2} - 3.10 + 0.87 S \right) \right\} \quad (\text{in practical metric units}) \quad (4.34)$$

• Interpretation:

The pressure varies linearly versus the right-hand member (between parentheses) of equations (4.33) and (4.34). The member is a function of flow rates and time and is called the superposition function.

If the value of the pressure measured in the bottom of the hole is plotted versus the superposition function, a straight line with a slope of m (Fig. 4.7) can be seen once the effect of wellbore storage has ended.

$$m = \frac{162.6 B\mu}{kh} \quad (\text{in practical US units}) \quad (4.35)$$

$$m = \frac{21.5 B\mu}{kh} \quad (\text{in practical metric units}) \quad (4.36)$$

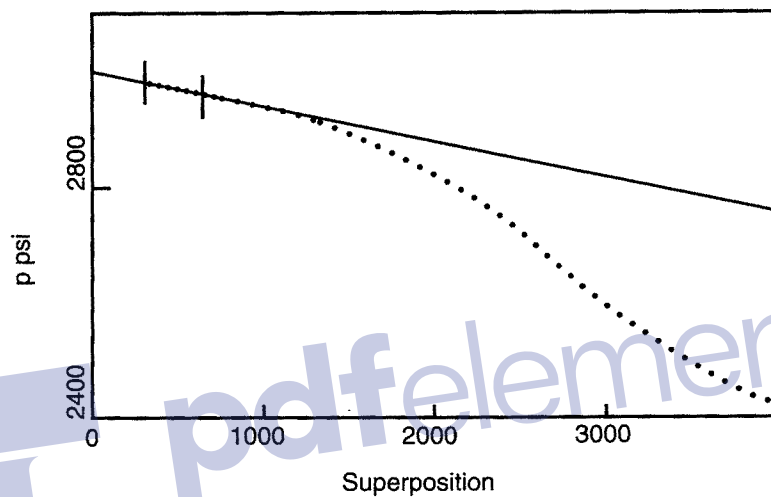


Fig. 4.7

The slope is independent of flow rate. This is the advantage of the representation: the results obtained with different flow rates can be compared on the same graph.

To find an expression of m which is dependent on flow rate comparable to what is obtained with Horner's method, the superposition function needs only to be divided by the last flow rate.

- **Reservoir kh :**

The slope, m , of the straight line is used to determine the reservoir's kh :

$$kh = \frac{162.6 B\mu}{m} \quad (\text{in practical US units}) \quad (4.37)$$

$$kh = \frac{21.5 B\mu}{m} \quad (\text{in practical metric units}) \quad (4.38)$$

- **Skin:**

The skin is determined based on the pressure value read on the straight line 1 hour after a last flow rate variation:

$$S = 1.15 \left(\frac{p_{1h} - p_{wf}(t_{n-1})}{(q_{n-1} - q_n) m} - \log \frac{k}{\phi \mu c_t r_w^2} + 3.23 \right) \quad (\text{in practical US units}) \quad (4.39)$$

$$S = 1.15 \left(\frac{p_{1h} - p_{wf}(t_{n-1})}{(q_{n-1} - q_n) m} - \log \frac{k}{\phi \mu c_t r_w^2} + 3.10 \right) \quad (\text{in practical metric units}) \quad (4.40)$$

- **Extrapolated pressure:**

If the last flow rate variation is a shut-in, the pressure reading for infinite time, i.e. for a value of the superposition function equal to zero, is used to determine the extrapolated reservoir pressure (Fig. 4.7).

The comments made in section 4.2 on the meaning of the extrapolated pressure are applicable here too.

4.5 SIMPLIFICATION OF THE FLOW RATE HISTORY

The superposition function takes the flow rate history into account.

It does not cause any problems when the interpreter has a computer to deal with it.

However few would try manual calculation even with two or three flow rates.

What equivalent function could be used in this case?

- **Equivalent time:**

To analyze the final buildup, the simplest method consists in reducing the flow rate history to one single rate and using Horner's method for the actual interpreting.

The single-rate production data that replace the n-1 multirate reality must be governed by the following principles:

- flow rate = the last rate;
- equivalent production time:

$$t_{pe} = \frac{\sum_{i=1}^{n-1} q_i (t_i - t_{i-1})}{q_n} \quad (4.41)$$

The production time is designed to provide a total production value identical to the production that was actually recorded.

The real production time should not be used in any case to compute an equivalent flow rate.

• **Validity of the method:**

As a rule of thumb, simplifying the flow rate history can be considered to introduce negligible error when the buildup duration is less than twice the duration of the last constant flow rate before shut-in (Fig. 4.8).

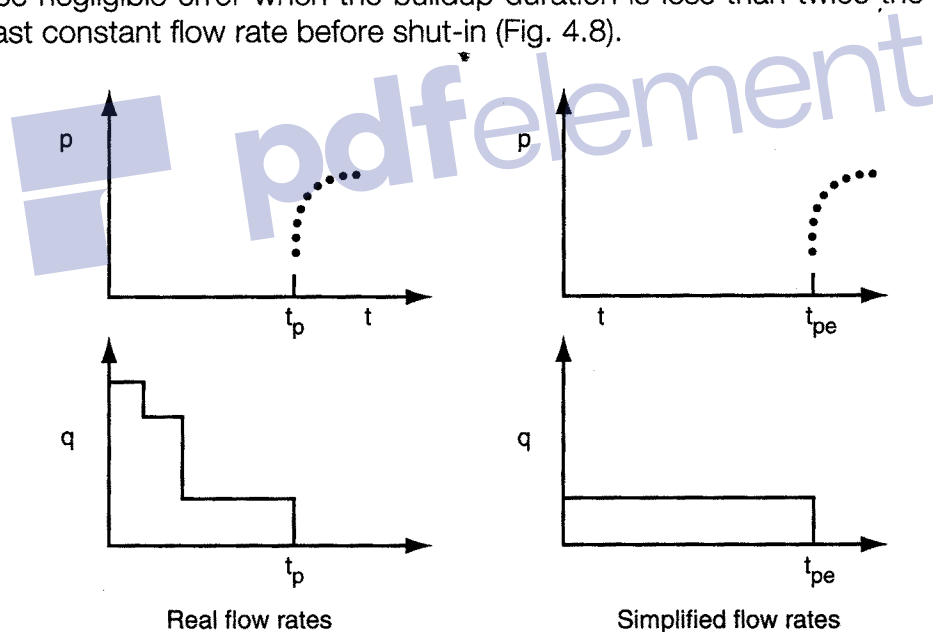


Fig. 4.8 Simplification of flow rate history introduces little error

If substantial rate variations occurred shortly before shut-in, the simplification will introduce error. The wider the variations and the closer they occurred before shut-in, the greater the error introduced.

Figure 4.9 indicates the direction the error takes on a Horner plot.

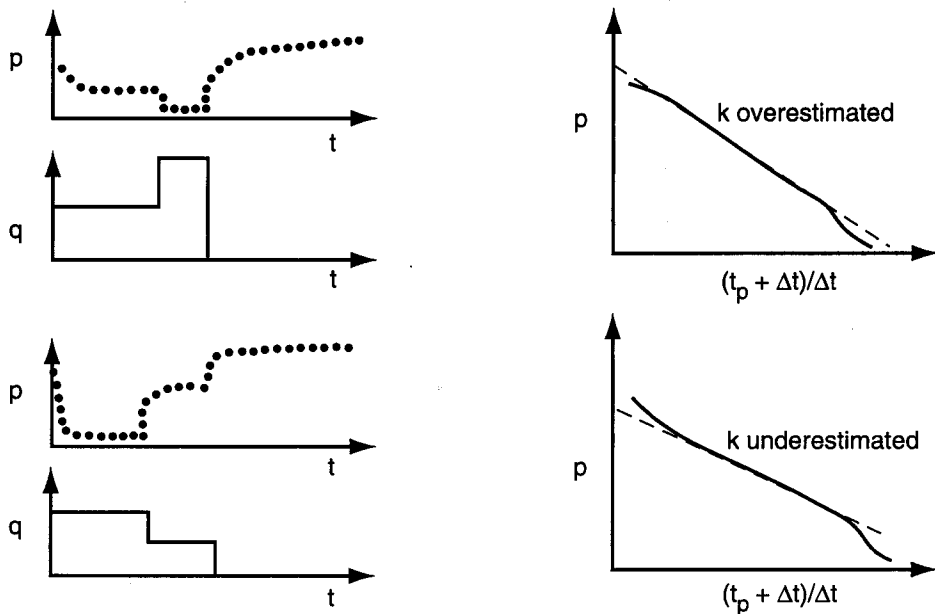


Fig. 4.9 Simplification of flow rate history introduces error

Let Δt be the buildup duration (Fig. 4.10). The simplification of flow rate history ($t_p - 2\Delta t_r$) and t_p can introduce error in the interpretation. Simplification before ($t_p - \Delta t_r$) usually introduces only a slight degree of error.

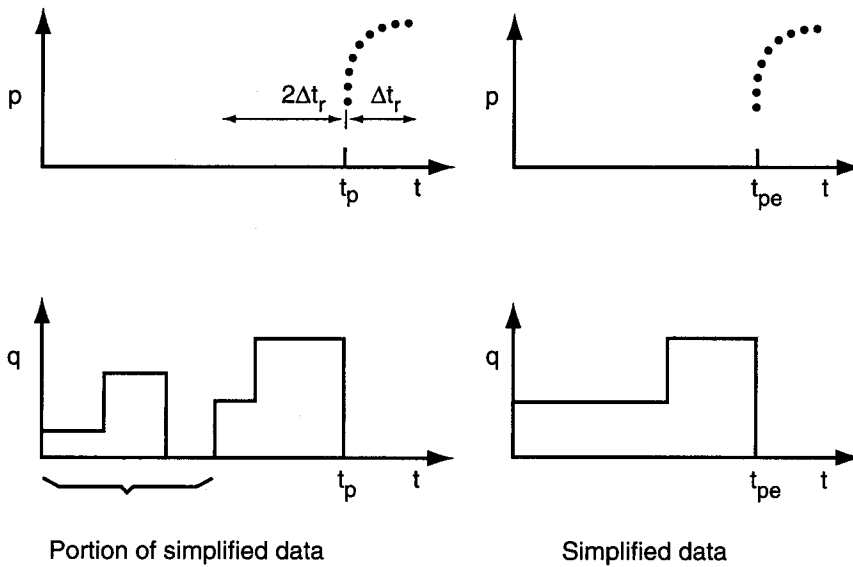


Fig. 4.10 Simplification of a multirate history

4.6 BUILDUP RADIUS OF INVESTIGATION

The theoretical radius of investigation depends only on the duration of the pressure buildup.

The radius of investigation can be estimated by using the formula proposed in section 1.7:

$$r_i = 0.032 \sqrt{\frac{k \Delta t}{\phi \mu c_t}} \quad (\text{in practical US units}) \quad (4.42)$$

$$r_i = 0.038 \sqrt{\frac{k \Delta t}{\phi \mu c_t}} \quad (\text{in practical metric units}) \quad (4.43)$$

It is theoretically independent of the duration of the drawdown period.

In contrast, the practical buildup radius of investigation is limited by the accuracy of pressure gauges. When the pressure buildup is long compared with the duration of the drawdown period, then the pressure drop recorded toward the end of the buildup may become too small to be measured.

To increase the practical radius of investigation of a pressure buildup, several methods can be used:

- use more accurate pressure gauges;
- increase the well flow rate to increase the pressure drop before buildup;
- increase the duration of the drawdown period for the same reason.

Care must also be taken since the production of other wells may interfere with the shut-in of the well itself during a buildup period that is too long. In this case, the signal measured would be nothing else but an interference signal (see Chapters 22 and 23).

Likewise, when buildup lasts several days, moon tides may disturb the pressure buildup by cyclic variations with an amplitude of approximately 0.1 psi (see Chapter 23 on interference).

Chapter 5

Type curves

5.1 INTRODUCTION

Type curves first appeared in oil industry literature in the seventies.

Several kinds, as listed below, are used to interpret a test in a vertical well with an infinite homogeneous reservoir:

- Agarwal et al. type curves;
- McKinley type curves;
- Earlougher and Kersch type curves;
- Gringarten et al. type curves.

F. Daviau [Réf. 1] has examined type curves in detail in his book on new well testing interpretation methods. He suggests that the Gringarten et al. curves are the most complete and practical to use. They are also the most widely used in oil industry literature. They are the only ones presented here.

5.2 GRINGARTEN TYPE CURVES

A type curve represents the variations in pressure versus time for a specified reservoir-well configuration.

It is calculated using an analytic model and expressed in dimensionless variables.

The analytic model used by Gringarten to describe a vertical well in an infinite homogeneous reservoir is discussed by F. Daviau [Ref. 1] in Chapters 1 and 4.

• **Dimensionless variables:**

The variables used are as follows in practical US units:

$$\text{Pressure:} \quad p_D = \frac{kh}{141.2 qB\mu} \Delta p \quad (5.1)$$

$$\text{Time:} \quad t_D = \frac{0.000264 k}{\phi\mu c_t r_w^2} \Delta t \quad (5.2)$$

$$\text{Well storage:} \quad C_D = \frac{0.89}{h\phi c_t r_w^2} C \quad (5.3)$$

$$\text{Skin:} \quad S$$

• **Representation:**

In a vertical well in an infinite homogeneous reservoir the dimensionless pressure variations depend on three factors: time, wellbore storage and skin.

Type curves therefore correspond to an expression of the following form:

$$p_D = p_D(t_D, C_D, S)$$

Representing the skin by an effective radius (see section 3.4):

$$r_w \text{ is replaced by } r'_w = r_w \exp(-S)$$

$$t_D \text{ is replaced by } t_D \exp(2S)$$

$$C_D \text{ is replaced by } C_D \exp(2S).$$

The pressure is represented by an expression of the following form:

$$p_D = p_D(t_D \exp(2S), C_D \exp(2S))$$

with Gringarten using the form below:

$$p_D = p_D\left(\frac{t_D}{C_D}, C_D \exp(2S)\right)$$

The pressure is represented on the abscissa versus t_D/C_D on a log-log graph. Each type curve differs from the following one by the value of the parameter $C_D \exp(2S)$ (Fig. 5.1).

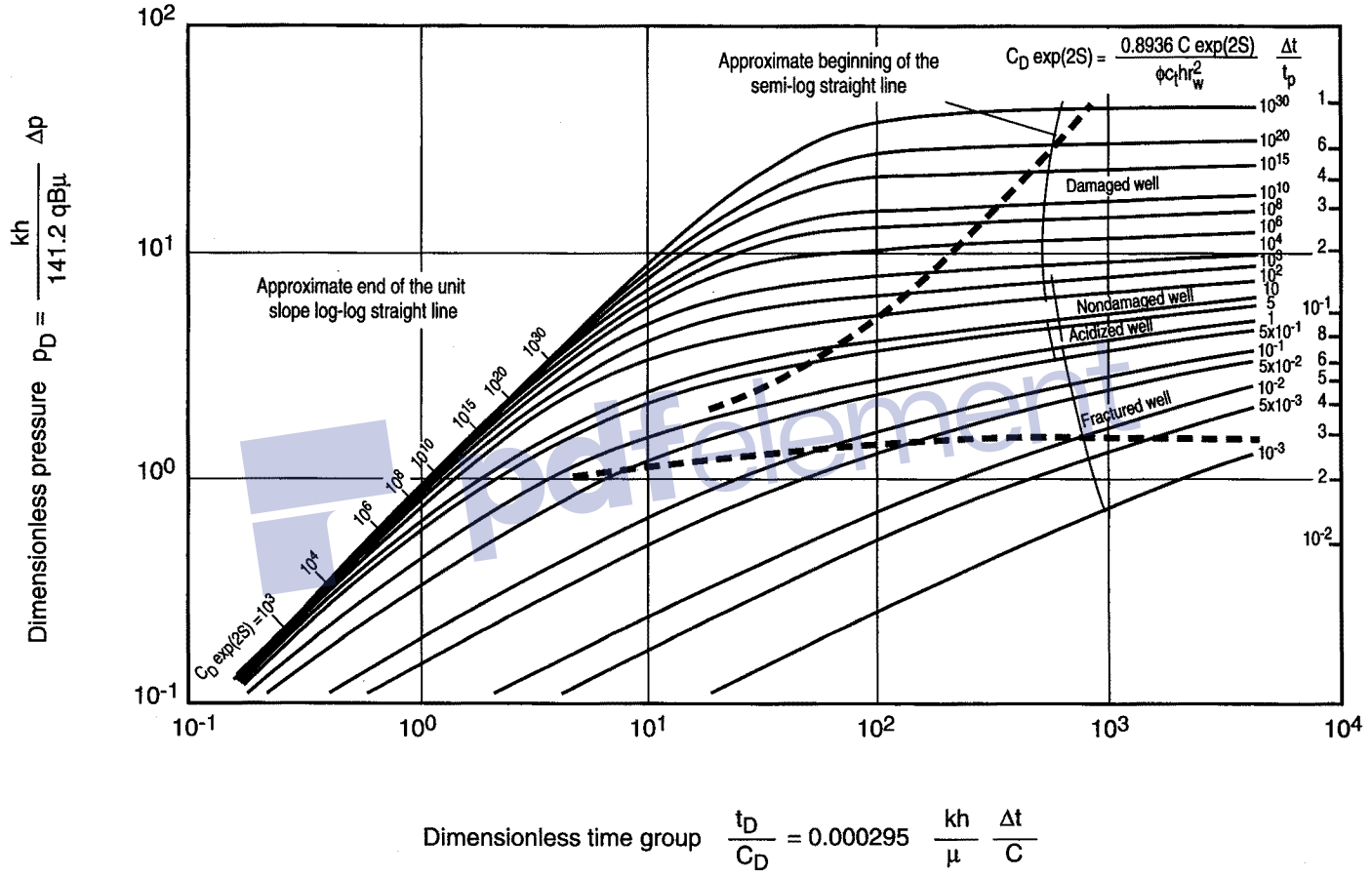


Fig. 5.1 Type curves for a well with wellbore storage and skin (infinite homogeneous reservoir)

The upper curves in the set correspond to high $C_D \exp(2S)$ values. Considering a realistic range of wellbore storage figures, these high values can only be obtained with high skins, i.e. they correspond to damaged wells.

Likewise, the lowest $C_D \exp(2S)$ values correspond to acidized or even fractured wells.

During the period of dominant wellbore storage effect the dimensionless pressure (see section 2.5) is equal to:

$$p_D = \frac{t_D}{C_D}$$

The points corresponding to this period are located on the straight line with a slope of 1 that goes through the time origin. All type curves have this straight line as asymptote for short times.

Two curves in the set indicate the end of the wellbore storage effect: the upper one corresponds to type curves where $C_D \exp(2S)$ is greater than 1, the lower one corresponds to those where $C_D \exp(2S)$ is less than 1.

5.3 INTERPRETATION METHOD

- **Procedure:**

The interpretation method is illustrated in Figure 5.2 and consists in the following steps:

- 1 Plot the measured pressure drop on tracing paper lying on the type curves, using the log-log scale of the type curves (Fig. 5.2a).
- 2 Look for the portion of an underlying type curve matching the data best (Fig. 5.2b).

Only translations are allowed during this step, keeping the two grids parallel.

- 3 Note the specifications of the type curve where the measured points match; they correspond to a value of $C_D \exp(2S)$.
- 4 Pick a match point, M, whose coordinates can be read in both the type curve system of axes (p_D , t_D/C_D) as well as in the field data system (Δp , Δt). The point M can be chosen anywhere on the plot, not necessarily on the curve (Fig. 5.2c).

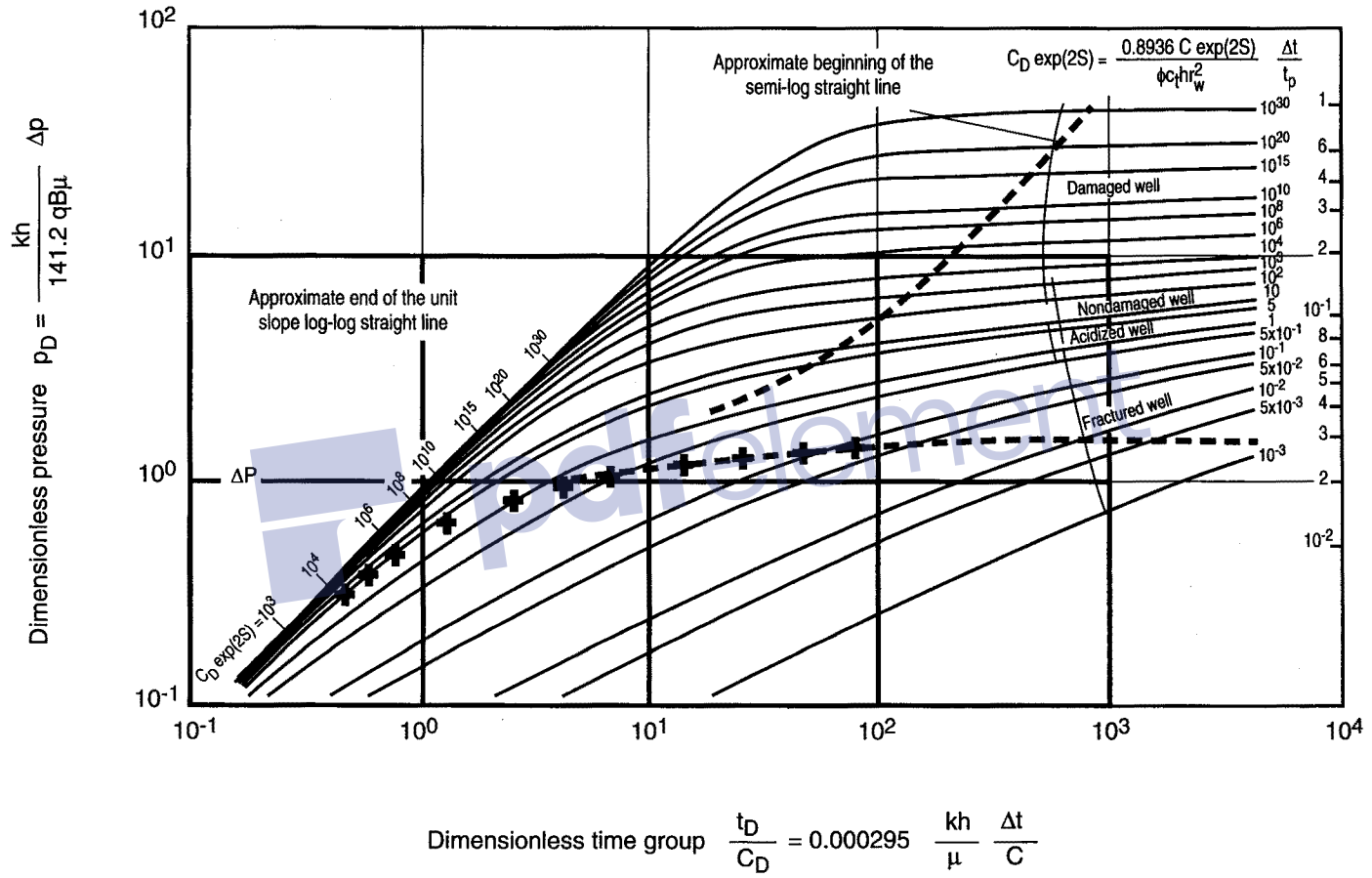


Fig. 5.2a

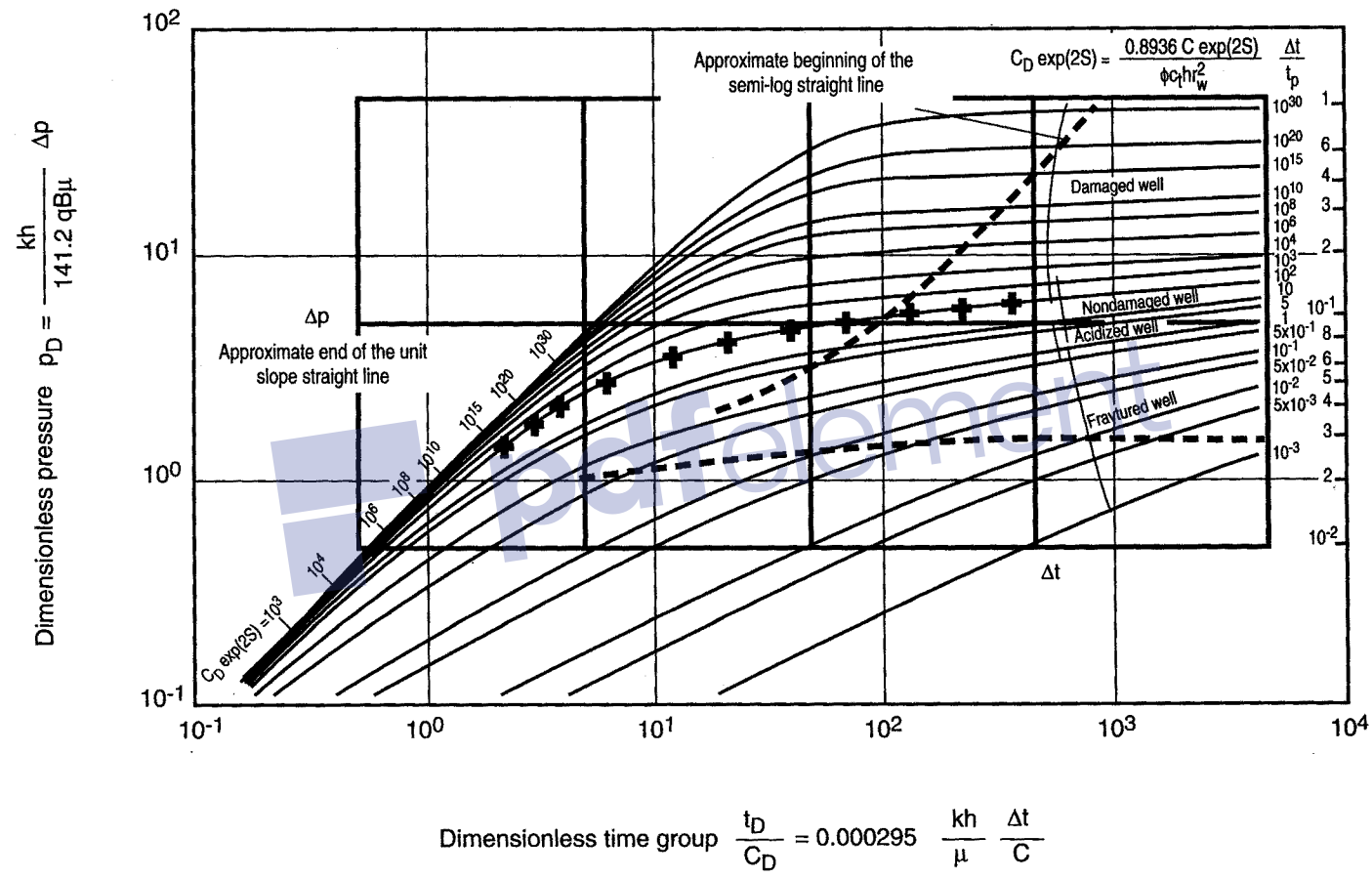


Fig. 5.2b

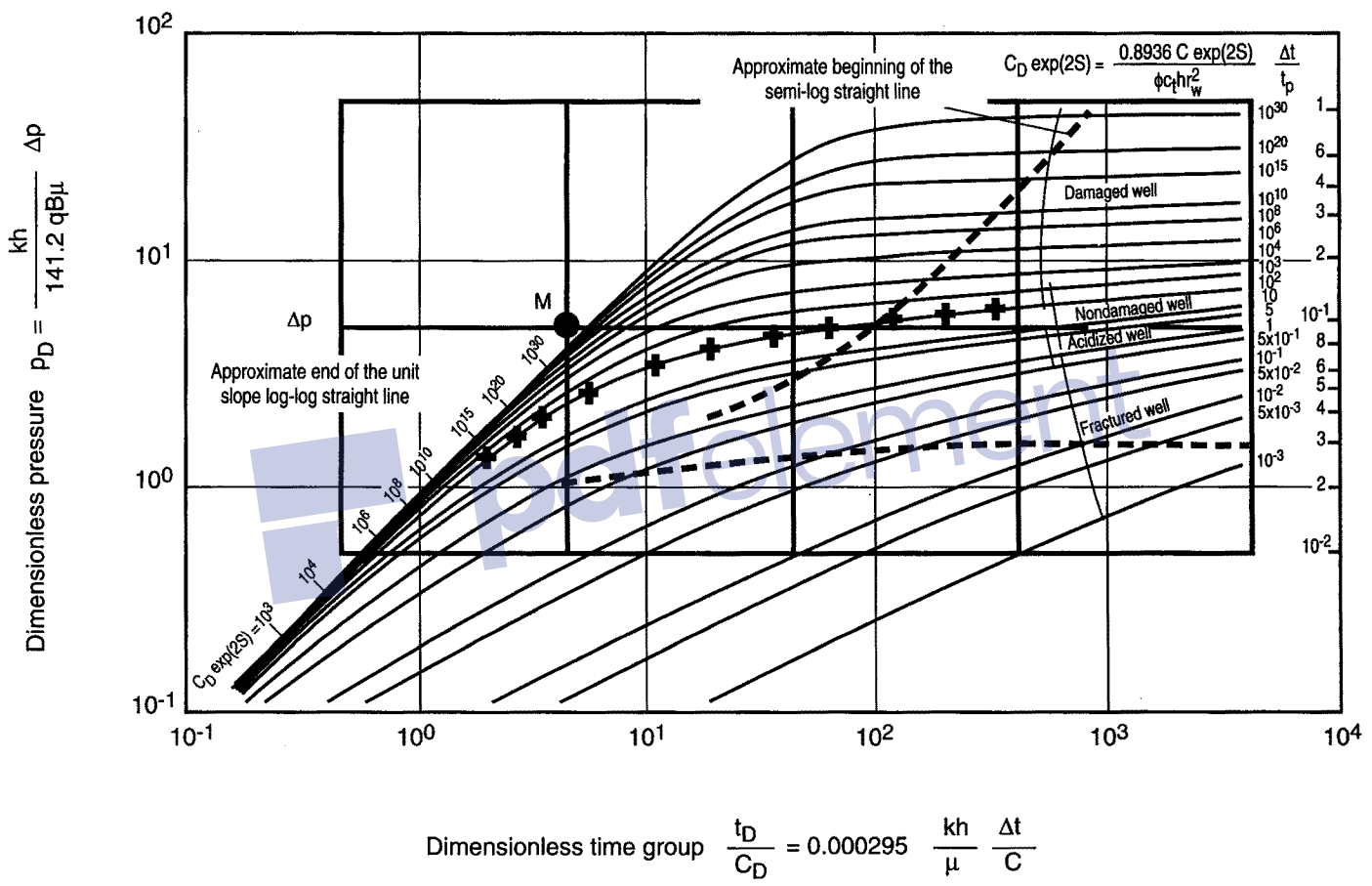


Fig. 5.2c

• **Interpretation :**

The ordinate of the match point is measured:

- in the type curve system of axes: p_D
- in the field data system of axes: Δp .

$$\text{As: } p_D = \frac{kh}{141.2 qB\mu} \Delta p \quad (\text{in practical US units})$$

The proportionality factor between p_D and Δp can be used to determine the reservoir's kh :

$$kh = 141.2 qB\mu \frac{(p_D)_M}{(\Delta p)_M} \quad (5.4)$$

In the same way the abscissa of the match point, M , is measured in the type curve system of axes, t_D/C_D and in the field data system of axes: Δt .

$$\text{As: } t_D/C_D = \frac{0.000295 kh}{\mu C} \Delta t \quad (\text{in practical US units}) \quad (5.5)$$

As kh is already determined.

The proportionality factor between t_D/C_D and Δt can be used to calculate C , the wellbore storage:

$$C = \frac{0.000295 kh}{\mu} \frac{(\Delta t)_M}{(t_D/C_D)_M} \quad (\text{in practical US units}) \quad (5.6)$$

The type curve where the data have been matched is characterized by $C_D \exp(2S)$.

C_D is then calculated:

$$C_D = \frac{0.89 C}{h\phi \cdot c_t r_w^2} \quad (\text{in practical US units}) \quad (5.7)$$

The value of $C_D \exp(2S)$ is used to determine the skin:

$$S = \frac{1}{2} \ln \frac{(C_D \exp(2S))}{C_D} \tag{5.8}$$

5.4 USING TYPE CURVES DURING BUILDUP

Type curves were established for constant flow rate production (drawdown). How can they be used to analyze pressure buildup?

• **Using the curves directly to analyze buildup:**

The curves can be used directly to analyze pressure buildup if:

$\Delta t \ll t_p$ after a constant flow rate;

$\Delta t \ll t_{p(n-1)}$ after a multirate history [Ref. 1, pp. 34-35];

$t_{p(n-1)}$ = duration of the last production period before shut-in.

These conditions are the same as for using the MDH method (see section 4.3).

If these conditions do not exist, using the type curves directly may lead to inaccurate results.

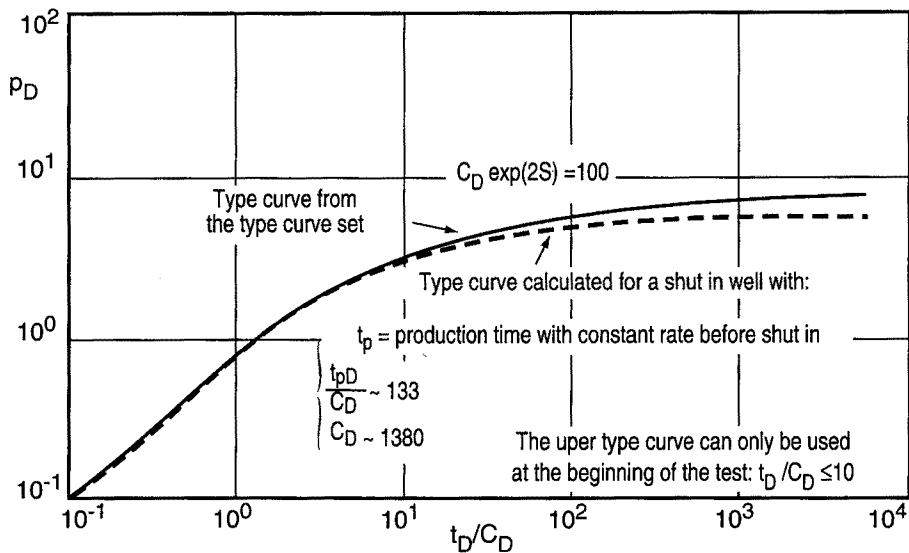


Fig. 5.3

The effect of short production time can be seen in a flattening out of the type curve, the buildup curve under the drawdown type curve (Fig. 5.3). Attempting to force a match between the buildup data points and a drawdown curve would result in a type curve located too high on the set of curves and therefore in inaccurate results.

• **Agarwal's equivalent time method:**

The most useful method of using drawdown type curves for buildup is Agarwal's method [Ref. 1, pp. 32-33 and Ref. 7, pp. 32-33].

It consists in plotting each measurement versus an equivalent time Δt_e as defined below instead of versus Δt :

$$\Delta t_e = \frac{\Delta t}{1 + \frac{\Delta t}{t_p}} \quad (5.9)$$

The equivalent time is very close to Δt for Δt values that are small compared to production time.

The equivalent time can be much smaller than Δt when Δt becomes large compared to t_p . The measured points are concentrated on a very limited portion of the type curve and matching loses reliability.

The buildup measured points plotted versus Δt_e are located on a drawdown curve and the flattening effect of buildup disappears (Fig. 5.4).

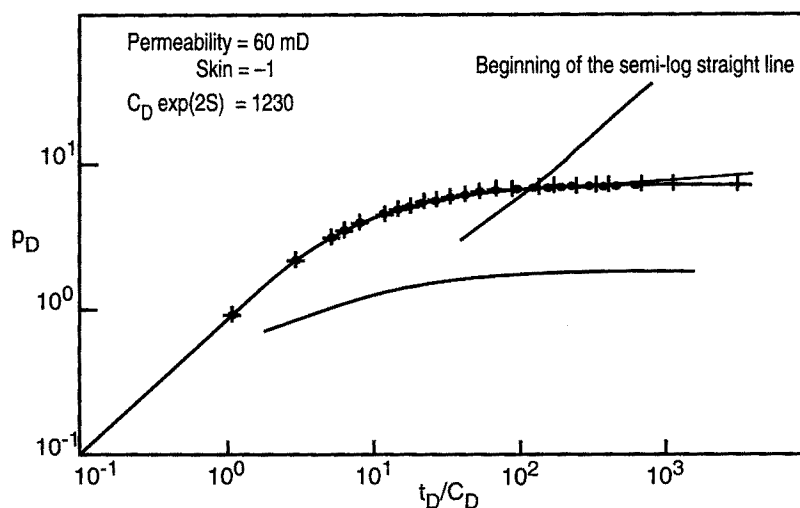


Fig. 5.4

F. Daviau indicates that Agarwal's method can be used for buildup provided that the semi-log straight line was reached during the previous drawdown period.

- **Advantages and limitations of type curves, well models:**

Type curves help the interpreter to:

- make a diagnosis about the type of reservoir and understand the flow regimes;
- use conventional methods by determining the sequence of flow regimes; in a homogeneous reservoir type curves can be used to locate the end of the wellbore storage effect and thereby situate the semi-log straight line correctly.

The type curve representation has two important limitations in an infinite homogeneous reservoir:

- the wellbore storage effect is represented by a constant value;
- a test needs to be interpreted with type curves established for drawdown.

The second limitation can be eliminated if the interpreter uses a well model instead of a set of type curves.

A well model is an analytic program used to generate type curves taking the flow rate history into account.

Additionally, the representation by a set of curves severely limits the number of parameters that can be taken into account.

It was possible to establish a set of type curves to interpret a test for an infinite homogeneous reservoir since only three parameters govern the pressure variations: wellbore storage, permeability and skin.

When the reservoir-well configuration is more complex, the number of parameters becomes too large for a type curve representation. A well model is the only way to generate appropriate type curves.

Type curves represented in sets or generated by a well model undergo the same flattening out effect due to the logarithmic representation.

The scale attenuates pressure variations. Because of this interpreting with type curves is often tricky. For a long time the problem discouraged interpreters who were used to the sensitivity of conventional methods.

The use of type curves combined with the pressure derivative has completely eliminated this difficulty.



Chapter 6

The derivative

The preceding chapter showed the advantages and drawbacks of type curves: advantages related to the fact that one single curve can deal with a whole test and drawbacks related to the log-log representation that makes it difficult to observe small relative pressure variations.

Methods using the pressure derivative take advantage of the advantages of the type curve representation and counteract the drawbacks of the logarithmic representation.

These methods are based on an observed fact: in a well test the pressure variation is more significant than the pressure itself. This is illustrated by the fact that it is the slope of the semi-log straight lines that is used to get information on the reservoir in conventional methods.

Different forms of derivatives were proposed in oil industry literature in the early eighties. Among them the most interesting is D. Bourdet's approach [Ref.9], which is the only one presented and used in this book.

6.1 REPRESENTATION

The pressure derivative as represented by D. Bourdet is calculated in relation to the **time function of radial flow in the transient regime**.

$$dp_D/d \ln (t_D/C_D) \quad \text{for a drawdown} \quad (6.1)$$

$$dp_D/d \ln \frac{tp + \Delta t}{\Delta t} \quad \text{for a buildup after a constant flow rate period} \quad (6.2)$$

$$dp_D/d \text{ (superposition function)} \quad \text{more generally, with a varying flow rate} \quad (6.3)$$

The derivative is represented on a log-log graph like a type curve.

6.2 PROPERTIES OF THE DERIVATIVE

• Radial flow:

In radial flow dimensionless pressure is expressed during drawdown by:

$$p_D = \frac{1}{2} (\ln t_D + 0.81 + 2S) \quad (6.4)$$

It can also be written as:

$$p_D = \frac{1}{2} \left(\ln \frac{t_D}{C_D} + 0.81 + \ln C_D \exp(2S) \right) \quad (6.5)$$

The pressure derivative is expressed as follows with the radial flow time function:

$$p_D' = \frac{dp_D}{d \ln \frac{t_D}{C_D}} = 0.5 \quad (6.6)$$

All type curves therefore have the 0.5 ordinate straight line as an asymptote during radial flow (Fig. 6.1).

• Wellbore storage effect:

When the wellbore storage effect prevails, dimensionless pressure is expressed by:

$$p_D = \frac{t_D}{C_D} \quad (6.7)$$

(see section 2.5).

The pressure derivative is expressed by:

$$p'_D = \frac{dp_D}{d \ln \frac{t_D}{C_D}} = \frac{t_D}{C_D} \frac{dp_D}{d \frac{t_D}{C_D}} \quad (6.8)$$

$$p'_D = \frac{t_D}{C_D} \quad (6.9)$$

Therefore, the derivative like the pressure has as an asymptote the unit slope straight line that passes through the origin of the coordinates on a log-log graph (Fig. 6.1)

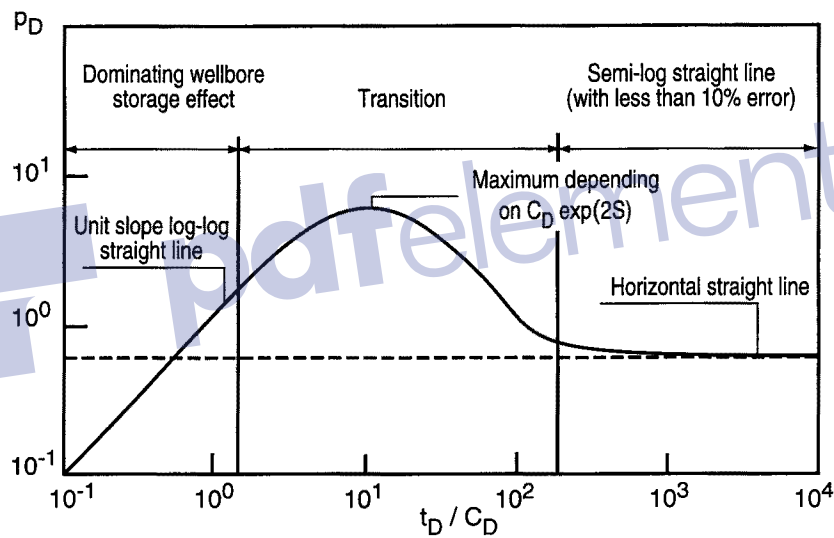


Fig. 6.1

6.3 THE DERIVATIVE AS DIAGNOSTIC TOOL

- Flows with a power function equation:

Generally speaking, whenever a flow presents pressure variations of the type:

$$p_D = a \left(\frac{t_D}{C_D} \right)^n + b \quad (6.10)$$

the derivative of the pressure during the flow is equal to:

$$p_D' = a n \left(\frac{t_D}{C_D} \right)^n \quad (6.11)$$

in other words the derivative appears on a log-log graph as a straight line with a slope of n .

- **Flows with a logarithmic function equation:**

Likewise, whenever a flow presents pressure variations of the type:

$$p_D = a \ln \left(\frac{t_D}{C_D} \right) + b \quad (6.12)$$

the derivative of the pressure during the flow is equal to:

$$p_D' = a \quad (6.13)$$

in other words the derivative appears on a log-log graph as a horizontal straight line with an ordinate of a .

- **Diagnosis:**

Most flows that can be seen during a well test have pressure variations that are either linear versus the logarithm of time or linear versus a power of time.

The characteristic shape of the derivative in both cases makes it an excellent diagnostic tool:

- all flows can be seen on the same graph;
- each flow corresponds to a horizontal straight line or a straight line with a slope of n .

The fact that the pressure drop is represented by the derivative attenuates the flattening out effect of the log-log representation. Interpretation sensitivity is similar to that of conventional interpretation.

6.4 ANALYSIS WITH TYPE CURVES

D. Bourdet's type curves with a derivative for homogeneous reservoirs are shown in Figure 6.2.

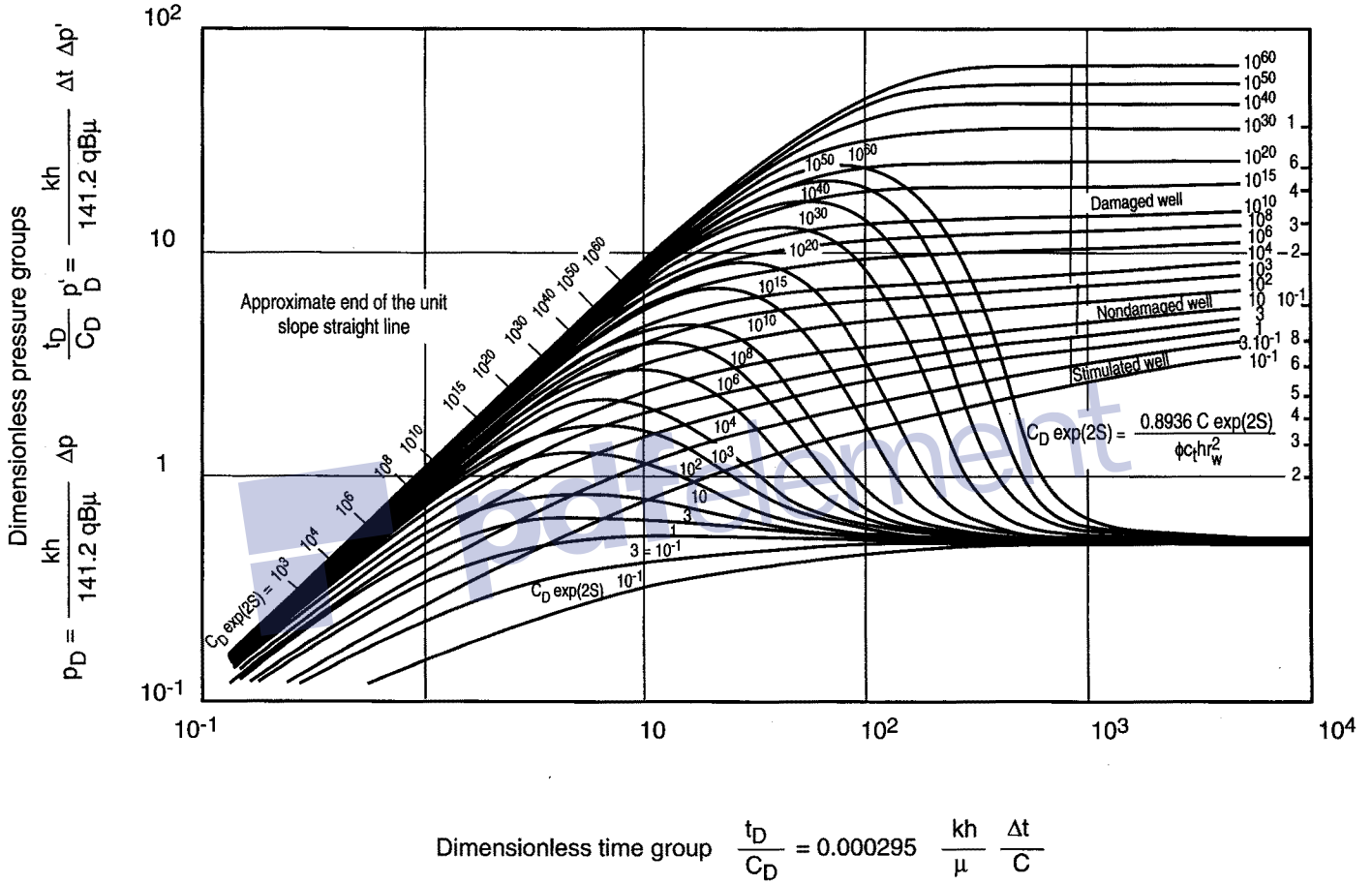


Fig. 6.2 Type curves for a well with wellbore storage and skin (infinite acting homogeneous reservoir)

His set of curves is similar to Gringarten's (Fig. 5.1), with the addition of the derivative of each curve.

As indicated in section 6.3, derivative type curves have the following remarkable properties:

- They have the slope 1 straight line passing through the origin of the coordinates as an asymptote as long as the wellbore storage effect is dominant.
- They have the 0.5 ordinate straight line as an asymptote when the wellbore storage effect is over.
- The curves corresponding to values of $C_D \exp(2S)$ greater than 1 exhibit a maximum. The ones corresponding to values less than or equal to 1 increase continually.

• **Analysis method:**

The analysis method is similar to the procedure without the derivative.

- 1 Plot the measured field data points and their derivative simultaneously on tracing paper using the scale provided by the type curves (Fig. 6.3a).
- 2 Look for a type curve to match the field data with.
- 3 Note the $(C_D \exp(2S))$ value of the type curve matching the data best.
- 4 Pick a match point in both the type curve coordinate system and the data system.
- 5 Analyze.

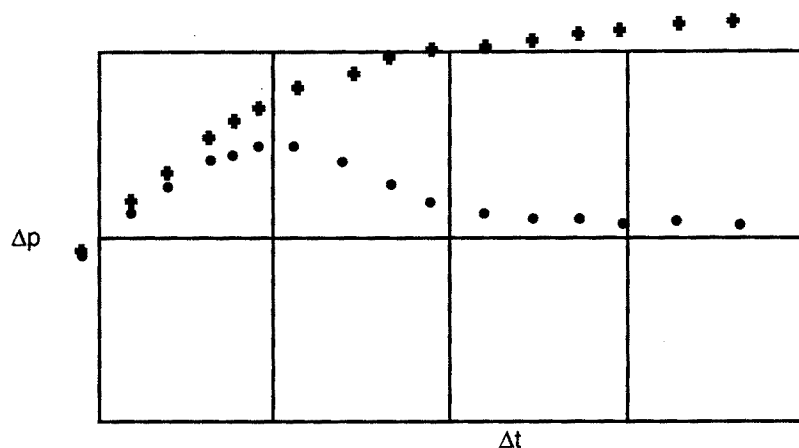


Fig. 6.3a Interpretation with the derivative

The major advantage of the derivative is the considerable help it gives in the matching step. The interpreter does it in two stages:

- The points of the derivative of radial flow measurements correspond to a horizontal straight line. The points are matched on the 0.5 ordinate horizontal straight line on the set of curves. This greatly simplifies vertical matching (Fig. 6.3b).
- The points of the derivative of wellbore storage effect measurements are located on a slope 1 straight line. They are matched on the slope 1 straight line passing through the origin of the coordinates on the set of type curves (Fig. 6.3c).

Once these two operations have been performed the measured points and their derivative are matched simultaneously on a type curve and its derivative. The only remaining step is to read the value of $C_D \exp(2S)$.

• **Beginning of the semi-log straight line:**

The beginning of the semi-log straight line is determined with the derivative by considering a deviation with respect to the semi-log straight line:

- The semi-log straight line is reached **theoretically** when the derivative is stabilized. It is then equal to 0.5 in dimensionless parameters.
- The semi-log straight line is considered as having been reached in practice when the deviation of the derivative in relation to stabilization is less than 10%, i.e. in dimensionless parameters when the derivative on the set of type curves is less than 0.55 for values of $C_D \exp(2S)$ greater than 1 and when it is greater than 0.45 for values of $C_D \exp(2S)$ that are lower than or equal to 1.

This is the criterion used to indicate the start of the semi-log straight line on the sets of type curves without derivatives.

The start of the semi-log straight line does not appear on the type curves with derivatives since the interpreter can judge by using the derivative how far the data are from the semi-log straight line.

Nota bene:

The use of sets of type curves with derivatives assumes that the interpreter has pressure measurements and their derivative.

It is difficult to calculate the derivative simply by hand for two reasons:

- The flow rate history has even more impact on the derivative than on the type curve itself. The derivative should therefore be calculated using the flow rate superposition function to be correct.

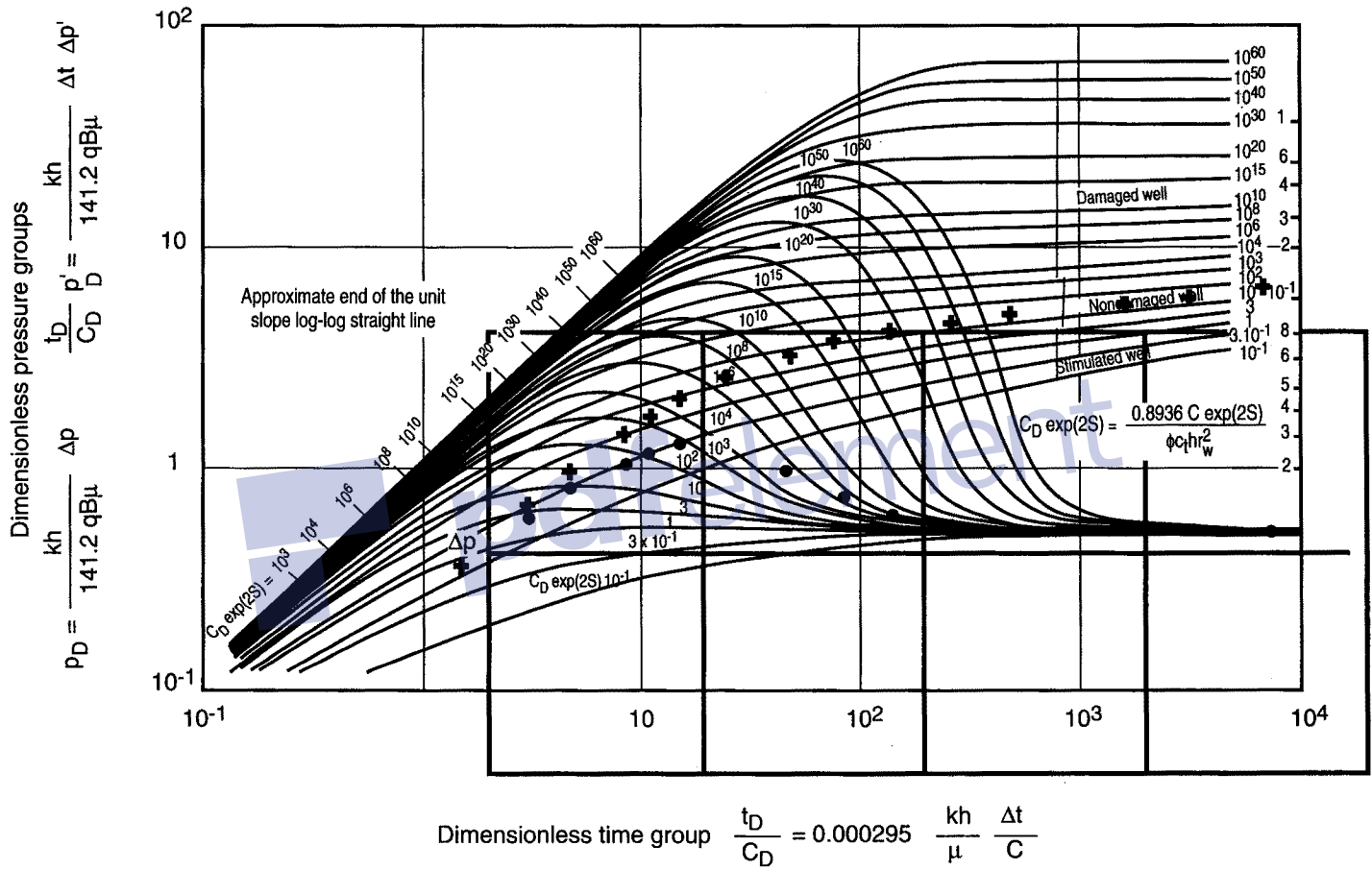


Fig. 6.3b Vertical matching
 Type curves for a well with wellbore storage and skin (infinite acting homogeneous reservoir)

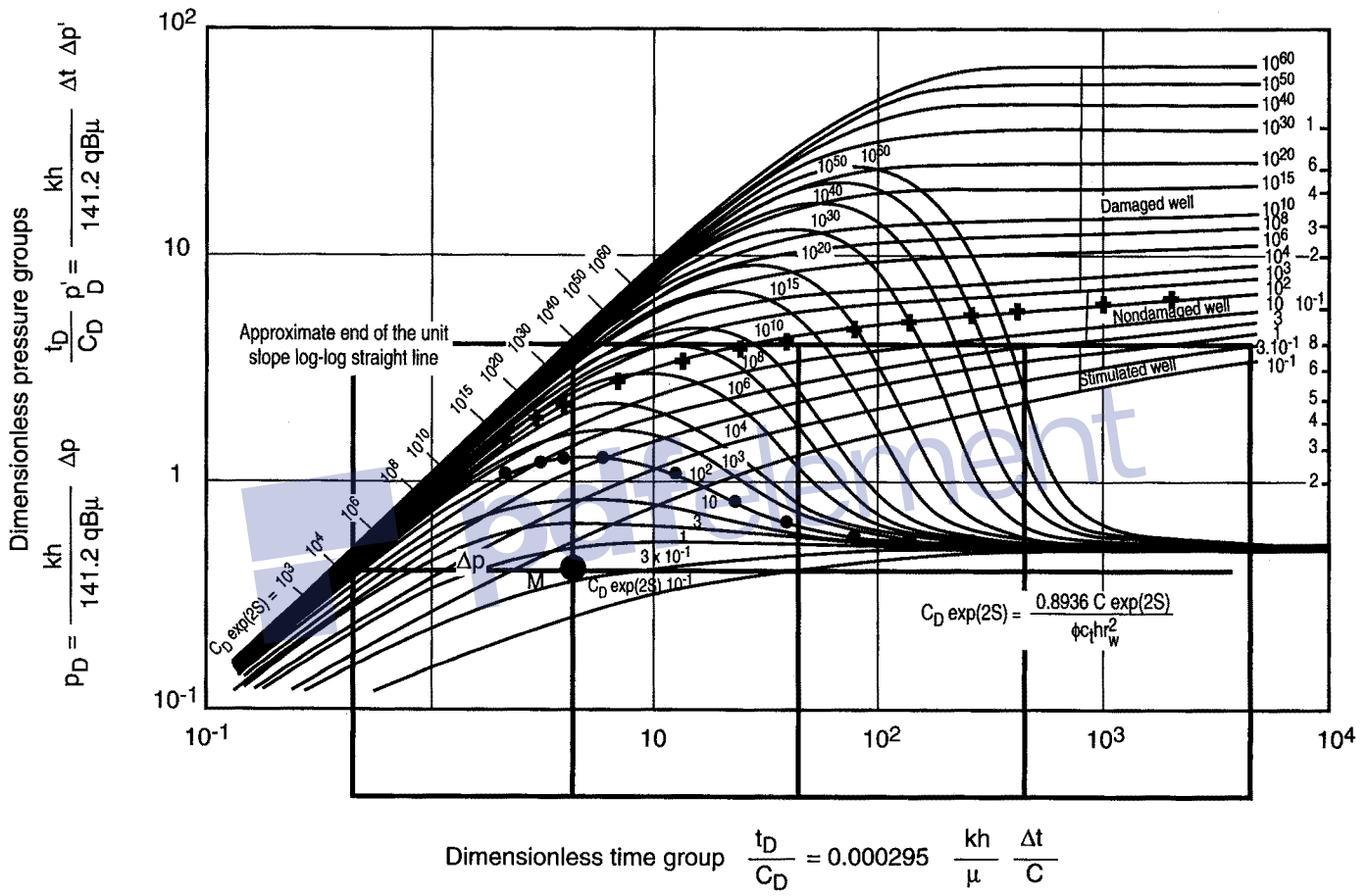


Fig. 6.3c Vertical + horizontal matching
 Type curves for a well with well storage and skin (infinite homogeneous reservoir behavior)

- The derivative measures the pressure variations produced by the varying flow rates. Unfortunately it also measures the noise caused by measuring the pressure signal. This is why the derivative is usually calculated with a smoothing algorithm, which should attenuate the noise of the pressure signal while preserving the main trends due to the different flows.

6.5 DIRECT INTERPRETATION BY MEANS OF THE DERIVATIVE

Reservoir permeability, wellbore storage and skin can be determined directly using the type curve and its derivative provided that the stabilization of the derivative has been reached.

- **Reservoir kh:**

Permeability is calculated based on the value $\Delta p'_{st}$ (Fig. 6.4) corresponding to the stabilization of the derivative.

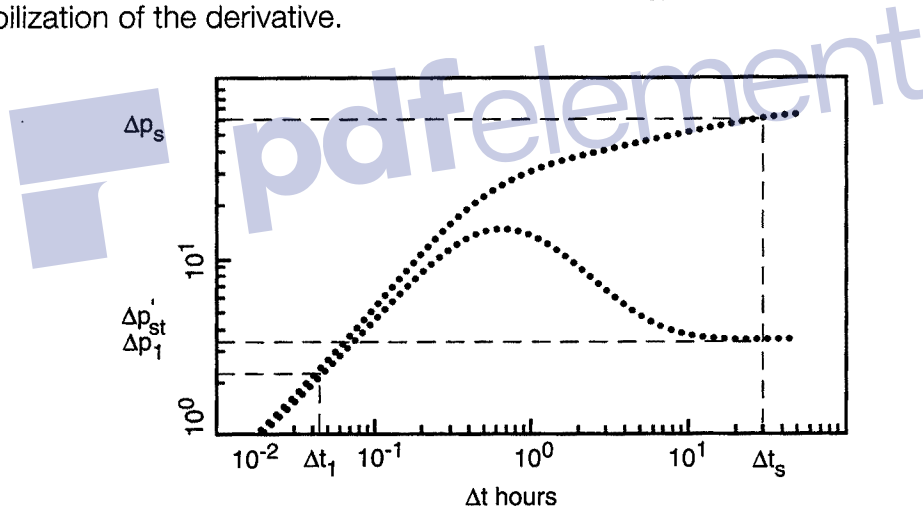


Fig. 6.4

The value of this derivative expressed in dimensionless terms is known, it is equal to 0.5.

The expression of $\Delta p'_{st}$ in relation to 0.5 is equal to:

$$\Delta p'_{st} = \frac{141.2 qB\mu}{kh} \times 0.5 \quad (\text{in practical US units}) \quad (6.14)$$

It is used to calculate the reservoir's kh:

$$kh = 141.2 qB\mu \times \frac{0.5}{\Delta p'_{st}} \quad (\text{in practical US units}) \quad (6.15)$$

- **Wellbore storage:**

Wellbore storage can be calculated if the coordinates of a point located on the slope 1 straight line are known: Δp_1 and Δt_1 (Fig. 6.4).

During dominating wellbore storage effect:

$$\Delta p_1 = \frac{qB}{24C} \Delta t_1 \quad (6.16)$$

hence:

$$C = \frac{qB}{24} \frac{\Delta t_1}{\Delta p_1} \quad (6.17)$$

- **Skin:**

The skin can be calculated if the coordinates of a point located on the semi-log straight line are known: Δp_s , Δt_s (Fig. 6.4).

Le skin est calculé à partir de l'expression conventionnelle donnée par la loi semi-log. Pour une remontée de pression suivant une période à débit constant :

$$S = 1.151 \left(\frac{\Delta p_s}{2.303 \Delta p'_{st}} - \log \frac{\Delta t_s}{1 + \frac{\Delta t_s}{t_p}} - \log \frac{k}{\phi \mu c_r^2 + 3.23} \right) \quad (6.18)$$

In the case of a varying flow rate, a superposition function must be used to calculate it.

6.6 CONCLUSION

Like type curves, the derivative offers the great advantage of allowing a complete well test to be taken into account and interpreted using one single curve.

Chapter 6 • THE DERIVATIVE

Each type of flow exhibits a characteristic facies on the derivative which represents an excellent **diagnostic** tool. By materializing pressure variations the derivative is similar to a **zoom** onto the data, amplifying variations that would otherwise not be noticed flattened out by the logarithmic representation.

The following chapters illustrate the contribution of the derivative in more complex reservoir-well configurations.

Smoothing algorithms are required to overcome the main limitation on its use due to the noise of the signal.

The derivative is practically impossible to calculate by hand: a computer is necessary. It has become one of the major tools in well test analysis software.



Reservoir boundaries



Introduction

At the beginning of a well test the compressible zone generated by the flow rate variation moves away from the wellbore without reaching any boundaries. The reservoir behaves as if it were infinite.

When a boundary is reached it is perceived a characteristic change in the pressure at the well.

The following chapters indicate the different pressure shapes and the interpretation methods that can be used when some characteristic boundaries are perceived during a well test:

- linear sealing fault;
- channel;
- intersecting linear boundaries;
- constant pressure boundary;
- closed reservoir.

For each of these cases, we will examine the characteristic flow corresponding to the effect the boundary, its conventional analysis and the effect the flow on the derivative and the type curves.



Chapter 7

Linear sealing faults

7.1 DESCRIPTION

The boundary condition corresponding to a linear fault is the linear no-flow boundary.

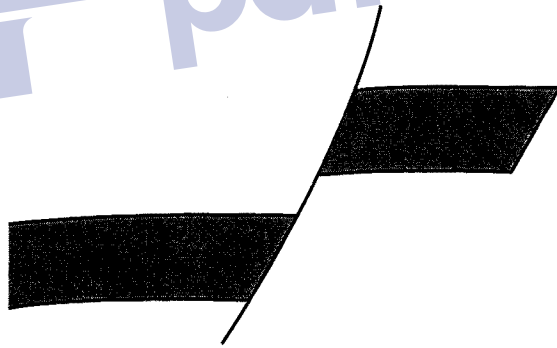


Fig. 7.1

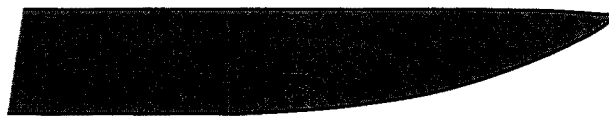


Fig. 7.2

Several field cases produce this boundary condition: the linear sealing fault of course (Fig. 7.1), but also disappearing facies (Fig. 7.2) and a number of unconformities (Fig. 7.3).



Fig. 7.3

7.2 THE METHOD OF IMAGES

A no-flow line at a distance, d , from the well is obtained analytically with the method of images by superposing:

- the pressure drop at the well in an infinite acting reservoir;
- the pressure drop due to an identical well with the same flow rate history located at a distance, $2d$, from the well and symmetric to the boundary (Fig. 7.4).

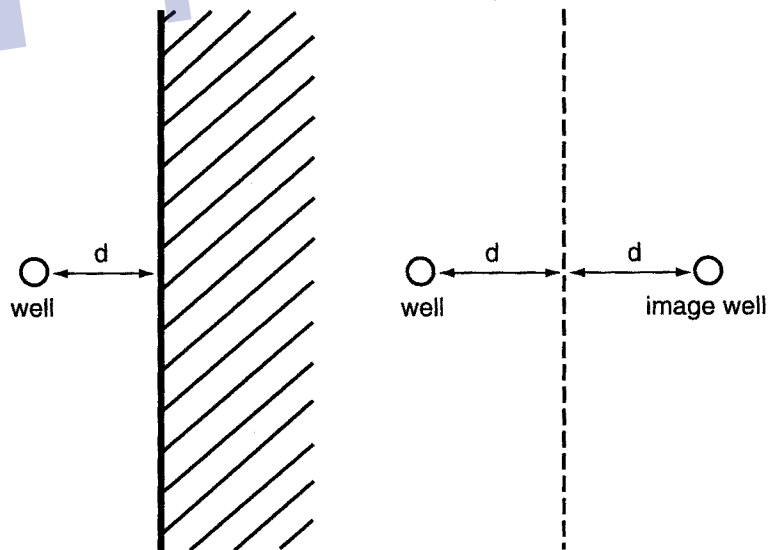


Fig. 7.4 Representation of a no-flow boundary by the method of images

In the presence of a no-flow boundary, the pressure at the well is expressed by:

$$p_D = p_D(t_D, r_D = 1, S) + p_D(t_D, 2r_D, 0) \quad (7.1)$$

\uparrow
 pressure drop
at the well

\uparrow
 pressure drop
due to the image well

where $r_D = \frac{d}{r_w}$ is the distance from the linear sealing fault to the well in dimensionless variables.

7.3 CONVENTIONAL INTERPRETATION METHOD

Assuming that the wellbore storage effect ends soon enough, the pressure drop at the well is written:

$$p_D = \frac{1}{2} \left[\underbrace{\ln t_D + 0.81 + 2S}_{\text{well}} - \text{Ei} \left(-\frac{(2r_D)^2}{4t_D} \right) \right] \quad (7.2)$$

$\underbrace{\ln t_D + 0.81 + 2S}_{\text{well}}$

$\text{Ei} \left(-\frac{(2r_D)^2}{4t_D} \right)$
 image well

- **Short times:**

Until the compressible zone has reached the fault, $\frac{(2r_D)^2}{4t_D}$ is large and the Ei term is almost equal to zero.

The pressure drop is the same as that of a well in an infinite reservoir. Once the wellbore storage effect has ended, the pressure drop can be expressed using the semi-log straight line:

$$p_D = \frac{1}{2} (\ln t_D + 0.81 + 2S) \quad (7.3)$$

- **Long times:**

When the compressible zone reaches the fault, the term corresponding to the image well is no longer negligible.

Once the fault has been reached, the pressure drops faster than in an infinite reservoir and the measurement points depart from the m-slope semi-log straight line.

When t is long enough, in practice as soon as $\frac{2r_D^2}{4t_D}$ is less than 1%, the Ei term corresponding to the image well can be calculated by its logarithmic approximation:

$$-Ei\left(-\frac{(2r_D)^2}{4t_D}\right) = \ln \frac{t_D}{(2r_D)^2} + 0.81 \quad (7.4)$$

The pressure drop at the well can then be written:

$$p_D = (\ln t_D + 0.81 + S - \ln (2r_D)) \quad (7.5)$$

If the test is long enough, the fault appears as a straight line with a slope double that of the initial one.

This property can be seen both in drawdown and in buildup (Fig. 7.5).

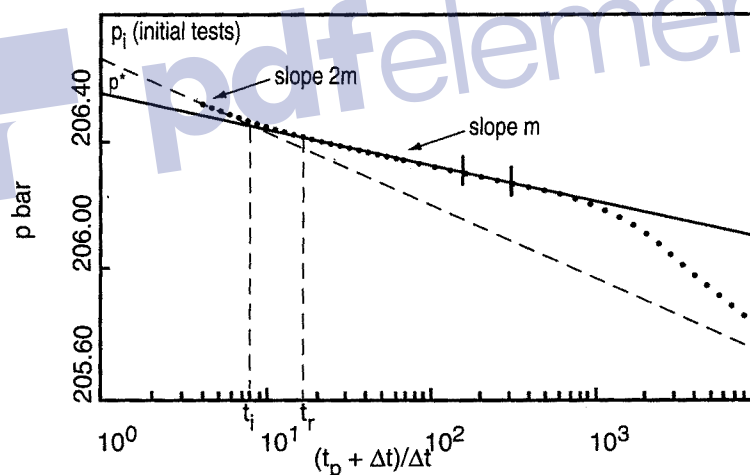


Fig. 7.5

• **Distance from the linear sealing fault:**

Two methods are habitually used to determine how far away the fault is:

- The first uses the intersection point of the two semi-log straight lines.
- The second uses the investigation range of the test at the time when the compressible zone reaches the fault.

- **Intersection of the semi-log straight lines:**

Let t_i be the time when the straight lines with a slope of m and $2m$ intersect. The distance, d , from the well to the fault is determined based on equations (7.3) and (7.5):

$$r_D = \frac{1}{2} \sqrt{\exp(0.81)} \sqrt{t_{Di}} \quad (7.6)$$

from which d is deduced:

$$d = \alpha \sqrt{\frac{kt_i}{\phi\mu c_t}}$$

- $\alpha = 0.75$ (in SI units)
- $\alpha = 0.012$ (in practical US units)
- $\alpha = 0.014$ (in practical metric units).

For this method to be applicable, the double slope straight line must be reached. This is seldom the case.

- **Radius of investigation:**

The distance from the well to the fault can be determined by considering the radius of investigation of the test at the time when the measurement points leave the first semi-log straight line.

Let t_r be this time (Fig. 7.5). The distance from the fault is equal to:

$$d = \alpha \sqrt{\frac{kt_r}{\phi\mu c_t}}$$

- $\alpha = 2$ (in SI units)
- $\alpha = 0.032$ (in practical US units)
- $\alpha = 0.038$ (in practical metric units).

The advantage of this method is that it can help determine the distance from the well of any event perceived during a well test.

It has two major drawbacks:

- It is not very accurate: it is hard to determine exactly when the measurement points depart from the semi-log straight line on a semi-log graph.

- It can not be used to characterize the event: a double slope straight line usually suggests the presence of a fault with some degree of certainty. The fact that points leave the semi-log straight line does not allow the type of event to be determined.

- **Extrapolated pressure, initial pressure:**

In buildup, whatever the flow rate history, the first semi-log straight line can be extrapolated to infinite time (i.e. $(t_p + \Delta t)/\Delta t = 1$ on a Horner plot) to determine the extrapolated pressure p^* . It is used in the MBH method (see Chapter 11) to calculate the average reservoir pressure.

During initial tests, the second semi-log straight line (with a slope of $2m$) is extrapolated to determine the initial reservoir pressure, p_i , when only one no-flow boundary has been perceived by the test (Fig. 7.5).

7.4 TYPE CURVES: THE DERIVATIVE

The presence of a fault is characterized by the fact that the slope of the semi-log straight line doubles.

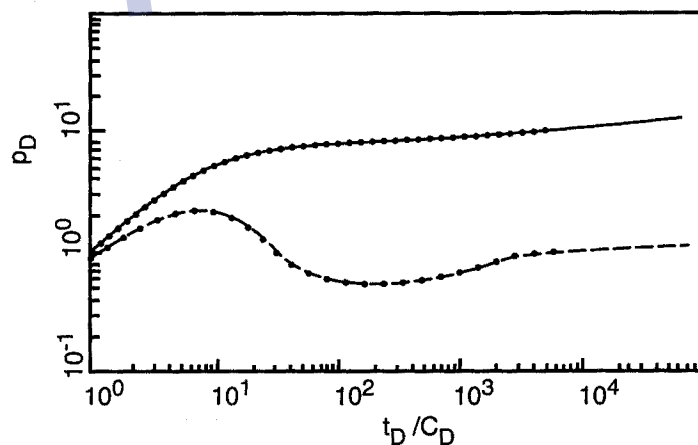


Fig. 7.6

The semi-log straight line is characterized on the log-log plot p_D versus t_D/C_D by a stabilization of the derivative at 0.5, that represents the value of the slope of the semi-log straight line in dimensionless terms (equation (7.4)).

The doubling of the slope characteristic of the fault is characterized on the derivative by a doubling of the level of the derivative. It goes from 0.5 to 1 (Fig. 7.6) on a dimensionless graph.

The time when the derivative leaves the first stabilization can be used to determine the radius of investigation of the test corresponding to the time when the compressible zone reaches the fault. Determination in this way is more accurate than the result obtained by the conventional method.





Chapter 8

Channels

8.1 DESCRIPTION OF FLOWS

The boundary condition dealt with under the term "channels" corresponds to two infinite parallel no-flow linear boundaries (Fig. 8.1).

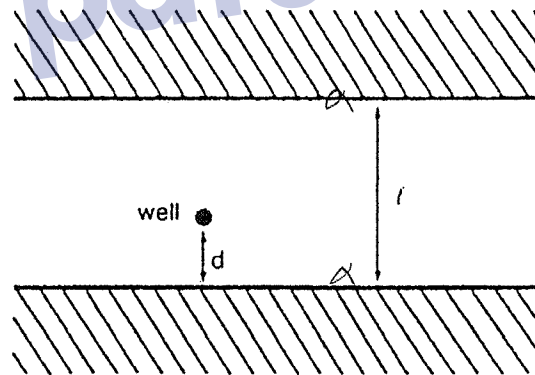


Fig. 8.1

"Channels" should be understood in terms of fluid mechanics. It does not necessarily correspond to the geological acceptance.

The dynamic channel can be due to a number of causes such as:

- two parallel sealing faults;
- a sedimentary deposit channel;
- two parallel lateral variations in facies.

The channel is defined by its width, l , and by the distance, d , from the well to one of its edges.

During a well test inside a channel, several flows follow one another:

- Radial flow until a no-flow boundary has been reached. The flow exhibits the usual infinite reservoir behavior: a semi-log straight line and stabilization of the derivative at 0.5 if the wellbore storage effect ended soon enough.
- First edge of the channel: fault effect. When the compressible zone reaches the nearer channel edge, the boundary has exactly the same effect as a sealing fault in an infinite reservoir: the slope of the semi-log straight line doubles, with the derivative going from a stabilization at 0.5 to a stabilization at 1.

This is observed only if the well is very much off center in the channel, otherwise the two edges are reached at the same time and no fault effect is observed.

- The channel. When the compressible zone reaches the two edges of the channel it expands linearly parallel to the edges of the channel.

The following sections present the properties of linear flow, the corresponding conventional analysis method and the variations in the pressure derivative during the flow.

8.2 LINEAR FLOW

The time function characteristic of radial flow is the logarithm function (Chapter 4). During radial flow the pressure varies as a time logarithmic superposition function, with superposition depending on the flow rate history.

Likewise, the characteristic function of linear flow is the square root of time. During linear flow the pressure varies as a superposition of square root of time functions, with superposition depending on the flow rate history.

The function that governs the pressure variations during linear flow when the well is put in production at a constant flow rate is described below.

- **In dimensionless terms:**

$$p_D(t_D) = \sqrt{4\pi t_D} + \sigma + S \quad (8.1)$$

where t_{Dl} is the dimensionless time calculated by taking the width, l , of the channel as a reference length [Ref. 10]:

$$t_{Dl} = \frac{\alpha kt}{\phi \mu c_t l^2} \quad (8.2)$$

$$\begin{aligned} \alpha &= 1 && \text{(in SI units)} \\ \alpha &= 0.000264 && \text{(in practical US units)} \\ \alpha &= 0.000355 && \text{(in practical metric units).} \end{aligned}$$

σ characterizes the eccentricity of the well in the channel:

$$\sigma = \ln \frac{l}{2\pi r_w} - \ln (\sin \pi e) \quad (8.3)$$

e is the eccentricity of the well:

$$e = \frac{d}{l} \quad (8.4)$$

• In practical units:

$$p_i - p_{wf}(t) = m_l \sqrt{t} + \frac{m}{1.151} (\sigma + S) \quad (8.5)$$

$$m_l = \frac{\alpha q B}{h l} \sqrt{\frac{\mu}{k \phi c_t}} \quad (8.6)$$

$$\begin{aligned} \alpha &= 0.56 && \text{(in SI units)} \\ \alpha &= 8.13 && \text{(in practical US units)} \\ \alpha &= 1.25 && \text{(in practical metric units).} \end{aligned}$$

m is the slope of the semi-log straight line.

8.3 CONVENTIONAL INTERPRETATION

Linear flow is used to determine the width of the channel and the eccentricity of the well.

Determination is based on the straight line obtained by plotting the pressure drop versus the square root of time (Fig. 8.2).

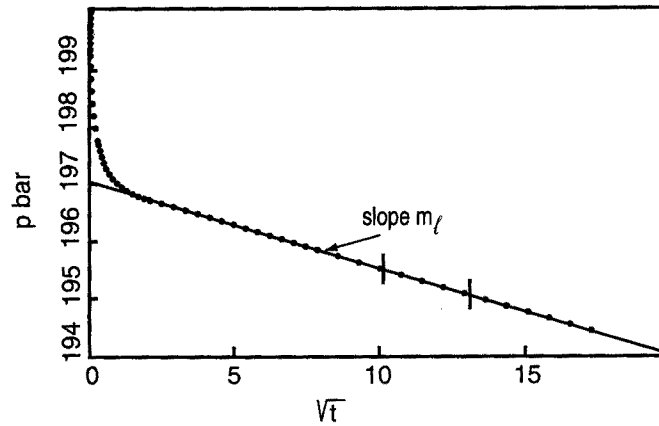


Fig. 8.2

The slope, m_l , of the straight line determines the width of the channel:

$$\ell = \frac{\alpha qB}{hm_l} \sqrt{\frac{\mu}{k\phi c_t}} \quad (8.7)$$

$\alpha = 0.56$ (in SI units)
 $\alpha = 8.13$ (in practical US units)
 $\alpha = 1.25$ (in practical metric units).

The ordinate, p_0 , of the straight line at the time origin determines the eccentricity, e , of the well:

$$\sigma = 1.151 \frac{p_i - p_0}{m} - S$$

with m the slope of the semi-log straight line:

$$e = \frac{1}{\pi} \text{Arcsin} \left(\frac{\ell}{2\pi r_w} \exp(-\sigma) \right) \quad (8.8)$$

8.4 BOUNDED CHANNELS

During a test the compressible zone may sometimes reach one end of the channel located at a distance, a , from the well (Fig. 8.3).

This case is dealt with analytically by the method of images in the same way as the case of a no-flow boundary in an infinite reservoir.

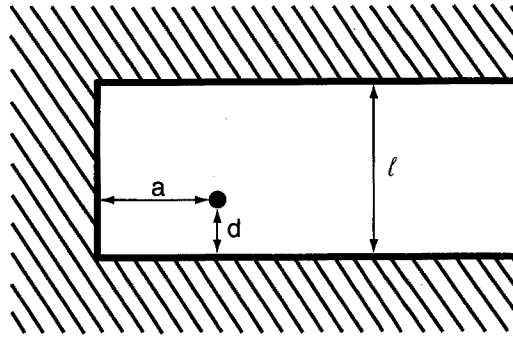


Fig. 8.3

The effect produced by the boundary is similar to that of a fault in an infinite reservoir, i.e. a doubling of the slope of the “semi-square root” straight line which is characteristic of linear flow (Fig. 8.4).

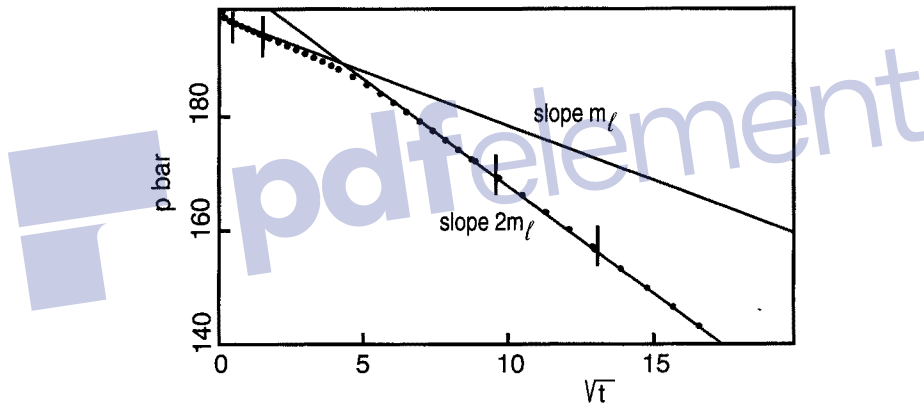


Fig. 8.4

The equation of the double-slope straight line is as follows in dimensionless terms:

$$p_D(t_D) = 2 \sqrt{4\pi t_{Dl}} + \sigma + \sigma' + S \quad (8.9)$$

with:

$$\sigma' = -2\pi r_{Dl} - \ln [1 - \exp(-2\pi r_{Dl})] - \frac{1}{2} \ln [1 - 2 \exp(-2\pi r_{Dl}) \cos(2\pi e) + \exp(-4\pi r_{Dl})] \quad (8.10)$$

where:

$$r_{Dl} = \frac{a}{l} \quad (8.11)$$

• **Distance to the boundary:**

The distance to the boundary can be obtained by using the intersection of the two straight lines with a slope of m_l and $2m_l$.

Let t_x be the time corresponding to the intersection of the two straight lines and let t_{Dxl} be its dimensionless expression:

$$\begin{aligned} \sqrt{2\pi t_{Dxl}} = 2\pi r_{Dl} + \ln(1 - \exp(-2\pi r_{Dl})) \\ - \frac{1}{2} \ln(1 - 2 \exp(-2\pi r_{Dl}) \cos(2\pi\epsilon) + \exp(-4\pi r_{Dl})) \end{aligned} \quad (8.12)$$

This equation implicit in r_{Dl} is not simple to solve except when the boundary is at a great distance compared to the width of the channel. In this case the last two right-hand terms of equation (8.12) are small compared to the first term and:

$$2\pi t_{Dxl} = 2\pi r_{Dl}$$

hence the distance to the end of the channel:

$$d = \alpha \sqrt{\frac{kt_x}{\phi\mu c_t}} \quad (\text{in SI units}) \quad (8.13)$$

$$\begin{aligned} \alpha &= \sqrt{2\pi} && (\text{in SI units}) \\ \alpha &= 0.040 && (\text{in practical US units}) \\ \alpha &= 0.048 && (\text{in practical metric units}). \end{aligned}$$

When the well is not far enough away from the end of the channel, the first “semi-square root” straight line may not be visible, making interpretation difficult.

The double-slope straight line may be mistaken for the first m -slope straight line. This leads to underestimation of the width of the channel and failure to take the boundary in the channel into account. The pressure derivative analysis or checking the interpretation with geological and seismic data is the only way to solve the indetermination.

8.5 PRESSURE BUILDUP WITH VARYING FLOW RATES

A buildup, or more generally speaking a test with varying flow rates is dealt with using a superposition function (see section 1.9), similar to the one developed for radial flow.

- **Buildup following constant flow rate:**

During buildup following a constant flow rate period with a duration of t_p , the superposition function is written:

$$p_i - p_{ws}(\Delta t) = m_l (\sqrt{t_p + \Delta t} - \sqrt{\Delta t}) \quad (8.14)$$

Taking as a reference the pressure $p_{wf}(t_p)$ at shut-in time:

$$p_{ws}(\Delta t) - p_{wf}(t_p) = m_l (\sqrt{t_p + \Delta t} + \sqrt{\Delta t} - \sqrt{t_p + \Delta t}) + \frac{m}{1.151} (\sigma + S) \quad (8.15)$$

The variations in $p_{ws}(\Delta t)$ versus $\sqrt{t_p + \Delta t} - \sqrt{\Delta t}$ (fig. 8.5) correspond to a straight line with a slope m_l with an ordinate p_0 at $\Delta t = 0$ (i.e. $\sqrt{t_p + \Delta t} - \sqrt{\Delta t} = \sqrt{t_p}$).

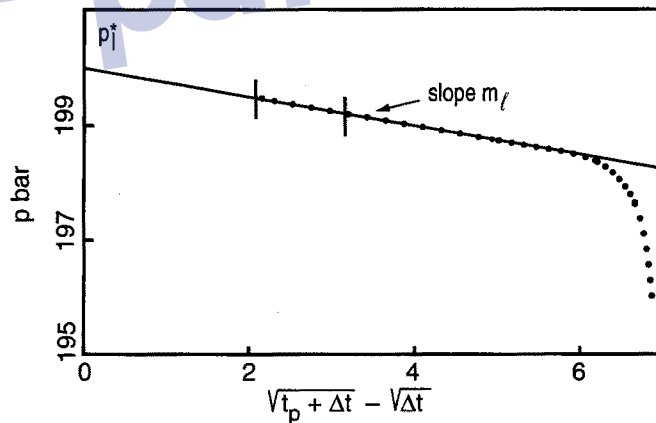


Fig. 8.5

The slope, m_l , of the straight line is used to determine the width of the channel:

$$l = \frac{\alpha q B}{k m_l} \sqrt{\frac{\mu}{k \phi c_t}} \quad (8.16)$$

- $\alpha = 0.56$ (in SI units)
- $\alpha = 8.13$ (in practical US units)
- $\alpha = 1.25$ (in practical metric units).

The value of the extrapolated pressure at the origin p_0 is used to calculate σ and to determine the eccentricity of the well:

$$e = \frac{1.151}{m} [p_0 - p_{wf}(t_p)] - S \quad (8.17)$$

$$e = \frac{1}{\pi} \text{Arcsin} \left(\frac{l}{2\pi r_w} \exp(-\sigma) \right)$$

- **Initial pressure, average pressure:**

The value of the pressure extrapolated at infinite buildup time, $\sqrt{t + \Delta t} - \sqrt{\Delta t} = 0$ is used to determine an extrapolated pressure p^* . This pressure is equal to the initial reservoir pressure in initial tests (negligible production compared to the amount of oil in place).

The average pressure calculated by the MBH method (see Chapter 11) must, however, use the pressure p^* extrapolated on the first semi-log straight line.

8.6 PRESSURE DERIVATIVE, TYPE CURVES

- **Characterizing the channel:**

The flow characteristic of a channel is linear flow. During linear flow the pressure varies linearly versus the square root of time or a square root of time superposition function.

When the pressure varies as a power, n , of time, the derivative has the form of a straight line with a slope n on a log-log graph (Chapter 6).

A channel is therefore characterized by a straight line with a slope $1/2$ on the pressure derivative.

• Infinite channel:

When a test is performed in a channel, the following flows can be diagnosed on the pressure derivative plotted on a dimensionless graph (Fig. 8.6):

- Wellbore storage effect: straight line with a slope 1.
- Radial effect: stabilization at 0.5. This flow can be masked by the wellbore storage effect.
- Effect of the first edge of the channel: stabilization at 1. The first edge of the channel behaves like a sealing fault. This effect is visible only if the well is off-centered enough in the channel ($d/l < 0.2$). Otherwise the characteristic flow of the channel is perceived first.
- Linear flow in the channel: straight line with a slope of 0.5. This is the flow characteristic of the presence of a channel.

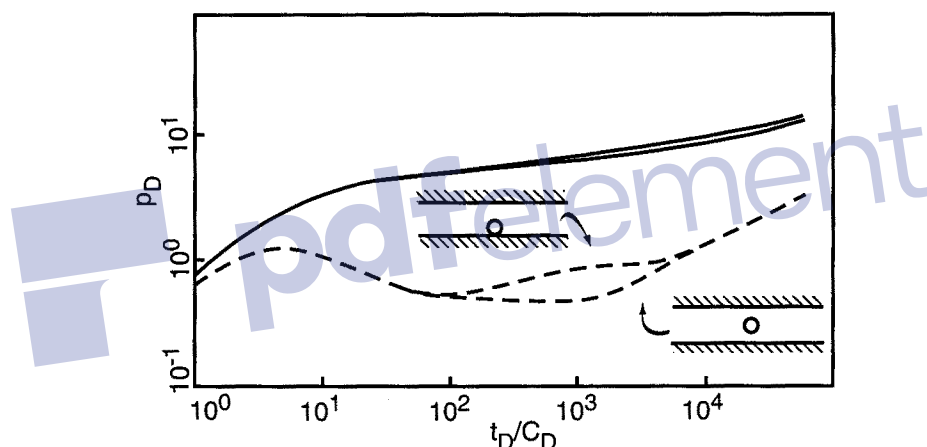


Fig. 8.6

• Bounded channel:

A no-flow boundary at one end of the channel is perceived by the doubling of the slope of the semi-square root straight line (see section 8.4).

On the log-log plot it corresponds to a pressure derivative going from an initial 0.5 slope straight line to a second 0.5 slope straight line. The doubling of the slope on the conventional plot corresponds to the translation of the second straight line by 2 on the log-log plot.

Figure 8.7 shows the derivative for different distances from the well to the boundary.

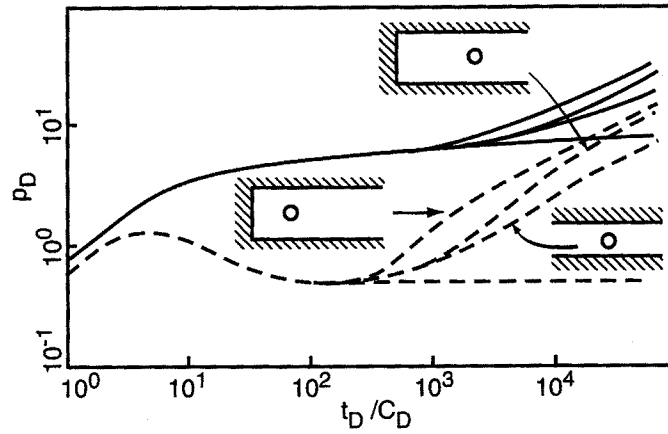


Fig. 8.7

When the boundary is close to the well, the steep increase of the derivative (i.e. slope greater than 0.5) before reaching the 0.5 slope is used to diagnose a boundary in the channel.

pdfelement

Chapter 9

Intersecting faults

During a test two intersecting no-flow boundaries (Fig. 9.1), faults for example, can be perceived.

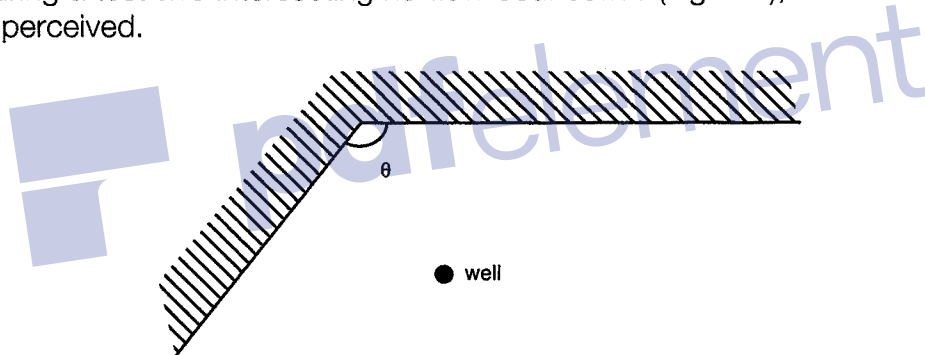


Fig. 9.1

The distance from the well to each one of them can be characterized by conventional methods [Ref. 11] and by using the pressure derivative.

9.1 CONVENTIONAL ANALYSIS

The presence of two intersecting no-flow boundaries may be felt by the transition from an initial m -slope semi-log straight line to a second one with a slope of $2\pi m/\theta$ (θ in radians). If the well is located closer to one of the boundaries than the other, a straight line with a slope of $2m$ may come before the transition to the one with a slope of $2\pi m/\theta$. Figure 9.2 shows the corresponding representation on a semi-log graph for buildup.

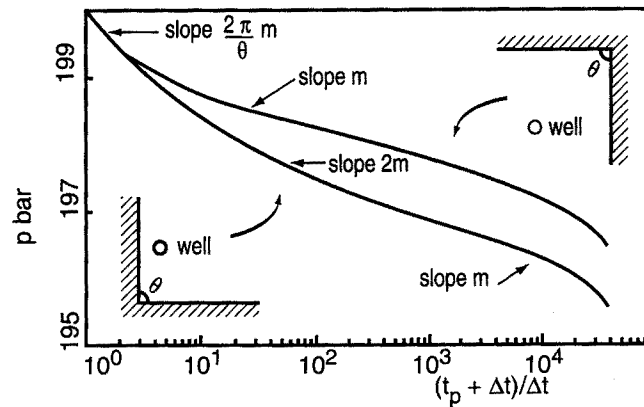


Fig. 9.2

The angle between the two boundaries is characterized by the ratio of the slopes of the two semi-log straight lines:

$$\theta = 2\pi \frac{m_1}{m_2}$$

The distance from the well to the closer boundary can be characterized by the radius of investigation of the test at the time when the boundary is perceived at the well.

Most of the time it is necessary to match the pressure and the pressure derivative data with a well test analytical model to determine the distance from the well to the farther boundary more precisely.

- **Extrapolated pressure, initial pressure:**

In buildup the extrapolated pressure p^* is read on the first semi-log straight line at infinite Δt . This pressure is used in the MBH method (see Chapter 11) to determine the average reservoir pressure.

During initial tests, the initial pressure can be read on the second semi-log straight line (the one with the slope of $2\pi m/\theta$) at infinite Δt .

9.2 TYPE CURVES; PRESSURE DERIVATIVE

The presence of two faults with an angle θ between them is characterized by the pressure derivative going from an initial stabilization at 0.5 to a second one at π/θ (θ in radians) on a dimensionless log-log plot (Fig. 9.3).

The smaller θ , the longer it takes to reach the second stabilization.

A stabilization at 1 (1 boundary) may come before the stabilization at π/θ if the well is located much closer to one of the boundaries than the other (Fig. 9.3).

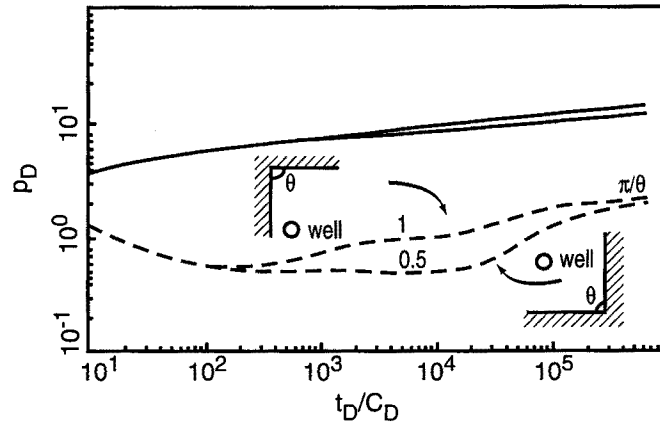


Fig. 9.3

When the angle is very small, the two faults can be considered as practically parallel: they behave like a channel. The transition between the stabilization at 0.5 and the one at π/θ corresponds to a quasi-linear flow with the derivative increasing as a 1/2 slope straight line (Fig. 9.4).

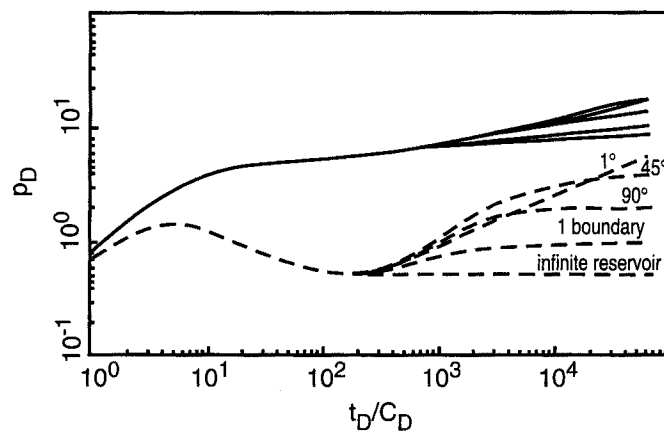


Fig. 9.4



Chapter 10

Constant pressure boundary

A constant pressure boundary effect can be seen during a well test in several cases (Fig. 10.1):

- when the compressible zone reaches a gas cap laterally;
- when the compressible zone reaches an aquifer with the mobility of the water much greater than that of the oil.

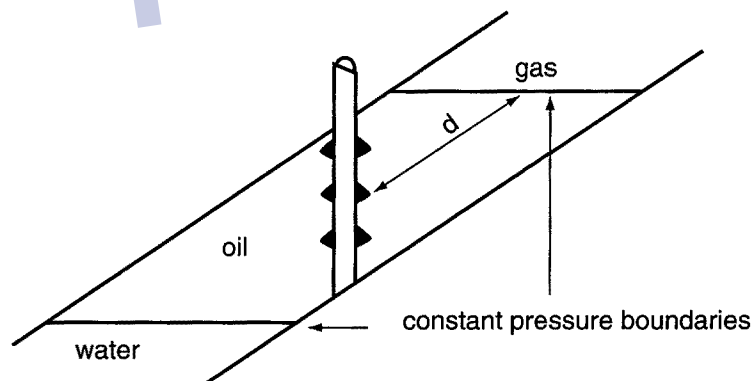


Fig. 10.1

A constant pressure boundary is obtained analytically using the method of images.

The image well is symmetrical to the tested well in relation to the boundary. It has a flow rate opposite that of the tested well (Fig. 10.2).

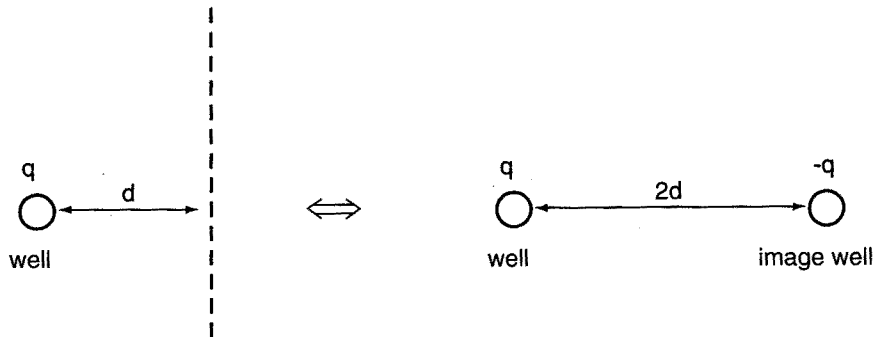


Fig. 10.2

Applying the image method, the pressure at the well is written

$$p_D = \underset{\substack{\uparrow \\ \text{pressure variation} \\ \text{due to the well}}}{p_D(t_D, r_D = 1, S)} - \underset{\substack{\uparrow \\ \text{pressure variation} \\ \text{due to the image well}}}{p_D(t_D, 2r_D)} \quad (10.1)$$

10.1 CONVENTIONAL INTERPRETATION METHOD

Provided the wellbore storage effect has ended soon enough, the pressure variation at the well is written:

$$p_D = \frac{1}{2} \left[\underbrace{\ln t_D + 0.81 + 2S}_{\text{well}} + \text{Ei} \left(-\frac{(2r_D)^2}{4t_D} \right) \right]_{\text{image well}}$$

• Short times:

Until the compressible zone reaches the constant pressure boundary, is $\frac{(2r_D)^2}{4t_D}$ small and the image well term is zero.

Pressure drop is that of a well in an infinite reservoir. Once the wellbore storage effect is over, pressure drop is given by the usual semi-log straight line:

$$p_D = \frac{1}{2} (\ln t_D + 0.81 + 2S) \quad (10.3)$$

• **Long times:**

When t is long enough, in practice as soon as $\frac{(2r_D)^2}{4t_D}$ is smaller than 1%, the image well term can be determined by its logarithmic approximation:

$$-Ei\left(-\frac{(2r_D)^2}{4t_D}\right) = \ln \frac{t_D}{(2r_D)^2} + 0.81 \quad (10.4)$$

The pressure drop at the well is then written:

$$p_D = S + \ln 2r_D \quad (10.5)$$

In other words, in real variables:

$$p_i - p_{wf} = \alpha \frac{qB\mu}{kh} \left(\ln \frac{d}{r_w} + S \right) \quad (10.6)$$

with:

$$\begin{aligned} \alpha &= 1/2 \pi && \text{(in SI units)} \\ \alpha &= 141.2 && \text{(in practical US units)} \\ \alpha &= 18.66 && \text{(in practical metric units).} \end{aligned}$$

Pressure is constant at the well.

The pressure at the boundary is equal to the initial pressure, The pressure drop between the boundary and the well is due to the sum of the pressure drop in the skin and the pressure due to Darcy's law.

• **Distance to the boundary:**

In the same way as for the fault, two methods can be used to determine the distance to the boundary:

- the intersection of the semi-log straight line and the constant pressure straight line that was reached at the end of the test;
- the radius of investigation at the time when the compressible zone reaches the boundary.

• **Intersection of the two straight lines:**

Let t_i be the time when the two straight lines intersect (Fig. 10.3).

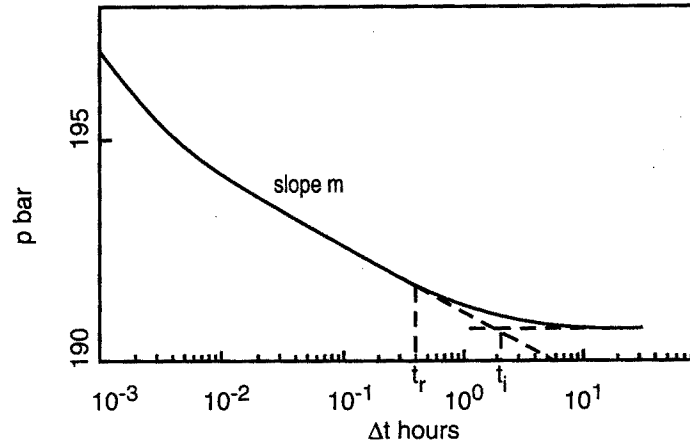


Fig. 10.3

Based on equations (10.3) and (10.5), the value of t_i is used to determine the distance from the well to the boundary.

The expression of the distance is identical to that obtained for a fault:

$$r_D = \frac{1}{2} \sqrt{\exp(0.81) t_{Di}}$$

from which d is deduced:

$$d = \alpha \sqrt{\frac{kt_i}{\phi\mu c_t}} \quad (10.7)$$

- $\alpha = 0.75$ (in SI units)
- $\alpha = 0.012$ (in practical US units)
- $\alpha = 0.014$ (in practical metric units).

• **Radius of investigation:**

The distance from the well to the boundary can be determined by the time t_r when the measurement points leave the semi-log straight line (Fig. 10.3).

The distance from the boundary is then equal to:

$$d = \alpha \sqrt{\frac{kt_r}{\phi\mu c_t}} \quad (10.8)$$

$\alpha = 2$ (in SI units)
 $\alpha = 0.032$ (in practical US units)
 $\alpha = 0.038$ (in practical metric units).

10.2 TYPE CURVES; DERIVATIVE

The presence of a constant pressure boundary is characterized by a pressure stabilization.

A pressure derivative going to zero and appearing as a sharp decrease on the log-log representation corresponds to this pressure stabilization (Fig. 10.4).

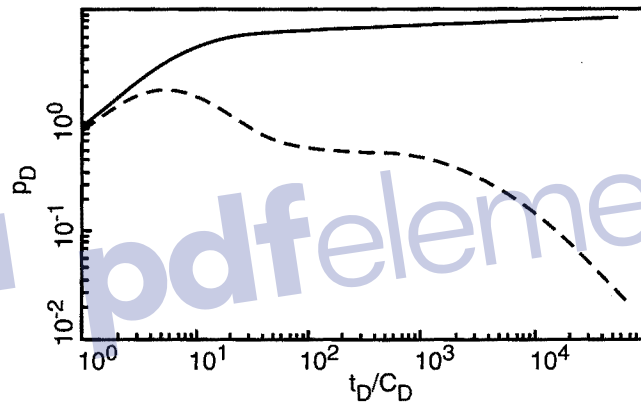


Fig. 10.4



Chapter 11

Closed reservoir

If the reservoir is limited by no-flow boundaries two cases can be distinguished when the compressible zone reaches the limits:

- **The well is producing:** when the no-flow boundaries are reached, the flow regime becomes **pseudosteady-state**.
- **The well is shut-in:** when the no-flow boundaries are reached, the pressure stabilizes at a value called average pressure in the whole area defined by the no-flow boundaries.

11.1 PRODUCING WELL, PSEUDOSTEADY-STATE REGIME

As long as the compressible zone generated by opening the well to production has not reached any boundary, the reservoir behaves as if it were infinite: i.e. the usual transient regime.

When all the no-flow boundaries have been reached, the flow regime becomes pseudosteady-state.

The no-flow boundaries define **the drainage area** of the well.

- **Drainage area:**

The boundaries of the drainage area may be due to several factors:

- physical barriers: sealing fault, disappearing facies, etc.;

- production from neighboring wells: the boundary between two wells is then fictive. The distance from each well is proportional to the pore volume, V_i , drained by each well:

$$V_i = \frac{V q_i}{q_t} \quad (11.1)$$

V : pore volume drained by the wells under consideration

q_t : $\sum_i q_i$

V_i : pore volume drained by well i .

The position of the boundary between the wells depends on the flow rate of the wells, but also on the thickness and the porosity of the reservoir in each drainage area.

- **Pseudosteady-state regime:**

Once the boundaries of the drainage area have been reached, the pressure at the well decreases linearly versus time:

- proportionally to the well flow rate;
- inversely proportional to the compressible volume of the drainage area.

The decline is expressed in dimensionless variables in equation (11.2) below [Ref. 12, 13]:

$$p_D = 2\pi t_{DA} + \frac{1}{2} \ln \frac{A}{r_w^2} + \frac{1}{2} \ln \frac{2.2458}{C_A} \quad (11.2)$$

$t_{DA} = \frac{\alpha kt}{\phi \mu c_t A}$ dimensionless time over drainage area

$\alpha = 1$ (in SI units)

$\alpha = 0.000264$ (in practical US units)

$\alpha = 0.000355$ (in practical metric units).

A is the drainage area of the well.

C_A is a shape factor that depends on the shape of the reservoir and the position of the well in it.

A table with shape factors (Table 11.1) corresponding to different reservoir-well configurations is presented by Earlougher in [Ref. 12].

In the case of a well in the center of a circular drainage area, equation (11.2) becomes:

$$p_D = 2\pi t_{DA} + \frac{1}{2} \ln \frac{r_e}{r_w} - 0.75 \quad (11.3)$$

r_e is the radius of the drainage area.

• **Conventional analysis:**

Equation (11.2) is expressed in real terms by:

$$p_i - p_{wf} = \frac{\alpha q B}{\phi c_t h A} t + \frac{\beta q B \mu}{kh} \left[\log \frac{A}{r_w^2} + \log \frac{2.2458}{C_A} + 0.87 S \right] \quad (11.4)$$

$\alpha = 0.234$	$\beta = 162.6$	(in practical US units)
$\alpha = 0.0417$	$\beta = 21.5$	(in practical metric units)
$\alpha = 1$	$\beta = 1.151$	(in SI units).

This equation is of the type:

$$p_{wf} = -m^*t + p_0 \quad (11.5)$$

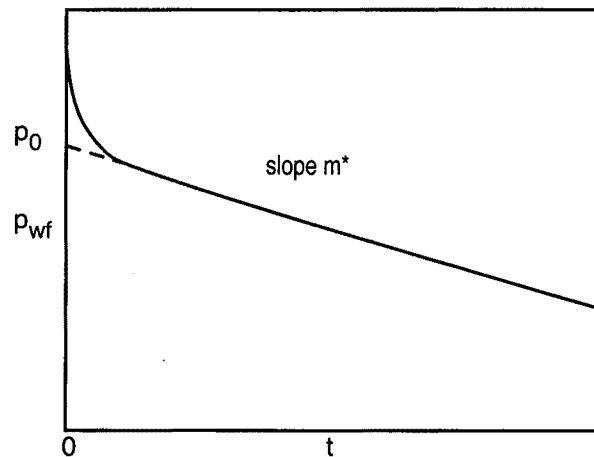



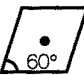



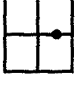
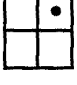
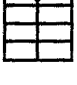
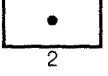
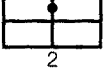

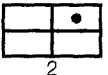



Fig. 11.1

Pressure drop on a pressure versus time plot shows up as a straight line with a slope of m^* and intercept p_0 at $t = 0$ (Fig. 11.1).

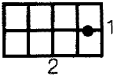

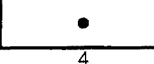

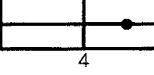
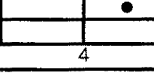


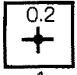
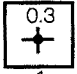
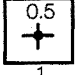
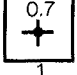
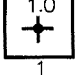
Table 11.1

In bounded reservoirs	C_A	$\ln C_A$	$1/2 \ln \frac{(2.2458)}{C_A}$	Exact for $t_{DA} >$	Less than 1% error for $t_{DA} >$	Use infinite system solution with less than 1% error for $t_{DA} <$
	31.62	3.4538	-1.3224	0.1	0.06	0.10
	31.6	3.4532	-1.3220	0.1	0.06	0.10
	27.6	3.378	-1.2544	0.2	0.07	0.09
	27.1	3.2995	-1.2452	0.2	0.07	0.09
	21.9	3.0865	-1.1387	0.4	0.12	0.08
	0.098	-2.3227	+1.5659	0.9	0.60	0.015
	30.8828	3.4302	-1.3106	0.1	0.05	0.09
	12.9851	2.5638	-0.8774	0.7	0.25	0.03
	4.5132	1.5070	-0.3490	0.6	0.30	0.025
	3.3351	1.2045	-0.1977	0.7	0.25	0.01
	21.8369	3.0836	-1.1373	0.3	0.15	0.025
	10.8374	2.3830	-0.7870	0.4	0.15	0.025
	4.5141	1.5072	-0.3491	1.5	0.50	0.06
	2.0769	0.7309	+0.0391	1.7	0.50	0.02
	3.1573	1.1497	-0.1703	0.4	0.15	0.005

Reproduced with the authorization of SPE (Society of Petroleum Engineers) Source : Advances in Well Test Analysis by Robert C. Earlougher Jr., Marathon Oil Co. (SPE Monograph Series 5, Second Printing, 1977, American Institute of Mining)

Chapter 11 • CLOSED RESERVOIR

Table 11.1 (continued)

In bounded reservoirs	C_A	$\ln C_A$	$1/2 \ln \frac{(2.2458)}{C_A}$	Exact for $t_{DA} >$	Less than 1% error for $t_{DA} >$	Use infinite system solution with less than 1% error for $t_{DA} <$
	0.5813	-0.5425	+0.6758	2.0	0.60	0.02
	0.1109	-2.1991	+1.5041	3.0	0.60	0.005
	5.3790	1.6825	-0.4367	0.8	0.30	0.01
	2.6896	0.9894	-0.0902	0.8	0.30	0.01
	0.2318	-1.4619	+1.1355	4.0	2.00	0.03
	0.1155	-2.1585	+1.4838	7.0	2.00	0.01
	2.3606	0.8589	-0.0249	1.0	0.40	0.025
5 in vertically fractured reservoirs	use $(x_e/x_f)^2$ instead of A/r_w^2 for fractured systems					
	2.6541	0.9761	-0.0835	0.175	0.08	inutilisable
	2.0348	0.7104	+0.0493	0.175	0.09	inutilisable
	1.9986	0.6924	+0.0583	0.175	0.09	inutilisable
	1.6620	0.5080	+0.1505	0.175	0.09	inutilisable
	1.3127	0.2721	+0.2685	0.175	0.09	inutilisable
	0.7887	-0.2374	+0.5232	0.175	0.09	inutilisable
1 in reservoirs with water drive	19.1	2.95	-1.07	-	-	-
1 in reservoirs of unknown production character	25.0	3.22	-1.20	-	-	-

The m^* slope of the straight line is used to determine the value of the drainage area A or the pore volume drained $hA\phi$:

$$A = \frac{\alpha q B}{\phi c_t h m^*} \quad (11.6)$$

α has the same values as in equation (11.4).

The value of p_0 is used to determine the shape factor, C_A :

$$C_A = 2.2458 \cdot 10 \left[-\frac{p_1 - p_0}{m} - \log \frac{A}{r_w^2} - 0.87 S \right] \quad (11.7)$$

with $m = \frac{\beta q B \mu}{kh}$ the absolute value of the slope of the semi-log straight line.

C_A can also be expressed using the pressure $t = 1$ h measured on the semi-log straight line one hour after well shut-in:

$$C_A = 5.456 \frac{m}{m^*} \cdot 10^{-\left[\frac{p_{1h} - p_0}{m} \right]} \quad (11.8)$$

By comparing C_A to the values listed in Table 11.1, it is possible to determine the reservoir-well configuration corresponding to the test.

On the table it can be seen that the highest value for ($C_A = 31.62$) corresponds to a circle. This is the most regular reservoir-well configuration. Small values of C_A correspond to an elongated reservoir or a well off center in the drainage area.

Table 11.1 can be used to determine the t_{DA} corresponding to the end of the transient flow and to the beginning of the pseudosteady-state flow for a given reservoir-well configuration:

- the fourth column of the table indicates the exact beginning of the pseudosteady-state flow;
- the fifth column shows the beginning of the pseudosteady-state flow with less than 1% error;
- the sixth column gives the end of the transient flow with less than 1% error.

A can be determined accurately. This is not the case for C_A . Matching the transition between the radial flow and the pseudosteady-state flow on the pressure

derivative gives much more reliable information on the shape of the drainage area and the position of the well.

- **Type curves, derivative:**

Since pressure varies linearly versus time during the pseudosteady-state flow, this flow is characterized on the pressure derivative by a straight line with a slope of 1 on a log-log plot (Fig. 11.2).

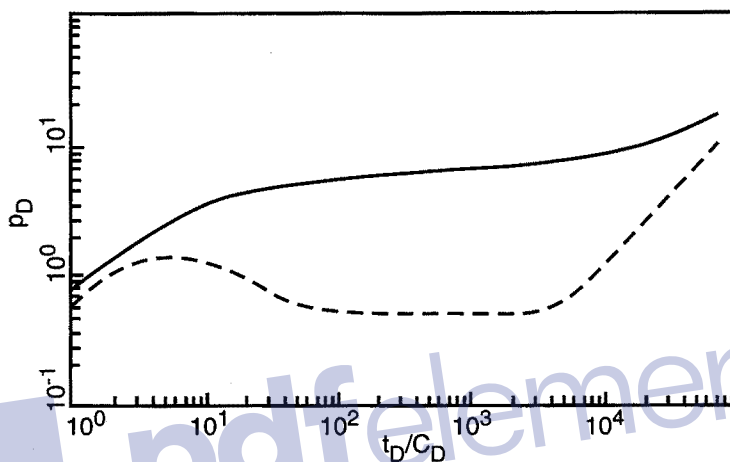


Fig. 11.2

The shape of the transition between the transient regime and the pseudosteady-state regime depends on the shape of the drainage area and on the position of the well in the area. The shape of the transition is used to characterize the reservoir-well configuration. Chapters 7, 8 and 9 indicate how the boundaries can be characterized during a test.

Figure 11.3 shows a number of typical configurations and how they are characterized on the pressure derivative plot.

It shows the boundary during a drawdown, but also during buildup (broken line).

The effect of the boundaries is not as characteristic during buildup as during drawdown: reaching the average pressure hides the end of buildup.

It is often difficult to determine the distance to the boundaries during drawdown as flow rate fluctuations cause pressure variations that are often greater than those due to the effect of the boundaries. The only thing that can sometimes be obtained is an estimate of the drainage area.

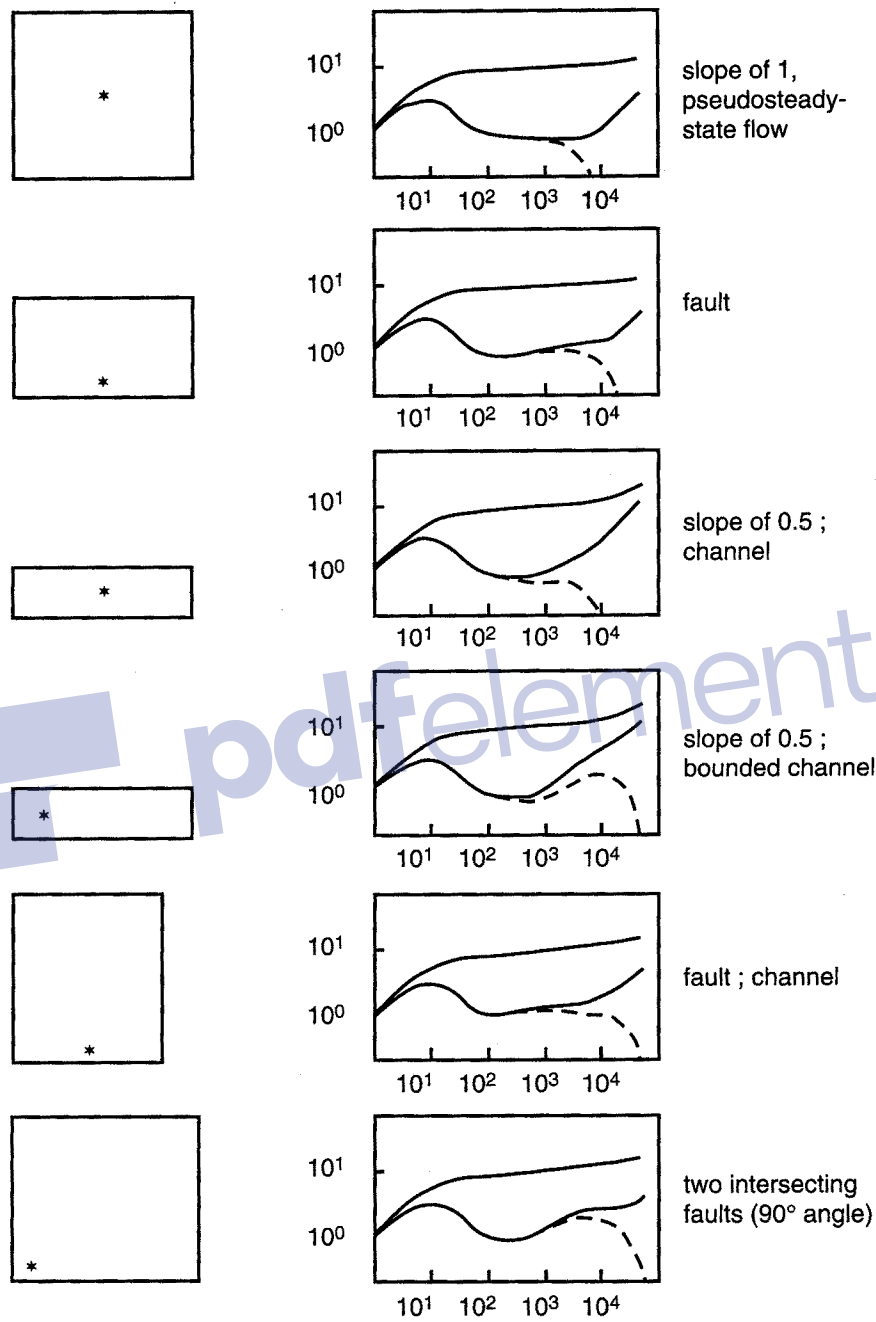


Fig. 11.3
Transitions between transient and pseudosteady-state flows

11.2 SHUT-IN WELL, AVERAGE PRESSURE

When the compressible zone reaches real no-flow physical boundaries during buildup, the pressure in the drainage area becomes uniform and constant. The pressure is called the average pressure of the drainage area.

This is characterized by a stabilization of pressure on pressure versus superposition function plots (Fig. 11.4).

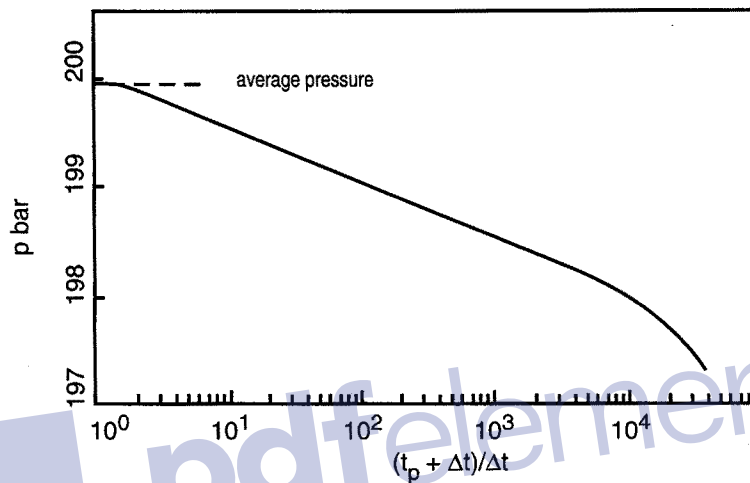


Fig. 11.4

A derivative going to zero corresponds to reaching the average pressure. It corresponds to a steep decrease of the derivative on a log-log plot (Fig 11.5).

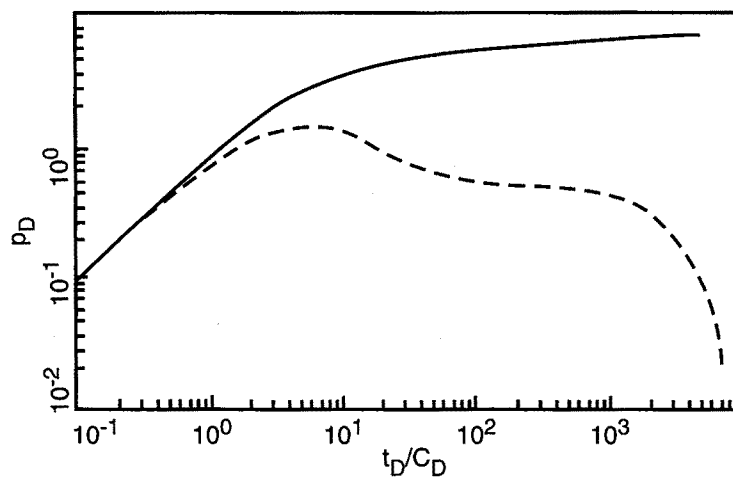


Fig. 11.5

• **Comparison with a constant pressure boundary:**

The pressure stabilization that corresponds to the average pressure of a closed area can be confused with a constant pressure boundary (Chapter 10).

The two phenomena have the same result in a pressure buildup. To distinguish between them, the data from the previous drawdown period must be used:

- The constant pressure boundary (Chapter 10) shows as a stabilization of pressure and a steep decrease on the derivative plot in both drawdown and buildup (Fig. 11.6).
- Reaching the average pressure in buildup corresponds to the beginning of the pseudosteady-state flow in drawdown. It looks very different from a constant pressure boundary (Fig. 11.6):
 - . linear pressure drop versus time instead of stabilization;
 - . a straight line with a slope of 1 increase instead of decrease.

When the drainage area is defined by the production of neighboring wells, the shut-in well pressure starts to decrease under the influence of the other wells after stabilizing.

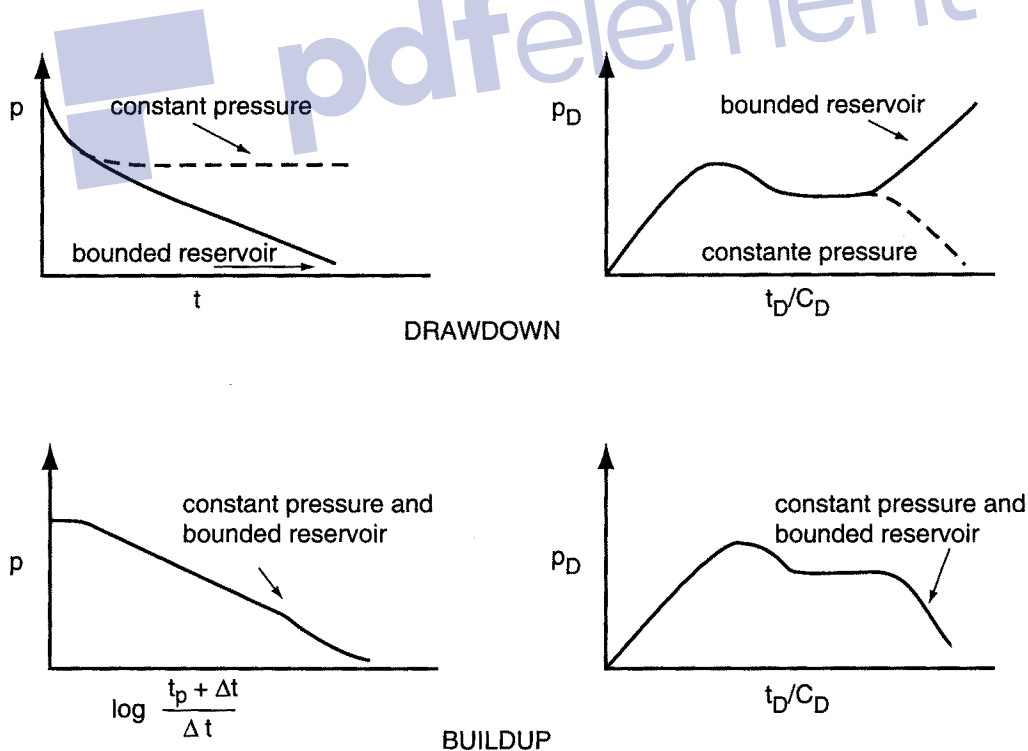


Fig. 11.6

- **Calculating the average pressure**
MBH (Matthews, Brons, Hazebroek) method:

During buildup extrapolation of the semi-log straight line to infinite buildup time gives a value p^* of the pressure. This is the pressure value for $\frac{t_p + \Delta t}{\Delta t} = 1$ on a Horner plot for instance (Fig. 11.7).

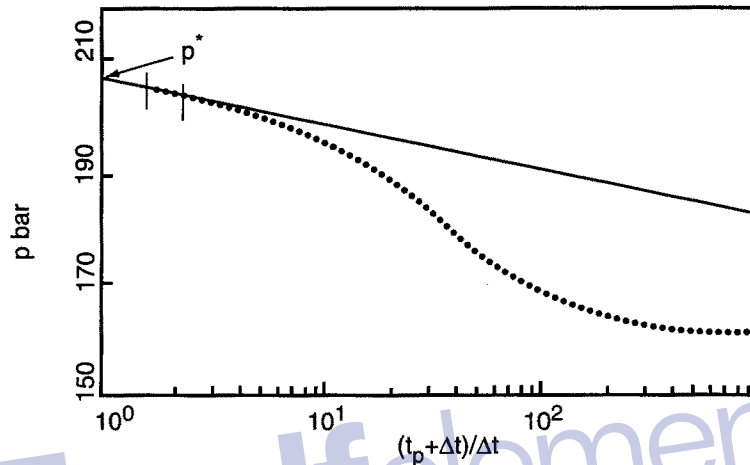


Fig. 11.7

If no reservoir boundary has been reached during the production period preceding buildup, p^* remains close to the initial pressure of the drainage area before the test.

If the production period is long enough, the average pressure has dropped in the drainage area during production. The value of p^* must then be corrected for the production effect in order to calculate the average reservoir pressure.

- **Principle of the method:**

The pressure inside a closed drainage area can be calculated analytically with the image method.

For a rectangular drainage area, four categories of images need to be considered corresponding to the images of the well relative to the four boundaries of the drainage area.

$$p_i - p_{ws} = \frac{m}{2.303} \left\{ \ln \frac{t_p + \Delta t}{\Delta t} + \sum_{i=1}^{\infty} \left[\text{Ei} \left(-\frac{\phi \mu c_t a_i^2}{4k \Delta t} \right) - \text{Ei} \left(\frac{\phi \mu c_t a_i^2}{4k (t_p + \Delta t)} \right) \right] \right\} \quad (11.9)$$

a_i : distance from the well to the images
 m : slope of the semi-log straight line.

For infinite Δt , this expression is of the type:

$$p_i - p^* = \frac{m}{2.303} F(t_p) \quad (11.10)$$

$F(t_p)$ is dependent on the production time, the drainage area and the position of the well.

A material balance gives the decline of the average pressure:

$$p_i - \bar{p} = \frac{qBt_p}{\phi c_t h A} \quad (11.11)$$

with \bar{p} the average pressure in the drainage area.

Equation (11.11) can also be written:

$$p_i - \bar{p} = \frac{m}{2.303} 4\pi t_{pDA} \quad (11.12)$$

with:

$$t_{pDA} = \frac{k t_p}{\phi \mu c_t A} \quad (11.13)$$

from (11.10) and (11.12):

$$\frac{2.303 (p^* - \bar{p})}{m} = 4\pi t_{pDA} + F(t_p) \quad (11.14)$$

The function of t_p can be calculated for different reservoir-well configurations.

It is used to calculate the average pressure in the drainage area of the well based on information about:

- the geometry and dimensions of the drainage area;
- the position of the well;
- the slope m of the semi-log straight line;
- the extrapolated pressure p^* ;
- the production time t_p .

• Analysis:

Matthews, Brons and Hazebroek computed and plotted the function of t_p corresponding to equation (11.14) for various reservoir-well configurations. The

resulting charts are shown in Figures 11.9 to 11.11. Figure 11.8 explains how they are used in four steps:

- 1 Calculating t_{pDA} :

$$t_{pDA} = \frac{0.000264 kt_p}{\phi \mu c_f A} \quad (\text{in practical US units})$$

- 2 Choosing the curve corresponding to the reservoir-well configuration of the test: here the well is located at one-quarter the width and half the length of a rectangular reservoir that is twice as long as it is wide.
- 3 Using the chart to determine:

$$P_{DMBH} = \frac{2.303 (p^* - p)}{m}$$

- 4 Calculating the average pressure based on the value of m and p^* above.

Nota bene:

- 1 It is absolutely necessary to know the drainage area data in order to calculate the average pressure: shape, dimensions, position of the well.
- 2 The method can be applied only if a drainage area bounded by no-flow boundaries can be defined. The MBH method can not be applied near injection wells or near a pressure support.
- 3 p^* must be determined on the first semi-log straight line that corresponds to the infinite acting period.
- 4 The average pressure is not always lower than p^* . It is higher for certain values of t_p when the well is located near one of the reservoir boundaries.

• **Dietz's method:**

The Dietz method [Ref. 15] is used to read the average pressure directly on a MDH graph (pressure versus $\log t$, see section 4.3).

Applying this method requires three assumptions to be verified:

- pseudosteady-state flow before the well is shut-in;
- a semi-log straight line on the MDH graph;
- skin greater than -3 .

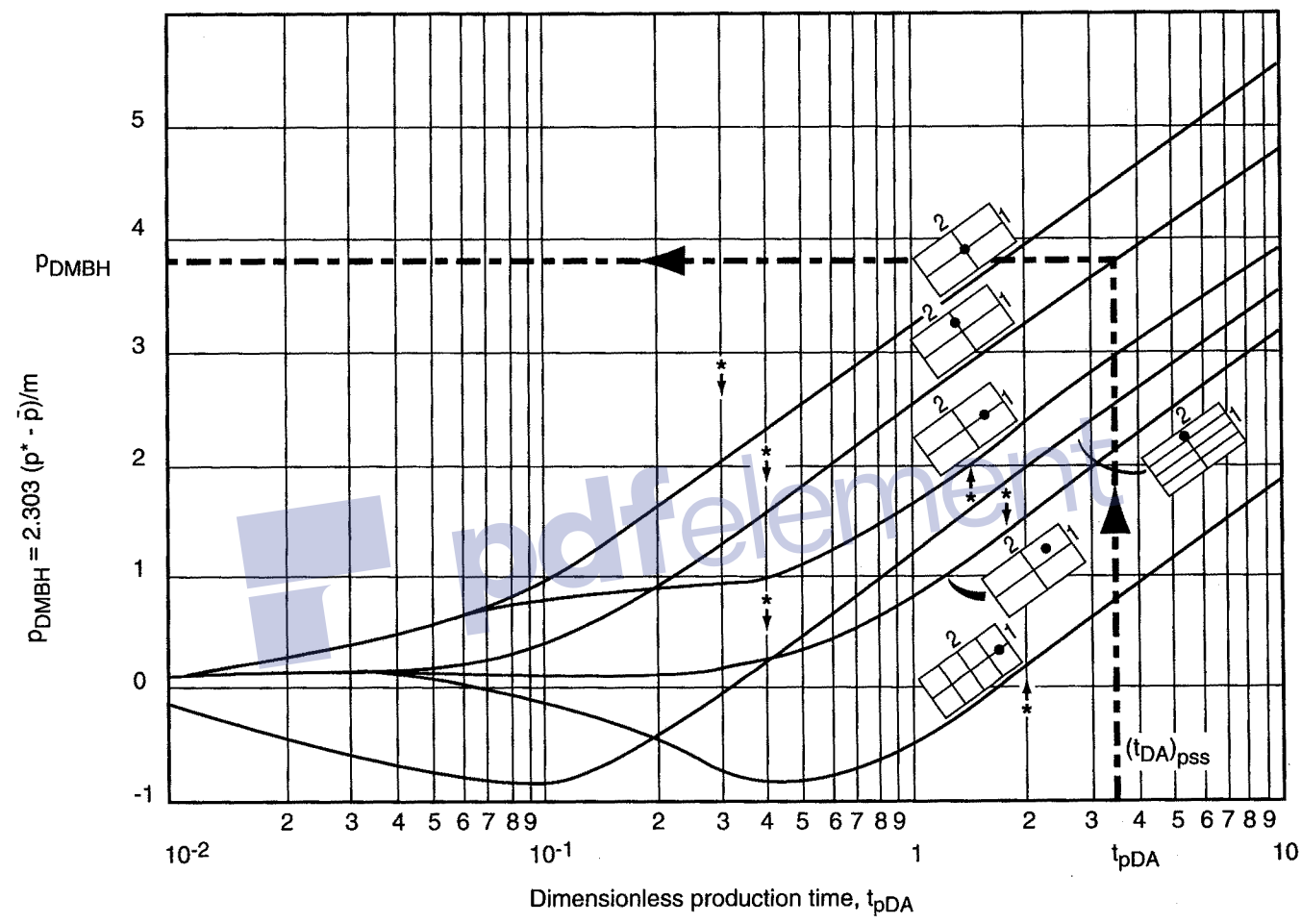


Fig. 11.8

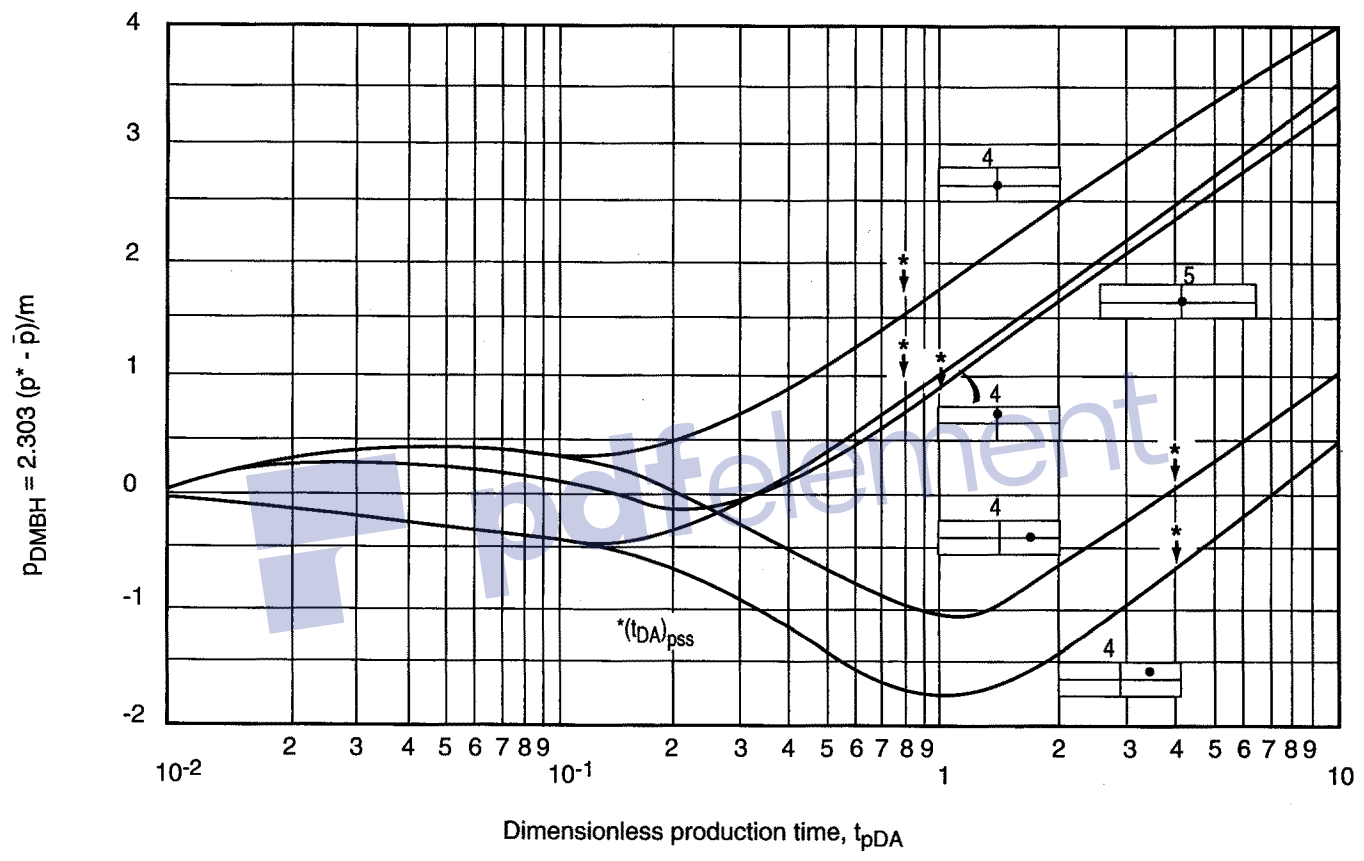


Fig. 11.9

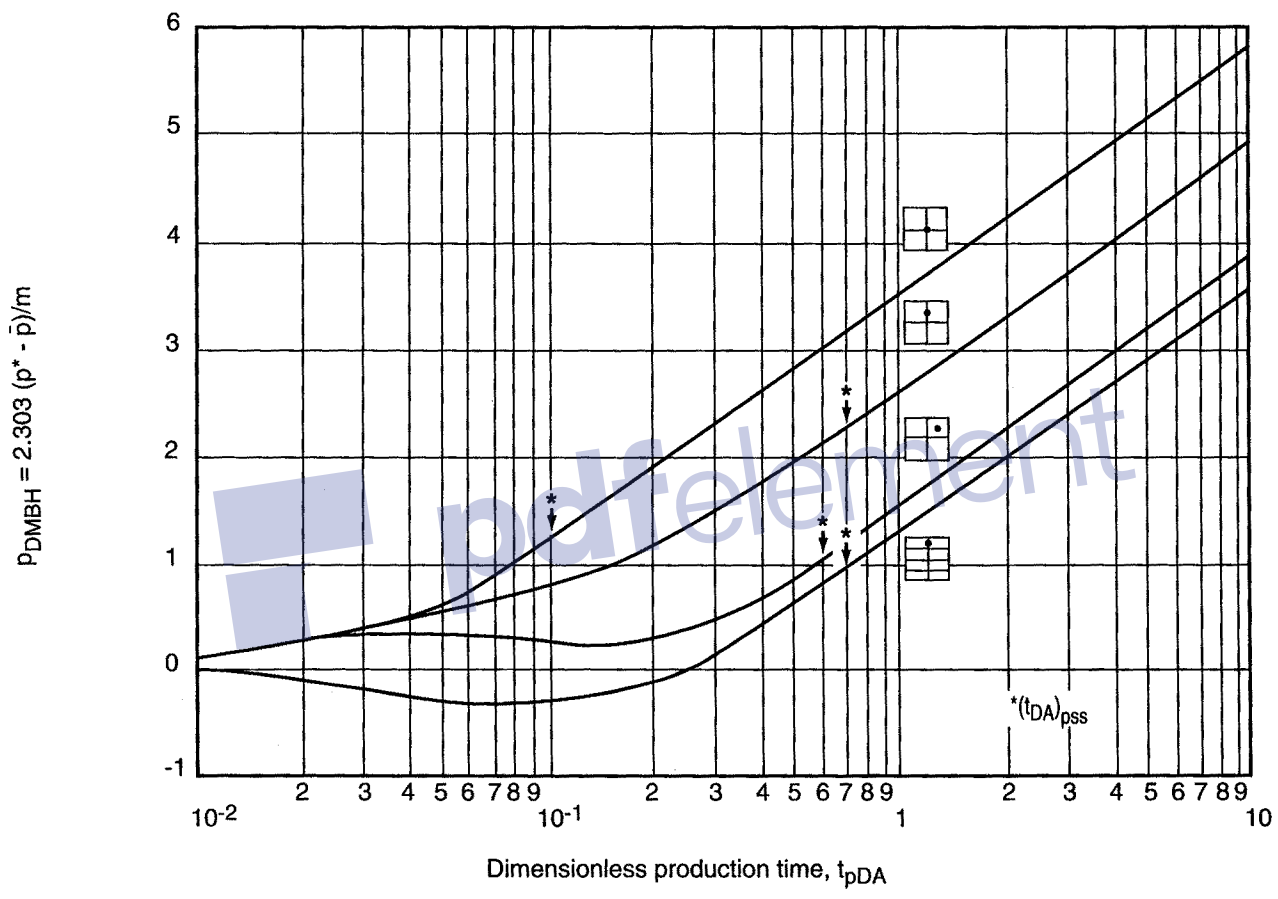


Fig. 11.10

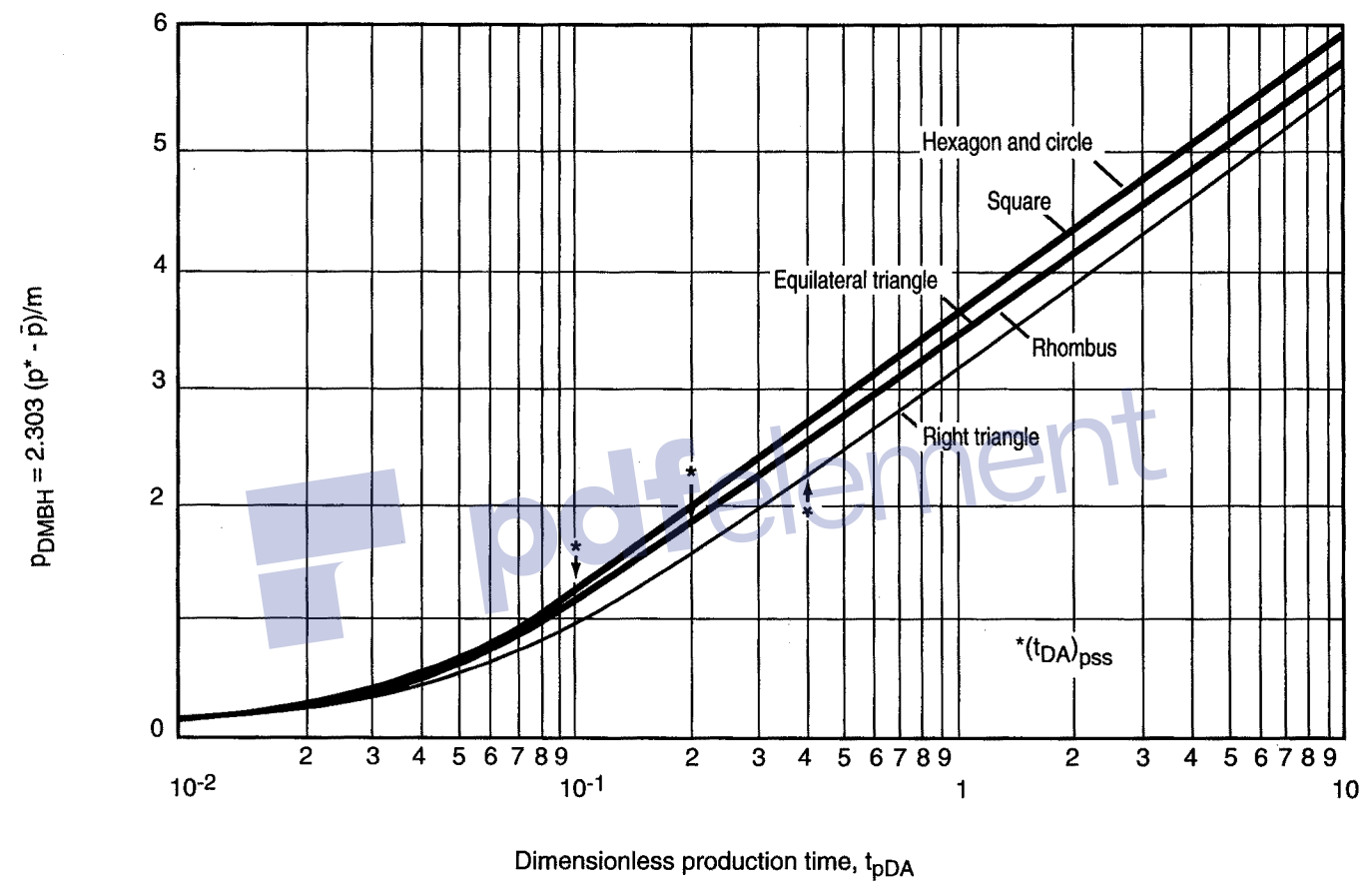


Fig. 11.11

Chapter 11 • CLOSED RESERVOIR

Provided the above are verified, the average pressure is read directly on the semi-log straight line at time Δt such that:

$$\Delta t_p = \frac{t_p}{C_A t_{pDA}} \quad (11.15)$$

$$\Delta t_p = \frac{\phi \mu C_A A}{\alpha k C_A} \quad (11.16)$$

$\alpha = 1$ (in SI units)
 $\alpha = 0.000264$ (in practical US units)
 $\alpha = 0.000355$ (in practical metric units).

C_A is the shape factor corresponding to the reservoir-well configuration (see Table 11.1).

Using the same hypotheses, Ramey and Cobb [Ref. 13] propose reading the average pressure on a Horner graph at a time Δt such that:

$$\left(\frac{t_p + \Delta t}{\Delta t} \right)_p = C_A t_{pDA} \quad (11.17)$$

$$\left(\frac{t_p + \Delta t}{\Delta t} \right)_p = \frac{\alpha k t_p C_A}{\phi \mu A} \quad (11.18)$$

with α having the same meaning as in the Dietz method.

Chapter 12

Productivity index

12.1 DEFINITION

The productivity index of a well is the ratio between:

- the well flow rate;
- the difference between the average pressure of the drainage area and the bottomhole pressure:

$$IP = \frac{q}{\bar{p} - p_{wf}} \quad (12.1)$$

Two cases can be distinguished, depending on whether the pressure is measured in the transient or in the pseudosteady-state flow.

The first corresponds to initial well tests and the second to measurements made during production.

12.2 PRODUCTIVITY INDEX DURING THE INFINITE-ACTING PERIOD

During the infinite-acting period, the average pressure in the drainage area of the well is close to the average pressure at the beginning of the test, p_i :

$$\bar{p} - p_{wf} \approx p_i - p_{wf}$$

$p_i - p_{wf}$ is calculated based on formulas (4.2) to (4.6) presented in Chapter 4:

$$IP = \frac{kh}{\alpha B \mu \left(\log t + \log \frac{k}{\phi \mu c_t r_w^2} - \beta + 0.87 S \right)} \quad (12.2)$$

$\alpha = 2.303/4\pi$	$\beta = -0.81/2.303$	(in SI units)
$\alpha = 162.6$	$\beta = 3.23$	(in practical US units)
$\alpha = 21.5$	$\beta = 3.10$	(in practical metric units).

The productivity index is a decreasing function of time during the transient flow.

12.3 PRODUCTIVITY INDEX DURING THE PSEUDOSTEADY-STATE FLOW

The productivity index is calculated using (formula 12.1) the difference between the average pressure of the drainage area and the pressure at the well: $\bar{p} - p_{wf}$. The difference can also be written:

$$\bar{p} - p_{wf} = (p_i - p_{wf}) - (p_i - \bar{p}) \quad (12.3)$$

$p_i - p_{wf}$ can be calculated based on equations (11.9) and (11.14) which govern the variations at the well in the pseudosteady-state regime:

$$p_i - p_{wf} = \frac{\gamma qB}{\phi c_t h A} t + \frac{\alpha qB \mu}{kh} \left(\log \frac{A}{r_w^2} + \log \frac{2.2458}{C_A} + 0.87 S \right) \quad (12.4)$$

$\alpha = 162.6$	$\gamma = 0.234$	(in practical US units)
$\alpha = 21.5$	$\gamma = 0.0417$	(in practical metric units)
$\alpha = 1.151$	$\gamma = 1$	(in SI units).

$p_i - \bar{p}$ is calculated using a simple material balance:

$$p_i - \bar{p} = \frac{\gamma qB}{\phi c_t h A} t \quad (12.5)$$

therefore:

$$IP = \frac{kh}{\alpha B \mu \left(\log \frac{A}{r_w^2} + \log \frac{2.2458}{C_A} + 0.87 S \right)} \quad (12.6)$$

The productivity index is constant during the pseudosteady-state flow. It can be considered as a characteristic of the well that involves:

- reservoir characteristics: kh ;
- well characteristics: S ;
- reservoir size, A ;
- reservoir-well geometry: C_A .

Nota bene:

The productivity index is the factor that is most widely used by producers to estimate the potential of a well.

During the pseudosteady-state flow, i.e. after a long production time, it does characterize the well's potential.

However, when it is measured during initial tests on a well, i.e. usually during the transient flow, it should be used with caution:

- This PI is continually decreasing.
- The lower the well's skin, the greater the PI decline in relative value.
- The decline lasts until the pseudosteady-state regime is reached.

12.4 REAL AND THEORETICAL PI

The real productivity index is the one measured on the well. The theoretical PI is the one the well would have if its skin were zero. The theoretical PI is used to estimate the gain in productivity that would be brought about by well stimulation, or the loss in productivity due to plugging, partial perforation, etc.:

$$IP_{th} = \frac{q}{(\bar{p} - p_{wf}) - \Delta p_s}$$

$$\Delta p_S = \alpha \frac{q\beta\mu}{kh} S$$

$$\begin{aligned}\alpha &= 1/2\pi && \text{(in SI units)} \\ \alpha &= 141.2 && \text{(in practical US units)} \\ \alpha &= 18.67 && \text{(in practical metric units).}\end{aligned}$$

Δp_S is the pressure drop caused by the skin around the well.



Reservoirs aspects



Chapter 13

Naturally fractured reservoirs

The presence of fractures changes the flows in a reservoir considerably [Ref. 21].

In a fractured reservoir a network of fractures coexists with a network of matrix.

The two porous networks have very different geometrical characteristics, porosities, capacities and permeabilities.

13.1 GEOMETRY

The geometrical representation of a fractured reservoir that is most widely used in well testing is the representation by Warren and Root [14]. It is illustrated by Figure 13.1:

- The matrix blocks are homogeneous and all identical.
- They have a rectangular parallelepiped shape with faces corresponding to orthogonal fracture planes.
- The matrix blocks are divided into three classifications, according to the relative dimensions of the sides of the parallelepiped.
- Cubic matrix blocs: the three sides have dimensions of the same order of magnitude (Fig. 13.1a).
- Match matrix blocs: one of the sides is much longer than the other two (Fig. 13.1b).
- Slab matrix blocs: one of the sides is much shorter than the other two (Fig. 13.1c).

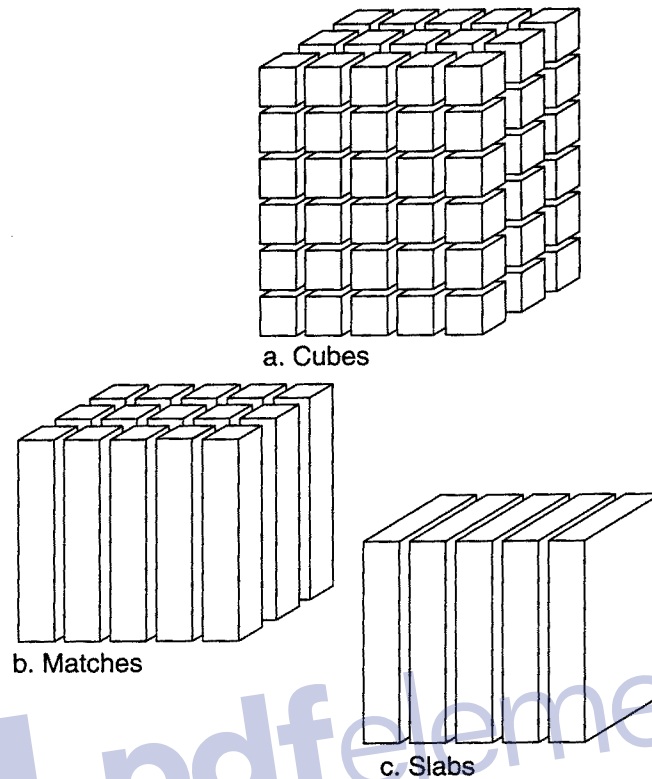


Fig. 13.1 Geometrical representation of a fractured reservoir

In Warren and Root's model, the parameter α reflects the effects of the geometry of the matrix blocks on fluid exchanges between the matrix and the fractures:

$$\alpha = \frac{n(n + 2)}{r_m^2} \quad (13.1)$$

Exchanges depend on the shape and size of the matrix blocks.

- **Shape:**

The shape of the blocks comes into play through the parameter n , which indicates the number of directions provided for fluid exchange:

- $n = 1$ for slab matrix blocs
- $n = 2$ for match matrix blocs
- $n = 3$ for cubic matrix blocs.

The higher n , the easier the exchanges.

- **Size:**

r_m is a characteristic length that defines the size of the matrix block:

$$r_m = \frac{\text{Volume of matrix block}}{\text{Area of the matrix block}} \times n \quad (13.2)$$

The smaller r_m , the easier the exchanges.

- **Cubes:**

For a cube with an edge of a :

$$r_m = \frac{a}{2} \quad \alpha = \frac{60}{a^2}$$

The flow occurs through the three faces of the cube.

- **Sheets:**

For sheets with a thickness of a :

$$r_m = \frac{a}{2} \quad \alpha = \frac{12}{a^2}$$

Flow occurs only perpendicularly to the sheet planes.

α is five times smaller than for a cube of the same thickness.

Generally speaking the larger α (small, cube-shaped blocks for example) the easier the flow between matrix and fractures.

13.2 POROSITY

The matrix and the fractures exhibit very different porosities.

The space occupied by each of the porous networks is defined by their relative volume:

$$V_f = \frac{\text{Total volume of fractures}}{\text{Total volume of the sample}} \quad (13.3)$$

$$V_m = \frac{\text{Total volume of the matrix}}{\text{Total volume of the sample}} \quad (13.4)$$

With this definition $V_f + V_m = 1$.

Each one of the volumes is porous:

$$\phi_f = \frac{\text{Volume of voids located in fractures}}{\text{Total volume of fractures}} \quad (13.5)$$

$$\phi_m = \frac{\text{Porous volume located in the matrix}}{\text{Total volume of the matrix}} \quad (13.6)$$

In terms of the total volume of the sample, the matrix and the fracture porosity are equal to:

- for matrix porosity: $\phi_m V_m$;
- for fracture porosity: $\phi_f V_f$.

The fracture porosity ϕ_f is usually close to 1, but the relative volume is very small (less than 1%). This means that in terms of the total volume of the sample, the fracture porosity is very small (less than 1%).

There might be some confusion between the symbols ϕ_f , ϕ_m and $\phi_f V_f$ and $\phi_m V_m$:

- $\phi_f V_f$ and $\phi_m V_m$ are porosities in relation to the whole reservoir;
- ϕ_f and ϕ_m are porosities in relation to the fractures alone and the matrix alone.

Although they may be confusing, this nomenclature is used here because this is what is usually found in oil industry literature.

13.3 CAPACITY

The total compressibility of each system is equal to:

- for the matrix:

$$c_{tm} = c_o S_o + c_w S_w + c_{pm} \quad (13.7)$$

- for the fractures:

$$c_{tf} = c_o + c_{pf} \quad (13.8)$$

c_{pf} et c_{pm} are the compressibility of the voids located respectively in the fractures and in the matrix. They are defined in relation to the volume of the voids and not in relation to the total volume of the rock sample.

The capacity of each system is equal to:

- for the matrix:

$$\mathcal{C}_m = \phi_m V_m c_{tm} \quad (13.9)$$

for which there is a corresponding dimensionless wellbore storage:

$$C_{Df} = \frac{\beta C}{\mathcal{E}_f h r_w^2} \quad (13.10)$$

$\beta = 1/2\pi$ (in practical metric units and in SI units)

$\beta = 0.89$ (in practical US units).

– for the fractures:

$$\mathcal{E}_f = \phi_f V_f c_{tf} \quad (13.11)$$

$$C_{Df} = \frac{\beta C}{\mathcal{E}_f h r_w^2} \quad (13.12)$$

– for the reservoir taken as a whole, the global reservoir capacity is the sum of the fracture and the matrix capacity:

$$\mathcal{E}_{f+m} = \phi_f V_f c_{tf} + \phi_m V_m c_{tm} \quad (13.13)$$

$$C_{Df+m} = \frac{\beta C}{\mathcal{E}_{f+m} h r_w^2} \quad (13.14)$$

Fracture porosity is usually negligible compared with matrix porosity, however it is not uncommon to find capacities of the same order of magnitude. This is due to the high degree of total compressibility of the fractures, c_{tf} .

The compressibility of the voids located in the fractures, c_{pf} , is generally often 10 to 100 times greater than that of the voids located in the matrix, c_{pm} .

• **Capacity contrast: the parameter ω**

The parameter ω characterizes the contrast in capacity between the fractures and the whole reservoir:

$$\omega = \frac{\mathcal{E}_f}{\mathcal{E}_{f+m}} \quad (13.15)$$

ω can also be written:

$$\omega = \frac{\mathcal{E}_{Df+m}}{\mathcal{E}_{Df}} \quad (13.16)$$

The smaller ω the more the fracture effect can be felt on pressure variations: with $\omega = 1$ the reservoir behaves like a homogeneous reservoir made up solely of fractures.

The fact that a capacity contrast exists is used to establish that the matrix takes part in flows, but does not prove that the matrix is impregnated with oil. The matrix's contribution can be due only to the compressibility of the water it is saturated with.

13.4 PERMEABILITY

Fracture permeability is much higher than matrix permeability, and because of this, fluids circulate mainly through the fractures. It is the fracture permeability that will be perceived by well testing.

A test can not determine the permeability of a reservoir directly: it determines the product of a permeability by a reservoir thickness.

It is necessary to know the thickness that kh must be divided by in order to determine reservoir permeability.

In the case of a fractured reservoir, it would be necessary to know the cumulative thickness of all the fractures to determine the intrinsic permeability of the fractures. This cumulative thickness is not easy to determine.

By convention and also in order to compare the permeability of a fractured reservoir and that of a homogeneous reservoir with the same net pay, the equivalent permeability of the fractures is calculated taking the net reservoir pay as the thickness.

Because of this, the permeability obtained is of the same order of magnitude as the permeability usually found in reservoirs (10 mD to a few darcys).

It does not reach the several tens of darcys that could be expected of the fractures' intrinsic permeability.

Despite this convention on thickness, the equivalent permeability of the fractures is generally higher than what is attributed to the matrix by measurements on core samples or interpretation of RFTs in the matrix (several millidarcys).

The fact that the permeability obtained from a test is much higher than that of the matrix (more than 10 times) suggests that the reservoir is fractured.

To be applicable, the mathematical model by Warren and Root used to interpret tests in fractured reservoirs requires matrix permeability to be small compared to the equivalent permeability of the fractures [Ref. 1, 14, 22].

13.5 MATRIX-FRACTURE EXCHANGE: λ

The ease with which fluids are exchanged between the matrix and the fractures depends on two factors:

- the geometry of matrix blocks;
- the ratio between matrix (k_m) and fracture (k_f) permeability.

The way the exchanges occur is described by the parameter λ :

$$\lambda = \alpha r_w^2 \frac{k_m}{k_f} \quad (13.17)$$

$\alpha = \frac{n(n+2)}{r_m^2}$ was defined in section 13.1.

α characterizes the influence of matrix block geometry (size and shape) on matrix-fracture exchanges.

The larger λ the easier the exchange of fluids between the matrix and the fractures:

- The higher the permeability, k_m ;
- the larger α i.e. the smaller the blocks (small r_m) and the larger the number of exchange directions, n , the larger.

The most common range for λ values is 10^{-4} and 10^{-8} .

13.6 ANALYSIS OF FLOWS

Three flow periods follow one another when a fractured reservoir is put in production:

- flow from the fractures;
- a transition period when the matrix starts to produce;
- flow from both matrix and fractures.

These three periods are indicated in Figure 13.2, which represents pressure and derivative changes that are typical of what is observed in a fractured reservoir using the type curve log-log plot.

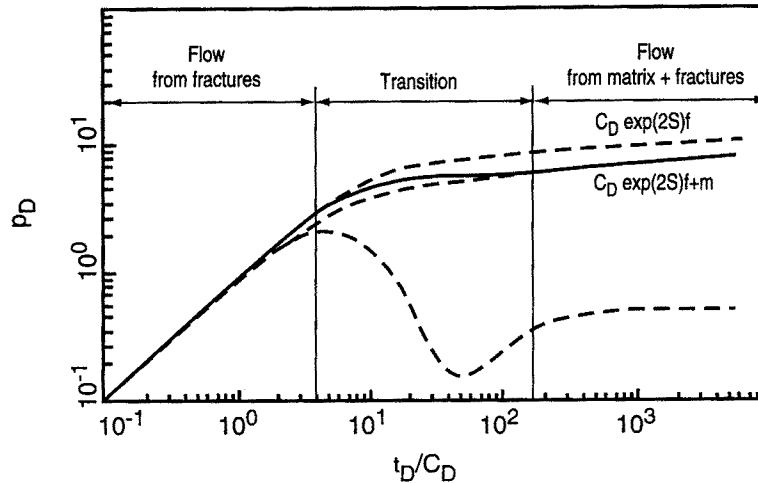


Fig. 13.2

13.6.1 Flow from the fractures

Because of their high permeability, the fractures take part in production first.

During this period, the fractured reservoir behaves like a homogeneous reservoir with a permeability of k_f and a capacity of \mathcal{C}_f .

Type curves:

The pressure variations during this flow can be described by the type curve for homogeneous reservoirs corresponding to (Fig. 13.2):

$$C_D \exp(2S) = C_{Df} \exp(2S)$$

Conventional analysis:

If the wellbore storage has ended before the transition period begins, the flow from the fractures corresponds to a semi-log straight line with the following equation:

$$p_i - p_{wf} = \frac{\delta q B \mu}{h_f h} \left(\log t + \log \frac{k_f}{c_f \mu r_w^2} - \beta + 0.87 S \right) \quad (13.18)$$

$$\begin{array}{lll} \delta = 162.6 & \beta = 3.23 & \text{(in practical US units)} \\ \delta = 21.5 & \beta = 3.10 & \text{(in practical metric units).} \end{array}$$

Derivative:

A stabilization at 0.5 of the dimensionless pressure derivative corresponds to this first semi-log straight line.

The first semi-log straight line and the stabilization of the derivative are almost never observed. The wellbore storage effect, even with a bottomhole shut-in device, is generally too great to allow them to be observed.

13.6.2 Transition period

This period corresponds to when the matrix begins to contribute to production.

Analysis of the depletion of a matrix block in a fractured medium shows that after a transient flow period, a pseudosteady-state regime is established in the matrix block.

Two approaches are proposed in technical literature to describe matrix-fracture flow:

- The first is by Warren and Root [Ref. 14, 22] and consists in considering that matrix-fracture interporosity flow is immediately pseudosteady-state. This matrix-fracture flow model is called **pseudosteady-state interporosity flow**.
- The second, by A. de Swann [Ref. 17], does not use this hypothesis. The matrix-fracture flow model is called **transient interporosity flow**.

The wellbore storage effect can hide the transition period.

However, when the transition period is visible it is characterized by the dip shown on the derivative (Fig. 13.2). The position and the amplitude of the dip depend respectively on the ease of matrix-fracture flow (the λ parameter) and on the capacity contrast between matrix and fractures (ω parameter).

- **Influence of matrix-fracture exchange: λ parameter**

The matrix-fracture flow is characterized differently depending on whether the pseudosteady-state or the transient model is used to describe it.

Pseudosteady-state model:

The matrix-fracture flow is characterized by the λ parameter (see section 13.5):

$$\lambda = \alpha r_w^2 \frac{k_m}{k_f}$$

or by the parameter $\lambda \exp(2S)$ when the effective radius method is used (the well with a radius r_w and skin S is replaced by a well with a radius $r_w' = r_w \exp(-S)$ and zero skin, see Chapter 3).

Transient model:

With this model, the matrix-fracture flow depends not only on λ but also on the geometry of the matrix blocks.

These two effects are taken into account by the parameter β' :

$$\beta' = a \frac{(C_D \exp(2S))_{f+m}}{\lambda} \quad (13.19)$$

The parameter a depends on the geometry of the matrix blocks.

Two shapes of matrix blocks are usually considered:

– Slab matrix blocs:

$$a = 1.8914$$

This model is call 1D transient (1 fracture plane).

– Cubic or spherical matrix blocs:

$$a = 1.0508$$

This model is called 3D transient (3 fracture planes).

For the same value of λ , Figure 13.3 shows the pressure derivative with the three matrix-fracture flow models (pseudosteady-state, 1D transient, 3D transient) for the same value of λ .

There is almost no difference between 1D and 3D transient interporosity flow.

A wide difference exists between the pseudosteady-state and the transient interporosity flow models:

– The dip of the derivative is much more accentuated with the pseudosteady-state model.

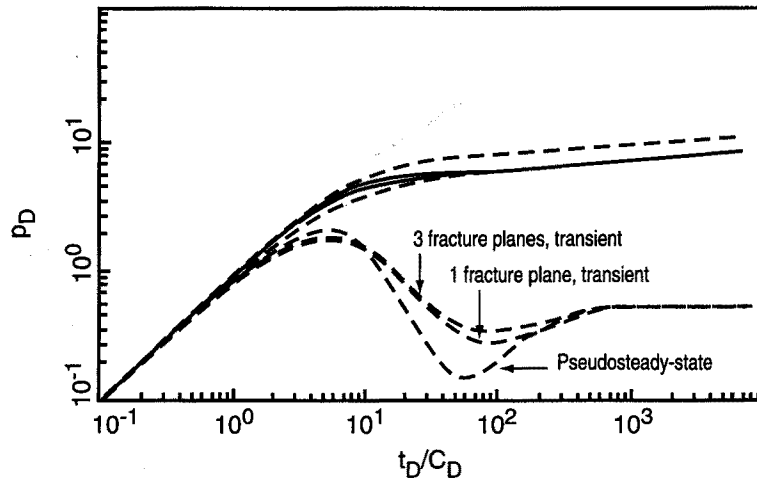


Fig. 13.3

- With the transient model, during transition the dimensionless pressure derivative is stabilized at 0.25, one-half the value observed during matrix-fracture flow.

Stabilization corresponds to a semi-log straight line with the following equation [Ref. 26]:

$$p_i - p_{wf} = \frac{1}{2} \frac{\delta q B \mu}{k_f h} \left(\log t + \log \frac{k}{\phi \mu c_f r_w^2} - \log \lambda (1 - \omega) - \beta + 1.74 S \right) \quad (13.20)$$

$$\begin{array}{lll} \delta = 162.6 & \beta = 3.13 & \text{(in practical US units)} \\ \delta = 21.5 & \beta = 3 & \text{(in practical metric units).} \end{array}$$

In buildup the derivative may however stabilize at a lower level (less than 0.25), should the global matrix-fracture flow not have been reached during the previous drawdown period.

Figures 13.4 and 13.5 show the effect of a variation in the λ parameter, with the pseudosteady-state and the transient model respectively.

They were plotted with negligible wellbore storage in order to highlight the influence of the λ parameter.

In both cases a decrease in the λ parameter delays the beginning of the transition period. The shape of the transition period does not depend on the value of λ .

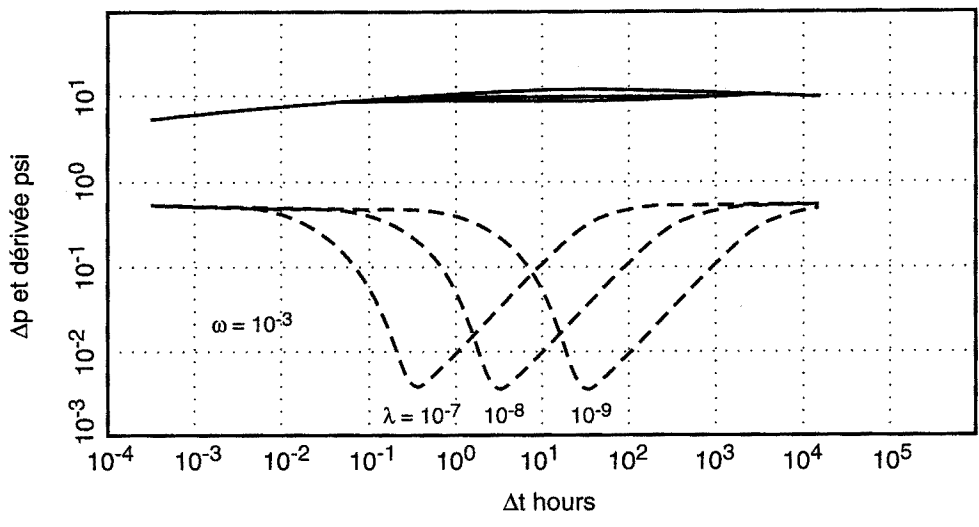


Fig. 13.4 Pseudosteady-state interporosity flow. Influence of λ

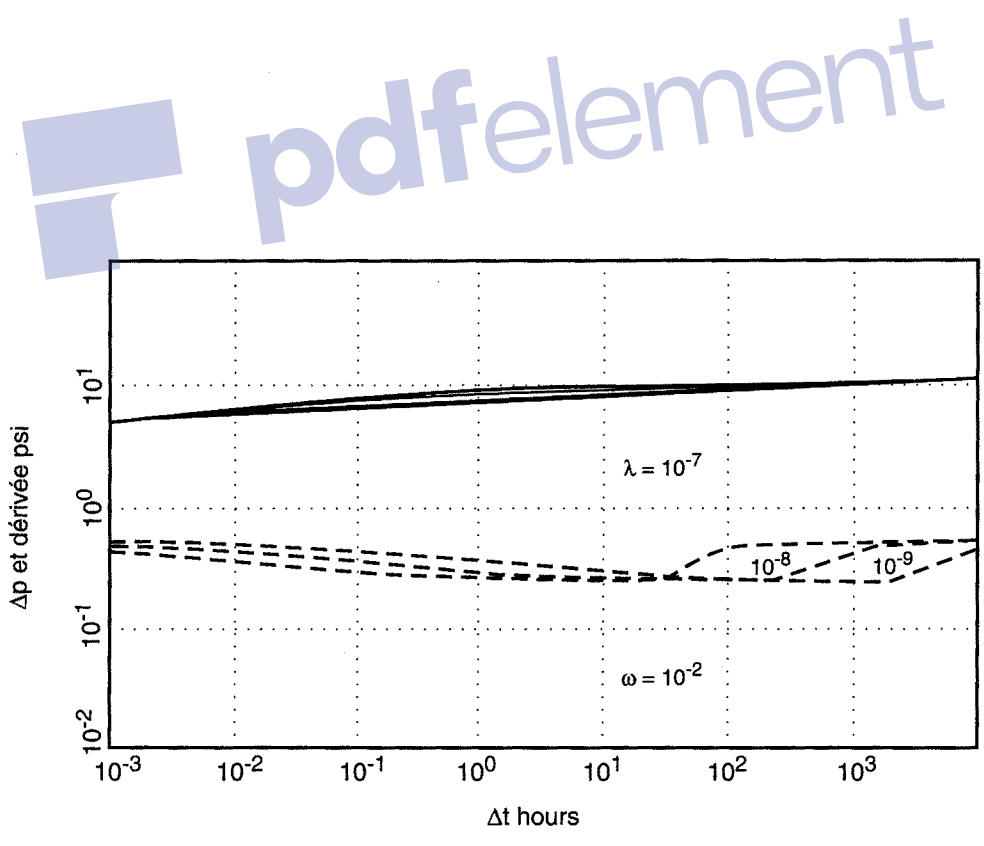


Fig. 13.5 1D Transient interporosity flow. Influence of λ

In reality the wellbore storage effect often hides part of the transition. It affects the way the transition looks on the derivative.

• **Influence of the capacity contrast: the ω parameter**

The ω parameter takes into account the capacity contrast that exists between the fractures and the reservoir:

$$\omega = \frac{\mathcal{C}_f}{\mathcal{C}_{f+m}} = \frac{(C_D \exp(2S))_{f+m}}{(C_D \exp(2S))_f} \quad (13.21)$$

During the transition from fracture flow to matrix-fracture flow, the capacity goes from \mathcal{C}_f to \mathcal{C}_{f+m} .

Figures 13.6 and 13.7 illustrate the influence of the capacity contrast ω on a type curve and its derivative with the two matrix-fracture interporosity flow models.

The wellbore storage is negligible in order to highlight the effect of the ω parameter.

The variation of ω has the same effect with the two models: the closer the value of ω is to 1, the later the beginning of transition.

With the transient model (Fig. 13.7) the dip in the derivative stabilizes at 0.25.

With the pseudosteady-state model (Fig. 13.6) the smaller the value of ω , the more accentuated the dip.

13.6.3 Global matrix-fracture flow

Once the transition period has ended, the reservoir behaves like a homogeneous reservoir again:

- with a permeability of k_f ;
- a capacity of \mathcal{C}_{f+m} .

Type curves:

The pressure variations during this flow are described by the type curve for homogeneous reservoirs corresponding to $C_D \exp(2S) = C_{Df+m} \exp(2S)$ (Fig. 13.2).

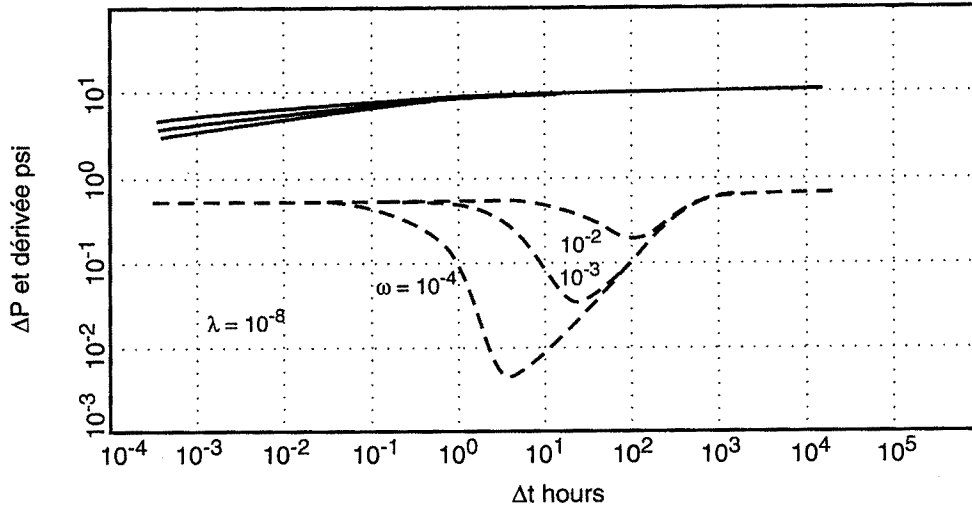


Fig.13.6 Pseudosteady-state interporosity flow. Influence of ω

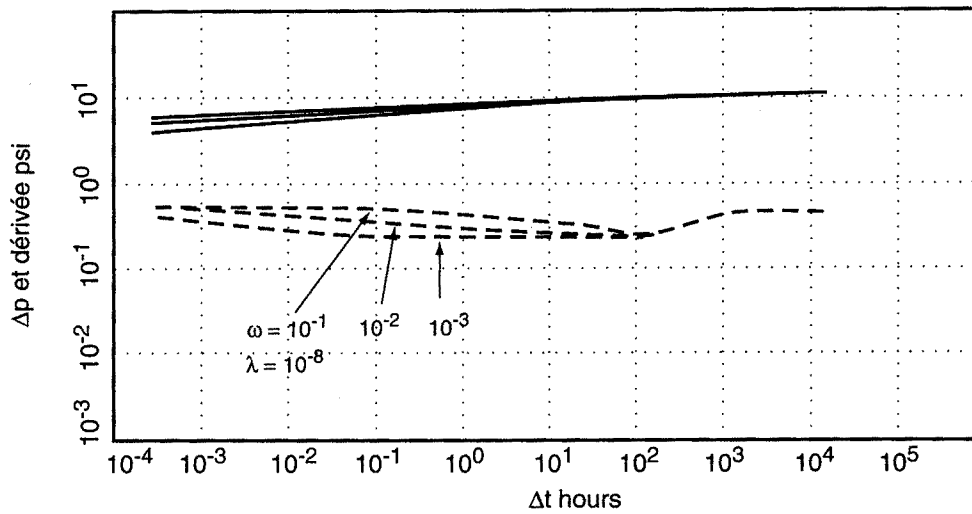


Fig. 13.7 Transient interporosity flow. Influence of ω

Conventional analysis:

The global matrix-fracture flow corresponds to a semi-log straight line with the following equation:

$$p_i - p_{wf} = \frac{\delta q B \mu}{k_f h} \left(\log t + \log \frac{k_f}{C_{f+m} \mu r_w^2} - \beta + 0.87 S \right) \quad (13.22)$$

$$\begin{array}{lll} \delta = 162.6 & \beta = 3.23 & \text{(in practical US units)} \\ \delta = 21.5 & \beta = 3.10 & \text{(in practical metric units).} \end{array}$$

This straight line is parallel to the first semi-log straight line that can be observed during fracture flow (Fig. 13.8).

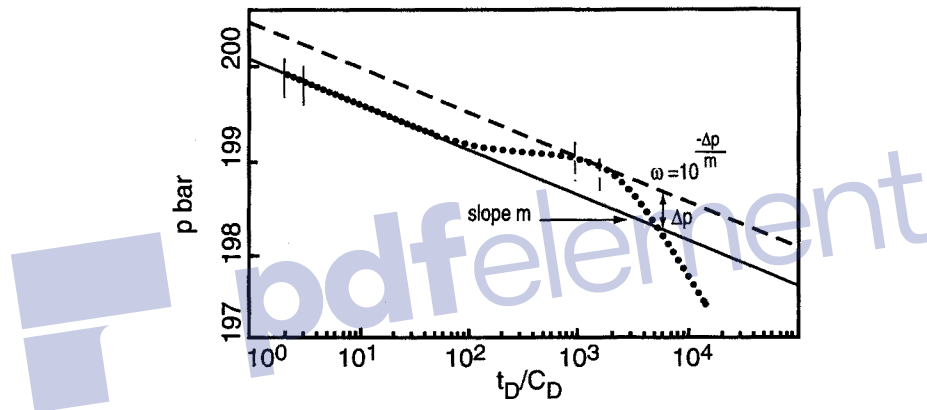


Fig. 13.8

The distance Δp , between the two straight lines depends on the value of ω :

$$\omega = 10^{-\Delta p/m} \quad (13.23)$$

where m is the slope of the two semi-log straight lines.

In fact, the first semi-log straight line is almost never observed. Trying to draw a parallel to the second semi-log straight line through the first measurement points usually corresponds to drawing a tangent to the pressure curve during the wellbore storage effect. Under these conditions, the value of ω estimated from the distance between these two parallel straight lines is a value by excess (Fig. 13.8).

Derivative:

The second semi-log straight line corresponds to a stabilization at 0.5 of the dimensionless pressure derivative (Fig. 13.2).

13.6.4 Nota bene

The wellbore storage effect often hides the first two flows. In this case the test can not be used to determine either λ or ω . No characterization of the fractures can be done.

The only way to realize that the reservoir is fractured using tests is to consider the skin and the reservoir permeability values. Two observations suggest a reservoir is fractured:

- when the permeability deduced from the test is substantially higher (factor of 10) than what has been measured on core samples or by RFT in the matrix;
- a negative skin lower than -2 .

13.7 CHOOSING BETWEEN THE PSEUDOSTEADY-STATE AND THE TRANSIENT INTERPOROSITY FLOW MODELS

There are two models to describe the interporosity flow:

- the transient model (A. de Swann);
- the pseudosteady-state model (Warren and Root).

From the standpoint of theory alone, the transient model seems to be closer to reality than the pseudosteady-state model. It involves no restrictive hypotheses on combined matrix-fracture interporosity flow.

In reality things are quite different since it is usually much easier to match a transition using a pseudosteady-state model than with a transient model.

An explanation for this paradox can be found in the fact that the model used to describe the fractured reservoir is very unsophisticated:

- the matrix blocks are all identical and of the same size;
- the matrix blocks are perfectly homogeneous.

This description was considerably improved on by H. Cinco et al. [Ref. 20]. In their model:

- The blocks are distributed according to several sizes.
- Each block has a skin at its interface with the fractures. The skin takes mineral deposits in the fractures into account.
- The matrix-fracture interporosity flow is a transient model.

The model accounts for behavior observed with the transient model as well as with the pseudosteady-state model:

- behavior corresponding to the pseudosteady-state model can be seen with a damage-type skin around the matrix blocks;
- reservoirs with regular distribution of block sizes behave in a way that can be accounted for with one single block size.

The Cinco model also shows that reservoirs where distribution of block size is irregular and varied behave in a way that mainly corresponds to small blocks. A good-quality pressure derivative is, however, required to use this model to determine matrix block sizes.

When this model is not available, the pseudosteady-state model can be used to interpret most tests in fractured media. This indicates that most matrix blocks produce in the fractures through a reduced permeability zone.

This representation corresponds to the conventional image of a fractured reservoir:

- a low-permeability matrix;
- partially plugged fractures where there is still a flow channel;
- fluids circulating from the matrix to the channel through filling up the fractures.

Fig. 13.9 from L.H. Reiss [Ref. 21] shows an example corresponding to this image.

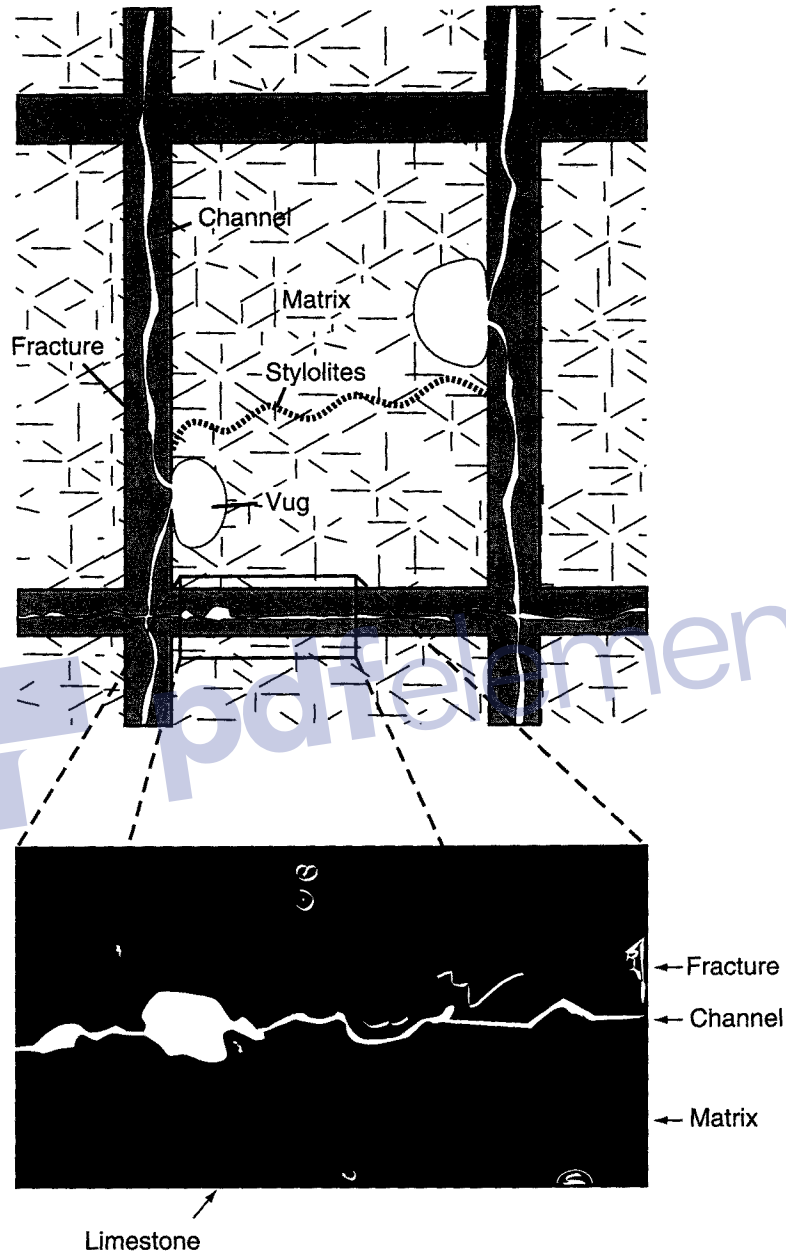
13.8 TYPE CURVE ANALYSIS

The type curves that can be used to analyze a test in a fractured reservoir were developed by A. Gringarten, D. Bourdet et al. [Ref. 18, 19].

They were described and analyzed in detail by F. Daviau in his *Interprétation des essais de puits. Les méthodes nouvelles* [Ref. 1]. Only the major points in his description and analysis will be discussed here.

• Description of the type curves

There are two sorts of type curves, adapted to the two matrix-fracture interporosity flow models: pseudosteady-state or transient (Fig. 13.10 and Fig. 13.11).



**Fig. 13.9 Schematic drawing of a matrix.
Secondary porosity inside a fracture**

(From L.H. Reiss [Ref. 21])

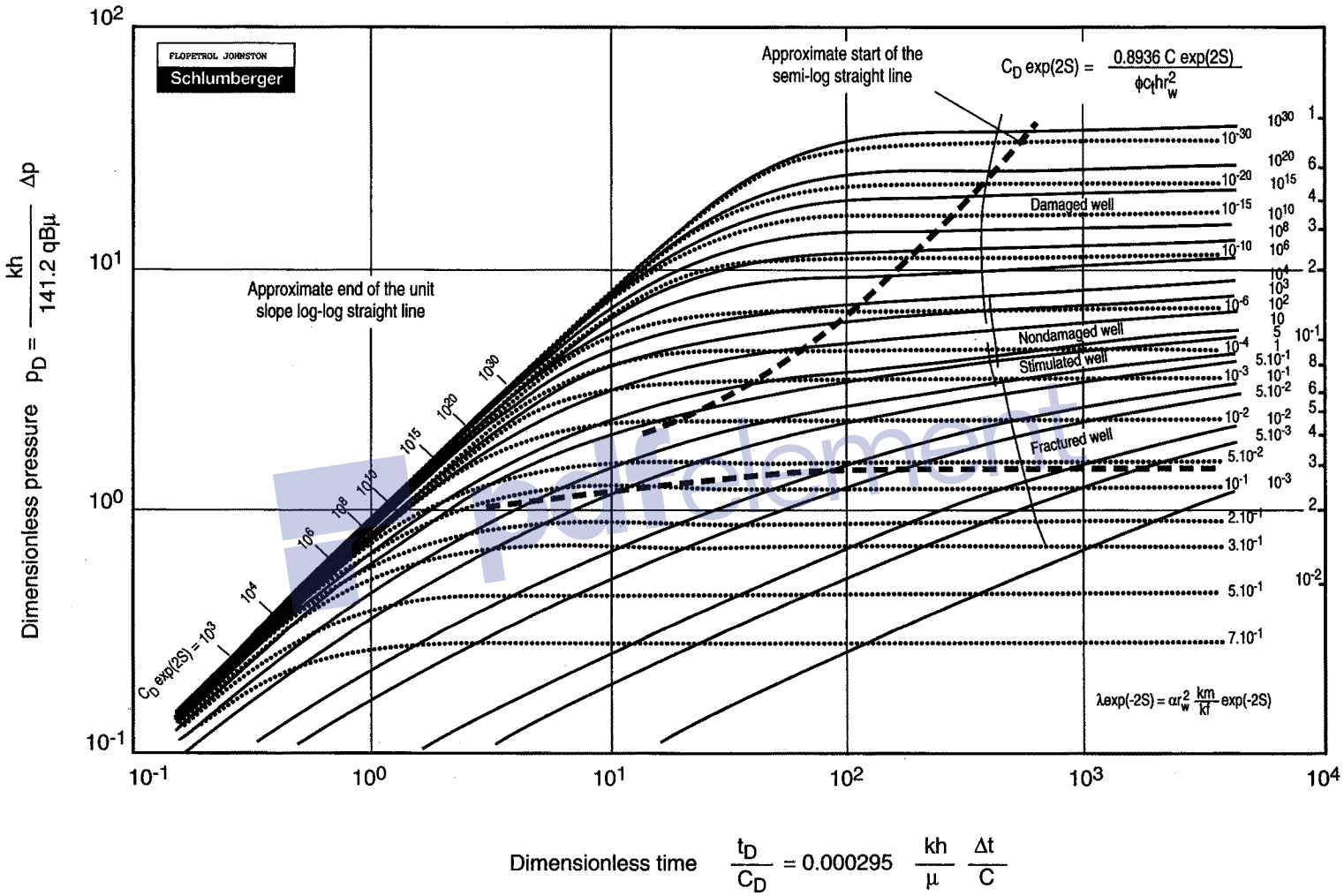


Fig. 13.10 Type curves for a well with wellbore storage and skin, reservoir with double porosity behavior (pseudosteady-state interporosity flow)

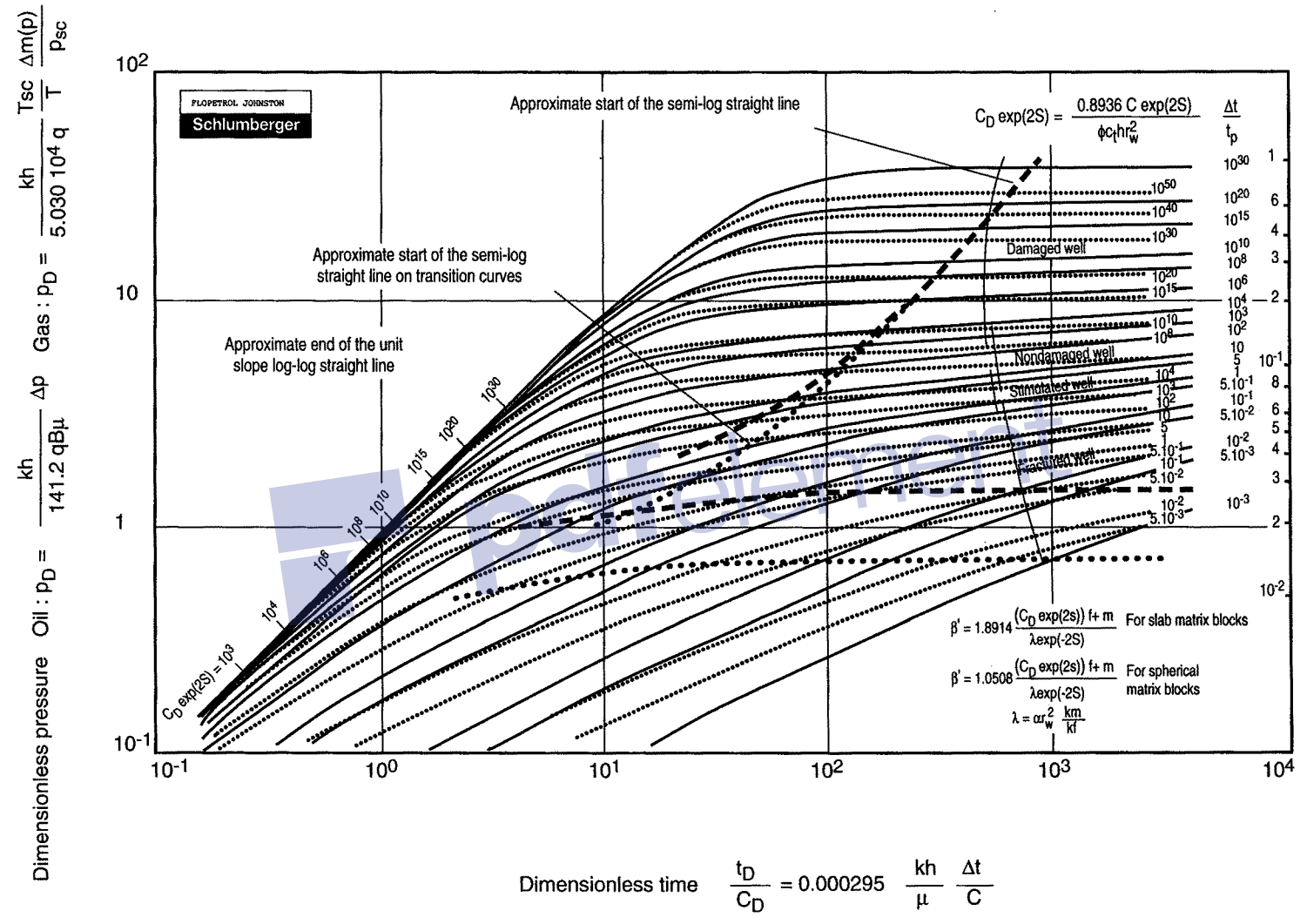


Fig. 13.11 Type curves for a well with wellbore storage and skin, reservoir with double porosity behavior (transient interporosity flow)

They have several points in common with the type curves for homogeneous reservoirs:

- a log-log scale;
- a representation of p_D versus t_D/C_D ;
- type curves changing from one to another by the value of $C_D \exp(2S)$.

The curves are identical to the ones used for homogeneous reservoirs (Fig. 5.1). They reflect the reservoir's behavior before and after the transition period.

Type curves for fractured reservoirs have an extra set of curves (dotted lines) that show the reservoir's behavior during the interporosity flow:

- $\lambda \exp(-2S)$ curves for the pseudosteady-state model (Fig. 13.10);
- β' curves for the transient model (Fig. 13.11).

• Steps in type curve matching

The interpretation method is similar to the one illustrated in section 5.3 for a homogeneous reservoir. It consists in the following steps:

- 1 Plot the measured pressure changes on tracing paper using the log-log scale of the type curves.
- 2 By translation, look for three type curves that the measurement points can simultaneously be superposed on (Fig. 13.12):
 - One type curve $C_D \exp(2S)$ for the first points: this one corresponds to the flow from fractures.
 - One curve $\lambda \exp(-2S)$ (or β' for the pseudosteady-state model) for the intermediate points: this one corresponds to the transition period.
 - One last curve $C_D \exp(2S)$ for the last points: this one corresponds to the combined matrix-fracture flow.
- 3 Note the values of $C_D \exp(2S)$ and one value of $\lambda \exp(-2S)$.
- 4 Note the coordinates of a match point M that is both in the type curve axis system (p_D , t_D/C_D) and in the measured field data point system (Δp , Δt).

• Interpretation

Permeability:

The proportionality ratio between the coordinates p_D and Δp of point M is used to determine the reservoir's $k_f h$:

$$k_f h = 141.2 \text{ qB } \mu \frac{(p_D)_M}{(\Delta p)_M} \quad (13.24)$$

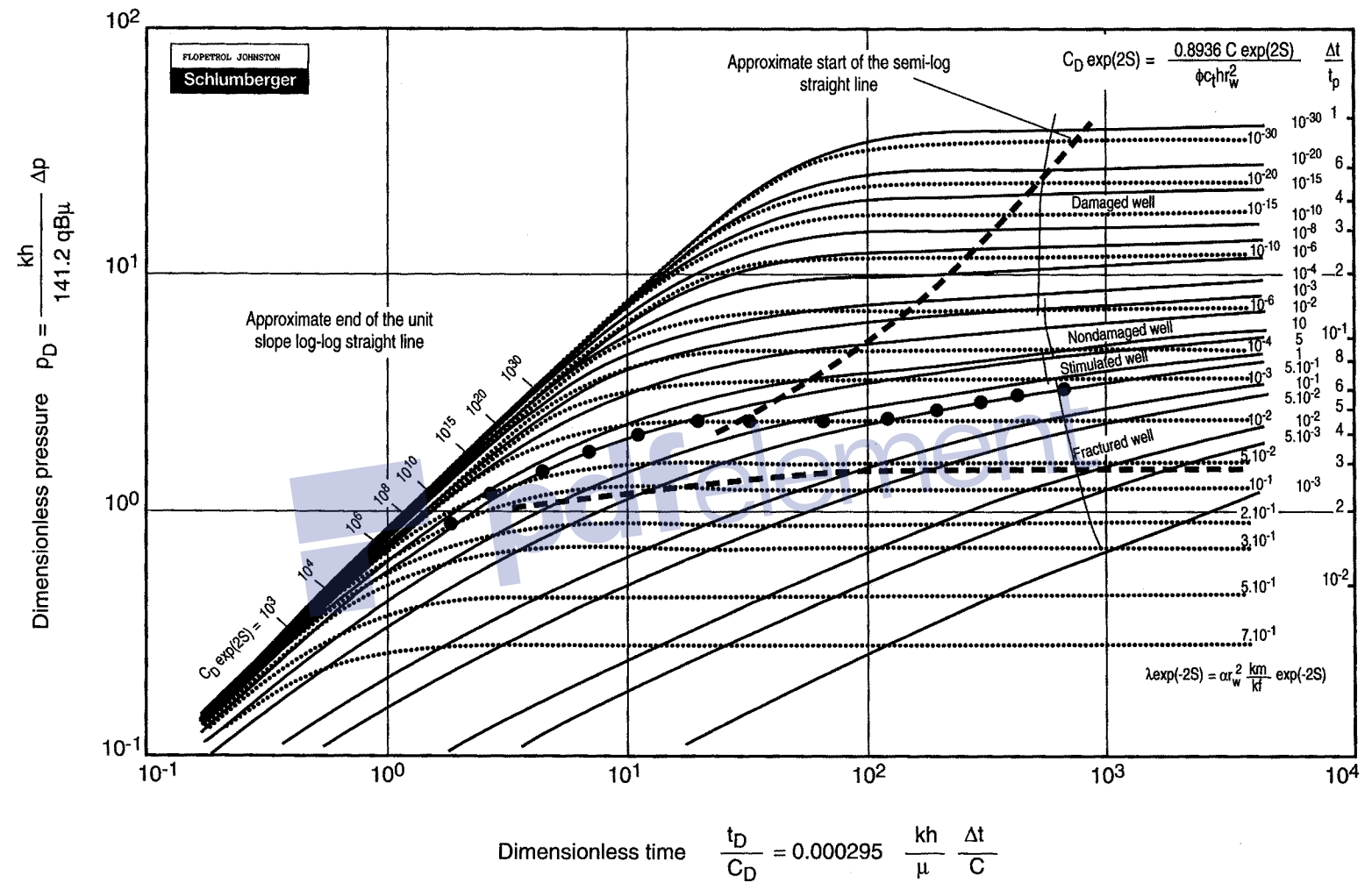


Fig. 13.12 Type curves for a well with wellbore storage and skin, double porosity behavior (pseudosteady-state regime between the two porosity systems)

The equivalent permeability of the fractures $k_f h$ is obtained by dividing $k_f h$ by the reservoir's net pay.

Wellbore storage:

The proportionality factor between the coordinates t_D/C_D and Δt of point M is used to determine the wellbore storage:

$$C = \frac{0.000295 k_f h (\Delta t)_M}{\mu (t_D/C_D)_M} \quad (13.25)$$

Capacity contrast ω :

The value of $C_D \exp(2S)$ of the type curves where the first and the last measurement points match corresponds to $(C_D \exp(2S))_f$ and $(C_D \exp(2S))_{f+m}$ respectively.

The ratio between these two values determines the capacity contrast between the reservoir and the fractures:

$$\omega = \frac{(C_D \exp(2S))_{f+m}}{(C_D \exp(2S))_f} \quad (13.26)$$

Skin:

The value of $C_D \exp(2S)$ from the type curve where the last measurement points match corresponds to the $C_D \exp(2S)$ of the reservoir: $(C_D \exp(2S))_{f+m}$.

The capacity \mathcal{C}_m (equation 13.9) of the matrix can be determined, the same as in a homogeneous reservoir, by well logs and core analysis.

The global capacity of the reservoir can be deduced from it by using the value of ω calculated before and equation (13.15):

$$\mathcal{C}_{f+m} = \frac{\mathcal{C}_m}{1 - \omega} \quad (13.27)$$

Once the wellbore storage C has been determined (equation 13.25), C_{Df+m} can be calculated:

$$C_{Df+m} = \frac{0.89 C}{\mathcal{C}_{f+m} h r_w^2} \quad (13.28)$$

The values of C_{Df+m} and of $(C_D \exp(2S))_{f+m}$ are used to calculate the skin of the well:

$$S = \frac{1}{2} \ln \frac{(C_D \exp(2S))_{f+m}}{C_{Df+m}} \quad (13.29)$$

Matrix-fracture flow; λ parameter:

The value of $\lambda \exp(-2S)$ from the type curve where the transition points match is used to determine the λ parameter. It characterizes how easily exchanges occur between the matrix and the fractures:

$$\lambda = (\lambda \exp(-2S)) \exp(2S) \quad (13.30)$$

In the transient model, the transition curves are specified in β' :

$$\beta = a \frac{(C_D \exp(2S))_{f+m}}{\lambda \exp(-2S)} \quad (13.31)$$

a depends on the geometry of the matrix blocks.

$a = 1.89$ for sheets ($n = 1$)

$a = 1.05$ for cubes ($n = 3$).

β' is used to calculate λ :

$$\lambda = \frac{a(C_D \exp(2S))_{f+m} \exp(2S)}{\beta'} \quad (13.32)$$

Limitations of using type curves for fractured reservoirs:

First of all, type curves for fractured reservoirs have the same limitations as those for homogeneous reservoirs:

- They can be used directly only if the flow rate history can be summed up to one single flow rate.
- They can be used directly in buildup provided that, before shut-in, there has been a constant flow rate period that is long compared to buildup time (condition for using the MDH method).
- When drawdown time is short, the Agarwal method (see section 4.4) can be applied with restrictions on its use similar to those mentioned for homogeneous reservoirs, i.e. the end of the wellbore storage effect and the end of the transition must have been reached during drawdown before shut-in.

- When one of these conditions is not verified, a well model with a flow rate superposition function is the only way to take the flow rate history into account.
- As for homogeneous reservoirs, the points corresponding to the wellbore storage effect are superposed on a type curve provided the wellbore storage can be considered constant. If wellbore storage is highly variable (a lot of low-pressure gas for example), superposition is often impossible and it is difficult to determine $(C_D \exp(2S))_f$ and ω .

In addition to the above-mentioned restrictions, there is a further limitation involving $\lambda \exp(-2S)$ or β' transition curves. They were plotted for one single value of ω ($\omega = 0$). To deal with other values, a set of curves should have been plotted for each value of $\lambda \exp(-2S)$ instead of only one curve. Only one value of ω ($\omega = 0$) is considered so that the curves are easier to read.

For high values of ω (greater than 0.1), measurement points can be superposed on a transition curve only on a few points.

The well model is the only way to overcome this limitation.

13.9 TYPE CURVES DERIVATIVES

Type curves derivatives were developed by Bourdet et al. [Ref. 19, 27] to analyze tests on fractured reservoirs.

Two sorts of curves exist depending on the matrix-fracture interporosity flow model:

- with pseudosteady-state interporosity flow (Fig. 13.13);
- with transient interporosity flow (Fig. 13.14).

Pseudosteady-state interporosity flow:

Figure 13.15 shows an example of a match using type curves derivatives.

Interpretation has similarities with homogeneous reservoir procedure:

- Points corresponding to the period of wellbore storage alone are matched on the 1-slope straight line passing through the origin.
- Points corresponding to the matrix-fracture flow are matched on the horizontal $1/2$ ordinate straight line.

FLOPETROL JOHNSON
Schlumberger

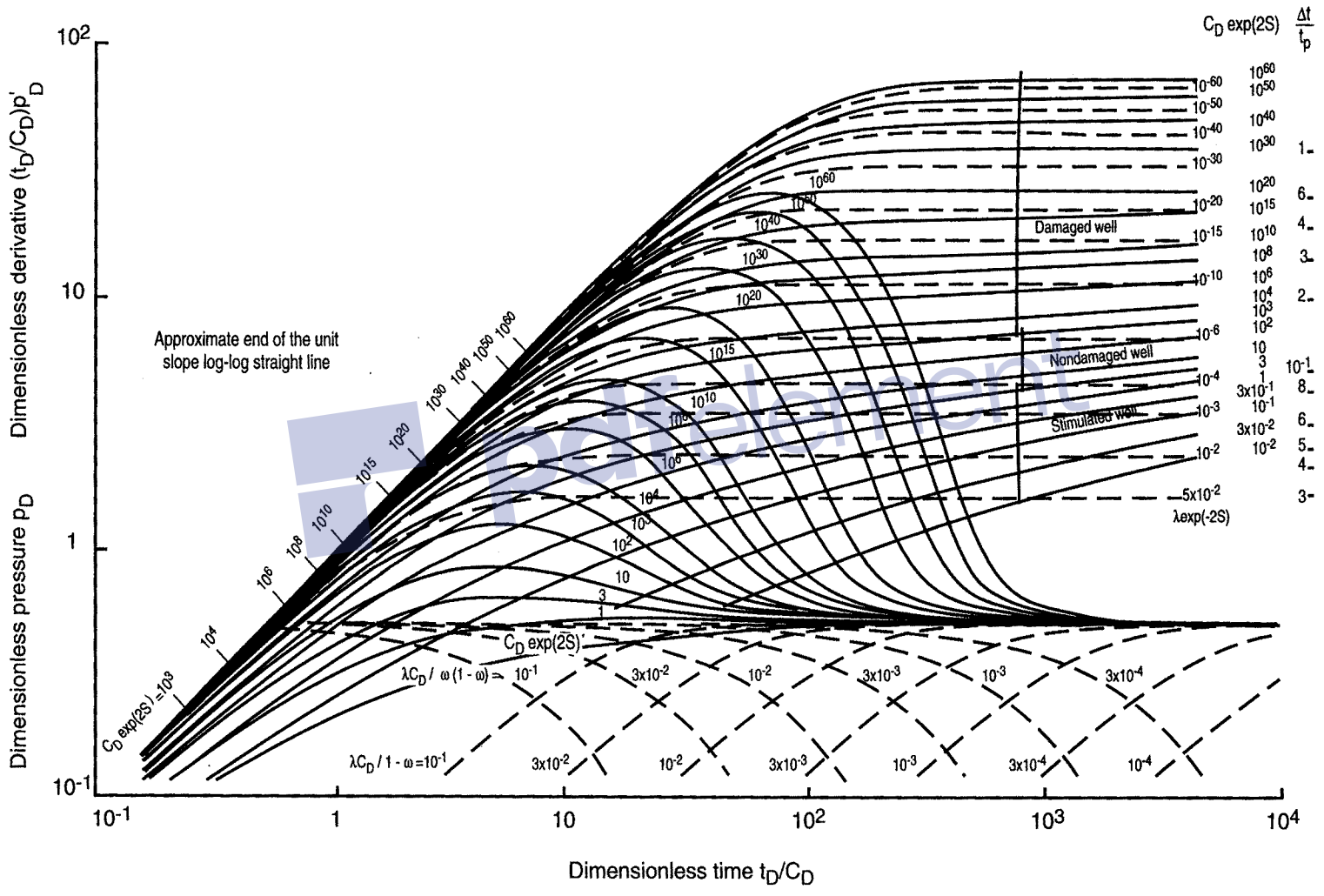


Fig. 13.13

FLOPETROL JOHNSTON
Schlumberger

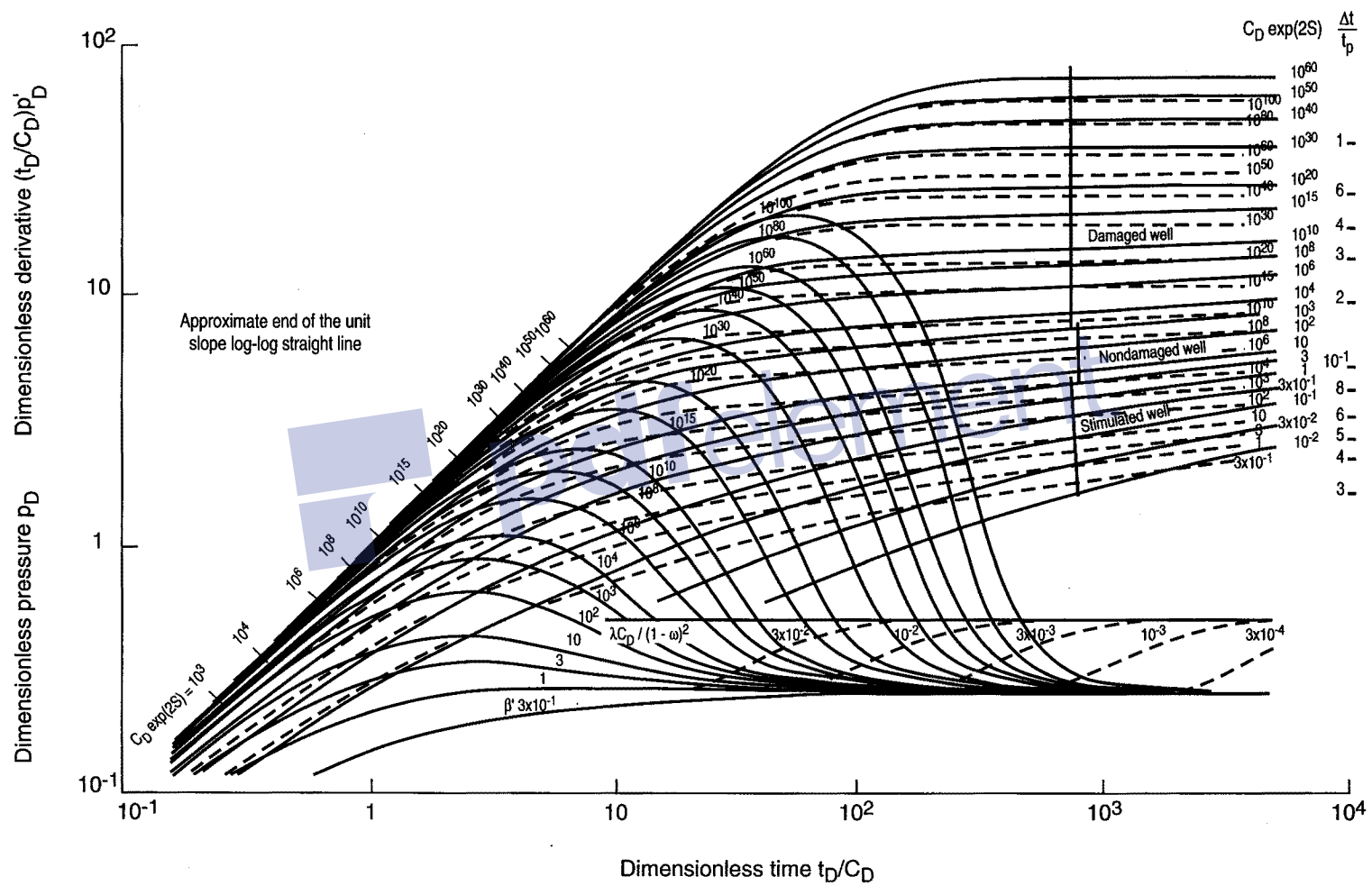


Fig. 13.14

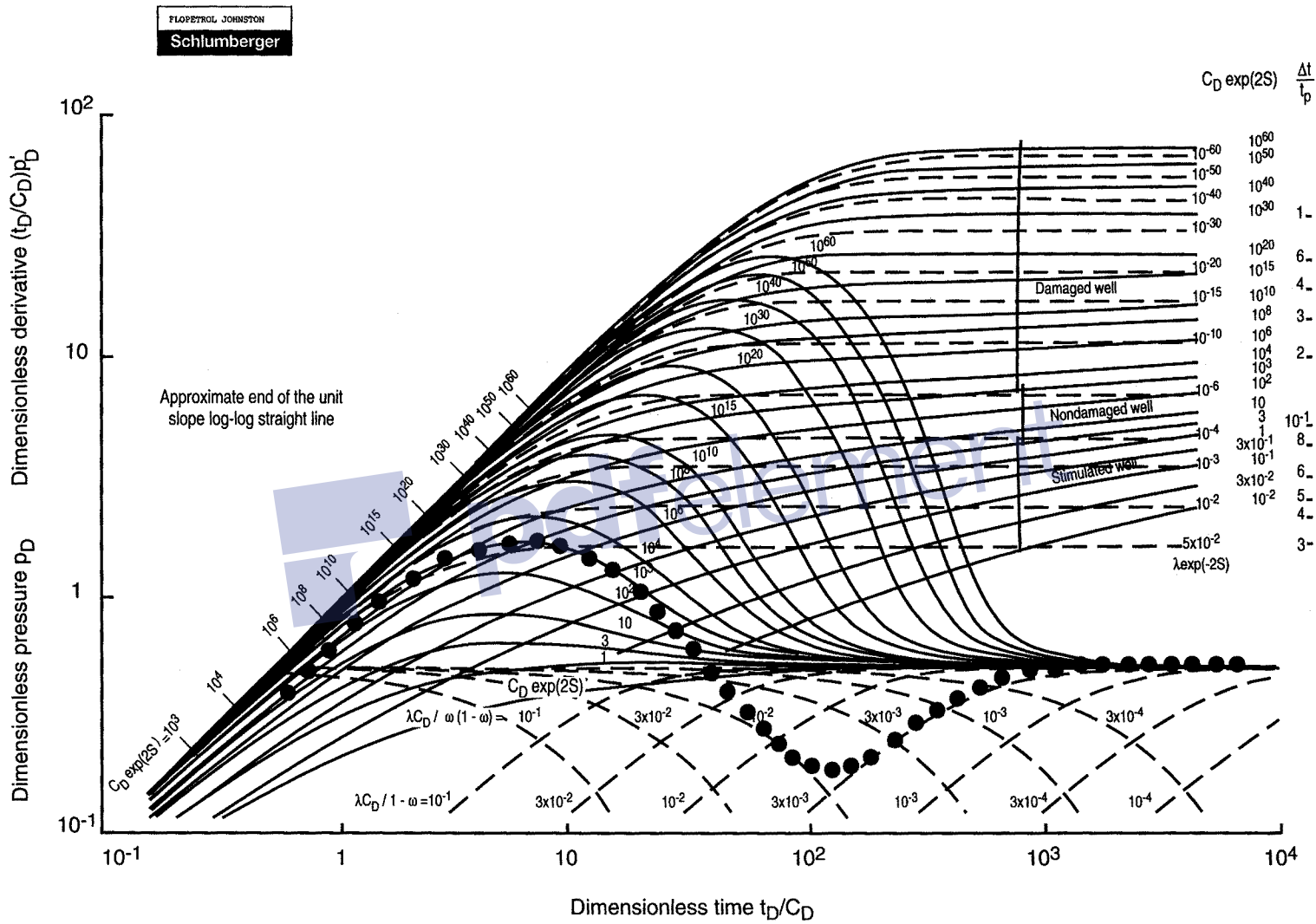


Fig. 13.15

If the wellbore storage effect is small enough, radial flow in the fractures is visible and corresponds to a dimensionless pressure derivative equal to 0.5.

The transition period is interpreted using two curves:

- one $\lambda C_D/\omega(1 - \omega)$ curve;
- one $\lambda C_D/(1 - \omega)$ curve.

The value of these two curves is used to calculate ω and λ .

Transient interporosity flow:

Figure 13.16 shows an example of a match using the derivative type curve for the transient model.

Three curves are used for interpretation:

- The derivative of transition curves β' : these curves stabilize at 0.25 for long times.
- Curves with $\lambda C_D(1 - \omega)^2$: they show the end of the transition period.
- The horizontal 0.5 ordinate straight line: it corresponds to the final stabilization reached with matrix-fracture interporosity flow.

13.10 TWO EXAMPLES OF INTERPRETATION IN A FRACTURED RESERVOIR

• **Example 1:**

The reservoir is composed of low-permeability silts alternating with fractured limestone beds through which fluids are produced. It can be treated like a fractured reservoir.

The matrix blocks are the silts. They can be considered slabs with metric thickness as estimated by well logs in the well considered in Figure 13.15.

Figure 13.17 show the multirate type curve and derivative that best fits the test pressure data. Interpretation was performed with a pseudosteady-state interporosity flow model for fractured reservoirs.

Figure 13.18 shows conventional interpretation of the second semi-log straight line, the only one visible in this test.

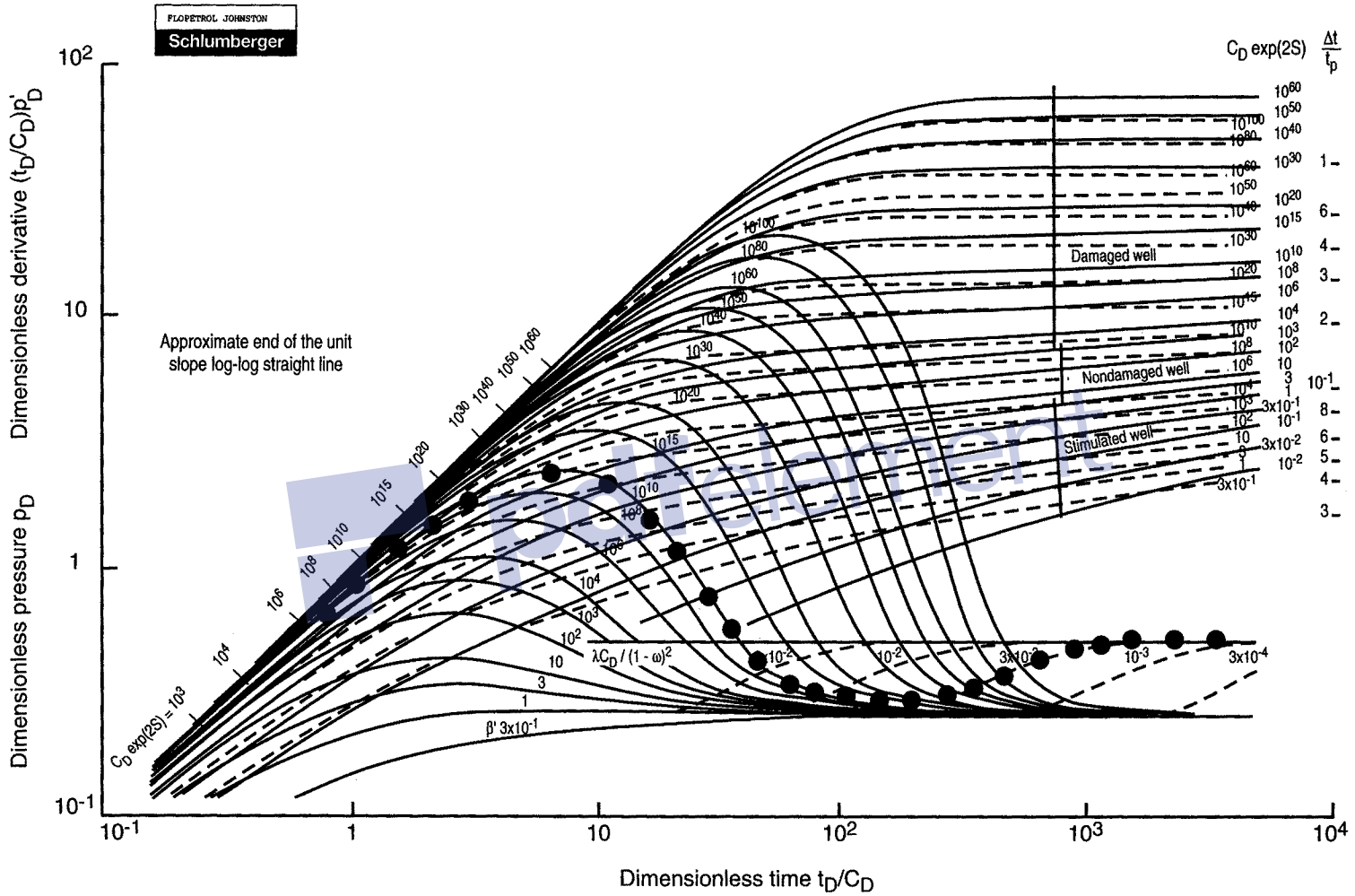


Fig. 13.16

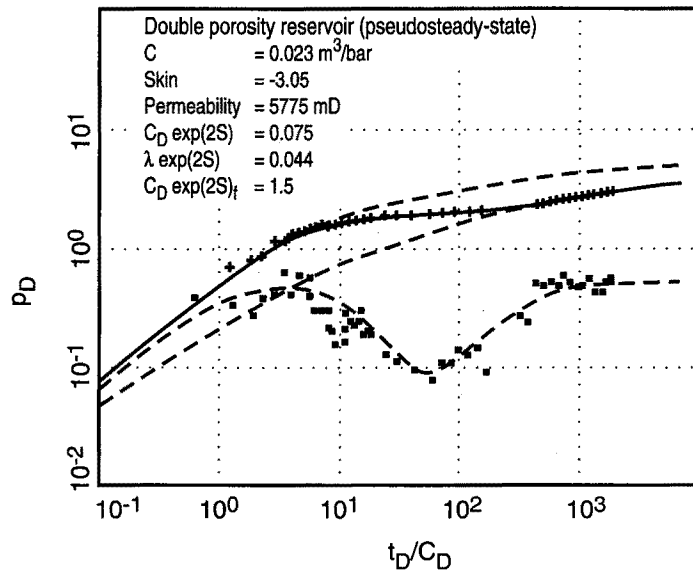


Fig. 13.17

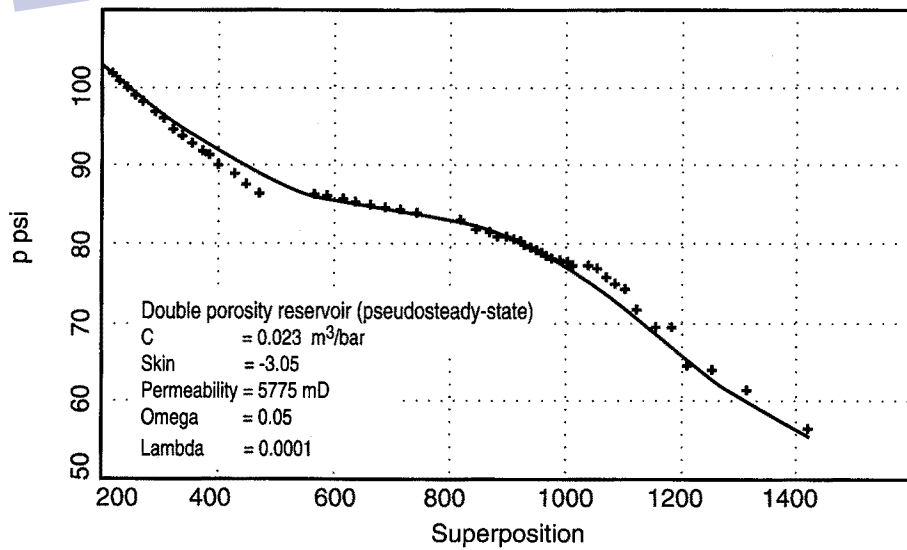


Fig. 13.18

Results:

The test is interpreted, as in most cases, using the pseudosteady-state model.

Test results confirm the presence of fractures:

$k_f = 5774$ mD whereas the permeability of core samples taken in the reservoir ranges between 0.2 and 20 mD.

Skin = -3 The well skin is lower than -2.

Interpretation of the transition gives:

- $\omega = 0.05$

This means that the fractures contribute to only 5% of the total reservoir production in terms of capacity.

- $\lambda = 10^{-4}$

The size of the blocks is determined by logs. The value of λ is used to determine the matrix permeability of the reservoir:

$$\lambda = \alpha r_w^2 \frac{k_m}{k_f}$$

$$\alpha = \frac{n(n+1)}{r_m^2}$$

Data:

$n = 1$ (slabs)

$r_m = 0.5$ m ($a = 1$ m, $n = 1$)

$r_w = 0.15$ m.

Test interpretation:

$\lambda = 10^{-4}$

$k_f = 5700$ mD.

Based on the data and on the test interpretation, a matrix permeability of 2 mD can be deduced which is in agreement with what was measured on core samples.

• Example 2:

Geologists describe this fractured reservoir as being made up of large slabs with a spacing distance of ten to several tens of meters. The large slabs are themselves microfractured.

Core samples taken from the well indicate a matrix permeability ranging between 0.1 and 1 mD.

Figure 13.19 shows the multirate fractured reservoir type curve and derivative that best fits the test pressure measurements.

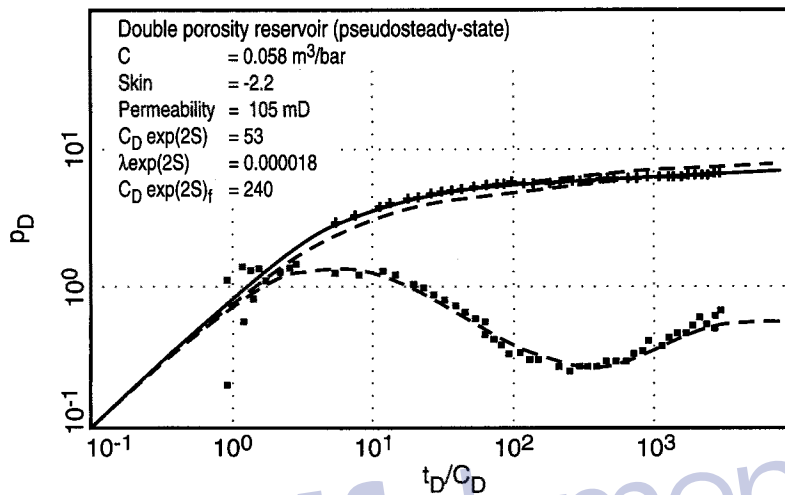


Fig. 13.19

Results:

The test is interpreted using the pseudosteady-state model.

The test results confirm the presence of fractures:

$k_f = 105$ mD whereas the matrix permeability ranges from 1 to 10 mD.

$S = -2.3$ The skin is lower than -2 .

The derivative exhibits a dip. The test interpretation gives:

- $\omega = 0.22$

This value means that 22% of the compressible capacity is located in the fractures, due to the high compressibility of the fractures:

$$\omega = \frac{C_f}{C_{f+m}}$$

$$C_f = (\phi_f V_f) (c_o + c_{pf})$$

$$C_m = (\phi_m V_m) c_{tm}$$

The total porosity of the matrix, $\phi_m V_m$ is 5%. Its total compressibility, c_{tm} , is $2 \cdot 10^{-5} \text{ psi}^{-1}$.

Assuming $\phi_f V_f$ is 0.1%, $c_{pf} = 0.0003 \text{ psi}^{-1}$. This value corresponds to the orders of magnitude observed in the most compressible porous media.

$$- \lambda = 10^{-7}$$

Since the matrix permeability is known, the value of λ can be used to determine the size of the matrix blocks.

Data:

$$n = 1 \text{ (slabs)}$$

$$k_m = 0.1 \text{ to } 1 \text{ mD}$$

$$r_w = 0.1 \text{ m.}$$

Test interpretation:

$$\lambda = 10^{-7}$$

$$k_f = 105 \text{ mD.}$$

From the data and the interpretation, a block size ranging between 15 and 50 m can be deduced. This is in agreement with the geological representation of the reservoir.

Chapter 14

Two-layer reservoirs

14.1 INTRODUCTION

The interpretation methods that have been presented in previous chapters assume that the reservoir is composed of one single layer.

Reservoirs are usually composed of a superposition of layers with different characteristics that may communicate in the reservoir.

This chapter deals with the simplest case of a multilayer reservoir: the reservoir made up of two layers.

It indicates how such a reservoir should be tested. It also justifies the assumption of homogeneous reservoir behavior that is adopted in most interpretations.

14.2 DESCRIPTION OF A TWO-LAYER RESERVOIR

The reservoir with two layers is illustrated by Figure 14.1. Each of the two layers is characterized by its:

- net thickness;
- porosity;
- saturation;
- pore compressibility;
- horizontal permeability;

- vertical permeability;
- skin.

The two layers communicate through a screen with a thickness h_e , and vertical permeability k_{ve} .

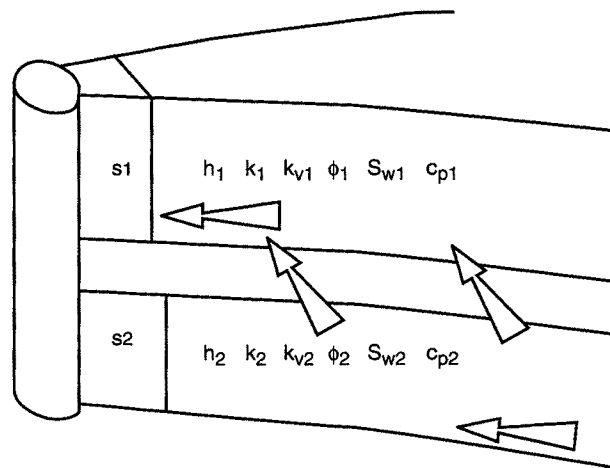


Fig. 14.1

14.3 THE BOURDET MODEL

The model used here to describe the two-layer reservoir was developed by D. Bourdet [Ref. 58]. It is based on the following assumptions:

- The fluids flow horizontally in each layer.
- The vertical flow between the two layers is instantaneously pseudosteady-state.

This model is similar to the pseudosteady-state double porosity reservoir model used to describe fissured reservoirs: two communicating reservoir systems with different characteristics. The flow from one system to the other is instantaneously pseudosteady-state.

There is, however, an important difference: the double porosity model makes the assumption that the permeability of one of the systems (matrix porosity in a fractured reservoir) is low compared to the other (fissure permeability). This hypothesis is not necessary in the D. Bourdet model. For this reason it can be qualified as a double porosity and double permeability model. It is used to describe the two-layer reservoir.

The main parameters that are involved in the model are:

- Total reservoir transmissivity:

$$kh = k_1 h_1 + k_2 h_2 \quad (14.1)$$

- Transmissivity contrast between the two layers described by the parameter κ :

$$\kappa = \frac{k_1 h_1}{k_1 h_1 + k_2 h_2} \quad (14.2)$$

- The skin of each layer: S_1, S_2 .
- Total reservoir capacity:

$$(\phi c_t) = \frac{(h \phi c_t)_1 + (h \phi c_t)_2}{h_1 + h_2} \quad (14.3)$$

- Capacity contrast between the two layers, which is described by the parameter ω the same as in the double porosity model:

$$\omega = \frac{(h \phi c_t)_1}{h \phi c_t} \quad (14.4)$$

- The exchange term between the two layers, which is described by the parameter λ the same as in the double porosity model.

This λ parameter can be related to the real reservoir parameters by using the Gao Cheng-Tai model [Ref. 59], used by C.A. Ehlig-Economides [Ref. 60] to describe multilayer reservoirs.

$$\lambda = \frac{r_w^2}{kh} \frac{2}{\frac{2h_e}{k_{ve}} + \frac{h_1}{k_{v1}} + \frac{h_2}{k_{v2}}} \quad (14.5)$$

The term λ has a simple meaning in two cases:

- The screen between the two layers severely limits communication between them. In this case h_e/k_{ve} is large compared to h_1/k_{v1} and h_2/k_{v2} . λ is used to determine the vertical permeability of the screen.

$$k_{ve} = \frac{kh}{r_w^2} h_e \lambda \quad (14.6)$$

- There is no screen between the two layers. λ is used to determine the vertical permeability of the reservoir. Assuming that $k_{v1} = k_{v2} = k_v$:

$$\frac{k_v}{k_h} = \frac{1}{2} \frac{h^2}{r_w^2} \lambda \quad (14.7)$$

- **Dimensionless wellbore storage**, which is described the same as in a homogenous reservoir by reference to the total reservoir capacity:

$$C_D = \frac{0.89 C}{h (\phi c_v) r_w^2} \quad (14.8)$$

14.4 TESTING A TWO-LAYER RESERVOIR

Several methods can be considered in testing a two-layer reservoir. They do not all allow the individual characteristics of each layer to be determined.

We will discuss three strategies:

- testing both layers simultaneously;
- testing each layer separately;
- testing one layer then both together.

14.4.1 Testing both layers simultaneously

This method consists in putting the two zones in production and testing them together.

This method generally provides only little information about the reservoir. *The reservoir usually behaves as if it were homogeneous* with the following characteristics:

- $kh = kh_1 + kh_2$;
- skin that can not be interpreted: it depends on the skin of each layer, the transmissivity contrast between the layers (κ parameter) and the exchange term between the layers (λ parameter).

This explains that even though reservoirs are very often vertically heterogeneous, they behave as if they were homogeneous during testing.

In some rare cases, a slight double porosity effect can be seen (Fig. 14.2). For this to be true, double porosity-type conditions must be observed:

- high capacity contrast between the two layers (ω close to 0 or to 1);
- high transmissivity contrast (κ close to 0 or to 1);
- the high capacity layer must have low transmissivity, therefore:
 - ω close to 0 when κ is close to 1
 - ω is close to 1 when κ is close to 0.

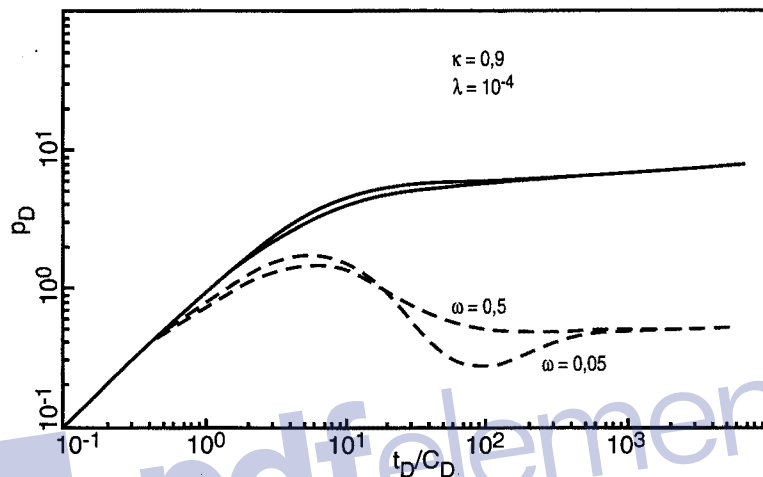


Fig. 14.2

14.4.2 Testing each layer separately

This method consists in producing only one of the two layers at a time in order to test it.

This procedure is often difficult to apply to each layer in succession. It is, however, the one that gives the most information.

The pressure change, and especially the derivative, show that three flow periods come one after the other during testing (Fig. 14.3):

- An initial radial flow period. Only the zone tested is involved in the flow. A stabilization of the derivative corresponds to it.
- A transition period when the derivative decreases. The decrease shows more reservoir thickness becoming involved. The time when it begins depends on the vertical communication between the two layers (λ parameter).
- A second radial flow period. Both layers are involved in flow and another stabilization of the derivative corresponds to it.

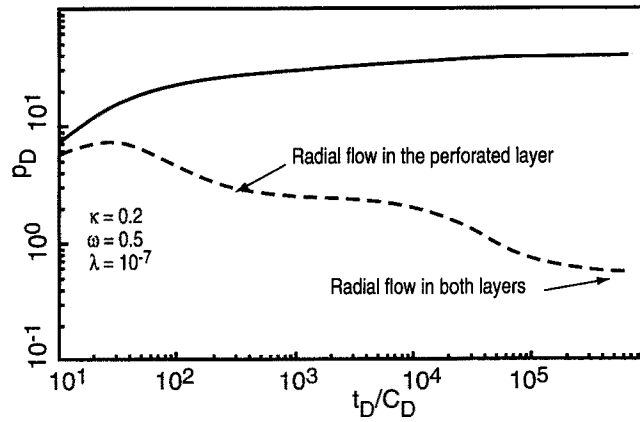


Fig. 14.3

Defining dimensionless pressure with respect to the thickness of both layers:

$$p_D = \frac{\alpha qB \mu}{k (h_1 + h_2)} \Delta p$$

$\alpha = 141.2$ (in practical US units)

$\alpha = 18.6$ (in practical metric units)

$\alpha = 1/2\pi$ (in SI units).

The derivative is stabilized respectively at:

$0.5 (h_1 + h_2)/h_1$ with the first stabilization (if the tested zone is zone 1);

0.5 with the second stabilization

The pressure curves look very similar to the curve observed during a test on a partially penetrating well (Fig. 14.4).

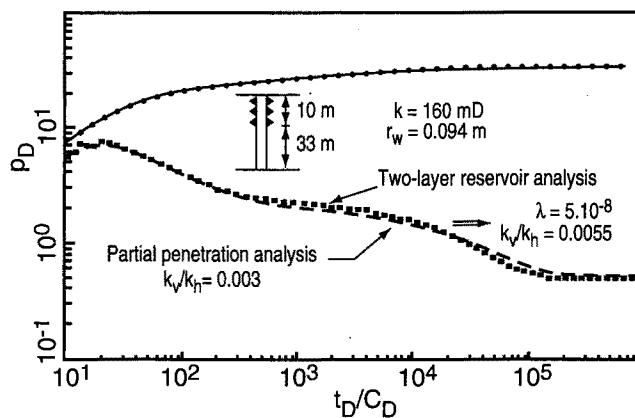


Fig. 14.4

Only the transition period is different:

- In partial perforation, transition corresponds to spherical flow. The derivative decreases with a slope of -0.5 .
- In a double-layer reservoir the transition is more sudden. The sudden transition is related to the hypothesis that the vertical flow between the two layers is instantaneously pseudosteady-state.

Here is the information provided by the analysis of each of the three flows described above:

• **Initial radial flow:**

Only the tested zone is involved during this flow.

If the wellbore storage effect is over soon enough, this flow corresponds to a stabilization of the derivative and a semi-log straight line with the following equation:

$$p_i - p_{wf} = \frac{\alpha q B \mu}{k_1 h_1} \left(\log t + \log \frac{k_1}{(\phi c_t)_1 \mu r_w^2} - \beta + 0.87 S_1 \right) \quad (14.9)$$

$\alpha = 162.6$	$\beta = 3.23$	(in practical US units)
$\alpha = 21.5$	$\beta = 3.10$	(in practical metric units)
$\alpha = 0.183$	$\beta = -0.35$	(in SI units).

The analysis of this flow is used to determine the kh and the skin of the tested zone (here zone 1) (Fig. 14.5 for a pressure buildup).

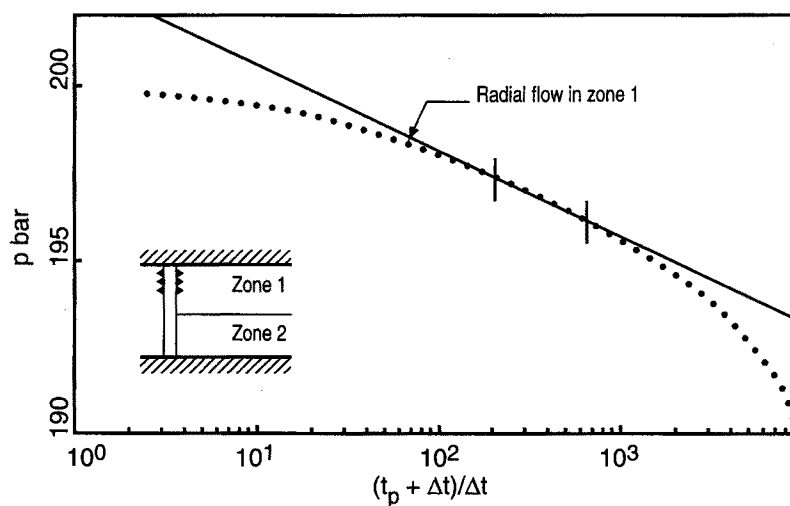


Fig. 14.5

- **Second radial flow:**

Both layers are involved in this flow. It corresponds to a stabilization of the derivative and to a semi-log straight line with the following equation:

$$p_i - p_{wf} = \frac{\alpha q B \mu}{kh} \left(\log t + \log \frac{k}{(\phi c_v) \mu r_w^2} - \beta + 0.87 S \right)$$

The analysis of this flow is used to determine the kh of both layers and one skin (Fig. 14.6).

It is difficult to analyze the skin. It is a function of the skin of each layer but also of the transmissivity contrast (κ parameter) between the layers and of the communication between the two layers (λ parameter).

The test is often too short or the vertical communication too poor for the second radial flow to be visible during the test.

- **Transition period:**

The time when the transition from one radial flow to the other begins depends on how the vertical flow from one layer to the other occurs, i.e. the λ parameter.

The better the flow, i.e. the higher λ , the earlier the transition (Fig. 14.7).

14.4.3 Testing one zone then both together

This method consists in putting the first zone in production, testing it then putting the second zone in production and testing it together with the first one.

- **Testing the first zone:**

The test is interpreted and provides information similar to what was mentioned above:

- kh and skin of the tested zone;
- communication between the two layers (λ parameter);
- equivalent skin and kh of both layers: this information is obtained only if the communication between the two layers is good and the test lasts long enough.

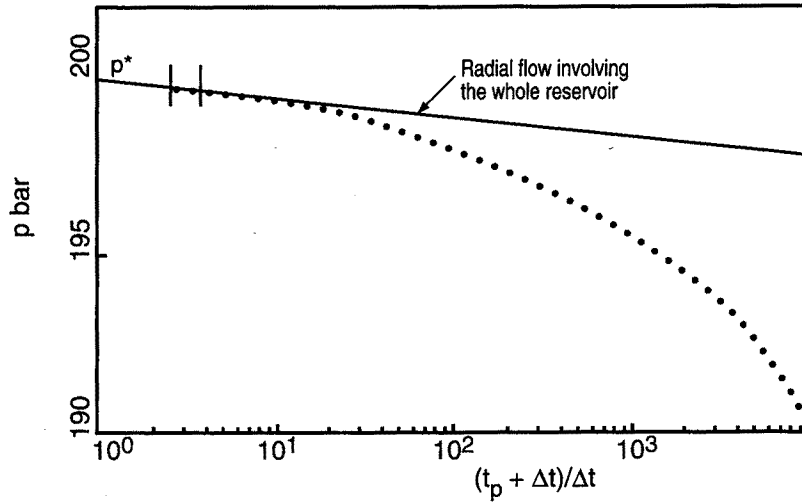


Fig. 14.6

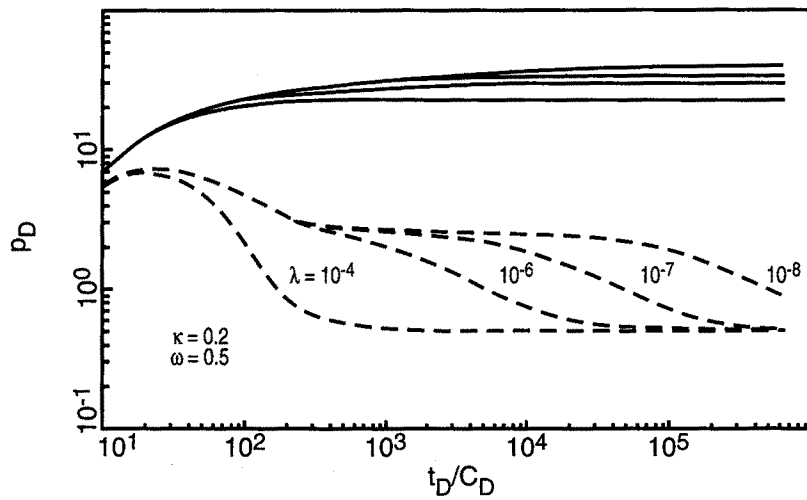


Fig. 14.7

- **Simultaneous testing of the two zones:**

This test provides information identical to information that may be obtained at the end of the test on the first zone: equivalent skin and kh for both the layers together.

- **Summary of the results:**

The test on the first zone is used to determine the characteristics (kh and skin) of the zone.

Testing the two together serves to determine the equivalent characteristics (kh and skin) of both zones.

The characteristics of the second zone can be obtained:

- by difference between the two tests for the kh ;
- by analysis with a well model for the skin.

In order to determine the characteristics of the second zone easily, there must be a substantial contrast between the results of the two tests. Accordingly, **the zone with the smaller kh must be tested first.**

Figure 14.8 illustrates the influence of the two possible test strategies in a particular case:

- testing the worse zone first;
- testing the better zone first.

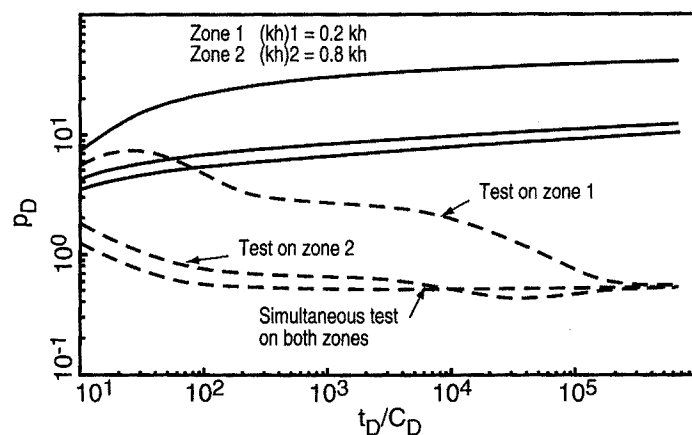


Fig. 14.8



Well aspects

pdfelement



Chapter 15

Partial penetration wells

15.1 INTRODUCTION

There is partial penetration whenever a well produces through a thickness that is smaller than the reservoir's net thickness.

Partial penetration may have been deliberate in order to:

- Avoid production of undesirable fluids. The well is perforated near the bottom of the pay zone when there is a gas-oil contact and near the top when there is an underlying aquifer (Fig. 15.1).
- Produce through the zones with the best characteristics when the total pay zone of a thick, heterogeneous reservoir can not be perforated due to economic or technical reasons (Fig. 15.2).

Partial penetration may occur unexpectedly when:

- A limited small portion of perforations is active. Production logs can be used to assess the effective perforated thickness.
- The net thickness is delimited by zones that are considered to be impermeable. Impermeability is usually estimated from measurements in the well, well logging for example, but impermeable zones may be discontinuous in the reservoir (Fig. 15.3). In this case the effective net thickness is difficult to determine. It may be considerably greater than what was originally estimated (when a regional aquifer is involved for example).

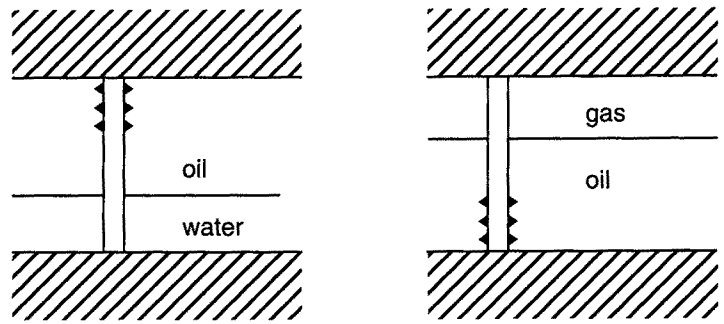


Fig. 15.1

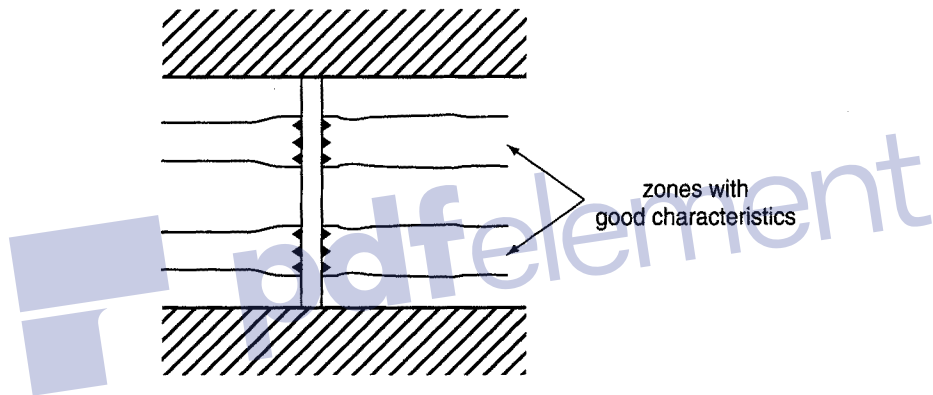


Fig. 15.2

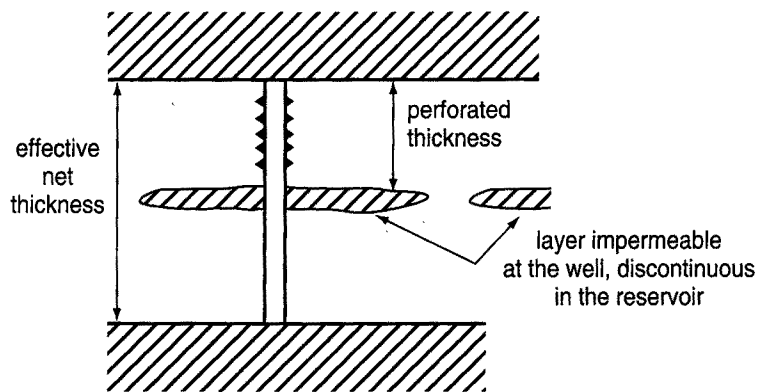


Fig. 15.3

Testing a partial penetration well is one of the best ways of measuring the vertical permeability of the reservoir.

This information is often of great importance and the well may be perforated in two stages in order to get it:

- partial perforation of the reservoir followed by a test;
- perforation of the relevant remaining thickness.

15.2 FLOW AROUND A PARTIAL PENETRATION WELL

The pressure change due to the beginning of production, or more generally due to each flow rate change, initially involves only the open interval.

Just after the reservoir starts producing, a radial flow develops around the well over a thickness equal to the open interval (Fig. 15.4). This flow can be hidden by the wellbore storage effect.

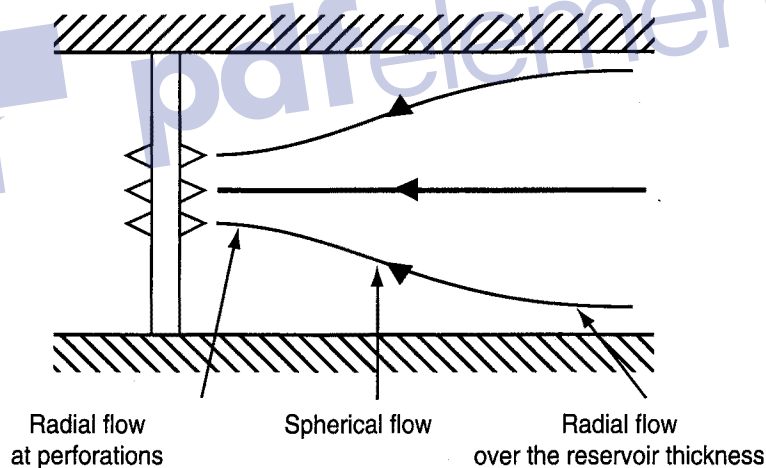


Fig. 15.4

The same as it develops radially, the compressible zone generated by perturbing the flow rate develops vertically to the shoulder beds.

Between the time when vertical development becomes significant and when the compressible zone has reached the shoulders, the fluid flow in the compressible zone is spherical (Fig. 15.4).

The time when spherical flow begins depends on the reservoir's permeability anisotropy (k_v/k_h):

- In an isotropic reservoir, it begins immediately after the perturbation.
- It may not be visible before the end of the test in a highly anisotropic reservoir.

Once the shoulder beds have been reached, the flow in the compressible zone become radial again and involves all of the net pay thickness (Fig. 15.4).

15.3 RADIAL FLOW AT THE PERFORATIONS

Let us consider that the well produces at a constant flow rate and that the wellbore storage effect does not hide any flow.

The radial flow at the perforations is characterized by a logarithmic variation of the bottomhole pressure change versus time (Fig. 15.5):

$$p_i - p_{wf} = \frac{\alpha q B \mu}{k h_p} \left(\log t + \log \frac{k}{\phi \mu c_r^2} - \beta + 0.87 S \right) \quad (15.1)$$

$\alpha = 1/4\pi$	$\beta = -0.35$	(in SI units)
$\alpha = 162.6$	$\beta = 3.23$	(in practical US units)
$\alpha = 21.5$	$\beta = 3.10$	(in practical metric units).

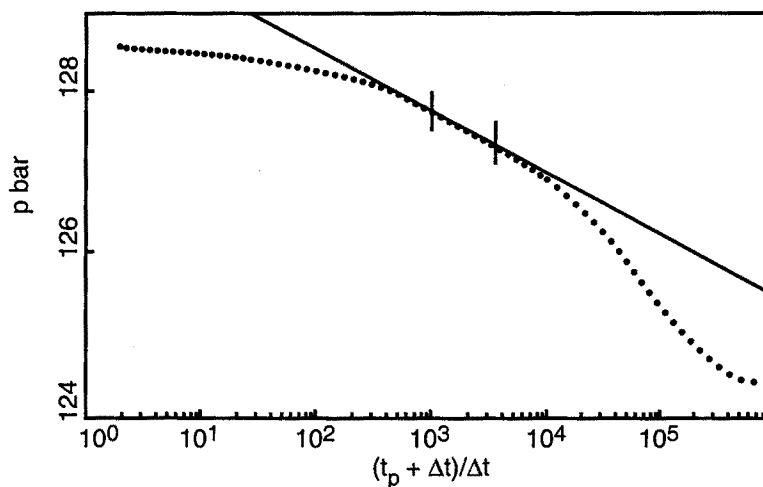


Fig. 15.5

• **Interpretation:**

This flow is used to determine:

- The kh of the perforated zone, i.e. kh_p .

Note bene: it is difficult to extrapolate kh to the whole pay zone, since permeability above and below the open interval may be different.

- The skin of the well.

15.4 SPHERICAL FLOW

When the vertical development of the compressible zone is significant, fluid flow becomes spherical. It is characterized in drawdown by a linear variation of bottomhole pressure versus the inverse of the square root of time:

$$p_i - p_{wf} = \frac{\alpha q B \mu}{k_s r_s} - \frac{\beta q B \mu \sqrt{\phi \mu c_t}}{k_s^{3/2}} \frac{1}{\sqrt{\Delta t}} \quad (15.2)$$

$\alpha = 1/4\pi$	$\beta = 1/4\pi^{3/2}$	(in SI units)
$\alpha = 70.6$	$\beta = 2453$	(in practical US units)
$\alpha = 9.3$	$\beta = 279.3$	(in practical metric units)

with:

$$k_s = (k_h^2 k_v)^{1/3} \text{ spherical permeability} \quad (15.3)$$

r_s equivalent radius of the source of the spherical flow: during this flow it is as if the well were a source with a radius of r_s .

In buildup this equation becomes (Fig. 15.6):

$$p_i - p_{ws} = \frac{\beta q B \mu \sqrt{\phi \mu c_t}}{k_s^{3/2}} \left[\frac{1}{\sqrt{t_p + \Delta t}} - \frac{1}{\sqrt{\Delta t}} \right] \quad (15.4)$$

Expressed in terms of the pressure at shut-in:

$$p_{ws}(\Delta t) - p_{wf}(t_p) = \frac{\alpha q B \mu}{k_s r_s} - \frac{\beta q B \mu \sqrt{\phi \mu c_t}}{k_s^{3/2}} \left[\frac{1}{\sqrt{t_p}} - \frac{1}{\sqrt{t_p + \Delta t}} + \frac{1}{\sqrt{\Delta t}} \right] \quad (15.5)$$

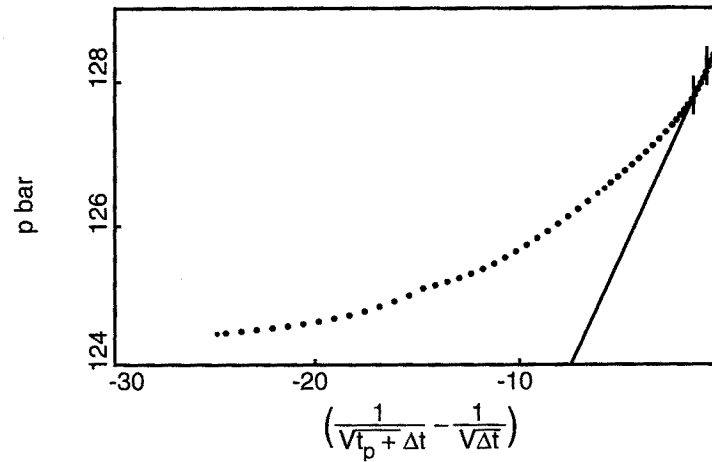


Fig. 15.6

• Interpretation:

The variations in bottomhole pressure versus:

– $\frac{1}{\sqrt{\Delta t}}$ in drawdown,

– $\frac{1}{\sqrt{t_p + \Delta t}} - \frac{1}{\sqrt{\Delta t}}$ in buildup,

– a spherical flow superposition function in more general terms, are characterized by a straight line with a slope of:

$$m_s = \frac{\beta q B \mu \sqrt{\phi \mu c_t}}{k_s^{3/2}} \quad (15.6)$$

which is used to calculate the spherical permeability:

$$k_s = \left(\frac{\beta q B \mu \sqrt{\phi \mu c_t}}{m} \right)^{2/3} \quad (15.7)$$

This information along with the horizontal permeability allows the reservoir's permeability anisotropy to be determined:

$$\frac{k_v}{k_h} = \left(\frac{k_s}{k_h} \right)^3 \quad (15.8)$$

The value of the pressure p_s^* extrapolated on the straight line at infinite t can be used to determine the radius r_s of the equivalent spherical source:

$$r_s = \frac{\alpha q B \mu}{(p_i - p_s^*) k_s} \quad \text{in drawdown} \quad (15.9)$$

$$r_s = \frac{\alpha q B \mu}{[p_s^* - p_{wf}(t_p)] k_s} \quad \text{in buildup} \quad (15.10)$$

Determining the radius may have a theoretical use but no practical application has ever been mentioned.

• Effect of shoulder beds:

When the compressible zone reaches the shoulder beds during spherical flow, there are two possible cases:

- The perforations are centered in the net thickness and the two shoulder beds are reached at the same time. The flow goes from spherical to radial all over the net pay thickness.
- The perforations are greatly off center in the pay zone and one of the shoulders is reached before the other. The first shoulder bed that is reached is perceived like a fault in an infinite reservoir or a boundary in a channel, i.e. the slope of the straight line corresponding to spherical flow doubles. When the well is highly eccentric, the double-slope straight line is seen immediately. This flow is termed hemispherical by several authors.

These phenomena are hard to see on the conventional graph, they are clearly visible on the derivative (Fig. 15.10).

15.5 RADIAL FLOW OVER THE WHOLE NET THICKNESS

When the compressible zone has reached all of the net thickness of the reservoir the flow becomes radial and is like the flow existing around a well perforated over all the reservoir thickness.

During this flow, the drawdown pressure follows the usual logarithmic variations versus time (Fig. 15.7):

$$p_i - p_{wf} = \frac{\alpha q B \mu}{kh} \left(\log t + \log \frac{k}{\phi \mu c_t r_w^2} - \beta + 0.87 S' \right) \quad (15.11)$$

$$\begin{array}{lll} \alpha = (1/4\pi) \ln 10 & \beta = -0.35 & \text{(in SI units)} \\ \alpha = 162.6 & \beta = 3.23 & \text{(in practical US units)} \\ \alpha = 21.5 & \beta = 3.10 & \text{(in practical metric units).} \end{array}$$

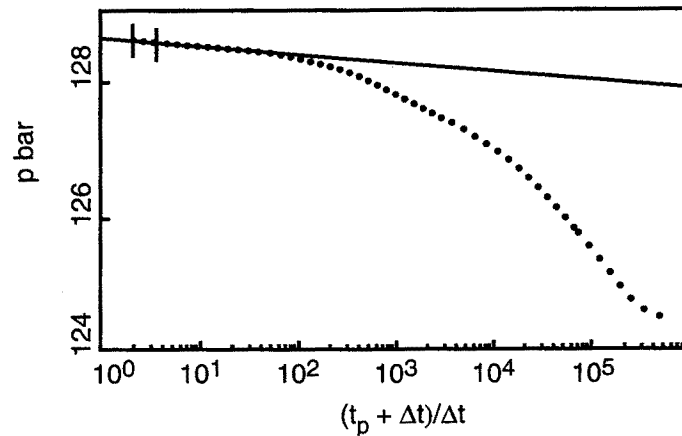


Fig. 15.7

This flow is used to determine:

- the reservoir kh ;
- an overall skin, S' .

The skin is the result of two effects:

- The skin S of the well.
- The effect of partial perforation. It causes restricted flow entry in the vicinity of the well, resulting in a positive skin S_{pp} :

$$S' = S_{pp} + S \frac{h}{h_p}$$

The partial perforation skin, S_{pp} , depends on several factors:

- the fraction of the reservoir thickness that is open;
- the reservoir's permeability anisotropy;
- the ratio between the net thickness and the well radius;
- the position of the perforations.

The charts in Figures 15.8 and 15.9 indicate how the partial perforation skin varies versus these different factors for a well perforated in the center of the reservoir and at the top or bottom of the reservoir respectively.

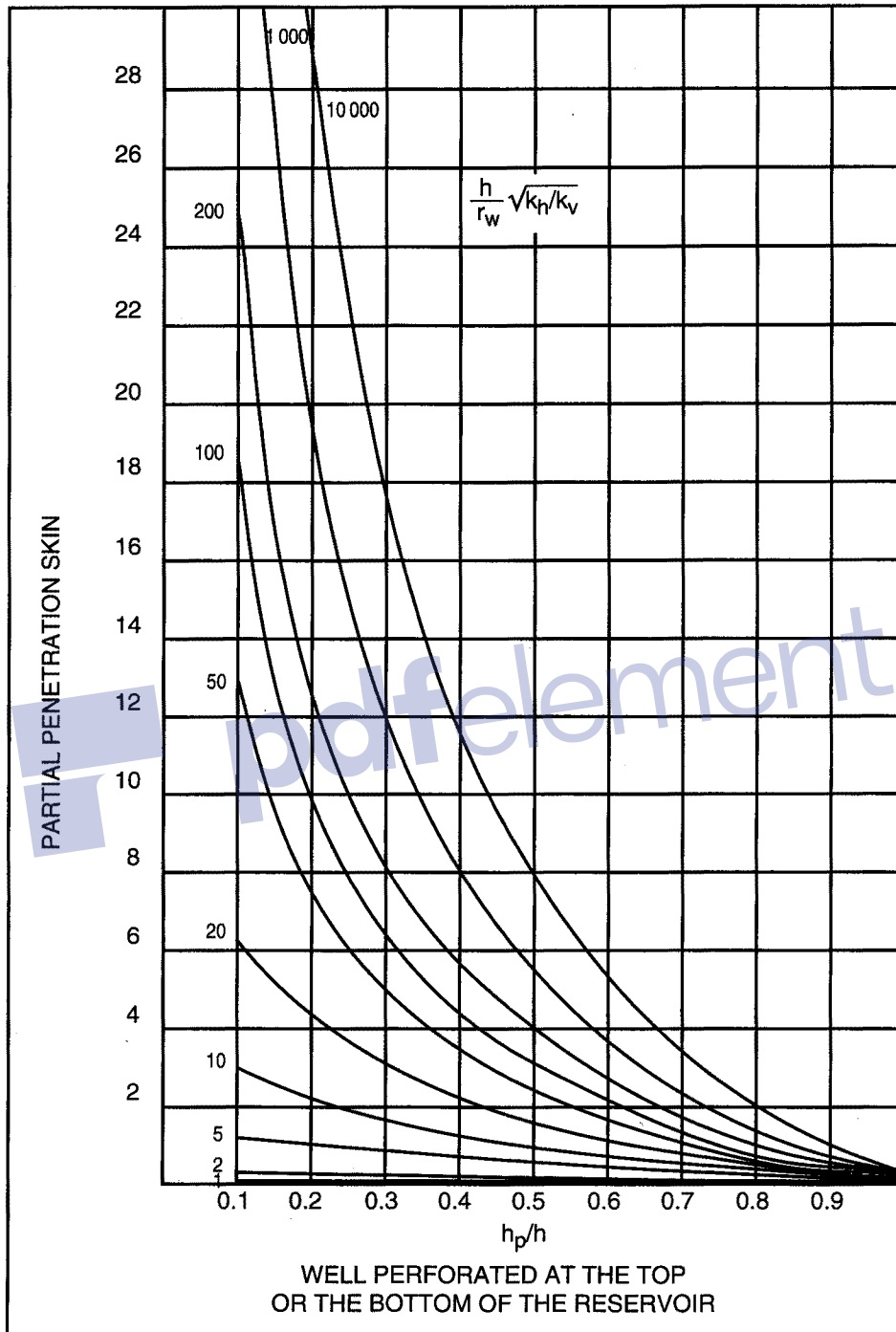


Fig. 15.8

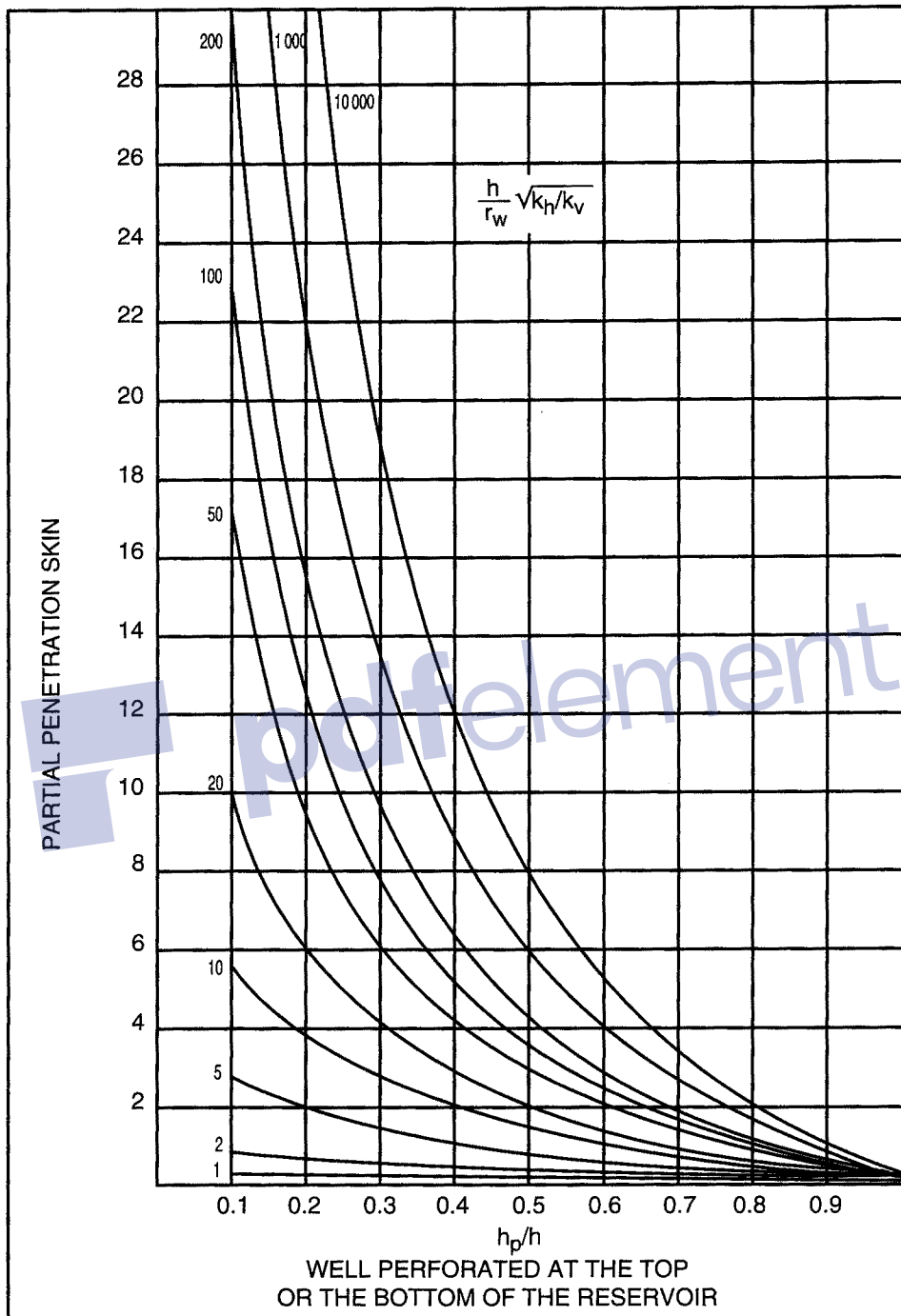


Fig. 15.9

15.6 EXTRAPOLATED PRESSURE, AVERAGE PRESSURE

Conventional methods of calculating the reservoir's average pressure (MBH, Dietz, see Chapter 11) can be used.

The extrapolated pressure must be read on the second semi-log straight line, the one that corresponds to flow over the whole of the net thickness.

It is possible to determine the extrapolated pressure only if the buildup was long enough to reach the second semi-log straight line.

When the second semi-log straight line has not been reached, only simulation with a well model can determine the average reservoir pressure.

15.7 PRESSURE DERIVATIVE

The pressure derivative (Fig. 15.10) is of great help in diagnosing the three flows described in the preceding sections.

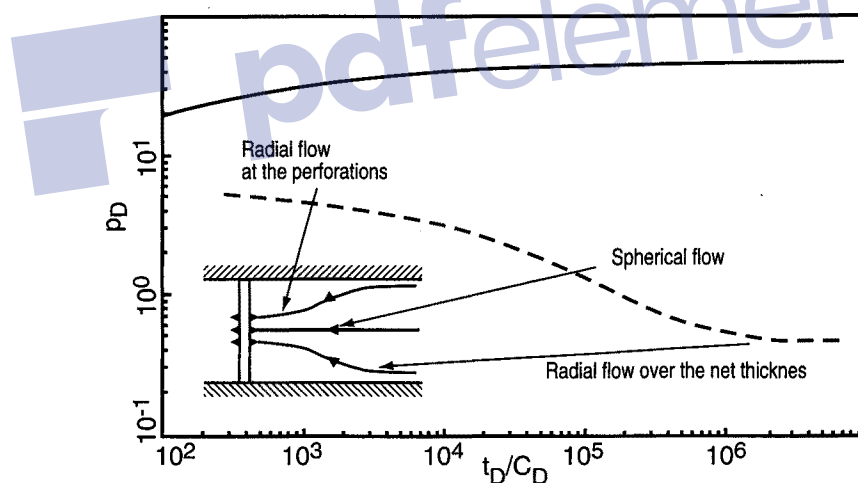


Fig. 15.10

Using the net thickness of the reservoir as the reference thickness in calculating dimensionless pressure $p_D = \frac{2\pi kh}{qB\mu} \Delta p$, the three flows are characterized in the following way:

- The radial flow at the perforations: by a stabilization of the derivative at $p'_D = 0.5 h/h_p$. This stabilization can be hidden by the wellbore storage effect.

- Spherical flow: by a decrease in the pressure derivative as a straight line with a slope of $-1/2$. It may also be hidden by the wellbore storage effect. The test may have been too short and spherical flow may appear only as a pressure derivative beginning to decline: the straight line with the slope of $-1/2$ has not yet been reached. The only way of determining the reservoir's permeability anisotropy is to match the beginning of the pressure derivative's decrease using a well model.
- Radial flow over all the net thickness: by a stabilization of the derivative at $p'_D = 0.5$.

• **Effect of shoulder beds:**

The position of the perforations in relation to the shoulder beds has an influence on the transition, i.e. spherical flow. Figure 15.11 illustrates the phenomenon:

- When the perforations are located in the middle of the net thickness, the two shoulder beds are reached at the same time. The transition between the two radial flows corresponds to the spherical flow which is seen by a drop in the pressure derivative with a slope of $-1/2$.
- When the perforations are much closer to one of the shoulder beds the other, transition occurs in two stages:
 - . An initial period of spherical flow with a slope of $-1/2$ until one of the shoulder beds is reached.
 - . Once the first shoulder bed is reached there is a translation of the pressure derivative by a factor of 2 until it starts its $-1/2$ slope decline again.
- When the perforations are immediately next to one of the shoulder beds the doubling occurs immediately. Spherical flow transition starts four times later than with perforations centered in the pay zone.

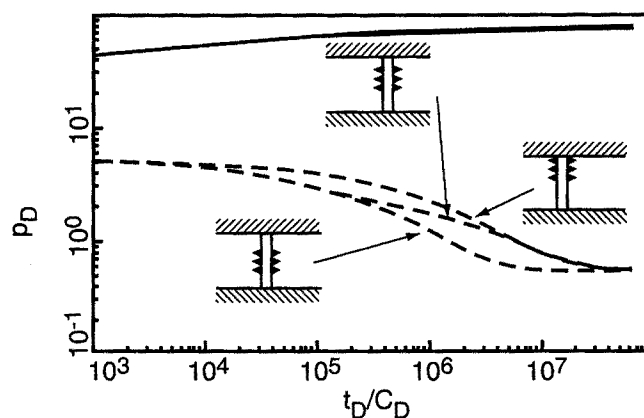


Fig. 15.11

15.8 AMBIGUOUS INTERPRETATION

In practice the sequence of flows described in the preceding sections is seldom observed in one test. Two situations are commonly found:

- **The test was too short to go on after the beginning of spherical flow** (Fig. 15.12)

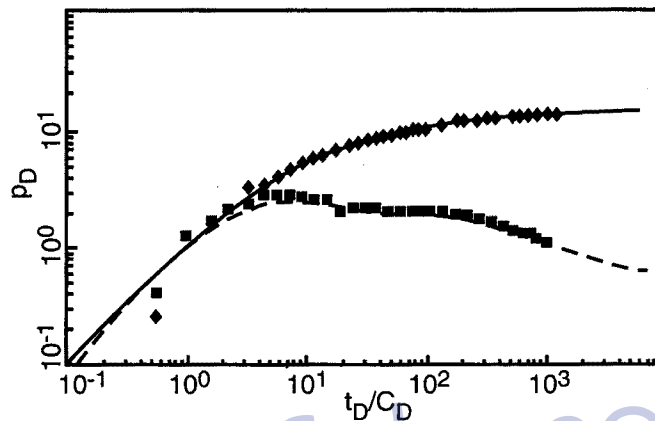


Fig. 15.12

The test allows the following to be determined:

- The permeability over the perforated thickness.
- The skin of the well.
- The permeability anisotropy using the beginning of spherical flow. When only the transition between radial flow at the perforations and spherical flow is visible, a well model is the only way to determine the permeability anisotropy by matching the transition.

This type of test can not be used to determine the permeability of the reservoir beyond the perforated zone.

- **Only one stabilization appears**

This situation is found in two cases that are not always easy to discriminate between:

- The test was too short for the spherical flow to begin, only radial flow at the perforations is visible.
- The wellbore storage effect hides the radial flow at the perforations and the spherical flow, only radial flow over the whole net thickness is visible.

The value of the skin can help determine which radial flow the end of the test corresponds to:

- Negative skin usually corresponds to the radial flow at the perforations.
- High skin (greater than 10) is usually due to partial perforation, although severe plugging in the vicinity of the wellbore can not always be excluded.

Comparison of permeability, calculated on the basis of the two thickness hypotheses, with the permeability measured on cores can also be used to settle the uncertainty.

Test simulation with a well model can usually settle the issue: one of the two hypotheses corresponds to an unrealistic permeability anisotropy.

15.9 COMPARISON WITH CORE SAMPLES

Interpretation of partial perforation well tests is a good way to determine the degree of vertical communication in reservoirs.

Vertical permeability values are also obtained by interpreting RFT pretests or by core analysis. Vertical permeabilities obtained in this way are often higher than vertical permeability determined by tests.

This difference can be explained by the dimensions of the zones involved in the two types of measurements:

- RFT pretests and core samples involve small areas that are usually homogeneous. The measured vertical permeability is that of these homogeneous zones.
- In addition to this, well tests measure the effect of average-size heterogeneities bypassed by flows and communication through discontinuous permeability screens as well. Measured vertical permeability is the resultant of permeability anisotropy and of tortuosity effects produced by the heterogeneities. Well tests lead to estimates of vertical permeability that are similar to those obtained from the analysis of water or gas breakthrough during a coning effect.

15.10 PARTIAL PERFORATION AND FRACTURED RESERVOIRS

The effects of fractures in reservoirs were described in Chapter 13. They can overlay the partial perforation effect.

They correspond to a minimum on the pressure derivative, which can appear sooner or later depending on how easy the flow from the matrix to the fractures is (value of λ).

The effect of fracturing usually shows up during the first radial flow period.

- **Permeability anisotropy:**

The permeability measured in a fractured reservoir is that of the fractures, which are usually vertical. Their development is not always continuous over the whole reservoir thickness. They can be transmitted from one sublevel to another by fracture relays (Fig. 15.13).

Vertical fluid communication depends on the reservoir permeability through these fracture relays.

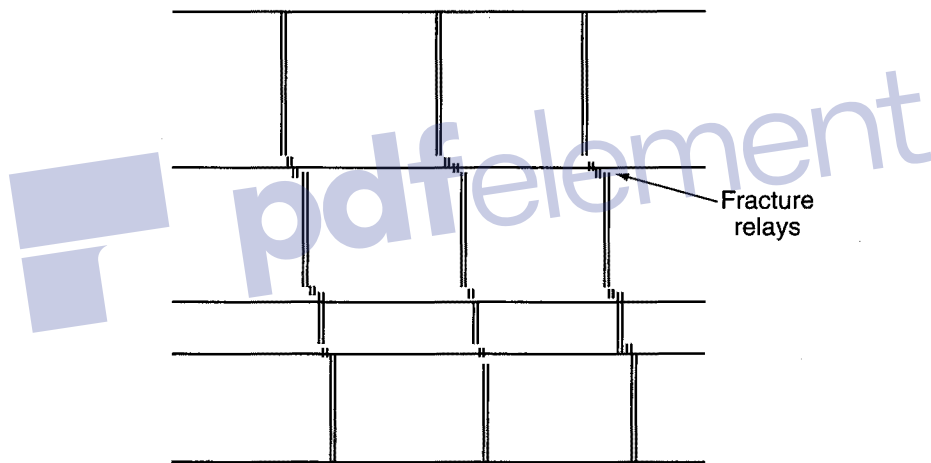


Fig. 15.13

It is important to understand this communication when a coning effect may perturb well production.

Local measurements such as core analysis or RFT interpretation are unable to determine this type of vertical communication. Vertical permeability, evaluated from the partial perforation, is generally similar to what is calculated from the analysis of a coning effect.



Chapter 16

Slanted wells

16.1 INTRODUCTION

Most wells go through the reservoir at an angle relative to the normal to the dip. The aim of this chapter is to study the modifications to interpretation caused by the slant of the well.

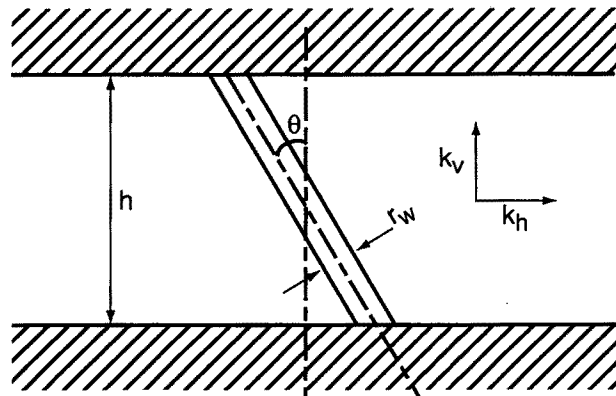


Fig. 16.1

Three parameters exert an influence:

- the inclination of the well relative to the normal to the dip: angle θ in Figure 16.1;

- permeability anisotropy: k_v/k_h ;
- the ratio between the net thickness and the well radius: h/r_w .

16.2 FLOWS AND SKIN FACTOR FOR SLANTED WELLS

Two flows can theoretically be seen one after the other around an inclined well:

- a radial flow around the well;
- a horizontal pseudoradial flow after a transition period.

The wellbore storage effect usually hides the first radial flow and the subsequent transition.

The first radial flow is visible only for very large angles of slant (larger than 75°), when the slanted well behaves like a horizontal well.

When the pseudoradial flow alone can be seen, the test is interpreted as if the well were vertical.

Inclination improves flow in the vicinity of the wellbore. This is seen by a negative skin of slant.

• Skin of slant:

H. Cinco et al. [Ref. 57] give an expression that can be used to calculate the skin of slant, S_i :

$$S_i = -\left(\frac{\theta'}{41}\right)^{2.06} - \left(\frac{\theta'}{56}\right)^{1.865} \times \log\left(\frac{h_D}{100}\right) \quad (16.1)$$

with $\theta' = \text{Arctg}\left(\sqrt{\frac{k_v}{k_h}} \text{tg } \theta\right)$ expressed in degrees:

$$h_D = \frac{h}{r_w} \sqrt{\frac{k_h}{k_v}}$$

This expression is valid for $0 < \theta' < 75^\circ$.

Figure 16.2 shows the variations of S_i versus h_D for different values of θ' .

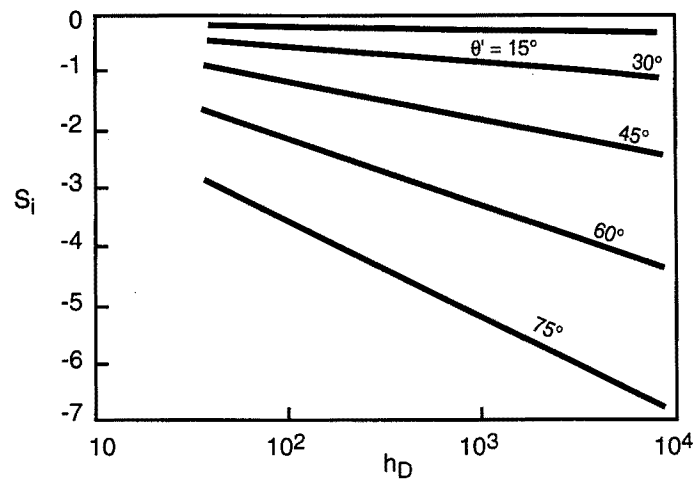


Fig. 16.2

16.3 INFLUENCE OF PERMEABILITY ANISOTROPY

Equation 16.1 shows that permeability anisotropy seriously reduces the effect of the slant.

The following example illustrates the influence of permeability anisotropy on the skin of slant.

For $\theta = 75^\circ$ and $h/r_w = 100$:

$\theta' = 75^\circ$	$S' = -3.5$	in an isotropic reservoir
$\theta' = 50^\circ$	$S' = -1.5$	for $k_v/k_h = 0.1$
$\theta' = 20^\circ$	$S' = -0.5$	for $k_v/k_h = 0.01$.

The higher the permeability anisotropy, the more reduced the effective angle of slant, θ' , of the well.

Since the permeability anisotropy of a reservoir is usually lower than 0.1, the slant of the well normally has a negligible effect on the well's productivity.



Chapter 17

Artificially fractured wells

17.1 DESCRIPTION OF THE FRACTURE

Natural fractures as discussed in Chapter 13 are considered to be distributed homogeneously throughout the reservoir. Artificial fractures are, however, located in the vicinity of the wellbore. They are caused by operations carried out on the well.

Fracturing can be intentional, it is the aim of hydraulic fracturing operations.

It can be accidentally induced on injection wells or on wells during acidizing when the injection pressure is greater than the reservoir fracture pressure.

- **Horizontal, vertical fractures:**

An artificial fracture can develop along horizontal or vertical planes. Interpretation methods have been developed for both cases [Ref. 28, 33].

At depths of less than 1000 m it is possible to achieve horizontal fractures. At greater depths, the overburden weight makes fractures develop only along vertical planes. This is the only case that will be dealt with here.

- **Description of the fracture:**

The description normally used in well testing is presented in figure 17.1:

- The fracture is vertical.
- It extends over all the reservoir's net thickness, h .

- It extends symmetrically from one side to the other of the well up to a distance x_f from the well.
- It has a uniform width, w .

17.2 FLOWS AROUND AN ARTIFICIALLY FRACTURED WELL. CONVENTIONAL INTERPRETATION METHODS

The presence of an artificial fracture modifies the flows near the wellbore considerably.

H.Cinco-Ley [Ref. 32] describes the flows that can develop around an artificially fractured well. Figure 17.2 gives a representation of the streamlines corresponding to each of them.

17.2.1 Linear flow in the fracture (Fig. 17.2a)

This flow exists theoretically at the very beginning of the test. During this flow most of the fluids produced at the well come from expansion in the fracture.

This flow is linear. The same as during any linear flow, pressure varies linearly versus \sqrt{t} .

This variation can be expressed in dimensionless variables as follows:

$$p_D = \frac{2\sqrt{\pi}}{C_r} \sqrt{\eta t_{Dxf}} \quad (17.1)$$

The following dimensionless terms are involved.

- **Time:**

$$t_{Dxf} = \frac{\beta kt}{\phi \mu c_t x_f^2} \quad (17.2)$$

Dimensionless time calculated with x_f as reference length.

$\beta = 1$	(in SI units)
$\beta = 0.000264$	(in practical US units)
$\beta = 0.00036$	(in practical metric units).

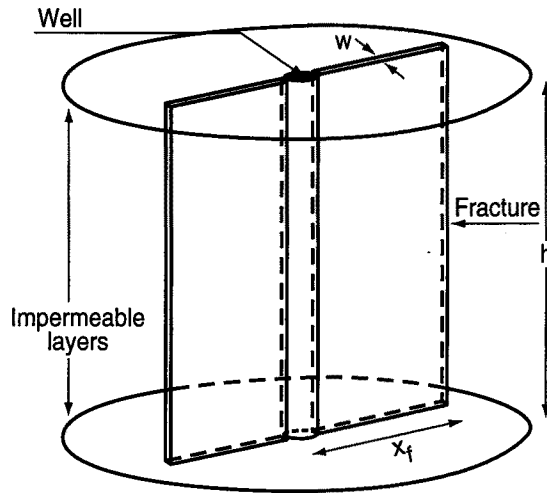


Fig. 17.1 Representing the fracture

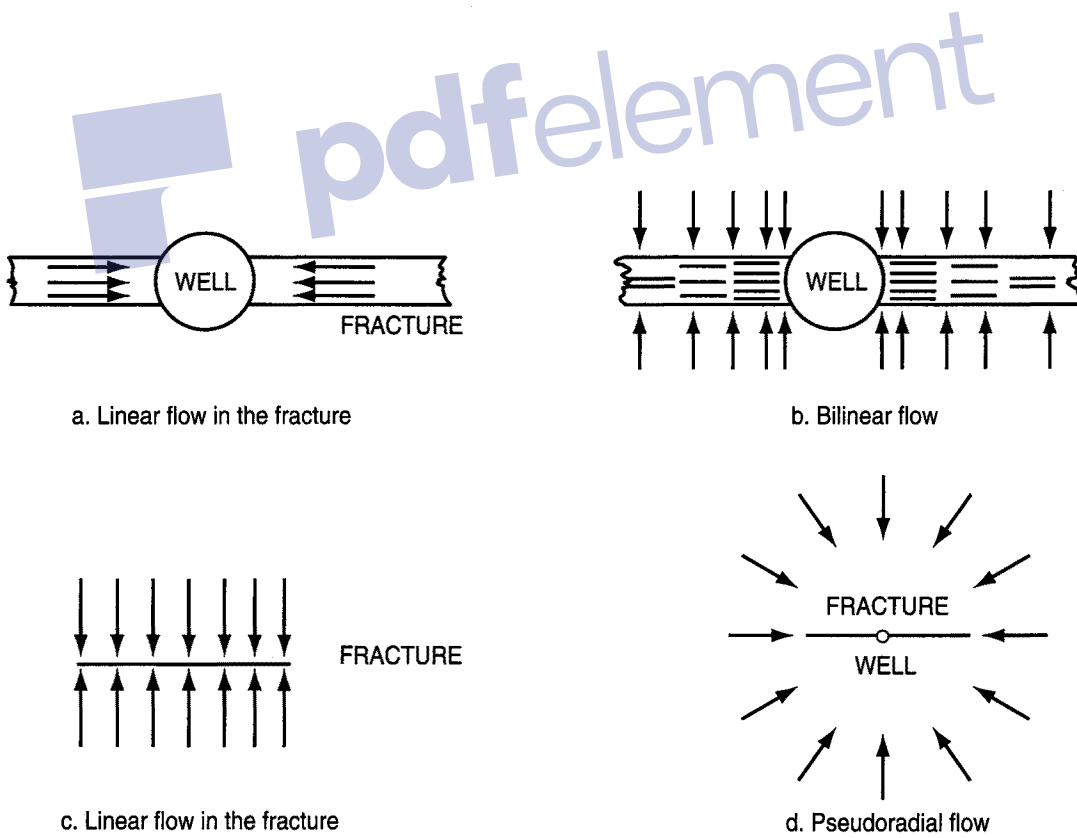


Fig. 17.2 Sequence of flows around the fracture

• **Diffusivity:**

$$\eta = \frac{k_f}{\mu(\phi c_t)_f} / \frac{k}{\phi \mu c_t} \quad (17.3)$$

Relationship between diffusivity inside the fracture and diffusivity in the reservoir.

• **Relative conductivity:**

$$Cr = \frac{wk_f}{x_f k} \quad (17.4)$$

The relative conductivity, Cr , expresses the relationship between:

- the factors governing emptying of the fracture (w and k_f): the wider (w) and the more permeable (k_f) the fracture, the better fluids circulate;
- and the factors governing supply to the fracture (x_f and k): the longer the fracture (x_f) and the more permeable the formation, the better supplied it is.

The greater the relative conductivity of the fracture, the more effective it is.

A fracture with a relative conductivity of over 100 behaves as if it had infinite conductivity.

The concept of relative conductivity explains why the smaller the formation permeability, the more effective the hydraulic fracturing is.

In reservoirs with permeability of over 10 mD, hydraulic fractures have a low relative conductivity and their effectiveness is poor.

In real terms, expression 17.1 becomes:

$$p_i - p_{wf} = \frac{\alpha qB}{wh} \sqrt{\frac{\mu t}{k_f (\phi c_t)_f}} \quad (17.5)$$

$\alpha = 8.128$ (in practical US units)

$\alpha = 0.3918$ (in SI units).

The slope of the straight line obtained by plotting pressure variations versus t depends on a group of several internal characteristics of the fracture: $wk_f (\phi c_t)_f$.

Cinco [Ref. 32] indicates that this flow ends for:

$$t_{Dxf} = \frac{0.1 C_r^2}{\eta^2} \quad (17.6)$$

This flow is always hidden by the wellbore storage effect.

17.2.2 Bilinear flow (Fig. 17.2b)

This flow was described for the first time by Cinco [Ref. 32] and has since been seen several times in field cases [Ref. 34].

It is called bilinear because it corresponds to two simultaneous linear flows:

- an incompressible linear flow in the fracture;
- a compressible linear flow in the formation.

Bilinear flow lasts as long as the ends of the fracture do not affect the flows.

It is characterized by linear pressure variations versus the fourth root of time.

The variations are expressed in dimensionless variables as follows:

$$p_D = \frac{1.38}{\sqrt{C_r}} (t_{Dxf})^{1/4} \quad (17.7)$$

In real terms the expression becomes:

$$\Delta p = \frac{\alpha q B \mu}{h \sqrt{C_r} (\phi \mu c_t k)^{1/4}} t^{1/4} \quad (17.8)$$

$\alpha = 44.1$ (in practical US units)

$\alpha = 34.97$ (in SI units).

The straight line that is obtained by plotting Δp versus $t^{1/4}$ through the origin of the coordinates. Its slope depends on both internal fracture characteristics (C_r) and on formation characteristics.

Cinco [Ref. 32, 33] points out that in some cases the straight line corresponding to bilinear flow does not pass through the origin of the coordinates:

- internal damage of the fracture;
- deviation from Darcy's law in the fracture (gas well).

In [Ref. 32] he gives a set of expressions that can be used to evaluate the end of the bilinear flow:

$$t_{Dxf} = \frac{0.1}{(\pi Cr)^2} \quad \text{for } \pi Cr > 3 \quad (17.9)$$

$$t_{Dxf} = 0.0205 (\pi Cr - 1.5)^{-1.53} \quad \text{for } 1.6 < \pi Cr < 3 \quad (17.10)$$

$$t_{Dxf} = \left(\frac{4.55}{\pi Cr} - 2.5 \right)^{-4} \quad \text{for } \pi Cr < 1.6 \quad (17.11)$$

Bilinear flow is seldom seen during testing, it is usually hidden by the wellbore storage effect.

17.2.3 Linear flow in the formation (Fig. 17.2c)

This flow is very often visible during testing of artificially fractured wells. It is an integral part of the conventional analysis methods of these tests.

The ends of the fracture have been reached. The dimension of the fracture has an influence on flows.

This flow corresponds, like any linear flow, to a linear variation of the pressure versus \sqrt{t} .

It is characterized by the following variation in dimensionless pressure:

$$p_D = \sqrt{\pi t_{Dxf}} \quad (17.12)$$

In real terms, this expression becomes:

$$p_i - p_{wf} = \frac{\alpha qB}{h} \sqrt{\frac{\mu}{\phi c_t} \frac{\sqrt{t}}{x_f \sqrt{k}}} \quad (17.13)$$

$$\alpha = 4.064 \quad (\text{in practical US units})$$

$$\alpha = 1/2 \sqrt{\pi} \quad (\text{in SI units}).$$

The slope of the straight line obtained by plotting bottomhole pressure change versus \sqrt{t} can be used to determine x_f , the fracture half-length.

Linear flow occurs only around high conductivity fractures (Cr over 100). It starts at:

$$t_{Dxf} = \frac{100}{(\pi Cr)^2} \quad (17.14)$$

and ends at:

$$t_{Dxf} = 0.016 \quad (17.15)$$

17.2.4 Pseudoradial flow (Fig. 17.2d)

The presence of an artificial fracture modifies the streamlines near the wellbore considerably.

Equipotentials recover a radial symmetry only at a certain distance from the well.

When the compressible zone reaches this area, flow becomes radial: pressure varies logarithmically versus time. The presence of the fracture near the wellbore corresponds to a geometrical skin.

This flow is characterized by the following dimensionless pressure variations:

$$p_D = \frac{1}{2} (\ln t_D + 0.81 + 2 S_f) \quad (17.16)$$

In real terms the expression becomes:

$$p_i - p_{wf} = \frac{\alpha q B \mu}{kh} \left(\log t + \log \frac{k}{\phi \mu c_t r_w^2} - \beta + 0.87 S_f \right) \quad (17.17)$$

$\alpha = 162.6$	$\beta = 3.23$	(in practical US units)
$\alpha = 21.5$	$\beta = 3.10$	(in practical metric units)
$\alpha = 0.183$	$\beta = 0.352$	(in SI units).

- **Geometrical skin:**

The geometrical skin, S_f , depends on the length of the fracture and on its conductivity:

$$S_f = G(Cr) - \ln \frac{x_f}{r_w} \quad (17.18)$$

$G(Cr)$ is a decreasing function of the fracture conductivity (Fig. 17.3).

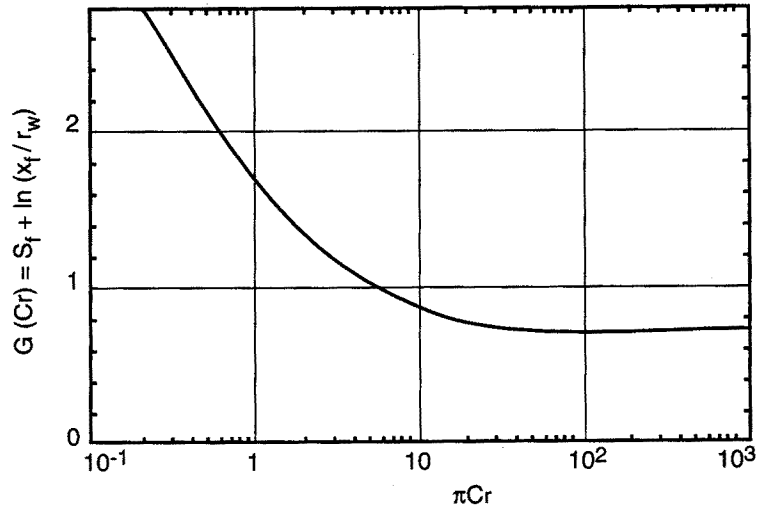


Fig. 17.3 $G(Cr)$

This figure shows that for relative conductivity values over 100, $G(Cr)$ is roughly constant and is equal to 0.69. Above 100, an increase in relative conductivity has no effect on flows. The fracture behaves as if it had infinite conductivity: it expels the fluids that feed it with a negligible internal pressure drop compared to those involved in the reservoir.

- **Effective radius:**

The geometrical skin due to the fracture can be expressed in terms of effective radius (see Chapter 3).

The effective radius due to the skin S_f is equal to:

$$r_{ef} = r_w \exp(-S_f)$$

and since $S_f = G(Cr) - \ln \frac{x_f}{r_w}$

$$r_{ef} = r_w \exp(-G(Cr)) \quad (17.19)$$

- **Infinite conductivity fracture:**

In an infinite conductivity fracture, $G(Cr) = 0.69$, therefore:

$$r_{ef} = \frac{x_f}{2}$$

With respect to productivity, the fractured well behaves like a vertical well with a diameter equal to the half-length of the fracture. A fracture usually extends for several tens of meters on each side of the well. The effective radius gives an idea of the fracture efficiency.

The value of the geometrical skin, S_f , can be used to determine the half-length of the infinite conductivity equivalent fracture:

$$x_f = 2 r_w \exp(-S_f) \quad (17.20)$$

This value must be compared to the one obtained with the linear flow if it is visible. Comparison helps verify the validity of the assumptions put forward about the fracture's conductivity.

- **Low-conductivity fracture:**

When the fracture's conductivity is low, the linear flow is not visible. The bilinear flow alone, if it exists, can be used to calculate the fracture's conductivity and determine its real half-length:

$$x_f = r_w \exp(-S_f) \exp(-G(Cr)) \quad (17.21)$$

When the bilinear flow is not visible, only interpretation with type curves can give the correct determination of x_f and Cr .

- **Beginning of pseudoradial flow:**

Cinco [35] situates the beginning of pseudoradial flow at:

$$t_{Df} = 5 \exp \left\{ -0.5 (\pi Cr)^{-0.6} \right\} \quad (17.22)$$

i.e. $t_{Df} = 5$ for an infinite conductivity fracture.

Therefore considerable time elapses between the end of linear flow ($t_{Df} = 0.016$) and the beginning of pseudoradial flow.

The transition between the two flows is of no use with conventional methods.

Tests are frequently too short to reach pseudoradial flow and often neither bilinear nor linear flow is visible during testing. Only type curves can be used to interpret these tests, with the analysis of transition periods.

17.3 TYPE CURVES, THE DERIVATIVE

17.3.1 Representation used

The most useful type curves represent dimensionless pressure p_D versus dimensionless time t_{Dxf} on a log-log plot.

This representation is derived from the one proposed by Agarwal [Ref. 36]. It is different from Gringarten's (p_D versus t_D/C_D used in the majority of other cases).

17.3.2 Parameters required to describe a type curve

Five parameters are required to describe a type curve for a fractured well in an infinite reservoir:

- the formation permeability, k ;
- the fracture half-length, x_f ;
- the wellbore storage, C ;
- the fracture's relative conductivity, C_r ;
- the skin around the fracture S .

- **Formation permeability:**

Formation permeability is obtained, like in a vertical well, after matching real data on a type curve by using the relationship of the real pressure Δp and the dimensionless pressure p_D of a match point.

When pseudoradial flow is reached during the test, a stabilization of the derivative corresponds to it. Matching this stabilization at 0.5 can determine formation permeability unambiguously. Otherwise, determination is more difficult: several groups of (k , x_f , C_r) can give similar results.

- **Fracture half-length:**

The horizontal match between real time and t_{Dxf} determines the fracture half-length:

$$x_f = \sqrt{\frac{\alpha k \Delta t}{\phi \mu c_t t_{Dxf}}} \quad (17.23)$$

$$\begin{aligned}\alpha &= 0.000264 && \text{(in practical US units)} \\ \alpha &= 0.000355 && \text{(in practical metric units)} \\ \alpha &= 1 && \text{(in SI units).}\end{aligned}$$

It may be difficult to match the time when few data are available at small t_{Dxf} values or when the wellbore storage effect is too great. Then several x_f , C_r pairs may give similar results.

- **Relative conductivity of the fracture, C_r :**

Its influence on pressure variations is indicated in Figure 17.4.

- **Wellbore storage:**

The dimensionless variable related to wellbore storage is C_{Dxf} :

$$C_{Dxf} = \frac{\alpha C}{h\phi c_x x_f^2} \quad (17.24)$$

$$\begin{aligned}\alpha &= 0.89 && \text{(in practical US units)} \\ \alpha &= 1/2\pi && \text{(in practical metric units)} \\ \alpha &= 1/2\pi && \text{(in SI units)}\end{aligned}$$

Its influence on pressure variations is indicated in Figure 17.5.

Like in a vertical well, the period when the wellbore storage dominates corresponds to a variation of dimensionless pressure and its derivative along a 1-slope straight line which does not go through the origin of the coordinates. It is off by C_{Dxf} on the t_{Dxf} axis.

- **The skin around the fracture:**

The skin, S , around the fracture corresponds to the additional pressure drops generated by the fact that the immediate vicinity of the fracture often has a permeability different from the permeability farther away in the reservoir. This difference may be due to hydraulic fracturing operations, for example, that modify saturations near the fracture.

Considering that the skin involves an area with a width of w_s around the fracture (Fig. 17.6) and that this area has a permeability of k_s , the additional pressure drop in the area is expressed by:

$$\Delta p_s = \frac{qB\mu w_s}{4k h x_f} \left(\frac{k}{k_s} - 1 \right) \quad (17.25)$$

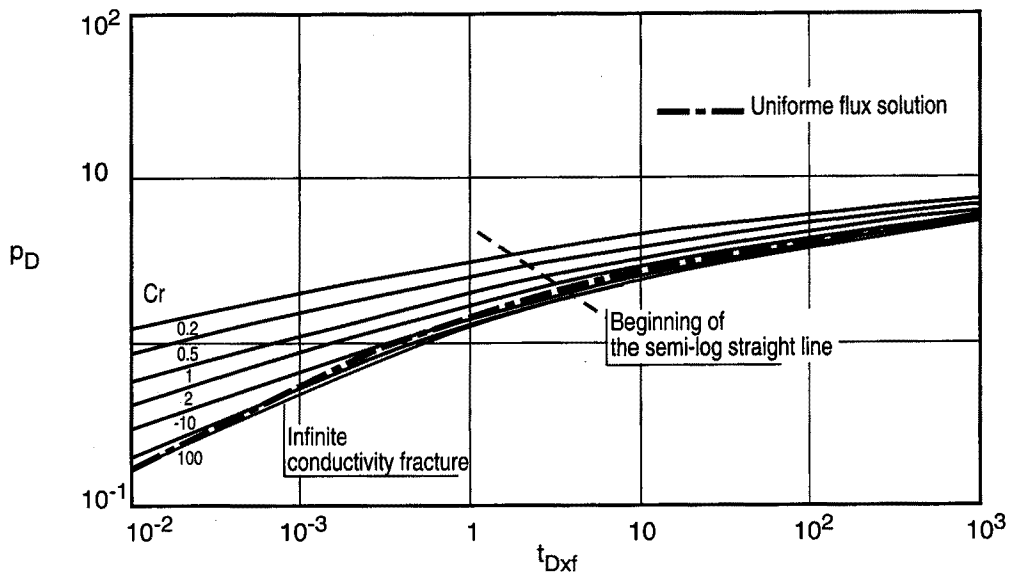


Fig. 17.4 Influence of the relative conductivity of the fracture

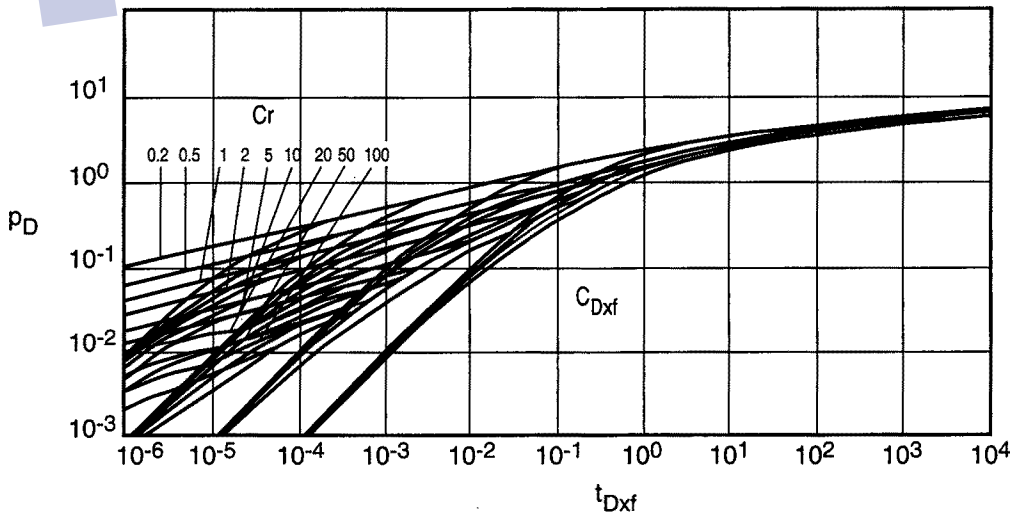


Fig. 17.5 Influence of the relative conductivity of the fracture and of wellbore storage

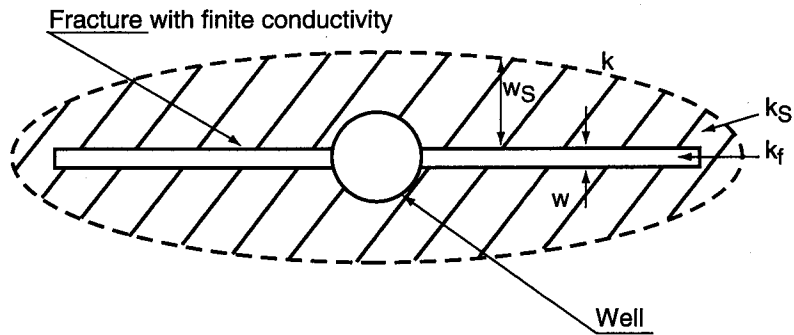


Fig. 17.6

The skin is defined by:

$$\Delta p_s = \frac{qB\mu}{2\pi kh} S$$

hence:

$$S = \frac{\pi}{2} \frac{w_s}{x_f} \left(\frac{k}{k_s} - 1 \right) \quad (17.26)$$

This expression should be compared to the one obtained with a cylindrical vertical well (see Chapter 3):

$$S = \left(\frac{k}{k_s} - 1 \right) \ln \frac{r_s}{r_w}$$

When permeability is reduced by a factor of 10 over a distance (r_s , w_s) of one meter around the well and the fracture, the following values are obtained:

$S = 20.7$ for a vertical well with a radius of 0.1 m;

$S = 0.7$ for a fracture extending 20 m on each side of the well.

The effect of reduced permeability is therefore much less severe, in terms of skin, around a fracture than around a vertical well.

The value of the skin around a fracture is usually between -0.1 and 1 .

Acidizing the reservoir around the fracture is of no use in terms of skin. The only gain is the improvement in internal fracture conductivity that may occur.

The effect of a hydraulic fracture is particularly beneficial for gas wells. Here the surface of the fracture is much larger than in a vertical well. Because of this, the

velocity of the gas at the entrance to the fracture and the coefficient of deviation from Darcy's law are much smaller than in a vertical well.

A small term of deviation from Darcy's law needs to be introduced inside the fracture, however.

The influence of the skin around the fracture was studied and described by Cinco [Ref. 31, 33]. Its influence on pressure is indicated in Figure 17.7 for an infinite conductivity fracture.

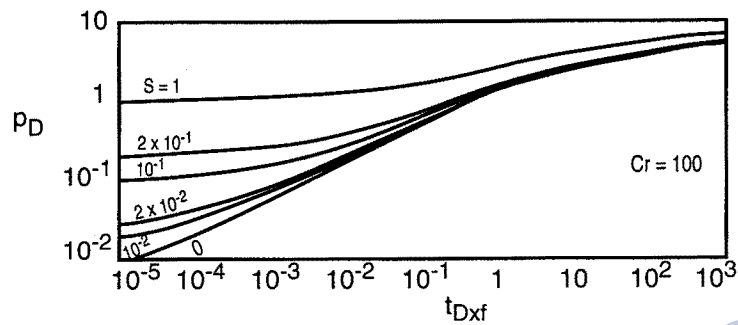


Fig. 17.7

17.3.3 Type curves and flows

Four flow periods can be identified during a test on a fractured well. In order of appearance they are:

- the wellbore storage effect;
- bilinear flow;
- linear flow;
- pseudoradial flow.

Linear flow in the fracture is not mentioned here since it is always hidden by the wellbore storage effect.

Each one of these flows has a corresponding characteristic pattern on the pressure derivative (Fig. 17.8):

- wellbore storage effect: straight line with a slope of 1;
- bilinear flow: straight line with a slope of 0.25;
- linear flow: straight line with a slope of 0.5;
- pseudoradial flow: stabilized derivative.

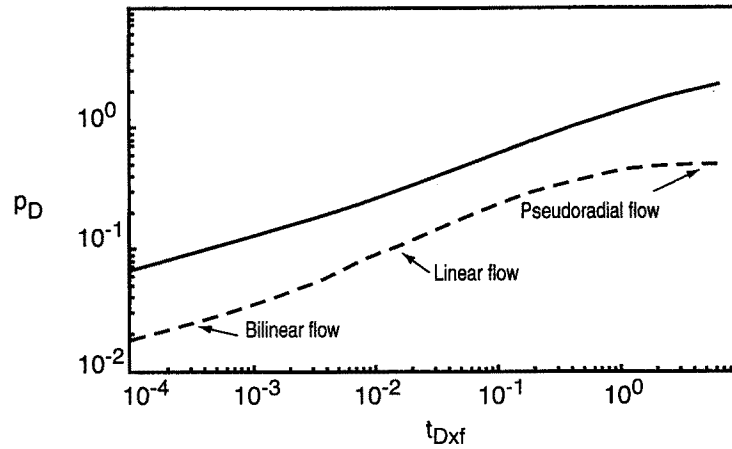


Fig. 17.8

Bilinear and linear flow can be hidden by the skin effect around the fracture.

- **Influence of the skin:**

The skin around the fracture corresponds to a flattening of the type curve at small t_{Dxf} .

This flattening may correspond to a dip in the derivative similar to what is observed for a fractured reservoir (Fig. 17.9).

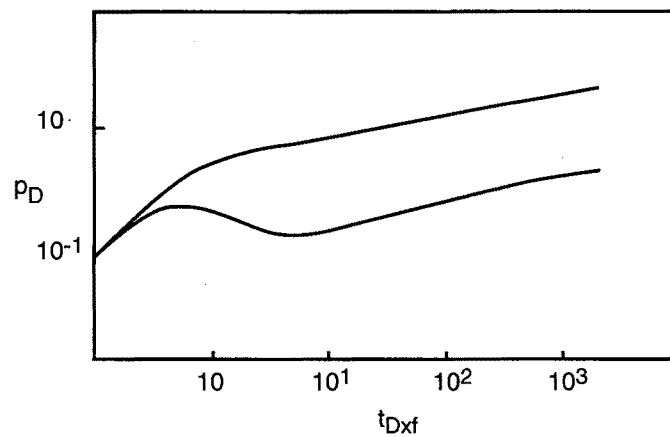


Fig. 17.9

This phenomenon may sometimes make it difficult to discriminate between a naturally fractured reservoir and an induced fracture of the reservoir at the well.

Comparison between test and core permeability can help make the difference between the two.

A fracture with intermediate conductivity (C_r ranging between 1 and 50) can be confused with a an infinite conductivity fracture with a skin.

The existence of a skin around the fracture can be detected at small t_{Dxt} by a type curve slope lower than 0.25. A fracture without any skin always gives a slope greater than 0.25 at short time periods.

17.4 TYPE CURVES

There are three sorts of type curves for fractured wells:

- the Gringarten type curves with a uniform flux in the fracture (Fig. 17.10);
- the Gringarten type curves with an infinite conductivity fracture (Fig. 17.11);
- the Cinco type curves: finite conductivity fracture and wellbore storage effect (Fig. 17.5).

These different type curves were analyzed and criticized by F. Daviau.

17.4.1 The Gringarten type curves (Figs. 17.10 and 17.11)

The two Gringarten type curves (infinite conductivity and uniform flux) represent the fracture in an infinite reservoir by a type curve.

They take the reservoir boundary effect into account. This advantage is of limited utility since the fractures are performed in reservoirs with low permeability. The boundaries are seldom reached during a test.

Besides the habitual limitations of type curves because they can not include previous flow rates, the Gringarten type curves also suffer from several specific limitations.

They do not take the following into account:

- fracture conductivity;
- the wellbore storage effect;
- the skin around the fracture.

These important limitations severely restrict their area of application.

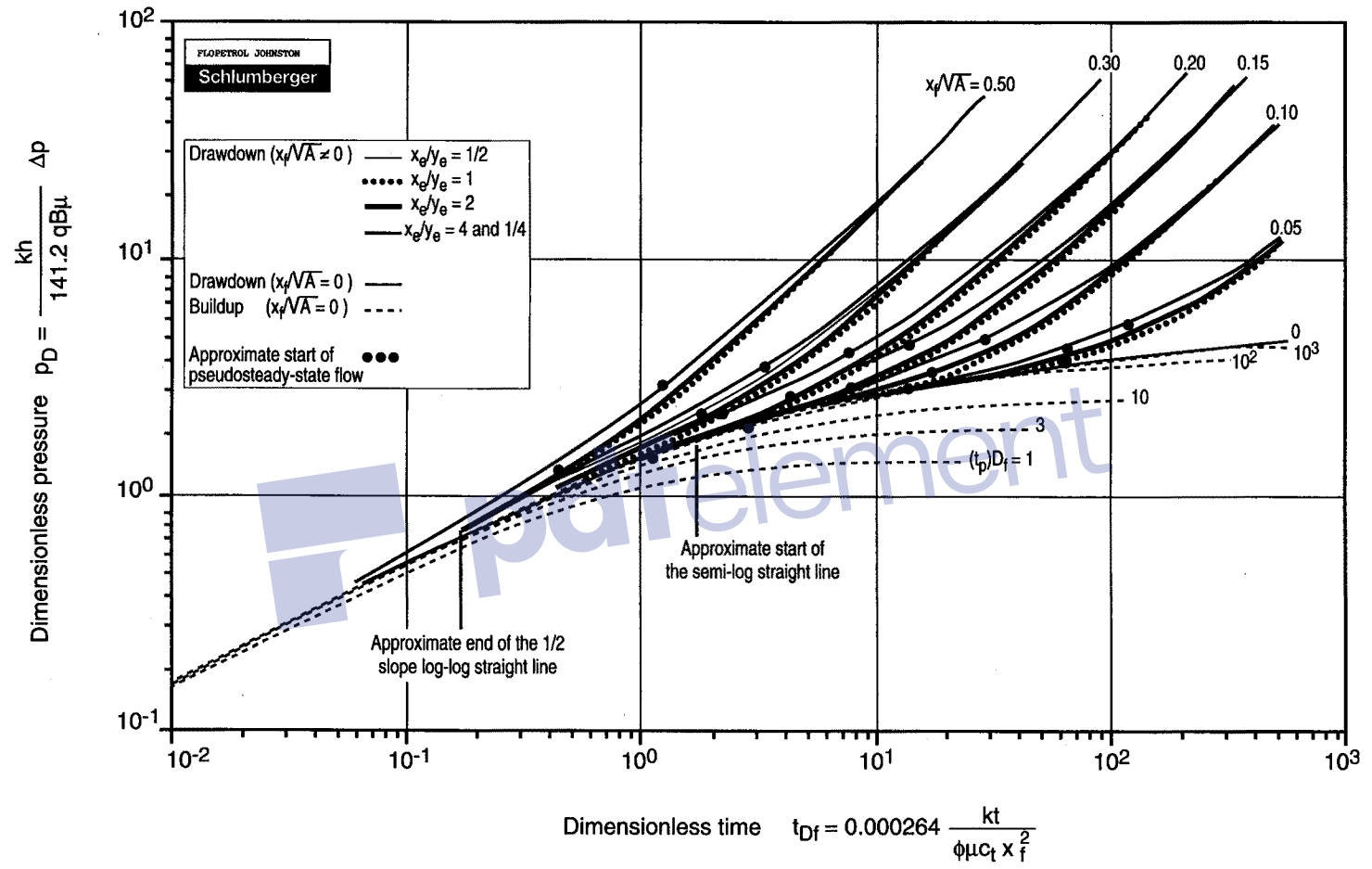


Fig. 17.10 Fracture with uniform flux

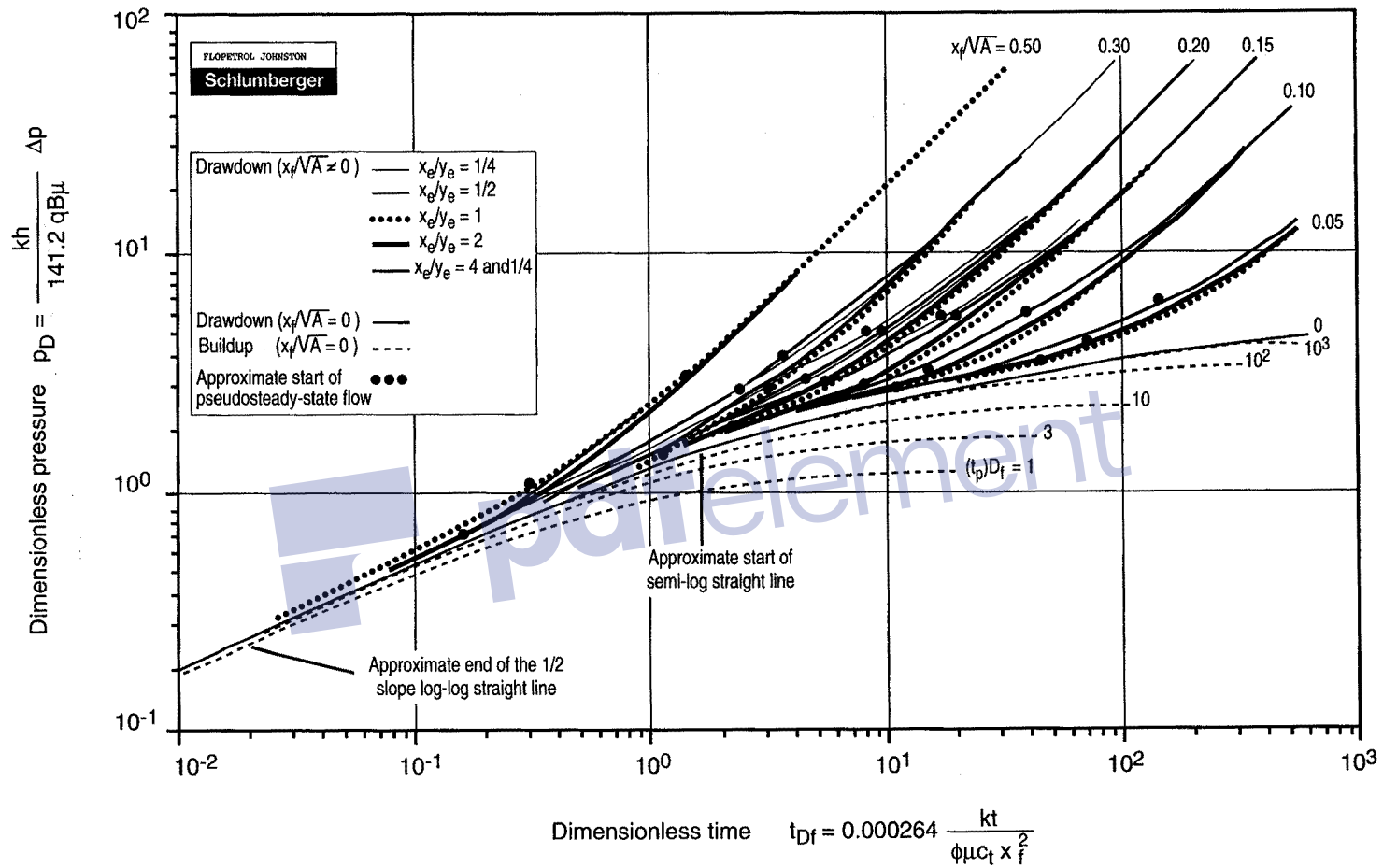


Fig. 17.11 Infinite conductivity fracture

17.4.2 The Cinco curves (Fig. 17.5)

The Cinco type curves take fracture conductivity into account and wellbore storage, but do not take the skin around the fracture into account.

They are used as described in section 17.3 and are the best for analyzing a test in a fractured well. They are, however, difficult to use because of the large number of parameters that have to be determined.

The same as for all the other curves, it is impossible to include the production history.

17.5 CONCLUSION

In this chapter we have detailed:

- the parameters required to describe a hydraulic fracture;
- the conventional interpretation methods;
- the advantages, but also the severe drawbacks, of type curves.

Often neither conventional methods nor type curves allow interpretation to be made. There may be several causes:

- The wellbore storage effect or the skin around the fracture hide bilinear and linear flow.
- The test is too short, the pseudoradial flow has not been reached.
- A skin around the fracture makes conventional methods and type curves unusable.
- The flow rate history does not allow curves to be used.

Under such conditions, a well model is the only recourse.

It can handle a larger number of parameters than type curves and it can also be used to:

- exploit the transitions from one flow to another;
- account for the skin around the fracture;
- account for the flow rate history.



Chapter 18

Horizontal wells

18.1 DESCRIPTION OF A HORIZONTAL WELL

Figure 18.1 gives a schematic illustration of a horizontal well.

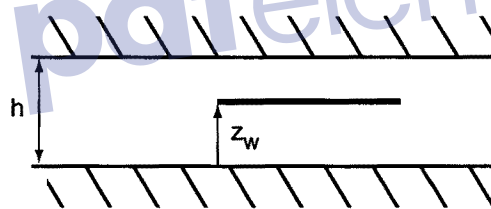


Fig. 18.1 Description of a horizontal well

The well with a radius, r_w , goes horizontally through the infinite reservoir over a length L . Reservoir thickness is h and it is bounded by impermeable shoulder beds. The well is located at a distance, z_w , from the bottom wall of the reservoir.

18.2 FLOWS AROUND A HORIZONTAL WELL. CONVENTIONAL INTERPRETATION METHODS

Assuming that the wellbore storage effect or the drainage area boundary effect do not hide them, two characteristic flow periods can be distinguished during a test on a horizontal well [Ref. 37]:

- Vertical radial flow (Fig. 18.2): The compressible zone generated by the flow rate change develops first in a vertical plane perpendicular to the well. The corresponding flow is radial. It ends when the shoulder beds are reached or when the well end effect is felt on the flows.

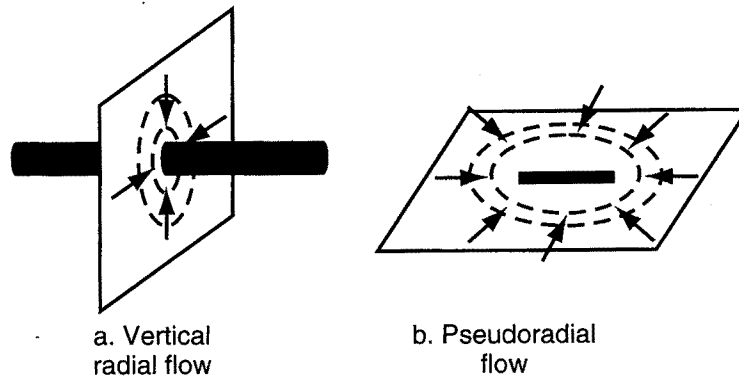


Fig. 18.2 The flows around a horizontal well

- Pseudoradial flow (Fig. 18.2): Once the vertical radial flow is over, a transition period begins.

After a certain time, the equipotentials become vertical cylinders similar to those around a vertical well. From then on the flow becomes radial circular in a horizontal plane. This flow is called pseudoradial.

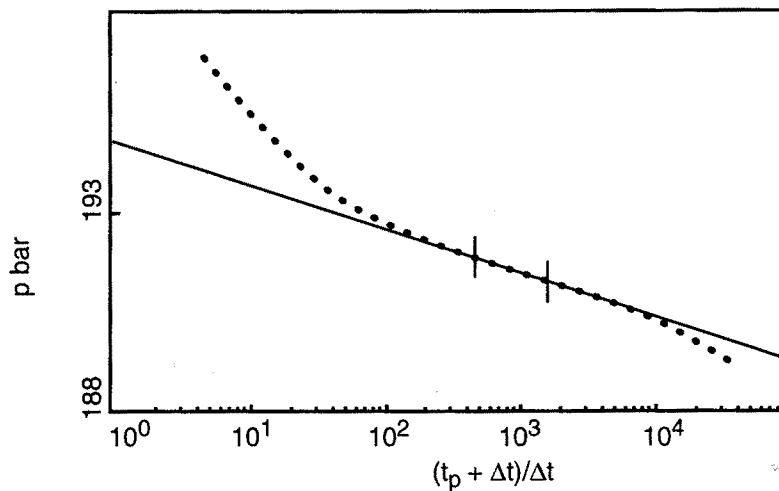


Fig. 18.3

18.2.1 Radial vertical flow

Like all radial flows, radial vertical flow corresponds to a linear variation of pressure versus the logarithm of time (Fig. 18.3).

During this period the horizontal well behaves like a vertical well in a reservoir with a thickness equal to the length L of the horizontal drain hole.

The compressible zone develops along vertical planes, so the pressure depends on both the horizontal and the vertical permeability of the reservoir.

The general equation showing pressure variations in a producing well versus time is as follows:

$$p_i - p_{wf} = \frac{\alpha qB\mu}{L\sqrt{k_v k_h}} \left(\log t + \log \frac{\sqrt{k_v k_h}}{\phi\mu c_t r_w^2} - \beta + 0.87 S \right) \quad (18.1)$$

$\alpha = 162.6$	$\beta = 3.23$	(in practical US units)
$\alpha = 21.5$	$\beta = 3.10$	(in practical metric units)
$\alpha = 0.183$	$\beta = -0.35$	(in SI units).

The slope of the semi-log straight line is used to determine $L\sqrt{k_v k_h}$. Information on the horizontal permeability, given by tests on vertical wells or by interpretation of pseudoradial flow, is used to determine the reservoir's permeability anisotropy (k_v/k_h).

The value of the pressure measured at one hour on the semi-log straight line is used to determine a skin:

$$S = 1.15 \left(\frac{p_i - p_{1h}}{m} - \log \frac{\sqrt{k_v k_h}}{\phi\mu c_t r_w^2} + \beta \right) \quad (18.2)$$

The skin is the sum of the well skin (plugging, deviation from Darcy's law), S_p , and a negative skin, S_a , due to the permeability anisotropy:

$$S = S_p + S_a$$

with:

$$S_a = \ln \left[\left(\frac{k_h}{k_v} \right)^{1/4} \frac{2}{1 + \sqrt{k_v k_h}} \right] \quad (18.3)$$

• **Beginning and end of radial vertical flow:**

Radial vertical flow is visible between the end of the wellbore storage effect and the time when the boundary formation or well end effect is felt.

The boundary formation effect is perceived [Ref. 37] from:

$$t_{DL} = 1.28 \left(\frac{h - z_w}{L} \right)^2 \quad (18.4)$$

with $t_{DL} = \frac{\gamma k_h t}{\phi \mu c_t L^2}$.

$\gamma = 0.000264$ (in practical US units)
 $\gamma = 0.000355$ (in practical metric units)
 $\gamma = 1$ (in SI units).

The well end effect is felt from:

$$t_{DL} = 0.015 \quad (18.5)$$

18.2.2 Pseudoradial flow

When the pseudoradial flow begins, the compressible zone has reached regions where the well geometry no longer affects the flows. From these areas the well is perceived like a vertical well.

The general pressure equation is the same as for a vertical well:

$$p_i - p_{wf} = \frac{\alpha q B \mu}{k_h h} \left(\log t + \log \frac{k_h}{\phi \mu c_t r_w^2} - \beta + 0.87 S' \right) \quad (18.6)$$

α and β have the same values as in formula 18.2 corresponding to radial vertical flow.

The same as for a vertical well, the slope of the semi-log straight line allows the reservoir's $k_h h$ to be determined (Fig. 18.4).

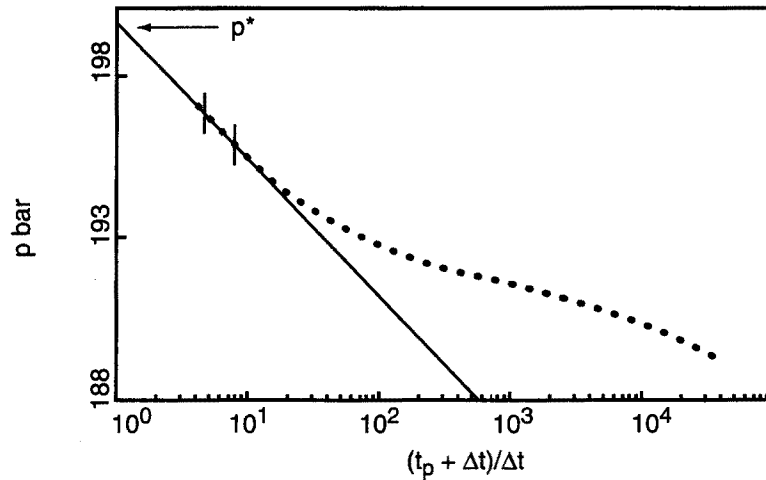


Fig. 18.4

The value of the pressure at one hour measured on the semi-log straight line is used to determine a skin S' which depends on both the well skin, S , and a geometrical skin, S_g :

$$S' = S_g + \frac{h}{L} \sqrt{\frac{k_h}{k_v}} S \quad (18.7)$$

The skin, S , is the sum of the well skin, S_p , and the anisotropy skin, S_a .

- **Geometrical skin:**

The geometrical skin measures the improvement to production due to the well geometry, when a horizontal and a vertical well are compared.

The geometrical skin can be calculated using the following expression [Ref. 37 and 38]:

$$S_g = \ln \frac{4r_w}{L} + \frac{h}{L} \sqrt{\frac{k_h}{k_v}} \ln \left(\frac{h}{2\pi r_w \sin \frac{\pi z_w}{h}} (k_h / k_v)^{1/4} \right) \quad (18.8)$$

This expression does not take into account the well end effect. The real value of the geometrical skin is slightly smaller than the one calculated from formula 18.8

and depends heavily on the reservoir's permeability anisotropy. The geometrical skin is negative, i.e. a horizontal well improves flow near the wellbore, as long as $L \sqrt{k_v/k_h}$ is greater than $k_h h$.

Example:

Length of the horizontal well	$L = 500$ m
Well radius	$r_w = 0.1$ m
Net pay	$h = 50$ m
Centered well	$z_w = 25$ m.

The table below shows the diminishing interest of a horizontal well from a geometrical standpoint when the reservoir's vertical permeability decreases.

k_v/k_h	1	0.1	0.01	0.0014	0.0001
S_g	-6.9	-6.3	-4.5	0	20.4

• **Start of the pseudoradial flow:**

According to F. Daviau [Ref. 37] pseudoradial flow begins at:

$$t_{DL} = 1.5 \text{ to } 2 \quad (18.9)$$

This is 100 times later than the beginning of the well end effect.

The late beginning of this flow means that it can be hidden by the reservoir boundary effect [Ref. 37] or by the drainage area effect and that it is observed only in reservoirs with high hydraulic diffusivity.

• **Extrapolated pressure:**

The extrapolated pressure, p^* , is read on the second semi-log straight line, the one that corresponds to pseudoradial flow. The same is true for determining the initial pressure during initial testing, as long as no reservoir boundary has been reached.

18.3 TYPE CURVES, THE DERIVATIVE

Three characteristic flows can be seen during the test of a horizontal well:

- The wellbore storage effect: characterized by linear variation in the pressure versus time. During this flow, the pressure and its derivative follow a straight line with a slope of 1 on a log-log plot.
- Radial vertical flow.
- Pseudoradial flow.

The sequence of flows is indicated in Figure 18.5.

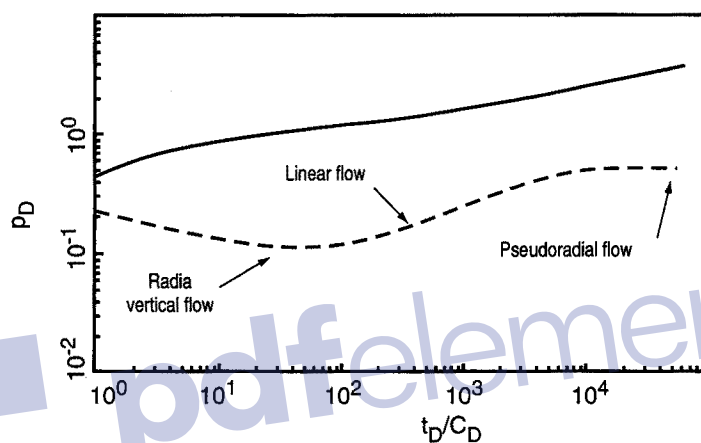


Fig. 18.5

- **Radial vertical flow:**

Radial vertical flow corresponds to a stabilization of the derivative. The dimensionless pressure derivative stabilizes at:

$$0.5 \times \frac{h}{L} \sqrt{\frac{k_h}{k_v}}$$

- **Pseudoradial flow:**

Pseudoradial flow corresponds to a stabilization at 0.5 of the dimensionless pressure derivative.

- **Transition between radial vertical and pseudoradial flow:**

The shape of the transition between radial vertical and pseudoradial flow depends on the ratio between $k_h h$ and $L \sqrt{k_v k_h}$.

Two main cases can be found:

First case: $L \sqrt{k_v k_h} > k_h h$

In this case the reservoir boundary formations have been reached before the well ends affect the radial vertical flow noticeably.

The shoulder beds channel the flows. A linear flow develops, characterized by a linear increase of the derivative with a slope of 0.5. This flow can be seen in Figures 18.5 and 18.6. It lasts as long as the well ends do not noticeably perturb the flows.

Second case: $L \sqrt{k_v k_h} < k_h h$

In this case the effect of the well ends is felt before the shoulder beds have been reached.

The flow becomes spherical and is characterized by a linear decrease of the derivative with a slope of -0.5 . This flow, visible in Figure 18.6, lasts as long as the shoulder beds have not been reached.

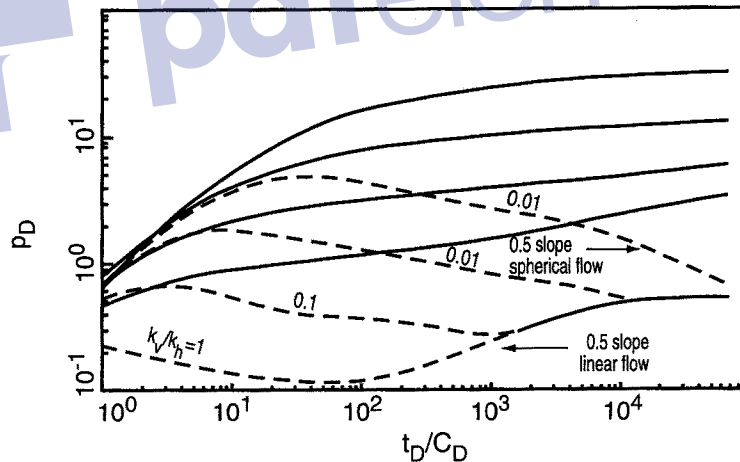


Fig. 18.6

Chapter 19

Injection wells

19.1 DESCRIPTION OF AN INJECTION WELL

Injecting a fluid into a homogeneous reservoir determines two zones around the well with different characteristics.

The interpretation methods presented in this chapter assume that the two zones are concentric (Fig. 19.1).

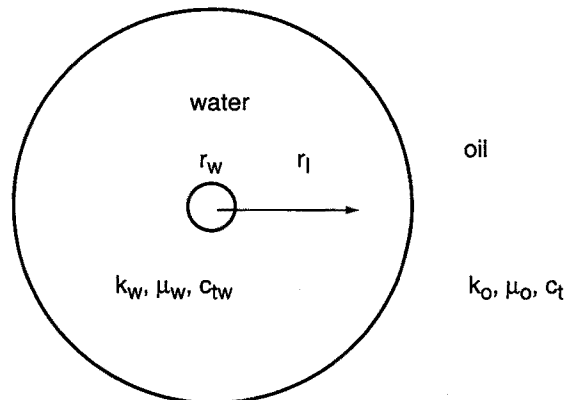


Fig. 19.1

This hypothesis is verified when the injected fluid's mobility (k_w/μ_w) is lower than that of the fluid in place (k_o/μ_o). When the opposite is true, fingering can take place.

The methods presented assume a piston-like displacement of the fluid in place by the injected fluid.

Injection determines two concentric zones:

- **The injection zone near the well:**

Its characteristics are the following:

- The viscosity of the fluid is that of the injected fluid and is expressed as μ_w .
- The permeability is that of the injected fluid in the presence of residual oil saturation after displacement by the injected fluid. It is generally different from the permeability to the fluid in place.
- The total compressibility in the zone near the wellbore is expressed as c_{tw} .
- The injection radius is the radius of the zone that extends near the well to a distance expressed as r_i . The value of r_i can be calculated from the injected volume V_i :

$$r_i = \sqrt{\frac{V_i}{\pi h \phi (S_w - S_{wi})}} \quad (19.1)$$

S_{wi} is the irreducible water saturation.

- **The zone farther from the well:**

Beyond the injection radius r_i the reservoir has the usual properties of a reservoir with a one-phase oil flow:

- The viscosity is that of the oil and it is noted μ_o .
- The permeability is the oil permeability at irreducible water saturation S_{wi} and is noted k_o .
- The total compressibility is c_t .

19.2 DESCRIPTION OF FLOWS

- **Conventional interpretation methods:**

When the wellbore storage effect does not hide them, two flow periods can be seen successively during the test of an injection well:

- An initial radial circular flow which corresponds to the compressible zone passing through the near-well zone where the injected fluid has displaced the oil in place.
- A second radial circular flow which corresponds to penetration of the zone farther from the well. It corresponds to the same as the flow normally found during a test on a vertical well in an oil reservoir.

• **Radial circular flow in the near-well zone:**

During this flow the bottomhole pressure follows a logarithmic variation versus time:

$$p_i - p_{wf} = \frac{\alpha q_w B_w \mu_w}{k_w h} \left(\log t + \log \frac{k_w}{\phi \mu_w c_{tw} r_w^2} - \beta + 0.87 S \right) \quad (19.2)$$

$\alpha = 141.2$	$\beta = 3.23$	(in practical US units)
$\alpha = 21.5$	$\beta = 3.10$	(in practical metric units)
$\alpha = 0.183$	$\beta = -0.35$	(in SI units).

The injection flow rate is counted negatively.

The first semi-log straight line corresponding to this variation (Fig. 19.2) is used to determine:

$$k_w h = \frac{\alpha q B \mu_w}{m_w} \quad (19.3)$$

with m_w , slope of this first semi-log straight line:

$$S = 1.151 \left(\frac{p_i - p_{1h}}{m} - \log \frac{k_w}{\phi \mu_w c_{tw} r_w^2} + \beta \right) \quad (19.4)$$

S is the real skin of the well.

Figure 19.2 indicates this straight line on a falloff (pressure drop).

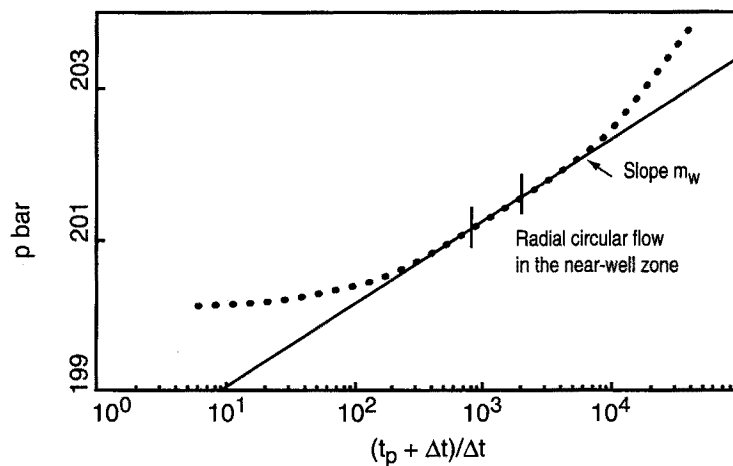


Fig. 19.2

The same as for production wells, injection wells are mainly tested during shut in.

In the same way as a production well has a pressure buildup during shut-in, an injection well has a falloff, when the well is shut in.

The skin of an injection well can be very low (less than -2). When the injection pressure is greater than the reservoir fracture pressure, injection may cause accidental fracturing of the reservoir at the well.

When there is extensive fracturing, a pressure variation typical of a hydraulically fractured well may be seen (see Chapter 16).

• **Radial circular flow farther from the well:**

Pressure also varies logarithmically for this flow and is described by the following equation:

$$p_i - p_{wf} = \frac{\alpha q_w B_w \mu_o}{k_o h} \left(\log t + \log \frac{k_o}{\phi \mu_o c_r r_w^2} - \beta + 0.87 S' \right) \quad (19.5)$$

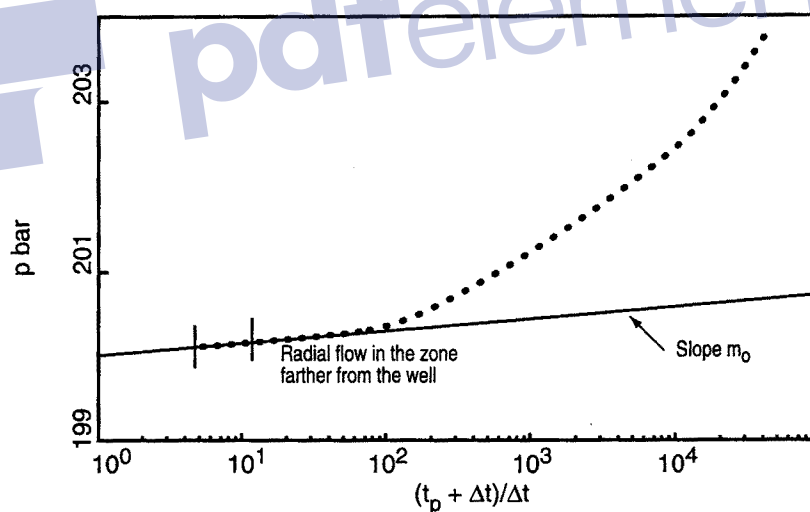


Fig. 19.3

The second semi-log straight line corresponding to this variation is used to determine (Fig. 19.3):

$$k_o h = \frac{\alpha q_w B_w \mu_o}{m_o} \quad (19.6)$$

with m_o , the slope of this second semi-log straight line:

$$S' = 1.151 \left(\frac{p_i - p_{1h}}{m_o} - \log \frac{k_o}{\phi \mu_o c_t r_w^2} + \beta \right) \quad (19.7)$$

• **Skin :**

The skin, S' , is composite, due to the well skin S and the injection effect S_i :

$$S' = \frac{k_o \mu_w}{\mu_o k_w} S + \left(\frac{k_o \mu_w}{\mu_o k_w} - 1 \right) \ln \frac{r_l}{r_w} \quad (19.8)$$

The second term S_i :

$$S_i = \left(\frac{k_o \mu_w}{\mu_o k_w} - 1 \right) \ln \frac{r_l}{r_w}$$

corresponds to the additional pressure drop in the vicinity of the wellbore due to the fact that the injected fluid has a different mobility from the fluid in place. This second term is calculated in a similar way as described in section 3.3.

This second term explains the substantial pressure drops that can be caused by injecting water that is less mobile than the oil in an oil reservoir.

Table 19.1 shows the value of the term S_i for two mobility ratio values, R_m (R_m = mobility of the water/mobility of the oil), in a well with a radius of 10 cm and for different injection radius values.

Table 19.1
Example of injection skin

$R_m = 0.5$

r_l	1 m	10 m	50 m
S_i	2.3	4.6	6.2

$R_m = 0.1$

r_l	1 m	10 m	50 m
S_i	20.7	41.4	55.9

Inversely, if the water is more mobile than the oil, the skin is negative. This type of configuration is also associated with water fingering. The interpretation methods presented can not be applied when fingering becomes significant.

- **Determining the injection radius:**

When S and S' are known, the injection radius can be calculated using equation 19.8:

$$r_i = r_w \exp \left(\left(S' - \frac{k_o \mu_w}{\mu_o k_w} S \right) / \left(\frac{k_o \mu_w}{\mu_o k_w} - 1 \right) \right) \quad (19.9)$$

This value can be compared to the one obtained from the material balance (equation 19.1).

A wide difference between the two can have several causes:

- inaccurate evaluation of the skins, S and S' ;
- mistaken evaluation of the saturation in injected fluid, S_w ;
- injection of part of the fluid outside the target level.

- **Extrapolated pressure:**

The extrapolated pressure must be read on the semi-log straight line corresponding to the radial circular flow in the zone farther from the wellbore (Fig. 19.3).

19.3 TYPE CURVES AND DERIVATIVE

Three characteristic flows are seen one after the other during an injection well test:

- The wellbore storage effect, characterized as usual by an increase in the pressure and its derivative corresponding to a straight line with a slope of 1 on a log-log plot.
- Radial circular flow in the injection zone near the well.
- Radial circular flow in the zone farther from the well.

The sequence of these flows is indicated in Figure 19.4.

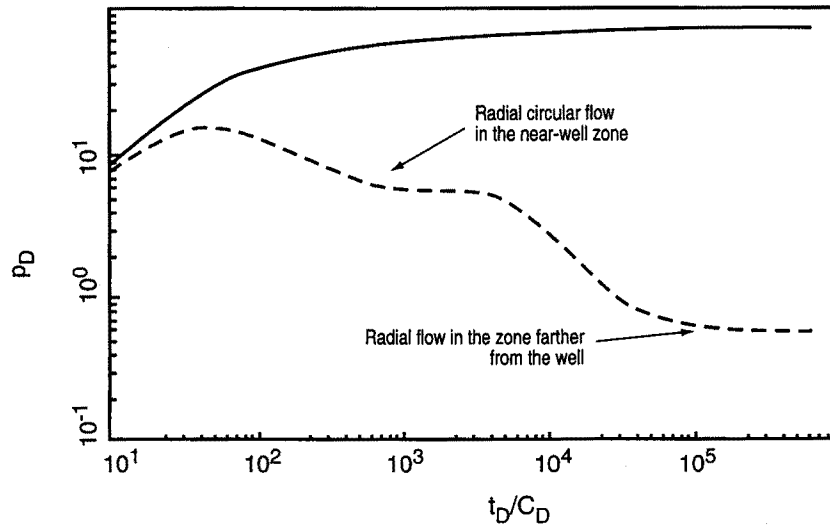


Fig. 19.4

- **Radial circular flow in the near-well zone:**

Radial circular flow in the near-well zone shows as a stabilization of the pressure derivative.

The level of stabilization of the dimensionless pressure derivative corresponds to:

$$0.5 \times \frac{k_o \mu_w}{\mu_o k_w}$$

when dimensionless pressure is defined by:

$$p_D = \frac{\alpha q_w B_w \mu_o}{k_o h}$$

$$\begin{aligned} \alpha &= 141.2 && \text{(in practical US units)} \\ \alpha &= 18.66 && \text{(in practical metric units)} \\ \alpha &= 1/2 \pi && \text{(in SI units).} \end{aligned}$$

- **Radial circular flow in the farther zone:**

Radial circular flow in the farther zone is characterized by a second stabilization of the derivative (Fig. 19.4).

The level of stabilization of the dimensionless pressure derivative corresponds to 0.5.

- **Transition between the two flows:**

The change in mobility corresponding to the transition from the near-well zone to the farther zone corresponds to a change in the level of stabilization of the derivative.

The change in zone is also associated with a change in the medium's hydraulic diffusivity (going from $k_w/\phi\mu_w c_{tw}$ to $k_o/\phi\mu_o c_t$).

The effect of the change in diffusivity is noticeable during the transition between the two flows. It is illustrated in Figure 19.5 where the mobility is assumed to be identical in the two zones. Only the total compressibility changes:

- Increasing diffusivity corresponds to a dip in the derivative. The same phenomenon is observed in a fractured reservoir when fracture flow turns into matrix-fracture flow (see Chapter 15).
- Decreasing diffusivity corresponds to a maximum of the derivative.

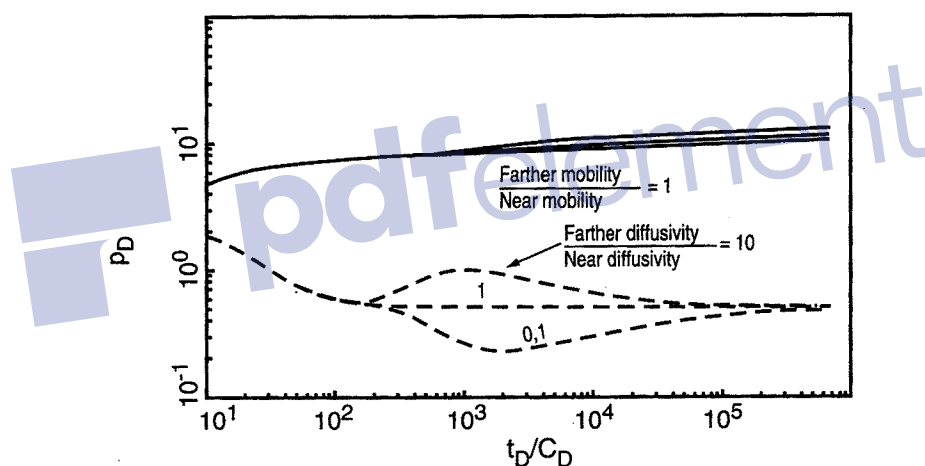


Fig. 19.5

19.4 THE OBJECTIVES OF TESTING AN INJECTION WELL

Five parameters can be determined by interpreting an injection well test:

- the wellbore storage, C ;
- the permeability in the injection zone, k_w ;
- the permeability in the oil zone, k_o ;
- the well skin, S ;
- the injection radius, r_i .

Interpreting one single test can give these parameters when the sequence of flows described in the preceding sections is visible.

There are two cases when the sequence is not visible:

- **The test is too short to reach the oil zone:**

Interpreting the test gives neither the permeability in the oil zone nor the injection radius.

- **The wellbore storage effect hides the flow in the injection zone:**

This can occur when the well is tested after injecting a very small volume.

Interpreting one single test gives neither the permeability in the near-well zone nor the well skin.

These parameters can, however, be obtained by testing the well after injecting further volumes.

Each of these tests can be used to determine an overall well skin, S' , which is dependent on the injection radius:

$$S' = \frac{S}{R_m} + \left(\frac{1}{R_m} - 1 \right) \ln \frac{r_i}{r_w} \quad (19.10)$$

In this expression R_m is the mobility ratio:

$$R_m = \frac{k_w}{\mu_w} / \frac{k_o}{\mu_o}$$

This expression can be written in another form versus the injected volume (see equation 19.1):

$$S' = \frac{S}{R_m} + 1.151 \left(\frac{1}{R_m} - 1 \right) \log \frac{V_i}{\pi r_w^2 h \phi (S_w - S_{wi})} \quad (19.11)$$

By plotting S' versus the logarithm of $V_i / \pi r_w^2 h \phi (S_w - S_{wi})$ a straight line is obtained (Fig. 19.6):

– with a slope of $1.151 \left(\frac{1}{R_m} - 1 \right)$

– with the ordinate at the origin $\frac{S}{R_m}$.

Chapter 19 • INJECTION WELLS

The slope is used to determine the mobility ratio R_m between the injected fluid and the fluid in place.

The ordinate at the origin serves to determine the well skin.

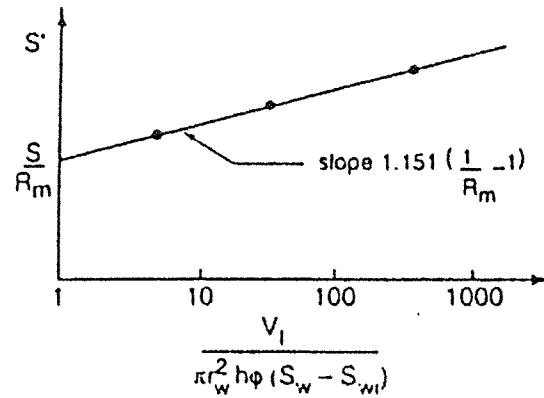


Fig. 19.6 Determining the skin and the mobility ratio by tests after injecting different volumes

pdfelement



Fluid aspects

pdfelement



Chapter 20

Gas wells

20.1 PSEUDOPRESSURE

The diffusivity equation was established for an oil well (Chapter 1), by making several hypotheses which are not usually acceptable in a gas well:

- low, constant compressibility;
- constant viscosity;
- low pressure gradients.

In a gas well viscosity and compressibility vary with pressure.

• Compressibility:

The variation in density of a real gas can be expressed using the following equation of state:

$$\rho = \frac{pM}{ZRT} \quad (20.1)$$

where:

M: molar mass of the gas

R: gas constant

Z: compressibility factor of the gas. Z shows the deviation of a real gas in relation to the ideal gas.

The compressibility of the gas is expressed by:

$$c_g = \frac{1}{\rho} \left(\frac{\partial \rho}{\partial p} \right)_T \quad (20.2)$$

i.e., replacing ρ by its value expressed by equation 20.1:

$$c_g = \frac{1}{\rho} - \frac{1}{Z} \left(\frac{\partial Z}{\partial p} \right)_T \quad (20.3)$$

• **Diffusion equation:**

The same as for oil, the diffusion equation that governs the behavior of flowing gas is established using:

– Darcy's law:

$$\vec{V} = - \frac{k}{\mu} \overrightarrow{\text{grad } p} \quad (20.4)$$

A non-linear term must be introduced into Darcy's law to take into account the effect of the high flow velocities that exist near the well. This non-linear term is taken into account by a skin of deviation from Darcy's law (see section 20.2).

– Material balance:

$$\text{div} (\rho \vec{V}) + \frac{\partial (\rho \phi S_g)}{\partial t} = 0 \quad (20.5)$$

– The equation of state which defines the equivalent compressibility of the gas:

$$c_g = \frac{1}{\rho} - \frac{1}{Z} \left(\frac{\partial Z}{\partial p} \right)_T \quad (20.6)$$

$$\frac{\partial (\rho \phi S_g)}{\partial t} = \left(\phi S_g \frac{\partial \rho}{\partial p} + \rho S_g \frac{\partial \phi}{\partial p} + \rho \phi \frac{\partial S_g}{\partial p} \right) \frac{\partial p}{\partial t}$$

but: $\frac{\partial \rho}{\partial p} = \rho c_g$

$$\frac{\partial \phi}{\partial p} = \phi c_p$$

$$\frac{\partial S_g}{\partial p} = \frac{\partial (1 - S_w)}{\partial p} = S_w (c_w + c_p) \quad \text{car} \quad S_w = V_w/V_p$$

hence:
$$\frac{\partial (\rho \phi S_g)}{\partial t} = \rho \phi c_t \frac{\partial p}{\partial t} .$$

By replacing ρ and \vec{V} by their expression in (20.1), (20.4) and (20.6), the material balance becomes:

$$\boxed{\text{div} \left(-\frac{\rho}{\mu Z} k \vec{\text{grad}} p \right) + \phi \mu c_t \frac{\rho}{\mu Z} \frac{\partial p}{\partial t} = 0} \quad (20.7)$$

• Pseudopressure:

Differential equation (20.7) does not have simple form when it is expressed directly in pressure terms. However, it takes on the form of a conventional diffusion equation when it is expressed using the pseudopressure function defined by:

$$\psi = 2 \int_{p_0}^p \frac{p}{\mu Z} dp \quad (20.8)$$

in fact:
$$\vec{\text{grad}} \psi = 2 \frac{p}{\mu Z} \vec{\text{grad}} p$$

$$\frac{\partial \psi}{\partial t} = 2 \frac{p}{\mu Z} \frac{\partial p}{\partial t}$$

Equation (20.7) becomes a pseudopressure diffusion equation:

$$\boxed{\Delta \psi - \frac{1}{K} \frac{\partial \psi}{\partial t} = 0} \quad (20.9)$$

with $K = \frac{k}{\phi \mu c_t}$ hydraulic diffusivity of the reservoir.

Pseudopressure is calculated directly based on the variation of μ and Z with pressure.

It takes on a simple expression in two extreme cases:

- At low pressure: $p < 2000$ psi (140 bar)

At low pressure the product μZ is roughly constant. Under these conditions:

$$\psi = \frac{p^2 - p_o^2}{\mu Z} \quad (20.10)$$

The diffusion equation is verified by the square of pressure:

$$\Delta p^2 - \frac{1}{K} \frac{\partial p^2}{\partial t} = 0 \quad (20.11)$$

- At high pressure: $p > 3000$ psi (210 bar)

At high pressure gases have a behavior that is similar to oil's. The pseudo-pressure varies linearly with pressure. The diffusion equation is verified by the pressure:

$$\Delta p - \frac{1}{K} \frac{\partial p}{\partial t} = 0 \quad (20.12)$$

To find out the domain of validity of the extreme forms it is recommended to calculate several values of ψ in the pressure domain corresponding to the interpretation domain and to plot ψ versus p and p^2 .

The domain where ψ varies linearly with p and p^2 is where p or p^2 can be used directly for interpretation (Fig. 20.1).

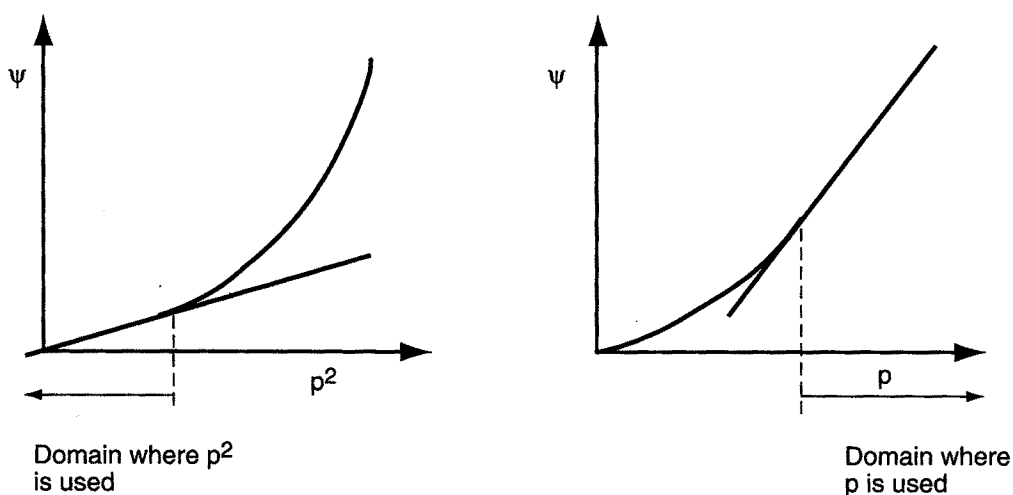


Fig. 20.1

20.2 DEVIATION FROM DARCY'S LAW

The high flow rates that are usually found in gas wells generate high flow velocities in the wellbore vicinity.

At high velocities Darcy's law can no longer be applied. In order to describe flows properly in the vicinity of the wellbore, a quadratic term needs to be added to Darcy's law:

$$\vec{\text{grad}} p = -\frac{\mu}{k} \vec{V} (1 + A |\vec{V}|) \quad (20.13)$$

This deviation term in Darcy's law generates an additional pressure drop in the vicinity of the wellbore that is a linear function of the flow rate. Since this pressure drop is particular to the wellbore vicinity, it is included in the skin.

• Skin with constant flow rate production:

When the well is opened to production at a constant flow rate, the overall skin is expressed by:

$$S' = S + qD \quad (20.14)$$

The term qD is the skin component due to the deviation from Darcy's law. D is called the deviation coefficient from Darcy's law.

To find out this coefficient and determine the real skin, S , of the well, it is necessary to measure the overall skin, S' , at several flow rates.

• Skin with a flow rate history:

The equation governing pseudopressure change with a flow rate history is of the following form:

$$\psi_i - \psi(t) = \alpha \left\{ \sum_{i=1}^n (q_i - q_{i-1}) p_D(t - t_{i-1}) + q_n (S + q_n D) \right\} \quad (20.15)$$

During interpretation of a well test, the pressure variations due to a change in flow rate are measured relative to the pressure at the time when the flow rate changes.

Interpretation deals with $\psi(t_{n-1}) - \psi(t)$ rather than $\psi_i - \psi(t)$ (Fig. 20.2).

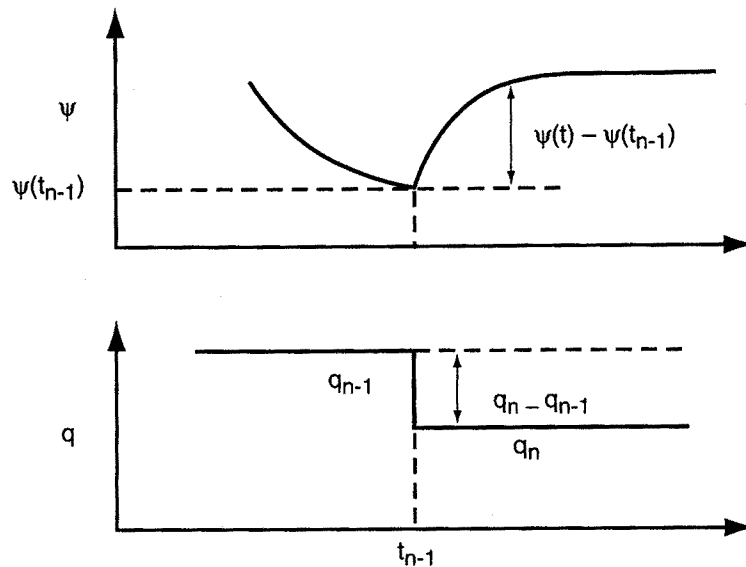


Fig. 20.2

Likewise, interpretation deals with the variation in flow rate ($q_n - q_{n-1}$) rather than the flow rate itself q_n . Under these conditions, the equation used to interpret a test is:

$$\psi(t_{n-1}) - \psi(t) = \alpha \left\{ \sum_{i=1}^{n-1} (q_i - q_{i-1}) [p_D(t - t_{i-1}) - p_D(t_{n-1} - t_{i-1})] + (q_n - q_{n-1}) p_D(t - t_{n-1}) + (q_n - q_{n-1}) [S + (q_n - q_{n-1}) D] \right\}$$

The skin to be considered is:

$$S' = S + (q_n + q_{n-1}) D \quad (20.16)$$

To find out S and D this overall skin must be measured at several flow rates.

When the overall skin is plotted versus $(q_n + q_{n-1})$ (Fig. 20.3), a straight line is obtained:

- with a slope of D ;
- an ordinate at the origin S .

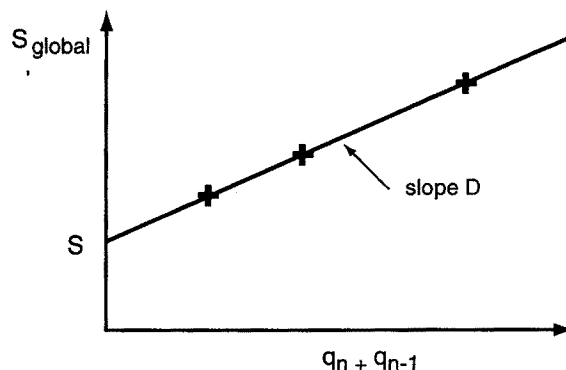


Fig. 20.3

Two important special cases should be considered:

- Pressure buildup: $q_n = 0$.
 $q_n + q_{n-1}$ is reduced to the last flow rate before shut-in q_{n-1} .
- Only one flow rate: $q_{n-1} = 0$.
 $q_n + q_{n-1}$ is reduced to flow rate q_n alone.

20.3 INTERPRETATION OF A GAS WELL TEST

Chapters 1 to 19 presented solutions to the diffusion equation expressed in dimensionless variables for different reservoir-well configurations. Several interpretation methods were developed.

These solutions and methods were designed for one-phase flow oil wells. All the solutions and methods are applicable directly to gas wells by replacing pressure by pseudopressure.

Tables 20.1 and 20.2 indicate how to go from dimensionless pressure to pseudopressure along with the expression of the slope of the semi-log straight line in pseudopressure.

Table 20.1 is in practical US units while Table 20.2 is in practical metric units.

The tables propose two sorts of standard conditions for measuring the gas flow on the surface:

- conditions to be defined by the user;
- usual standard conditions: $T = 520^\circ\text{R}$; $p = 14.7$ psia.

Table 20.1 US units
(*q* bbl/d ; *q_{sc}* scft/d)

		Dimensionless pressure	Slope of the semi-log straight line
Oil		$p_D = \frac{kh}{141.2 qB\mu} (p_i - p_{wf})$	$m = \frac{162.6 qB\mu}{kh}$
Gas	<i>p</i>	$p_D = \frac{kh \bar{p} T_{sc}}{25 150 \bar{\mu} \bar{Z} T q_{sc} p_{sc}} (p_i - p_{wf})$	$m = 28 955 \frac{q_{sc} \bar{\mu} \bar{Z} T p_{sc}}{kh \bar{p} T_{sc}}$
	<i>p</i> ²	$p_D = \frac{kh T_{sc}}{50 300 \bar{\mu} \bar{Z} T q_{sc} p_{sc}} (p_i^2 - p_{wf}^2)$	$m = 57 910 \frac{q_{sc} \bar{\mu} \bar{Z} T p_{sc}}{kh T_{sc}}$
	ψ	$p_D = \frac{kh}{50 300 T q_{sc}} \frac{T_{sc}}{p_{sc}} (\psi - \psi_{wf})$	$m = 57 910 \frac{qT p_{sc}}{kh T_{sc}}$
Gas	<i>p</i>	$p_D = \frac{kh \bar{p}}{711 \bar{\mu} \bar{Z} T q_{sc}} (p_i - p_{wf})$	$m = 818 \frac{q_{sc} \bar{\mu} \bar{Z} T}{kh \bar{p}}$
	<i>p</i> ²	$p_D = \frac{kh}{1 422 \bar{\mu} \bar{Z} T q_{sc}} (p_i^2 - p_{wf}^2)$	$m = 1 637 \frac{q_{sc} \bar{\mu} \bar{Z} T}{kh}$
	ψ	$p_D = \frac{kh}{1 422 T q_{sc}} (\psi - \psi_{wf})$	$m = 1 637 \frac{q_{sc} T}{kh}$

Table 20.2 Metric units
(q et q_{sc} m^3/lj)

		Dimensionless pressure	Slope of the semi-log straight line
Oil		$p_D = \frac{kh}{18.66 qB\mu} (p_i - p_{wf})$	$m = \frac{21.5 qB\mu}{kh}$
Gas	p	$p_D = \frac{kh\bar{p}T_{sc}}{18.66 \bar{\mu} \bar{Z} T q_{sc} p_{sc}} (p_i - p_{wf})$	$m = 21.5 \frac{q_{sc} \bar{\mu} \bar{Z} T}{kh \bar{p} T_{sc}} p_{sc}$
	p^2	$p_D = \frac{khT_{sc}}{37.32 \bar{\mu} \bar{Z} T q_{sc} p_{sc}} (p_i^2 - p_{wf}^2)$	$m = 43 \frac{q_{sc} \bar{\mu} \bar{Z} T}{kh T_{sc}} p_{sc}$
	ψ	$p_D = \frac{kh}{37.32 T q_{sc} p_{sc}} T_{sc} (\psi - \psi_{wf})$	$m = 43 \frac{qT}{kh T_{sc}} p_{sc}$
Gas	p	$p_D = \frac{kh\bar{p}}{0.0648 \bar{\mu} \bar{Z} T q_{sc}} (p_i - p_{wf})$	$m = 0.0746 \frac{q_{sc} \bar{\mu} \bar{Z} T}{kh \bar{p}}$
$p_{sc} = 1 \text{ bar}$	p^2	$p_D = \frac{kh}{0.1296 \bar{\mu} \bar{Z} T q_{sc}} (p_i^2 - p_{wf}^2)$	$m = 0.1492 \frac{q_{sc} \bar{\mu} \bar{Z} T}{kh}$
$T_{sc} = 289 \text{ °K}$	ψ	$p_D = \frac{kh}{0.1296 T q_{sc}} (\psi - \psi_{wf})$	$m = 0.1492 \frac{q_{sc} T}{kh}$

Table 20.3 SI units

		Dimensionless pressure	Slope of the semi-log straight line
Oil		$p_D = \frac{2\pi kh}{qB\mu} (p_i - p_{wf})$	$m = \frac{0.183 qB\mu}{kh}$
Gas	P	$p_D = \frac{2 kh\bar{p}T_{sc}}{\bar{\mu}ZTq_{sc} p_{sc}} (p_i - p_{wf})$	$m = 0.183 \frac{q_{sc} \bar{\mu}ZT}{kh\bar{p}} \frac{p_{sc}}{T_{sc}}$
	p ²	$p_D = \frac{\pi khT_{sc}}{\bar{\mu}ZTq_{sc} p_{sc}} (p_i^2 - p_{wf}^2)$	$m = 0.367 \frac{q_{sc} \bar{\mu}ZT}{kh} \frac{p_{sc}}{T_{sc}}$
	ψ	$p_D = \frac{\pi kh}{Tq_{sc} p_{sc}} (\psi - \psi_{wf})$	$m = 0.367 \frac{qT}{kh} \frac{p_{sc}}{T_{sc}}$
Gas	p	$p_D = \frac{kh\bar{p}}{55.82 \bar{\mu}ZTq_{sc}} (p_i - p_{wf})$	$m = 64.27 \frac{q_{sc} \bar{\mu}ZT}{kh\bar{p}}$
	p ²	$p_D = \frac{kh}{111.65 \bar{\mu}ZTq_{sc}} (p_i^2 - p_{wf}^2)$	$m = 128.54 \frac{q_{sc} \bar{\mu}ZT}{kh}$
	ψ	$p_D = \frac{kh}{111.65 Tq_{sc}} (\psi - \psi_{wf})$	$m = 128.54 \frac{q_{sc} T}{kh}$

20.4 PRESENTATION OF ABSOLUTE OPEN-FLOW POTENTIAL TESTS

Besides conventional well tests, gas wells also undergo special tests called absolute open-flow potential tests or AOF. They fulfill two needs:

- testing the well at several flow rates to determine the contribution of the deviation from Darcy's law to the skin;
- meeting the constraints of gas contracts that force the producer to determine the well's potential in the pseudosteady-state regime very early on in the life of the well.

The second objective is not particular to gas wells, it is also the aim of extended well tests on oil wells. What is specific to gas wells is that this type of test is incorporated in the initial test procedures.

Whatever the procedure used, an AOF test will include the following stages:

- a cleaning flow rate, that is the highest in the whole test;
- several different flow rates;
- a flow period that is long enough to reach the boundaries of the drainage area or at least to reach a pressure close to the pressure at the beginning of the pseudosteady-state regime.

Section 20.5 presents conventional test procedures and sections 20.6 and 20.7 indicate how to interpret them. Section 20.8 presents other procedures that are less constraining but still allow the same objectives to be attained.

20.5 CONVENTIONAL AOF TESTS

Three conventional procedures are used to test a gas well:

- the back-pressure test;
- the isochronal test;
- the modified isochronal test.

- **Back-pressure test** (Fig. 20.4):

The back-pressure test consists in producing the well at several different successive flow rates.

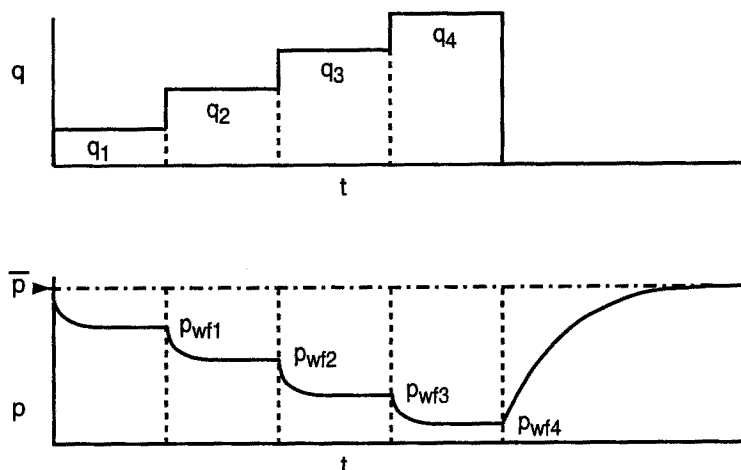


Fig. 20.4 Back Pressure Test

During the test each flow rate is held long enough so that the bottomhole pressure “stabilizes”. Stabilization depends of course on the sensitivity of the gauges and on the interval of time used to measure the stabilization.

Theoretically, for the test to be right, the flow rate would have to be long enough for the pressure reached at the end of each flow period to be as close as possible to the pressure that would be reached at the beginning of the pseudosteady-state regime.

This condition means long-lasting tests in low-permeability formations. For this reason back-pressure tests are mainly conducted in highly permeable formations. Isochronal and modified isochronal tests are preferred in reservoirs with poor characteristics.

The sequence of flow rates (increasing, decreasing, alternating) has no influence on interpretation.

In contrast, it is important to have cleaned the well at a rate higher than the highest test rate. Otherwise, the real skin can vary from one drawdown period to the other and this makes the test impossible to analyze.

- **Isochronal test** (Fig. 20.5):

In an isochronal test production periods all last the same time. They are separated by shut-in periods that are long enough for the pressure to come back to the level before opening.

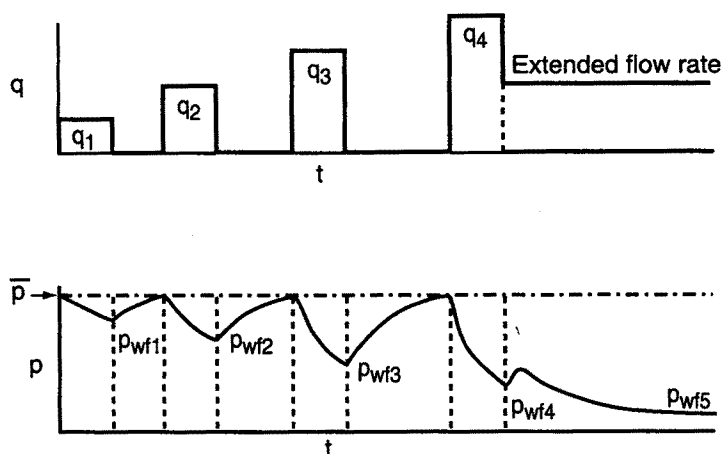


Fig. 20.5 Test isochrone

The test ends with a flow period that is long enough to reach the boundaries of the well drainage area.

The duration, t_p , of flow periods is generally taken equal to:

$$t_p = 4 \max(t_{ws}, t_{100}) \quad (20.17)$$

Here, t_{ws} is the time required to reach the end of the wellbore storage effect and t_{100} is the time required for the test to investigate 100 ft around the well:

$$t_{100} = 10^7 \frac{\phi \mu}{k_p} \quad \text{in practical US units} \quad (20.18)$$

The duration of buildup periods in the isochronal test explains why the modified isochronal test is often preferred.

• **Modified isochronal test** (Fig. 20.6):

The modified isochronal test differs from the isochronal test by the duration of buildup periods, which last just as long as drawdown periods. In the modified test the pressure does not come back to the initial level at the end of intermediate buildup periods.

Two methods are used to analyze the tests:

- An empirical method developed in 1936 by Rawlins and Schellhardt [Réf. 23] ;
- A method that uses the theory of flows around a gas well. This method was developed in the seventies by Houpeurt [Ref. 24] and will be presented first since it justifies the different procedures used.

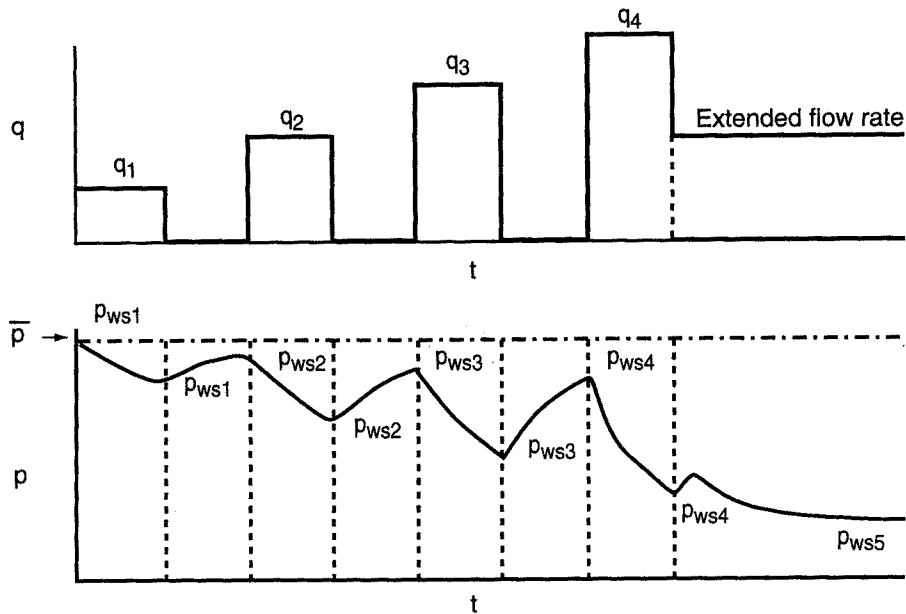


Fig. 20.6

20.6 INTERPRETATION OF AOFPT TESTS: HOUEURT'S METHOD

Absolute open-flow potential tests involve two flow regimes:

- The transient flow regime which is reached at the end of the first drawdown periods in isochronal tests. Each period must be long enough for the well-bore storage effect to be over.
- The pseudosteady-state flow regime which is theoretically reached at the end of each drawdown period in the back-pressure test and at the end of the last extended drawdown period in isochronal tests.

• Transient flow regime:

During the transient flow regime the pseudopressure at the well is expressed by:

$$\bar{\psi} - \psi_{wf} = \frac{\alpha T}{kh} q \left(\log t + \log \frac{k}{\phi \mu c_t r_w^2} - \beta + 0.87 S' \right) \quad (20.19)$$

Like $S' = S + Dq$, equation (20.19) can be written in the form:

$$\bar{\psi} - \psi_{wf} = A_t q + Bq^2 \quad (20.20)$$

with:

$$A_t = \frac{\alpha T}{kh} \left(\log t + \log \frac{k}{\phi \mu c_t r_w^2} - \beta + 0.87 S \right) \quad (20.21)$$

$$B = \frac{\gamma T}{kh} D$$

A_t depends on the duration of the drawdown period.

$\alpha = 1637$	$\beta = 3.23$	$\gamma = 1422$	(in practical US units)
$\alpha = 0.1492$	$\beta = 3.10$	$\gamma = 0.1296$	(in practical metric units)
$\alpha = 128.5$	$\beta = -0.35$	$\gamma = 111.7$	(in SI units).

• Pseudosteady-state flow regime:

During the pseudosteady-state flow regime the deviation of the pressure at the well relative to the average pressure is expressed by:

$$\bar{\psi} - \psi_{wf} = \frac{2\alpha q T}{kh} \left(\log \frac{0.472 r_e}{r_w} + \frac{S'}{2.303} \right) \quad (20.22)$$

assuming a circular drainage area with a radius of r_e .

This equation can be written in the form:

$$\bar{\psi} - \psi_{wf} = Aq + Bq^2 \quad (20.23)$$

with:

$$A = \frac{2\alpha T}{kh} \left(\log \frac{0.472 r_e}{r_w} + \frac{S}{2.303} \right) \quad (20.24)$$

$$B = \frac{\gamma T}{kh} D \quad (20.25)$$

The coefficient B is identical to the one obtained in the transient flow regime. α and γ have the same values as in the transient flow regime.

- **Deliverability straight line of the well :**

The variation of $(\psi - \psi_{wf})/q$ versus flow rate during the pseudosteady-state flow regime is linear and corresponds to a straight line:

- with a slope of B;
- with an ordinate at the origin A.

This straight line is called the deliverability straight line of the well. It is used to calculate the value of the bottomhole pressure when the well is put in production at a specified flow rate.

- **Absolute open-flow potential:**

The AOF is the theoretical production flow rate of the well reached with the bottomhole pressure equal to atmospheric pressure.

This rate can not be reached practically because of the pressure drops in the well and in production facilities.

The AOF is calculated using A and B:

$$\text{AOF} = \frac{-A + \sqrt{A^2 + 4B(\bar{\psi} - \psi_a)}}{2B} \quad (20.26)$$

ψ_a is the pseudopressure that corresponds to atmospheric pressure.

- **Interpretation of a back-pressure test:**

In a back-pressure test each drawdown period ends with the pseudosteady-state regime.

At the end of each flow period the difference between the initial test pseudopressure, ψ_i , and the pseudopressure at the end of drawdown is governed by equation (20.22) (making the realistic assumption that the produced volumes do not make the average reservoir pressure vary noticeably).

The deliverability straight line of the well is obtained directly by plotting $(\psi_i - \psi_{wf})/q$ versus q (Fig. 20.7).

The well's open-flow potential is calculated using equation (20.26).

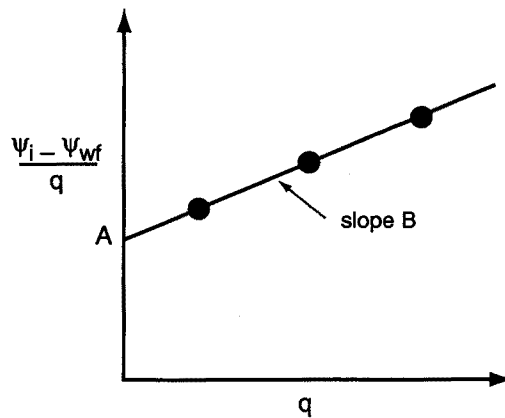


Fig. 20.7

• Interpretation of an isochronal test:

In an isochronal test each of the drawdown periods ends with the transient flow regime.

The difference between the initial test pseudopressure, $\bar{\psi}_i$, and the pseudopressure at the end of drawdown is governed by equation (20.20):

$$\bar{\psi}_i - \psi_{wf} = A_t q + Bq^2$$

A_t is a function of time and depends on the duration of the drawdown period. Since all drawdown periods in an isochronal test last the same time, A_t is the same from one period to another.

The variations in $(\bar{\psi}_i - \psi_{wf})/q$ versus q correspond to a straight line (Fig. 20.8):

- with a slope of B ;
- with an ordinate at the origin A_t .

The extended drawdown ends in the pseudosteady-state flow regime. The corresponding point $(\bar{\psi}_i - \psi_{wf})/q$ is found on a straight line:

- with a slope of B ;
- with an ordinate at the origin A .

To determine the deliverability straight line of the well, the following steps are required:

- Plot the points $(\bar{\psi}_i - \psi_{wf})/q$ corresponding to the different transient flow rates versus q .

- Draw the straight line passing through these points. Its slope is B, its ordinate at the origin is A_t .
- Draw a line passing through the point corresponding to the extended flow rate and parallel to the straight line. The ordinate at the origin of the parallel line is equal to A (Fig. 20.8)

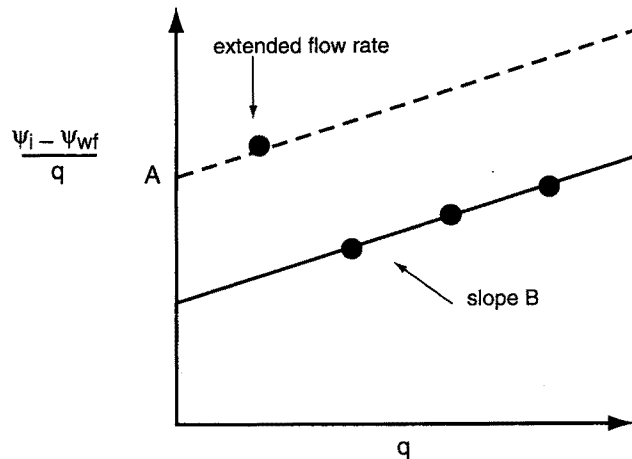


Fig. 20.8

• Interpretation of a modified isochronal test:

Katz [Ref. 25] showed that by considering the pseudopressure ψ_{ws} at the beginning of each transient flow period instead of the initial pseudopressure (Fig. 20.9), a modified isochronal test can be analyzed in exactly the same way as an isochronal test.

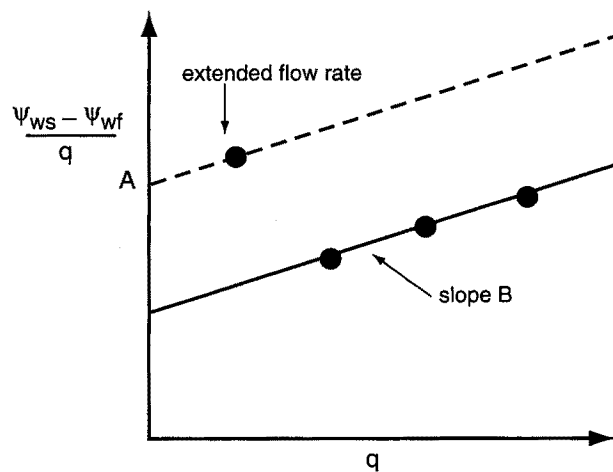


Fig. 20.9

The variations in $(\psi_{ws} - \psi_{wf})/q$ versus q correspond to a straight line with a slope of B and an ordinate at the origin A_t .

For the final drawdown period, the one that attains the pseudosteady-state flow regime, the initial pseudopressure must, however, always be considered and $(\psi_i - \psi_{wf})/q$ plotted.

The straight line with a slope of B passing through this point has an ordinate at the origin A the same as in an isochronal test.

20.7 INTERPRETATION OF ABSOLUTE OPEN-FLOW POTENTIAL TESTS: EMPIRICAL METHOD

In 1936 after studying a large number of gas wells in the United States, Rawlins and Schellhardt [Ref. 23] showed that there was a relationship between bottomhole pressure and the flow rate with the following form:

$$q = C(\Delta p^2)^n \quad (20.27)$$

with:

$$\Delta p^2 = p_i^2 - p_{wf}^2 \quad (20.28)$$

C is a constant related to the dimension of the well's drainage area, similar to coefficient A in the Houpeurt method.

n is a constant that depends on the deviation from Darcy's law, similar to D in the Houpeurt method. n is comprised between 0.5 and 1: near 1 when the deviation from Darcy's law is small and near 0.5 when the deviation is large.

D.N. Cornelson [Ref. 26] established a relationship between the coefficients A and B of the Houpeurt method and the coefficients C and n of the Rawlins and Schellhardt method:

$$a = \left(\frac{1}{C}\right)^{\frac{1}{n}} q^{\frac{1}{n}-1} \left(2 - \frac{1}{n}\right) \quad (20.29)$$

$$b = \left(\frac{1}{C}\right)^{\frac{1}{n}} q^{\frac{1}{n}-2} \left(\frac{1}{n} - 1\right) \quad (20.30)$$

- **Interpretation:**

Equation (20.27) shows that $\log q$ varies linearly versus Δp^2 :

$$\log q = n \log \Delta p^2 + \log C$$

The straight line obtained by plotting $\log \Delta p^2$ versus $\log q$ has a slope of $1/n$. It allows the well's open flow potential to be read directly. The open flow potential is the flow rate that corresponds to $\Delta p^2 = p_i^2 - p_a^2$.

• **Back Pressure Test :**

The variations of $\log \Delta p^2$ versus $\log q$ (Fig. 20.10) correspond to a straight line with a slope of $1/n$:

$$\Delta p^2 = p_i^2 - p_{wf}^2$$

p_{wf} is measured at the end of each drawdown period.

The AOF is read on the straight line for:

$$\Delta p^2 = p_i^2 - p_a^2$$

p_a is atmospheric pressure.

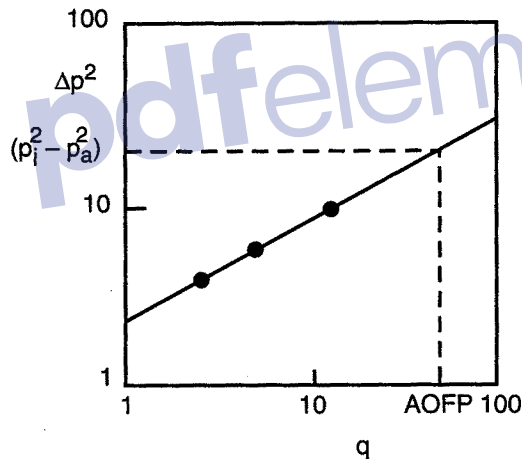


Fig. 20.10 Back Pressure test

• **Isochronal test:**

An isochronal test is interpreted using a procedure similar to the Houpeurt method:

- Plot the variations of $\log \Delta p^2$ versus $\log q$ for each of the transient flow rates (Fig. 20.11):

$$\Delta p^2 = p_i^2 - p_{wf}^2$$

These variations correspond to a straight line with a slope of $1/n$.

- Plot the point that corresponds to the extended drawdown period.
- Draw the straight line with the slope of $1/n$ passing through this point. The straight line obtained is the deliverability straight line for the well.
- The AOPF is read on the straight line. It corresponds to the ordinate point $\Delta p^2 = p_i^2 - p_a^2$.

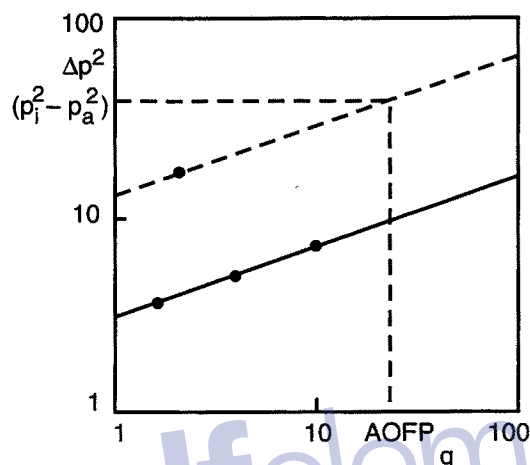


Fig. 20.11

• Modified isochronal test:

A modified isochronal test is interpreted in the same way as an isochronal test.

The only difference lies in the fact that, for transient flow rates, $\Delta p^2 = p_i^2 - p_{wf}^2$ needs to be plotted instead of $\Delta p^2 = p_i^2 - p_{wf}^2$.

p_{qi} is the value of the pressure at the beginning of the considered drawdown period.

For the final drawdown period, the one that reaches the pseudosteady-state regime, p_i must be used. The AOPF is read at:

$$\Delta p^2 = p_i^2 - p_a^2$$

Nota bene:

The method developed by Rawlins and Schellhardt is empirical.

The straight line with a slope of $1/n$ is in fact only the tangent to a curve with a slight curvature on a log-log graph.

The method provides a correct estimate of the AOF as long as it is not too high compared to the highest test flow rate.

Otherwise the log-log extrapolation gives an incorrect estimate. The Houpeurt method must be utilized to get an accurate evaluation.

20.8 OTHER TEST PROCEDURES

Absolute open-flow potential tests are designed to reach several objectives:

- Determine the deviation from Darcy's law near the wellbore: to do this the test must involve several different flow rates.
- Determine the well's behavior in the pseudosteady-state regime: which requires an extended flow period.

The advantage of conventional tests is that these objectives are met by measuring only one pressure at the end of drawdown.

They are, however, constraining from the standpoint of operational procedure:

- the back-pressure test lasts a long time;
- the modified isochronal test requires strict control of each different draw-down period's duration.

Continuous recording of pressure during the different periods, which tends to be the rule today, allows other more flexible procedures to be used to attain the same objectives.

• Modified back-pressure test:

The major drawback of the back-pressure test is that it lasts a long time. Each drawdown period must reach the pseudosteady-state regime.

Its main advantage is that it is simple to operate.

The modified back-pressure test retains the simplicity of the back-pressure test but lasts less time.

- **Description of the test:**

The sequence of flow rates in a modified back-pressure test is represented in Figure 20.12.

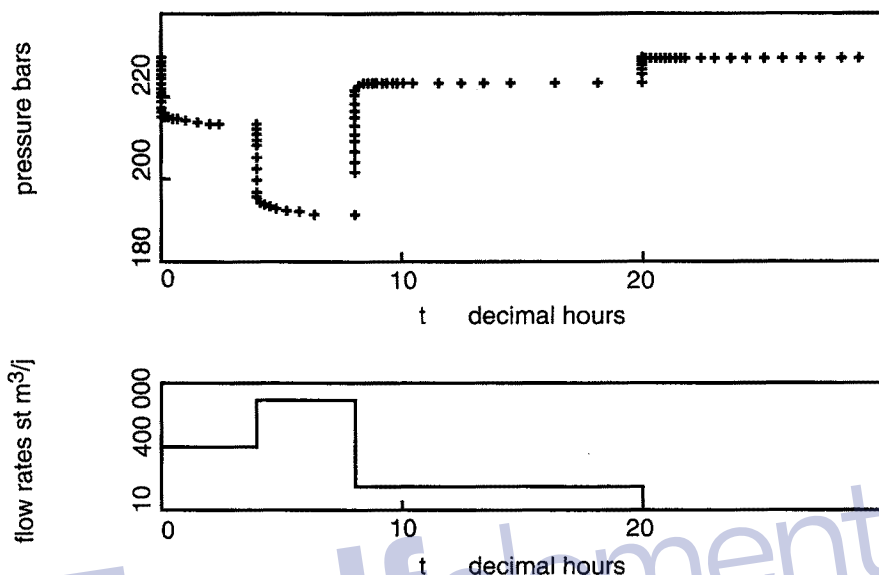


Fig. 20.12

The main characteristics of the test are:

- Several transient flow periods: each one meeting the same duration criterion as a drawdown period in an isochronal test: $t_p = 4 \max(t_{ws}, t_{100 \text{ ft}})$.
- One single long drawdown period.

A recording of the bottomhole pressure is needed to interpret the modified back-pressure test:

- continuous during each transient flow period;
- at the end of the extended flow period.

- **Interpretation:**

Interpretation includes several steps:

- 1 Analyze each drawdown period: this analysis made with a superposition function gives a skin value for each flow rate. The skin is a global skin, S' .
- 2 Determine the well skin and the Darcy's law deviation coefficient: by plotting S' versus $q_n + q_{n-1}$ (Fig. 20.13).

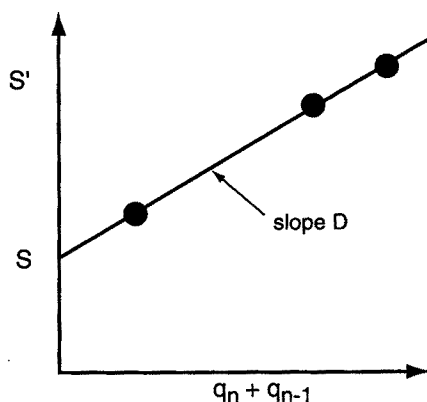


Fig. 20.13

The corresponding points are on a straight line:

- with the equation $S' = S + D (q_n + q_{n-1})$;
- with a slope of D ;
- with an ordinate at the origin S . S is the real well skin.

3 Calculate B , which is the slope of the well's deliverability straight line:

$$B = \frac{\alpha T}{kh} D$$

$\alpha = 1422$

$\alpha = 0.1296$

$\alpha = 111.7$

(in practical US units).

(in practical metric units).

(in SI units).

4 - Deliverability straight line (Fig. 20.14)

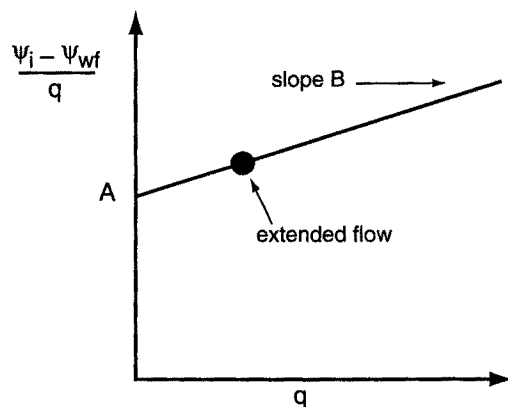


Fig. 20.14

The well's deliverability straight line:

- goes through the point with the coordinates $\Delta\psi/q$, with q corresponding to the long period;
- has B as a slope (calculated in step 3);
- has an ordinate at the origin A .

5 The absolute open-flow potential is equal to:

$$\text{AOFP} = \frac{-A + \sqrt{A^2 + 4B(\bar{\psi} - \psi_a)}}{2B}$$

Nota bene:

The advantage of this test is that it is considerably shorter than a back-pressure test.

When one or more flow periods are too short, the interpretation method uses the pressure recording for the analysis. Conventional interpretation of this test provides inaccurate results.

The drawback of the procedure is that it requires interpretation of tests when the well is flowing. The flow rate fluctuations that often exist in a producing well sometimes make it difficult to analyze the test.

• **A variation on the isochronal test:**

The advantage of isochronal and modified isochronal tests is that they are shorter than a back-pressure test.

The major drawback is that they are difficult to manage: the drawdown periods must all last the same length of time. This is because the same coefficient, A_t , is required at the end of each flow period.

Drawdown periods are separated by pressure buildups which are designed to make the influence of the prior flow periods negligible.

The constraints can be eliminated by using a superposition function.

This superposition function is used to interpret a modified isochronal test with drawdown and buildup periods lasting any length of time.

- **Test description:**

The variation on the isochronal test must comply with two constraints:

- be made up of several different flow rates so that the D coefficient can be determined;
- include a flow period that is long enough to reach the pseudosteady-state regime.

Figure 20.15 shows such a test. In order to interpret it, the bottomhole pressure must be recorded:

- continuously during each buildup period;
- at the end of the extended flow rate.

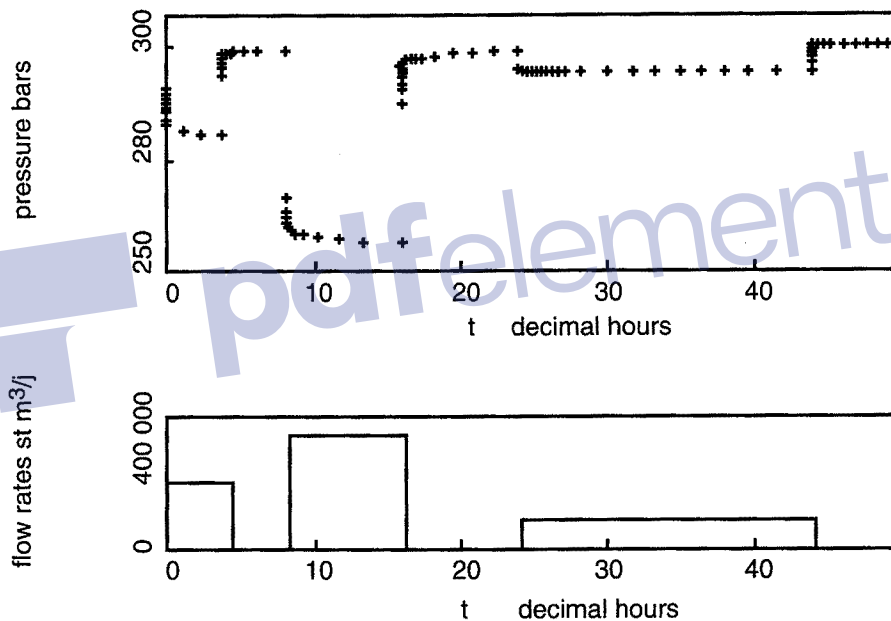


Fig. 20.15

- **Interpretation:**

Interpretation includes several steps:

- 1 Interpret each pressure buildup: each one has a different skin value, S' , S' being a global skin.
- 2 Determine the well skin and the Darcy's law deviation coefficient by plotting S' versus the flow rate (Fig. 20.16).

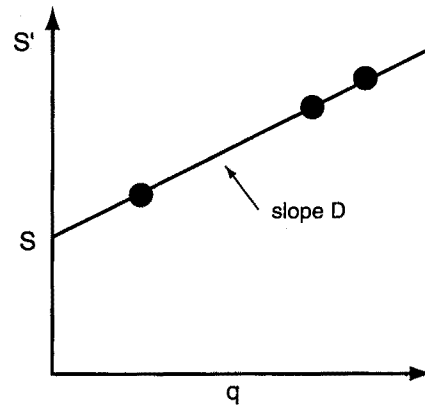


Fig. 20.16

The corresponding points are on a straight line:

- with the equation $S' = S + Dq$;
- with a slope D ;
- with an ordinate at the origin S , the true well skin.

3 Calculate B : B is the slope of the deliverability straight line:

$$B = \frac{\alpha T}{kh} D$$

$\alpha = 1422$ (in practical US units)
 $\alpha = 0.1296$ (in practical metric units)
 $\alpha = 111.7$ (in SI units).

4 The deliverability straight line (Fig. 20.17)

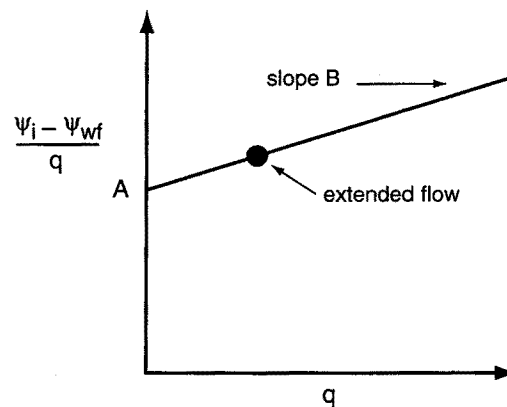


Fig. 20.17

This straight line:

- goes through the point with coordinates $\Delta\psi/q$, where q is the extended flow rate;
- has a slope B , which was calculated in step 3;
- has an ordinate at the origin A .

5 The well's absolute open-flow potential is equal to:

$$\text{AOFP} = \frac{-A + \sqrt{A^2 + 4B(\bar{\psi} - \psi_a)}}{2B}$$

Nota bene:

This test is a little longer than the modified back-pressure test.

It has an important advantage: the values of the well skin and of the D coefficient are obtained from interpreting pressure buildups. This is always preferable to interpreting pressure values that are measured during drawdown.

It is not always possible to make the long drawdown period last long enough to reach the pseudosteady-state regime. When the flow period is too short, the AOFP of the well is overestimated.

Chapter 21

Multiphase flows

21.1 INTRODUCTION

The interpretation methods discussed up to now have dealt with a one-phase fluid flow.

The fluid is generally a liquid. Chapter 20 indicates what modifications need to be made in testing and interpretation methods when the fluid is a gas.

The present chapter covers interpretation of tests with multiphase flow in the reservoir, i.e. simultaneous flow of water, oil and gas usually.

The fluids are assumed to be distributed uniformly. This means that the methods presented do not apply to an influx of different fluids from other levels into the tested zone (Fig. 21.1).

Several interpretation methods are presented in oil industry literature [Ref. 39 and 42].

In this chapter only the method developed by R.L. Perrine will be discussed as it is easy to use, has been thoroughly tested and gives correct results in most cases. The Perrine method is based on highly simplified hypotheses.

The other methods [Ref. 40 and 42] are more rigorous, but are not as simple to use and, more importantly, require relative permeability curves to be known beforehand. This is not always the case when the test is performed.

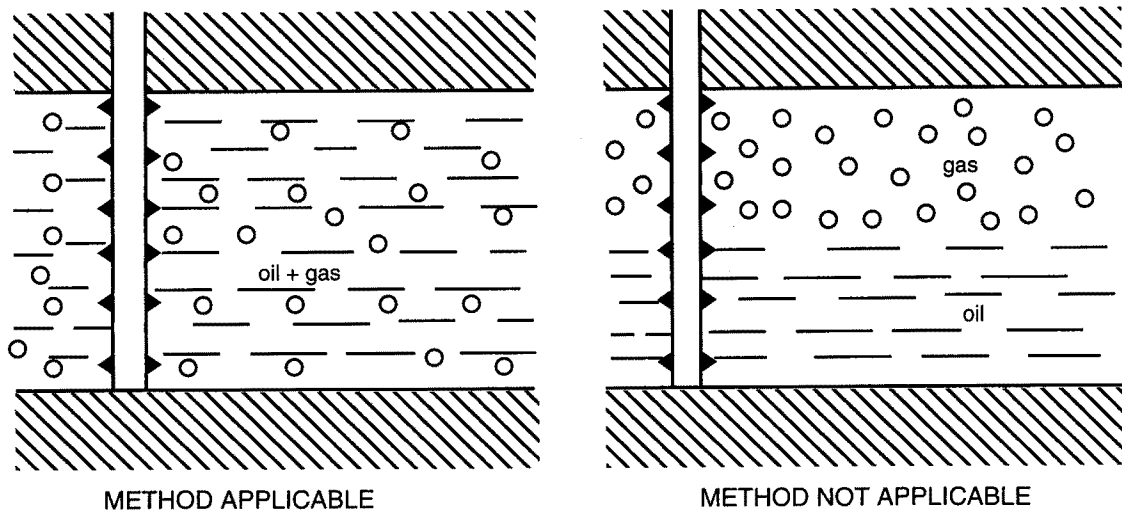


Fig. 21.1 The methods are applicable with uniform fluid distribution

21.2 PERRINE METHOD HYPOTHESES

Like all the other multiphase flow interpretation methods, the Perrine method assumes that fluid distribution is uniform. It also makes two further simplifying hypotheses:

- **Capillary pressures are negligible:** this means that the pressure in one place at a specified time is the same in all the fluids. This hypothesis is usually correct since capillary pressures are normally low.
- **Saturations are uniform:** assuming that the saturation in each fluid is uniform implies that in a homogeneous reservoir the permeability to each fluid is uniform.

This hypothesis is not verified in the wellbore vicinity in reservoirs whose pressure is lower than the bubble point pressure. Since the widest pressure variations take place in the near-well zone, this is also where the widest variations in gas saturation are located.

The fact that variations in saturation are disregarded in the vicinity of the well affects the skin value.

The uniform-saturation hypothesis is approximately verified at a certain distance from the wellbore. The distance depends on the properties of the reservoir and the fluids, and on production conditions.

21.3 PERRINE'S METHOD

In Perrine's method the multiphase fluid is considered as one single phase where the various fluids are dispersed.

The representation, which is correct when a reservoir has just gone under the bubble point for example, is no longer true as soon as segregation occurs.

When there is segregation it is preferable to treat the reservoir like a two-layer reservoir, each layer having the capacity and mobility of the phase circulating through it.

In Perrine's method the multiphase fluid is treated like an equivalent one-phase fluid.

21.3.1 Equivalent one-phase fluid

- **Mobility:**

The total mobility of the one-phase fluid equivalent to the multiphase fluid is equal to the sum of the mobility of each fluid:

$$\left(\frac{k}{\mu}\right)_t = \frac{k_o}{\mu_o} + \frac{k_w}{\mu_w} + \frac{k_g}{\mu_g} \quad (21.1)$$

The mobility of each phase is proportional to the flow rate of the phase.

- **Flow rate:**

The total bottomhole flow rate of the equivalent one-phase fluid is equal to the sum of the bottomhole flow rate of each fluid:

$$q_{tf} = q_o B_o + q_w B_w + q_g B_g \quad (21.2)$$

The gas flow rate, q_g , to be taken into account is the flow produced by the formation.

The gas produced at the wellhead is the sum of the gas produced at the bottom of the hole and the gas released by the oil.

The gas produced at the bottom of the hole, $q_g B_g$, is expressed with respect to the flow rate, q_{gt} , measured at the wellhead by:

$$q_g B_g = (q_{gt} - q_o R_s) B_g \quad (21.3)$$

Expression (21.2) is also expressed as follows:

$$q_{tf} = q_o \left(B_o + \frac{BSW}{1 - BSW} B_w + (GOR - R_s) B_g \right) \quad (21.4)$$

• Compressibility:

The total compressibility of the equivalent fluid is equal to:

$$c_t = c_o S_o + c_w S_w + c_g S_g + c_p \quad (21.5)$$

The oil compressibility term is equal to:

$$c_o = \frac{B_g}{B_o} \left(\frac{\partial R_s}{\partial p} \right)_T - \frac{1}{B_o} \left(\frac{\partial B_o}{\partial p} \right)_T \quad (21.6)$$

Oil compressibility is due to two factors:

– The compressibility of the oil itself: $-\frac{1}{B_o} \left(\frac{\partial B_o}{\partial p} \right)_T$

This term can be calculated from the B_o of the oil in the PVT study (Fig. 21.2).

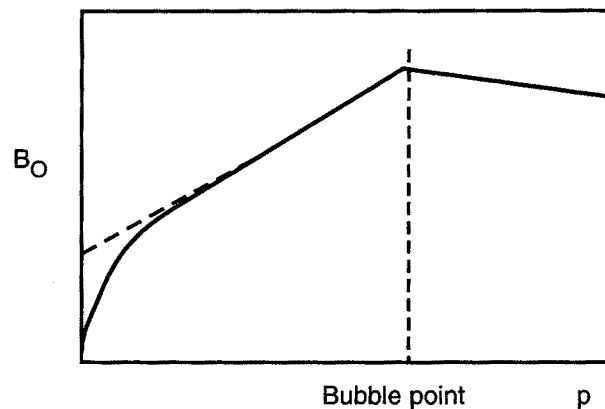


Fig. 21.2

The variation in B_o versus the pressure is roughly linear below and above the bubble point, allowing simple determination of the term $(\partial B_o / \partial p)_T$.

– Gas dissolution or gas release:
$$\frac{B_g}{B_o} \left(\frac{\partial R_s}{\partial p} \right)_T$$

This term can also be calculated from the R_s of the oil in the PVT study (Fig. 21.3).

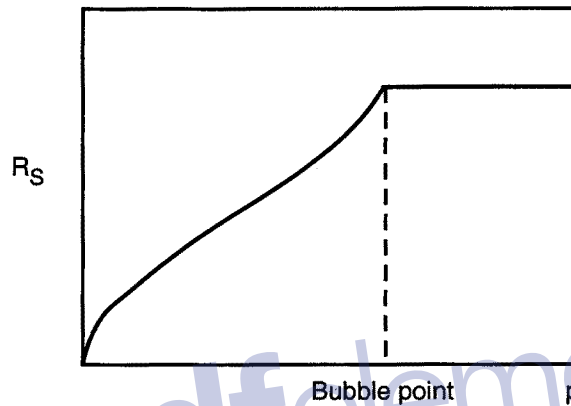


Fig. 21.3

The variation of R_s versus the pressure is also roughly linear.

The dissolution-release term is positive and is 10 to 100 times greater than the compressibility term of the oil itself.

Compressibility expression (21.6) assumes that all the gas released during drawdown is redissolved during buildup. This is not necessarily true, however.

21.3.2 Interpretation

All the interpretation methods discussed for an oil well can be applied to a well with a bottomhole multiphase flow.

In the Perrine method capillary pressures are considered to be negligible, so the pressure is the same in each phase at any given time and place. Because of this, for a specified total flow rate, each fluid is produced in proportion to its mobility.

When a multiphase well test is interpreted, the reservoir's permeability to each phase can be determined on the basis of the flow rate of each phase.

For example, in conventional interpretation the slope m of the semi-log straight line allows the following to be determined:

– the permeability to the oil:

$$k_o = \frac{\alpha q_o B_o \mu_o}{m h} \quad (21.7)$$

– the permeability to the water:

$$k_w = \frac{\alpha q_o B_{SW} B_w \mu_w}{(1 - B_{SW}) m h} \quad (21.8)$$

– the permeability to the gas:

$$k_g = \frac{\alpha q_o (GOR - R_s) B_g \mu_g}{m h} \quad (21.9)$$

The skin is equal to:

$$S = 1.151 \left[\frac{p_i - p_{1h}}{m} - \log \left(\left(\frac{k}{\mu} \right) t \frac{1}{\phi c_t r_w^2} \right) + \beta \right] \quad (21.10)$$

$\alpha = 162.6$	$\beta = 3.23$	(in practical US units)
$\alpha = 21.5$	$\beta = 3.10$	(in practical metric units)
$\alpha = 0.183$	$\beta = 0.35$	(in SI units).

The skin expression involves the overall properties of the equivalent fluid: mobility and compressibility.

The value of the skin must be considered with caution in reservoirs whose pressure is lower than the bubble point. The Perrine method puts forward the hypothesis that saturation is uniform around the well. In actual fact the gas saturation around a production well is greater than it is farther away in the reservoir. The higher saturation leads to an overall mobility that is greater around the wellbore. This can be seen by a negative skin. The main weakness of the Perrine method is that the skin can not be correctly evaluated.

21.4 PRODUCTIVITY INDEX OF AN OIL WELL PRODUCING UNDER THE BUBBLE POINT; VOGEL'S EQUATION

In an oil well that produces a reservoir whose pressure is greater than the bubble point, there is a linear relationship between the well flow rate and the difference between the average pressure and the bottomhole pressure in the pseudosteady-state regime. This relationship is shown by the well's productivity index:

$$IP = \frac{q_o}{\bar{p} - p_{wf}} \quad (21.11)$$

The relationship can be expressed in the following standardized way:

$$\frac{q_o}{q_{max}} = 1 - \frac{p_{wf}}{\bar{p}} \quad (21.12)$$

which is shown in Figure 21.4.

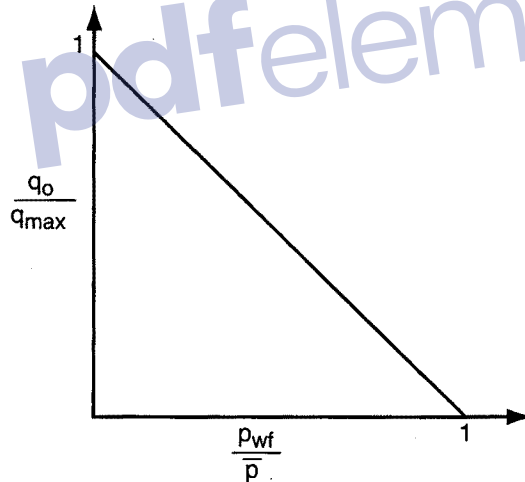


Fig. 21.4

In a well producing a reservoir whose pressure is lower than the bubble point, the relationship between q_o/q_{max} and p_{wf}/\bar{p} is not linear. Vogel [43] established an empirical relationship between the two terms. It is of the following form:

$$\frac{q_o}{q_{max}} = 1 - 0.2 \left(\frac{p_{wf}}{\bar{p}} \right) - 0.8 \left(\frac{p_{wf}}{\bar{p}} \right)^2 \quad (21.13)$$

It can be seen in Figures 21.5 and 21.6. In Figure 21.5 equation (21.12) is also indicated for comparison.

Based on the bottomhole pressure measurement at a specified flow rate and the average reservoir pressure data, the equation is used to determine:

- the well's maximum flow rate (q_{\max} , open-flow potential),
- the oil flow rate that can be obtained for a given bottomhole pressure.

Standing [Ref. 44] proposes a modification in the equation to account for the variations in relative permeability and in fluid properties during depletion. He proposes the following equation:

$$\left(\frac{q_o}{q_{\max}}\right)_F = \left(\frac{q_o}{q_{\max}}\right)_p \times \frac{\left(\frac{k_{ro}}{\mu_o B_o}\right)_F}{\left(\frac{k_{ro}}{\mu_o B_o}\right)_p} \quad (21.14)$$

The value of $(q_o/q_{\max})_F$, value of q_o/q_{\max} that is to be determined can be calculated from the measured value $(q_o/q_{\max})_p$ and an estimate of k_{ro} , μ_o et B_o .

• **Example using Vogel's equation:**

Vogel [Ref. 43] gives an example using equation (21.13). Assuming a well produces under the following conditions:

$$\begin{aligned} q_o &= 65 \text{ bbl/j} \\ p_{wf} &= 1500 \text{ psi} \\ \bar{p} &= 2000 \text{ psi.} \end{aligned}$$

Determine the absolute open-flow potential of the well and the flow rate that would be attained if a gas lift installation (mechanical pumping) could bring the bottomhole pressure down to 500 psi.

Based on equation (21.13), the data can be used to calculate:

$$q_{\max} = 162 \text{ bbl/j}$$

Using equation (21.13) with a bottomhole pressure of 500 psi gives:

$$\frac{q_o}{q_{\max}} = 0.9 \quad \text{then} \quad q_o = 146 \text{ bbl/j}$$

Using linear equation (21.12) directly would have given $q_o = 195 \text{ bbl/d}$.

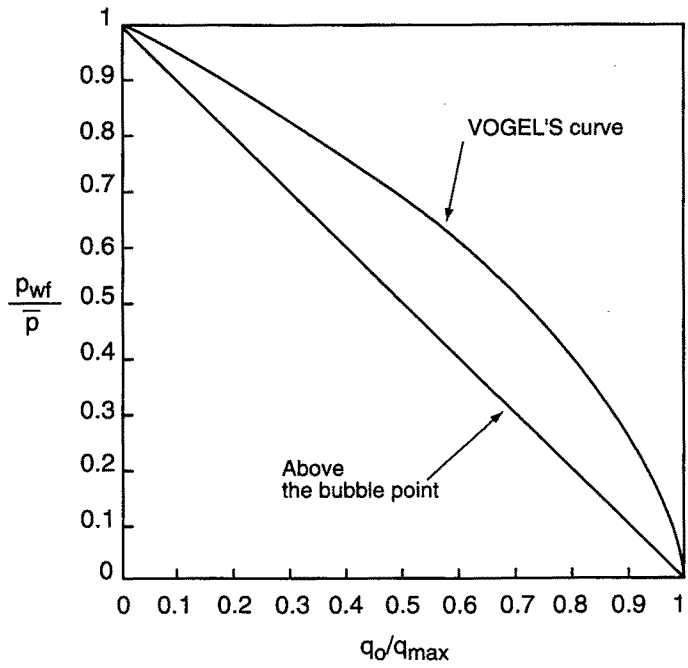


Fig. 21.5

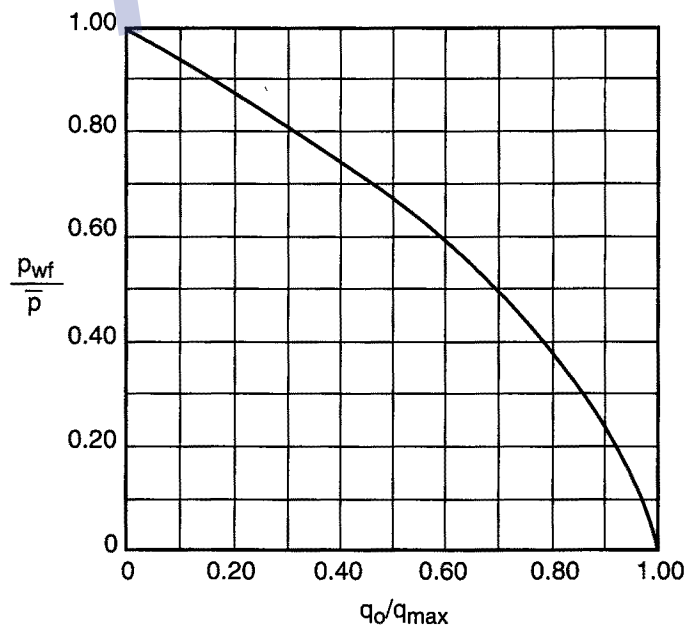


Fig. 21.6





Interferences

pdfelement



Chapter 22

Interference tests

22.1 PRESENTATION, PARTICULARS

In the previous chapters tests involved only one well: pressure was measured in the well where the flow rate was changed.

Interference tests involve several wells. The well where the flow rate is changed is called the **active well** and the one where the pressure is measured is called the **observation well**.

Interference tests are used to find out whether there is any communication between the two wells and to characterize the communication if there is one. They are also the only tests that can determine a reservoir's horizontal permeability anisotropy.

Measuring the pressure in a well other than the source well has two practical consequences:

- the measured signal is weak;
- the signal is observed after a delay.

- **Weak signal:**

The variation in flow rate causes wide variations in pressure in the active well.

In the observation well the pressure variations are often very weak. They usually range between 0.1 and 10 psi. The fact that the signal is so weak has several practical consequences:

- The pressure gauge on the observation well must be sensitive.
- The observation well must be shut in during the whole interference test: the flow rate of a producing well always fluctuates a little. These fluctuations produce pressure changes of the same level, or even greater than, the variations due to interference and therefore disturb the test.
- Tides [Réf. 46] can disturb interference. The sun and moon's attraction on the reservoir rock and fluids causes cyclic pressure variations of approximately 0.1 psi.
Tides make it difficult to observe any interference lower than this level.

- **The signal is measured after a delay:**

A well test lasts between several hours and several tens of hours, but an interference test can last several weeks. This duration is necessary so that the perturbation generated by the active well can reach the observation well.

This long duration has two major operational consequences:

- The sensor must have little drift over a long time. The pressure gauges used in an interference test must be able to measure weak pressure variations over several days to several weeks.
It is therefore crucial to use sensitive pressure gauges that do not drift with time. At the present, only quartz pressure gauges meet these requirements. Strain gauges have enough sensitivity, but too much drift (several psi per week).

- Other wells may perturb the interference test, whereas the operator usually wants interference to be due only to the flow rate variation in the active well. In practice other wells are located at a comparable distance. They may also interfere with the observation well.

It is of utmost importance to keep the flow rate constant all throughout the test in these other wells so that the signal measured at the observation well is easy to interpret.

22.2 INTERPRETATION METHODS IN A HOMOGENEOUS RESERVOIR

- **The Theis type curve:**

The active well is put in production at a constant flow rate.

The pressure measured in the observation well, which is shut in, is assumed to be constant at the beginning of the test.

The general equation for pressure variations is the one developed in section 1.5 for a well in production at a constant flow rate. Pressure at a distance, r , from the active well is equal to:

$$p_i - p(r, t) = - \frac{qB\mu}{4\pi kh} \operatorname{Ei} \left(- \frac{r^2}{4 Kt} \right) \quad (22.1)$$

Or, with dimensionless variables:

$$p_D = - \frac{1}{2} \operatorname{Ei} \left(- \frac{r_D^2}{4t_D} \right) \quad (22.2)$$

with: $r_D = \frac{r}{r_w}$.

This solution is based on the following hypotheses:

- the well radius is zero;
- the wellbore storage effect of each well is negligible;
- each well has zero skin.

Equation (22.2) is for a type curve presented for the first time in hydrology by Theis [Ref. 45] in 1935. It is illustrated in Figure 22.1, which represents dimensionless pressure variations, p_D , versus the term t_D/r_D^2 on a log-log graph.

• Procedure:

The usual procedure is followed in order to analyze an interference test with this type curve:

- plot measurement points on tracing paper using the existing log-log scale underneath;
- look for the part of the type curve where the measurement points match by translation of the tracing paper;
- note the coordinates of a match point in both the type curve system of axes (p_D , t_D/r_D^2) and in the measured field data system (Δp , Δt). The procedure is illustrated in Figure 22.2.

• Interpretation:

The interpretation method presented here assumes the reservoir is homogeneous and isotropic. The problem of anisotropy is dealt with a little later on.

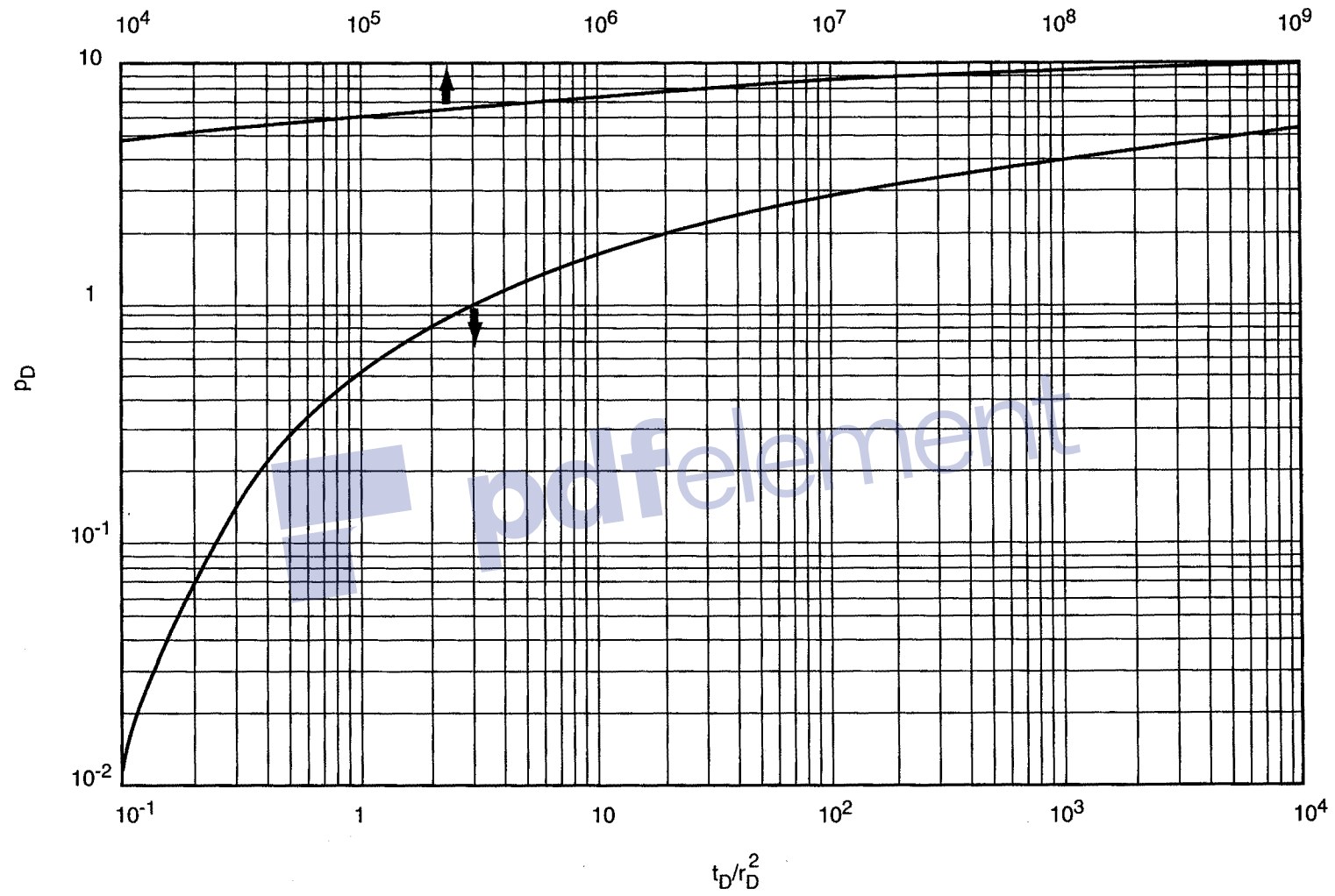


Fig. 22.1 This curve

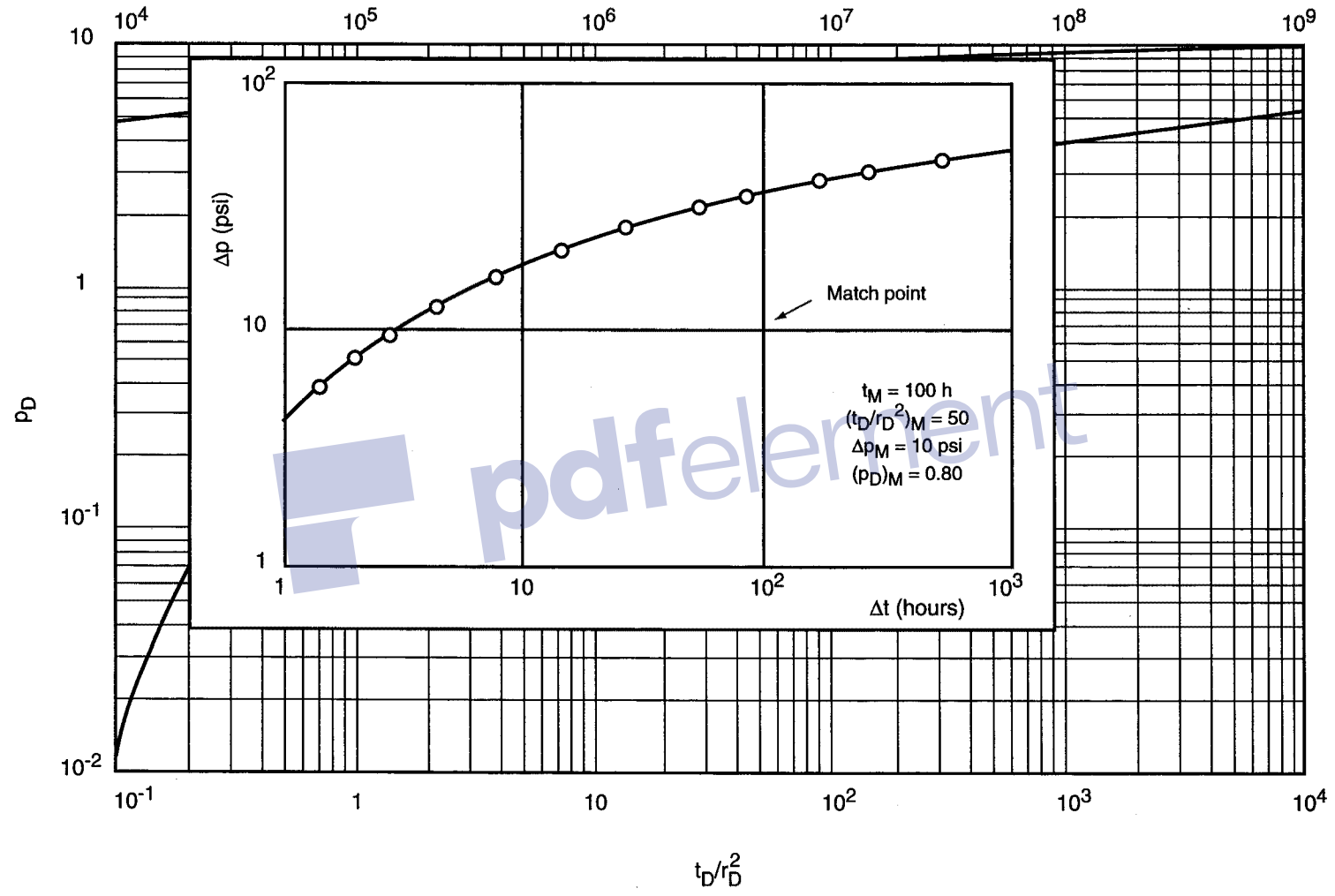


Fig. 22.2

As usual, the ordinate of the match point, M , measured in the two systems determines the reservoir's kh :

$$kh = 141.2 qB\mu \frac{(p_D)_M}{(\Delta p)_M} \quad (22.3)$$

The abscissas of point M are related by the following equation:

$$(t_D/r_D^2)_M = \frac{0.000264 k (\Delta t)_M}{\phi \mu c_t r^2} \quad (22.4)$$

This equation is used to determine the reservoir's capacity ϕc_t :

$$\phi c_t = \frac{0.000264 k (\Delta t)_M}{\mu r^2 (t_D/r_D^2)_M} \quad (22.5)$$

Nota bene:

It is normally easy to achieve vertical matching and as a result determine kh accurately.

However, it is often more difficult to do the horizontal matching and determine ϕc_t . If horizontal matching is to be accurate, there must be match points for small t_D/r_D^2 , ($t_D/r_D^2 < 10$). These points may not exist for several reasons:

- The measured pressure variation corresponding to small t_D/r_D^2 is too weak.
- Sometimes the wellbore storage effect and skin of the active well are not negligible (see section 22.4). In this case the points corresponding to small t_D/r_D^2 do not match on the Theis curve.

Because of this, porosity and ϕc_t determined by interference tests must always be considered with circumspection.

• **Semi-log approximation:**

The pressure complies with the general equation in (22.2):

$$p_D = -\frac{1}{2} \text{Ei} \left(\frac{-r_D^2}{4t_D} \right)$$

This equation can be replaced by its logarithmic approximation as long as $4 t_D/r_D^2$ is greater than 100. The approximation is valid to 1% as long as t_D/r_D^2 is greater than 10:

$$p_D = \frac{1}{2} \left(\ln \frac{t_D}{r_D^2} + 0.81 \right) \quad (22.6)$$

Or, in real variables:

$$p_i - p_{wf} = \frac{\alpha q B \mu}{kh} \left(\log t + \log \frac{k}{\phi \mu c_t r^2} - \beta \right) \quad (22.7)$$

$\alpha = 162.6$	$\beta = 3.23$	(in practical US units)
$\alpha = 21.5$	$\beta = 3.10$	(in practical metric units)
$\alpha = 1.151$	$\beta = -0.352$	(in SI units).

The slope m of the semi-log straight line obtained by plotting the variations in $p_i - p_{wf}$ versus $\log t$ is used to determine the reservoir's kh :

$$kh = \frac{\alpha q B \mu}{m} \quad (22.8)$$

The value of the pressure measured after one hour serves to determine the reservoir capacity, ϕc_t :

$$\phi c_t = \frac{k}{\mu r^2} \exp \left(-\frac{p_i - p_{1h}}{m} + \beta \right) \quad (22.9)$$

22.3 INTERFERENCE TESTS IN FRACTURED RESERVOIRS

The description of the fractured reservoir used to interpret interference tests is the same as in Chapter 13.

D. Bourdet, A. Gringarten [Ref. 47] and B. Deruyck et al. [Ref. 48] established two sets of type curves based on this description.

The curves are shown in Figures 22.3 and 22.4:

- Figure 22.3 is the set corresponding to the pseudosteady-state matrix-fracture flow model;
- Figure 22.4 is the transient model set.

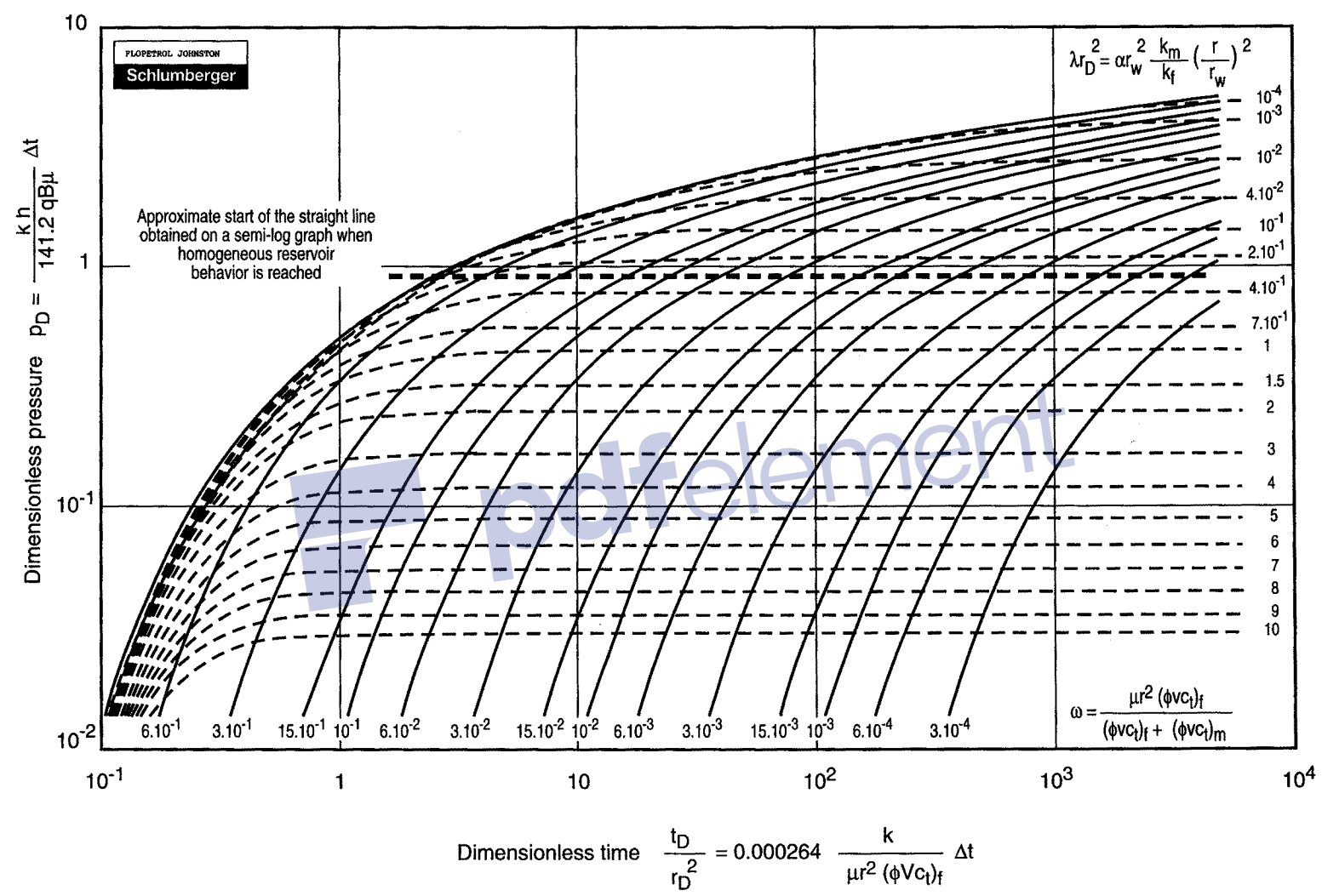


Fig. 22.3 Type curves for an observation well, double porosity reservoir behavior (steady-state interporosity flow)

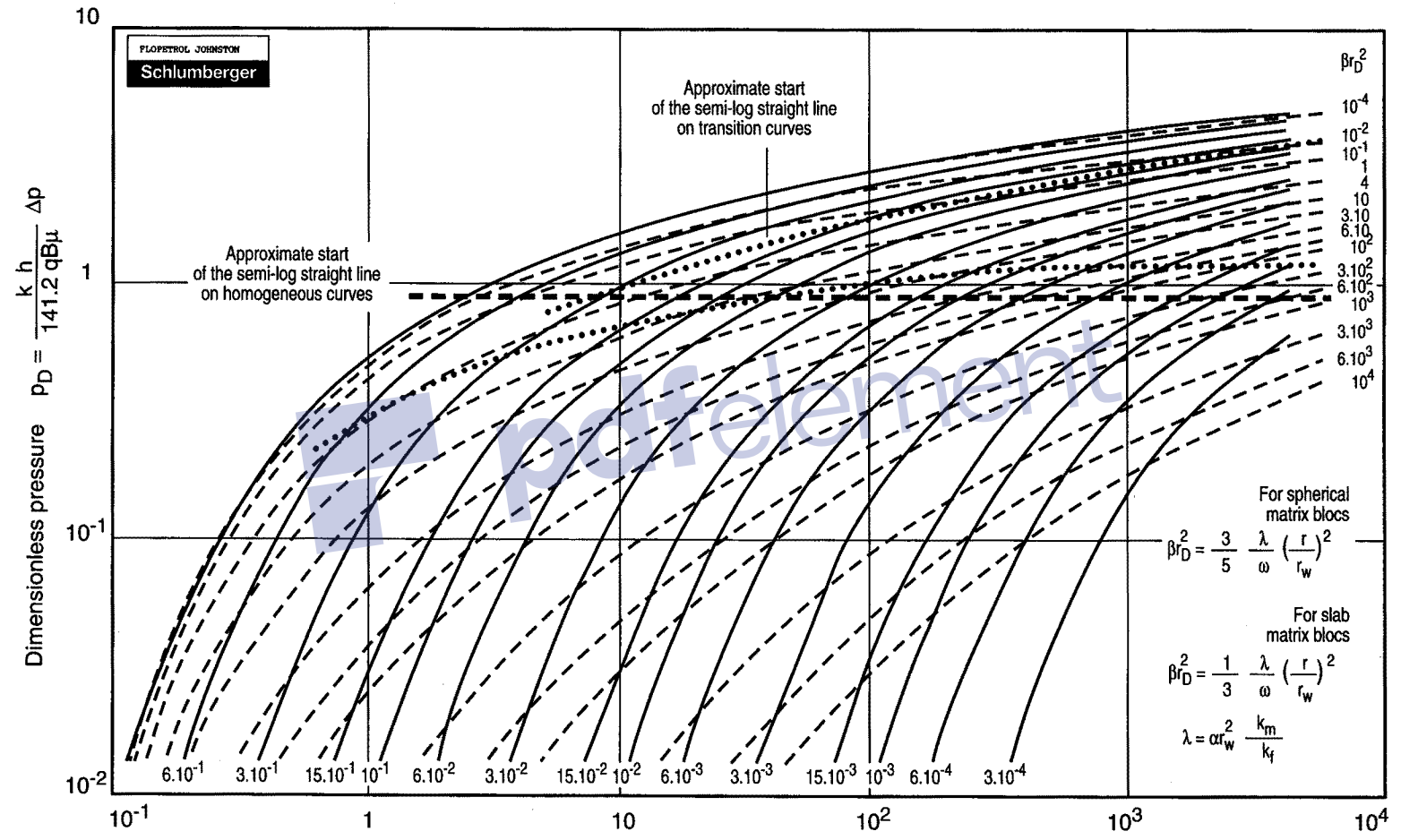


Fig. 22.4 Type curves for an observation well, reservoir with double porosity transient interporosity flow

• **Description of the curves:**

The curves represent the variations in p_D versus t_D/r_D^2 , like the Theis curve in Figure 22.1.

Two sets of curves can be seen in each figure:

- One set drawn in continuous line. The uppermost one is the Theis curve. The others are deduced from the first curve by simple translation parallel to the time axis. The translation value is equal to ω , capacity contrast between the fractures and the reservoir as a whole.
- Another set of curves drawn with dotted lines. These are transition curves. They are labeled in λr_D^2 terms in the pseudosteady-state interporosity flow model and βr_D^2 when the transient model is utilized.

• **Matching:**

The same as for one-well tests in fractured media, the measurement points are matched on three curves:

- The Theis curve ($\omega = 1$) for the first points, which correspond to flow from the fractures alone.
- A transition curve (λr_D^2 ou βr_D^2) for intermediate points.
- A curve labeled in ω terms for the last points, which correspond to the flow from both matrix and fractures.

• **Interpretation:**

Interpreting an interference test in a fractured medium can provide four types of information:

- The reservoir's kh value.
- The value of the capacity of the fractures: $(\phi C_t)_f$, which is obtained by horizontal matching.
- The value of the total reservoir capacity: $(\phi C_t)_f + (\phi C_t)_m$, which is obtained from $(\phi C_t)_f$ and ω :

$$(\phi C_t)_f + (\phi C_t)_m = (\phi C_t)_f / \omega \quad (22.10)$$

- The value of λ : λ characterizes how easily the flow occurs from the matrix to the fractures (see Chapter 13).

Nota bene:

It is even more difficult to characterize a fractured reservoir with an interference test than with a one-well test.

The information on fractures is obtained from the transition period, situated at small t_D/r_D^2 petits ($t_D/r_D^2 < 10$). The same as for a homogeneous reservoir, two conditions must be met for interpretation to be reliable:

- pressure variations must be measurable at small t_D/r_D^2 ;
- the wellbore storage effect and well skins must be negligible (see section 22.4).

Curves for interference tests in fractured media have the same limitations as curves for one-well tests:

- they are valid only for a producing active well;
- transition curves correspond to $\omega = 0$.

22.4 INFLUENCE OF FLOW RATE HISTORY

The interpretation methods presented in section 22.3 consider that:

- the active well is producing at a constant flow rate;
- the observation well does not flow and has constant pressure before interference.

How can interference be analyzed when the flow rate history for the two wells is more complex?

The most rigorous method is to account for the two flow histories by using a flow rate superposition function. The only way to generate type curves easily in this case is to use an analytical well simulator.

What happens when there is no well simulator available for interpretation?

The question is to determine the share due to the last flow rate variation at the active well in the pressure variation at the observation well.

The simplest method consists in:

- measuring the pressure at the observation well before interference;
- extrapolating the variations after interference begins;
- the pressure variation due to interference is the difference between the measured pressure and the extrapolated pressure.

The difficulty resides in extrapolating the pressure. It is crucial to measure the pressure in the observation well long enough in advance before changing the flow rate in the active well to have a reliable extrapolation.

Extrapolation is simple to perform with the following flow rate history of the active well:

- production or injection at a constant flow rate;
- well shut in.

First the interference due to opening the well for production is interpreted. Interpretation is done with the Theis type curve (Fig. 22.5) with the semi-log method (Fig. 22.6) when it is applicable.

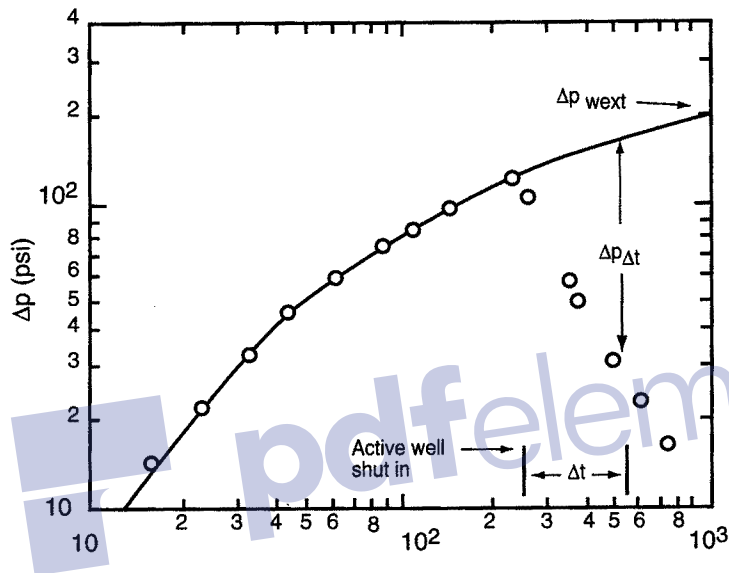


Fig. 22.5

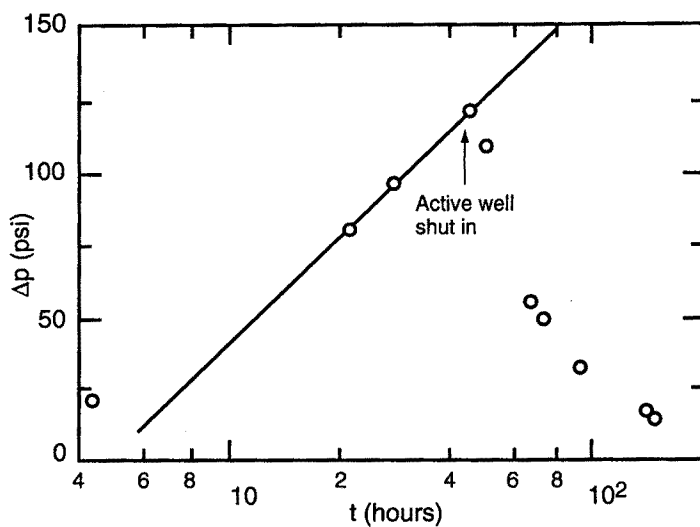


Fig. 22.6

The pressure variations due to the first flow rate are extrapolated (Figures 22.6 and 22.5) to allow interpretation of the interference due to the active well being shut in.

22.5 SKIN AND WELLBORE STORAGE EFFECT

The interpretation methods presented in this chapter assume that the wellbore storage effect and the skin of the two wells are of negligible importance.

This is not always the case. Jargon [Ref. 49] studied the influence of non-zero wellbore storage and skin in an active well.

The type curve is located under the Theis curve with positive skin or with non-zero wellbore storage (Fig. 22.7). Negative skin tends to push the type curve up.

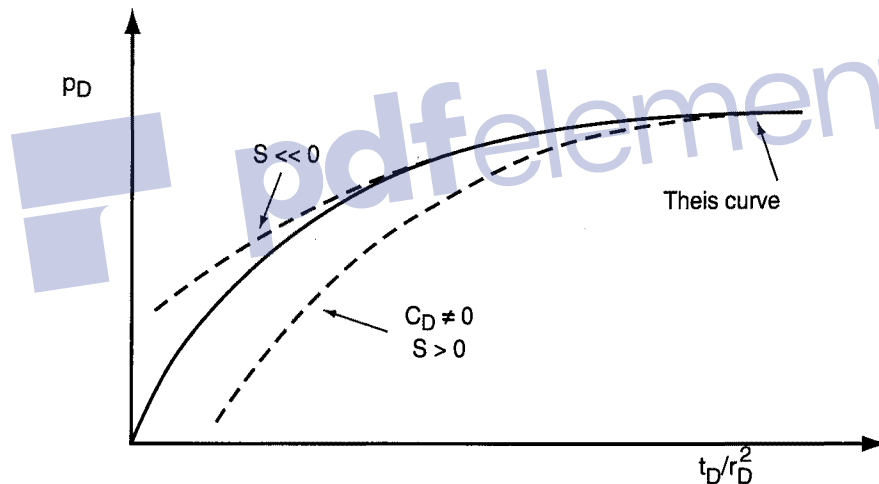


Fig. 22.7

The skin and wellbore storage effect is greater at small t_D/r_D^2 .

Jargon considers that disregarding the skin and the wellbore storage introduces error of less than 1% for p_D as long as:

$$\frac{t_D}{r_D^2} > (230 + 155) \left(\frac{C_D}{r_D^2} \right)^{0.86} \quad \text{for } S > 0 \quad (22.11)$$

F. Daviau [Ref. 1] points out that this criterion is severe and that the 10% criterion generally used for type curves would have been preferable.

He proposes another criterion, that wellbore storage and skin can be disregarded when:

$$[(C_D \exp(2S)] C_D / r_D^2 < 10^{0.005} \quad (22.12)$$

The terms of this equation are drawn from D.O. Ogbe and W.E. Brigham [Ref. 50], who deal with interferences including skin and wellbore storage at the two wells.

The criterion in equation (22.12) is valid as long as:

$$S > \log \frac{100}{r_D^2} \quad (22.13)$$

Using a well simulator helps avoid mistakenly disregarding the importance of the skin and the wellbore storage of the two wells.

22.6 OBJECTIVE OF INTERFERENCE TESTS, TWO EXAMPLES

An interference test is more complicated to perform than a simple well test. An operator uses it only to reach objectives that can not be achieved by a well test.

There are two specific objectives with an interference test:

- determine and characterize the communication between two wells;
- estimate the horizontal permeability anisotropy of the reservoir.

• Communication between two wells:

An interference test usually serves to establish whether two wells are in hydraulic communication. Communication is crucial whenever injection is planned to maintain pressure in the area drained by the other well.

When there is communication, interpretation of the interference characterizes the permeability, or more generally speaking, the kh/μ of the reservoir between the two wells.

The case below illustrates this first objective.

The map in Figure 22.8 shows wells N1 and N2 involved in the interference test.

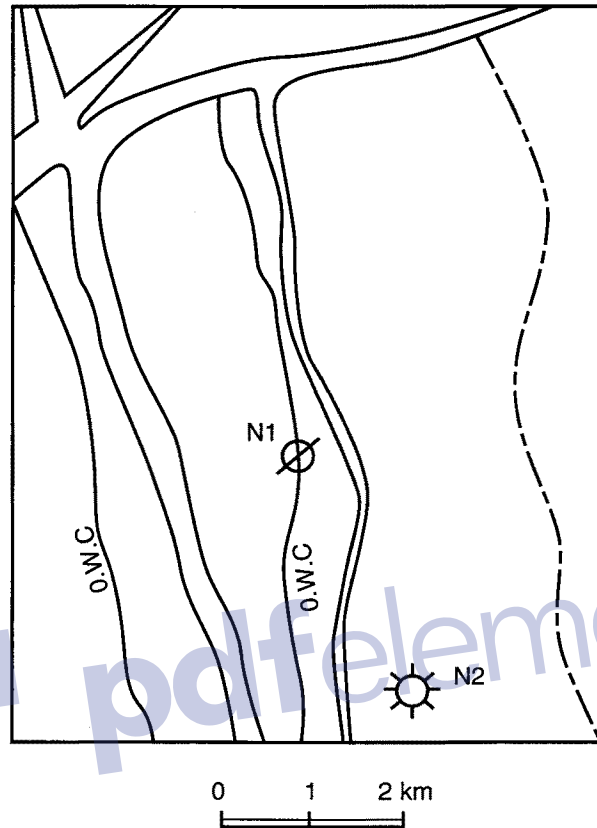


Fig. 22.8

Well N1 is in a water zone. Well N2 is in an oil zone. The two wells are separated by a fault, at the time of the test it is not known whether the fault is sealing.

It is of utmost importance for the two wells to communicate. N1 is to become a water injection well to maintain the pressure in the zone produced by well N2.

Well N2 is the observation well. It is shut in long before the test begins.

Well N1 is the active well. Interference is obtained by putting it in production (it is a naturally eruptive well).

Figure 22.9 shows the interference observed on N2 subsequent to N1 being opened for production.

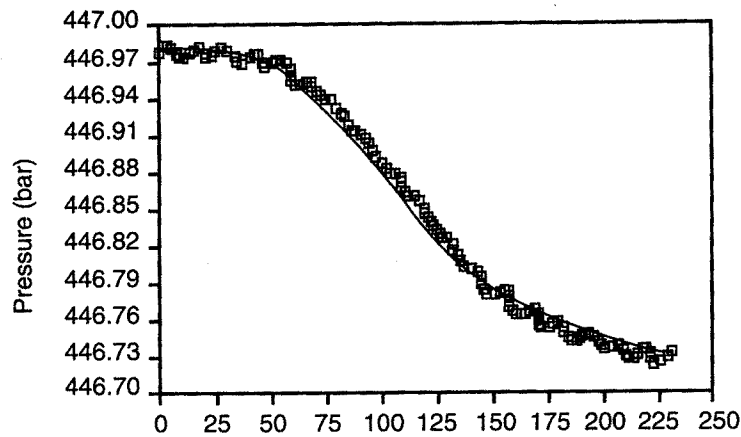


Fig. 22.9

The pressure measured on N2 is initially constant (446.98 bars).

Opening N1 produces a clear-cut interference from $t = 50$ hours elapsed.

Three things can be noted:

- the test lasts a long time: nearly 10 days;
- the interference is weak: less than 0.3 bar;
- there is a tide effect: very clear cyclic variations can be seen at the beginning and the end of the test, with a period of 12 hours and an amplitude of 0.01 bar (0.14 psi).

The duration of the test and the weak signal require the use of quartz pressure gauges.

The fact that an interference signal exists indicates that the fault throw is less than the reservoir thickness.

Since there is communication between the two wells, it is possible to drill injection wells to the west of fault F.

• Permeability anisotropy:

Reservoirs are naturally heterogeneous. Despite this fact, it is impossible to see anything but homogeneous reservoir behavior during a well test because of an averaging effect.

Interference tests are more directional and help highlight the heterogeneous nature of reservoirs.

The first type of heterogeneity that an interference test serves to characterize is the permeability anisotropy.

Under certain conditions an anisotropic reservoir can be described by means of a permeability tensor: k_x , k_y , k_{xy} are the components of this symmetrical tensor.

Two principal directions, k_{\min} and k_{\max} , correspond to the tensor and are illustrated in Figure 22.10.

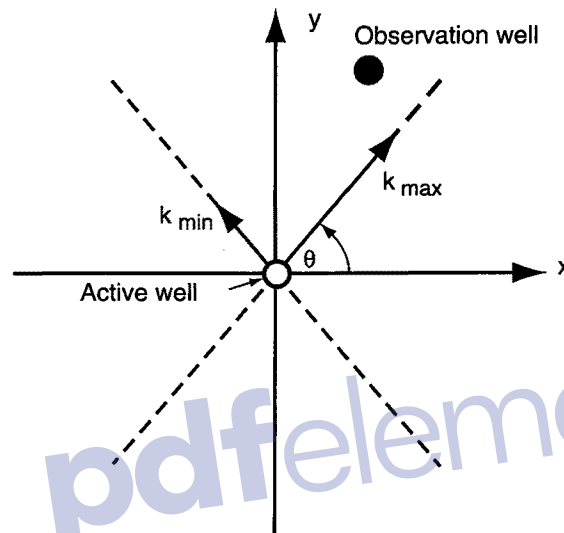


Fig. 22.10

The dimensionless pressure p_D and the dimensionless variable t_D/r_D^2 are related respectively to Δp and Δt by the equation:

$$p_D = \frac{k_{\max} k_{\min} h}{qB\mu} \Delta p$$

$$\frac{t_D}{r_D^2} = \frac{0.000264 \Delta t}{\phi \mu c_t} \left(\frac{k_{\max} k_{\min}}{k_x y^2 + k_y x^2 - 2k_{xy} xy} \right) \quad (\text{in practical US units})$$

$$k_{\max} k_{\min} = k_x k_y - k_{xy}^2$$

$$k_{\max} = 0.5 k_x + k_y + \sqrt{(k_x - k_y)^2 + 4 k_{xy}^2}$$

$$k_{\min} = 0.5 k_x + k_y - \sqrt{(k_x - k_y)^2 + 4 k_{xy}^2}$$

Three interference tests in three different directions are required to determine k_x , k_y and k_{xy} .

Such determination is seldom possible operationally. Reality may very often not be described by a tensor. This is notably the case when the heterogeneity is due to a drain that causes preferential communication between two wells.

Conventional interpretation of the interference test between the two wells gives a permeability value. The permeability is that of the homogeneous reservoir which is equivalent to the drain area.

The following case on the Chateaufrenard field (France) illustrates this type of determination.

• **The Chateaufrenard field [Ref. 51]:**

The interference test described here involves the zone of the microemulsion industrial pilot project. This zone is shown in Figure 22.11 and is characterized by:

- four neighboring five spots;
- an injection well in the middle of each five spot;
- the most significant results are expected on well CHU 18 located in the center of the panel.

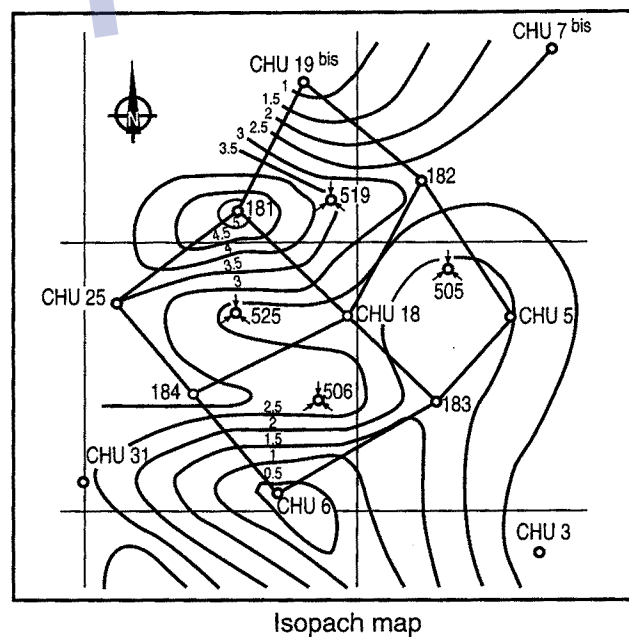
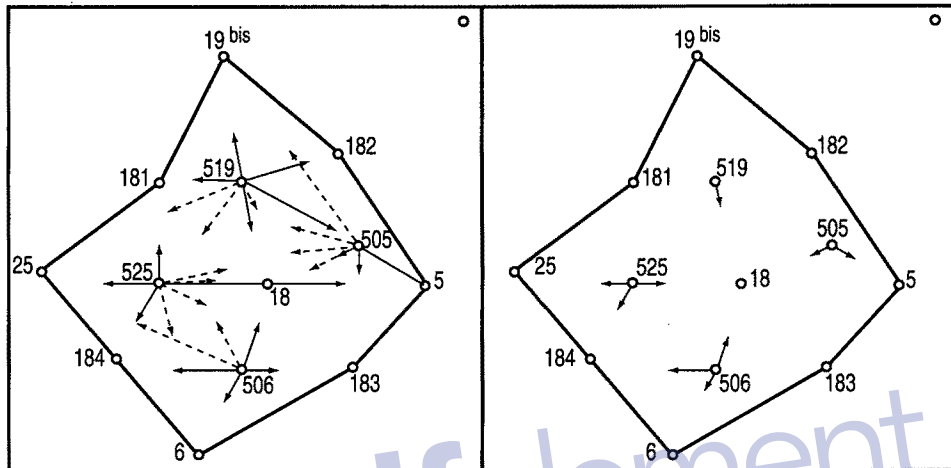


Fig. 22.11 Isopach map

An interference test is conducted before the pilot project starts:

- the injection wells are the active wells;
- the other wells are the observation wells.

Interpretation of this test shows uniform distribution of mobility around the injection wells except in the direction CHU 525-CHU 18 (Fig. 22.12).



Mobility (june, 1983)

Mobility after injection of 0.15 pore volume
(november, 1983)

Fig. 22.12

Fig. 22.13

Rapid breakthrough of the chemicals injected in CHU 525 is observed in the central production well CHU 18. Breakthrough confirms the results of the interference test.

The injection of highly viscous polymers in CHU 525 decreases the mobility of the fluids in the CHU 525-CHU 18 drainage zone. A further interference test (Fig. 22.13) confirms that the polymer injection has made mobility distribution more regular around injection well CHU 525.



Chapter 23

Pulse tests

23.1 PRESENTATION

- **Description of a pulse test:**

In an interference test the pressure change at the observation well is due to one single flow rate variation at the active well.

The pulse test is another type of multiwell test. It consists in having a sequence of flow rate variations in the active well, usually alternating periods of production and shut in.

In a pulse test each constant flow period is short compared to an interference test. Because of this the pressure variations measured at the observation well are small: often approximately 0.1 to 0.01 psi. To measure them correctly the observation well must be shut in and the pressure gauges must be highly sensitive.

- **Comparison between a pulse test and an interference test:**

A pulse test has two advantages over an interference test:

- The fact that each constant flow period is short means that the pressure drift in the observation well can be disregarded;
- The number of flow rate variations gives several estimates of k/μ and $\phi\mu c_t$: one for each variation.

However, a pulse test is economically feasible only when the duration of each constant flow period is short (a few hours to a few days). This is possible in two cases:

- a reservoir with high hydraulic diffusivity (high $k/\phi\mu c_f$);
- an observation well close to an active well.

• Pulse test or interference test?

The first use of pulse tests was described by Johnson, Greenkorn and Woods [Ref. 52]. It corresponds to the development of the first highly sensitive pressure gauges (sensitivity: 0.01 psi). The authors state that a pulse test lasts less time than an interference test and allows multiwell test time to be shortened.

Their comparison was biased then, since they were comparing a pulse test using a highly sensitive pressure gauge and an interference test conducted with conventional gauges from the seventies.

In actual fact each of these two types of multiwell tests has its area of application:

- Pulse tests are recommended in a reservoir where mobility (k/μ) and hydraulic diffusivity ($k/\phi\mu c_f$) are high (e.g. a very permeable gas reservoir). In this type of reservoir the pressure variation is small, but is felt very quickly in the observation well. Repeating the signal and eliminating the reservoir pressure trend at the observation well is particularly useful in this case.
- Interference tests are recommended in a reservoir where fluid mobility and hydraulic diffusivity are low, e.g. a low-permeability reservoir, viscous oil. In this type of reservoir the pressure change is greater, but requires a long-lasting test to be observed. Repeating the test, i.e. conducting a pulse test, in this case demands prohibitively long testing times.

The main factor involved in the decision to conduct a multiwell test is in both cases the distance between active and observation well.

The farther away the two wells:

- the smaller the pressure change at the observation well;
- the longer the test needs to last.

When the wells are a certain distance apart, each flow period has to last too long for the pulse test to be economically feasible. Only an interference test can be attempted.

For greater distances, even an interference test will be of no benefit, the pressure variation will be too small to be measured by the gauges.

23.2 INTERPRETING PULSE TESTS: THE KAMAL AND BRIGHAM METHOD

A pulse test consists in having a series of flow rate variations at the active well.

Like any multirate test it can be interpreted with a superposition function calculated using an analytical well simulator. In this case there can be any duration and value of the flow rate during each period.

A manual interpretation method was developed by Kamal and Brigham [Ref. 55 and 56], but the drawback is that it imposes some constraints on the flow rate history. This is the method that will be discussed here.

• Active well:

Let us assume that the active well is initially producing at a flow rate q . The first flow variation consists in shutting in the well.

To be applicable, the Kamal and Brigham method has the following requirements in relation to the active well:

- the well must produce with the same flow rate, q , during each flow period;
- the shut-in periods must all have the same duration, i.e. Δt_p (Fig. 23.1);
- the production periods must also all last the same length of time.

The production periods can have a different duration from the shut-in periods (Fig. 23.1).

A cycle consists of a shut-in period and the production period that comes after it. Its duration is Δt_c .

Kamal and Brigham define F' as the ratio of pulse length to the total cycle length:

$$F' = \frac{\Delta t_p}{\Delta t_c} \quad (23.1)$$

A pulse is defined by two successive flow rate variations. They are numbered according to the order they come in, with the first one numbered 1. The following can be distinguished on a well that is initially open (Fig. 23.1):

- the odd numbered pulses due to the well's shut-in/open/shut-in sequence;
- the even numbered pulses due to the open/shut-in/open sequence.

Nota bene:

A similar logic can be used with a well that is initially shut in. In this case the odd pulses are due to open/shut-in/open and the even ones to the inverse.

Likewise, instead of a production well, the active well can be an injection well.

• Observation well:

The signal obtained at the observation well looks like Figure 23.2.

In this figure an odd pulse is associated with a peak and each even one is associated with a dip.

The Kamal and Brigham interpretation method uses two components in this pressure history:

- the pressure variation between a peak and a dip;
- the time lag between the end of a pulse and the corresponding peak or dip.

The two phenomena are characterized in the following way:

- assuming a pulse and the peak or dip that is associated with it (see pulse 3 and peak 3 in Figure 23.3);
- draw the tangent to the two adjacent dips or peaks: dips 2 and 4 in Figure 23.2;
- draw a straight line parallel to the tangent which is itself tangent to the peak or dip under consideration (see Figure 23.2);
- the time lag t_L is the time elapsed between the end of the pulse and the point of tangency to the peak or dip (see Figure 23.2);
- the pressure variation, Δp is the difference in pressure between the two parallel straight lines (Fig. 23.2).

• The Kamal and Brigham charts:

A pulse test can be interpreted manually with the charts developed by Kamal and Brigham. It is the charts' domain of application that imposes constraints on the flow rate history of the active well.

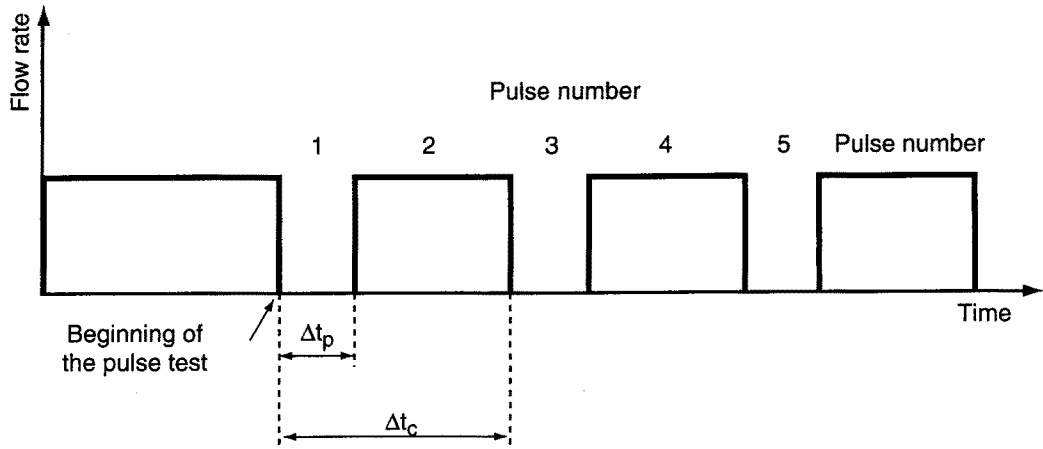


Fig. 23.1

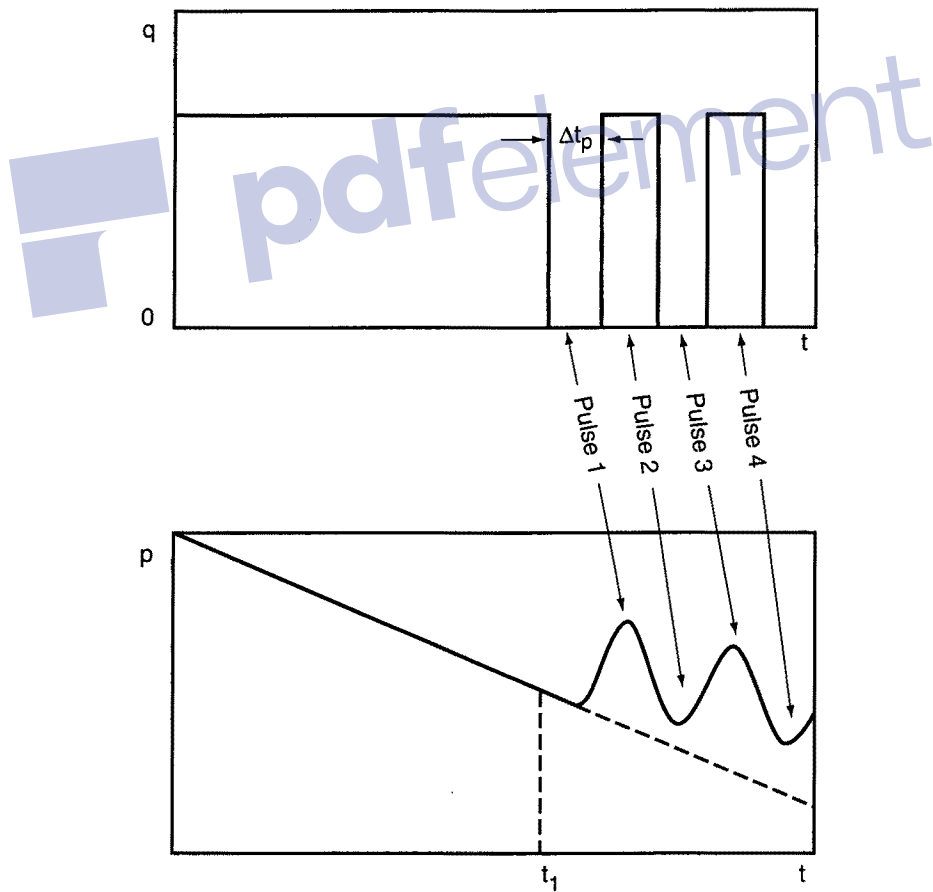


Fig. 23.2

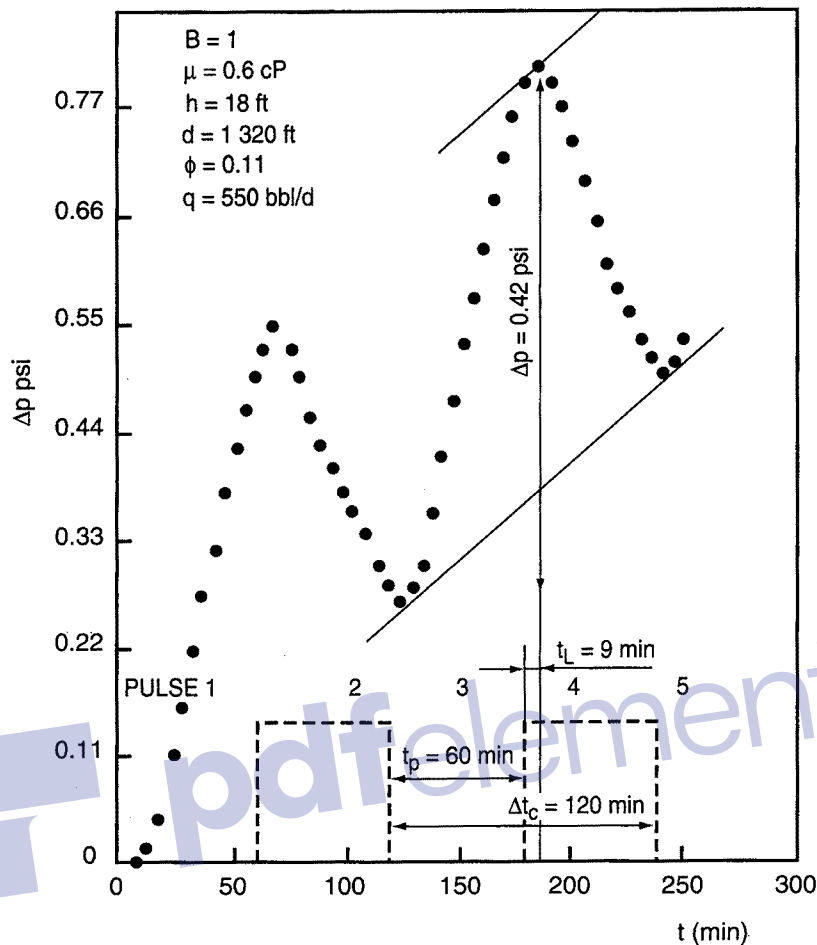


Fig. 23.3

Pulse tests are interpreted with four sets of two charts:

- one set of two charts for the first odd pulse (Figs. 23.4 and 23.5);
- a second set for the first even pulse (Figs. 23.6 and 23.7);
- a third set for the other odd pulses (Figs. 23.8 and 23.9);
- a fourth set for the other even pulses (Fig. 23.10 and 23.11).

Each chart is made up of curves that differ by the value of F' (equation 23.1) and each is graduated semi-logarithmically: logarithmic on the abscissa and linear on the ordinate.

The value of $t_L/\Delta t_c$ is plotted on the abscissa, while on the ordinate the value of:

- $\Delta p_D (t_L/\Delta t_c)^2$ is plotted on one of the charts in each set
- t_{LD}/r_D^2 is plotted on the other one in each set

with $r_D = r/r_w$, r being the distance between the active well and the observation well

$$\text{and } t_{LD} = \frac{\alpha k t_L}{\phi \mu c_t r_w^2}$$

$$\begin{aligned} \alpha &= 0.000264 && \text{(in practical US units)} \\ \alpha &= 0.00036 && \text{(in practical metric units)} \\ \alpha &= 1 && \text{(in SI units).} \end{aligned}$$

• **Interpretation:**

Interpretation of a pulse test involves several steps, which are illustrated in Figures 23.12 and 23.13 by the interpretation of pulse 3 in Figure 23.3.

- 1 Calculate Δt_c and F' corresponding to the flow rate history of the active well.
In the example $\Delta t_c = 2$ h; $F' = 0.5$.
- 2 Determine the time lag, t_L , and the pressure variation, Δp , associated with the pulse. $t_L = 9$ min; $\Delta p = 0.42$ psi.
- 3 Choose the right set of charts, i.e. other odd pulses in this case.
- 4 Calculate $t_L/\Delta t_c$: $t_L/\Delta t_c = 0.075$ in the chosen example.
- 5 Read $\Delta p_D (t_L/\Delta t_c)^2$ and t_{LD}/r_D^2 ; here $\Delta p_D (t_L/\Delta t_c)^2 = 0.0013$;
 $t_{LD}/r_D^2 = 0.0875$.
- 6 Determine the reservoir's permeability:

$$k = \frac{\beta q B \mu \Delta p_D (t_L/\Delta t_c)^2}{h \Delta p (t_L/\Delta t_c)^2}$$

$$\begin{aligned} \beta &= 141.2 && \text{(in practical US units)} \\ \beta &= 18.67 && \text{(in practical metric units)} \\ \beta &= 1/2 \pi && \text{(in SI units).} \end{aligned}$$

In the chosen example: $k = 1410$ mD.

- 7 Determine the reservoir's capacity:

$$\phi c_t = \frac{\alpha k t_L}{\mu r^2 t_{LD}/r_D^2}$$

In the chosen example: $\phi c_t = 6 \cdot 10^{-6}$ psi⁻¹.

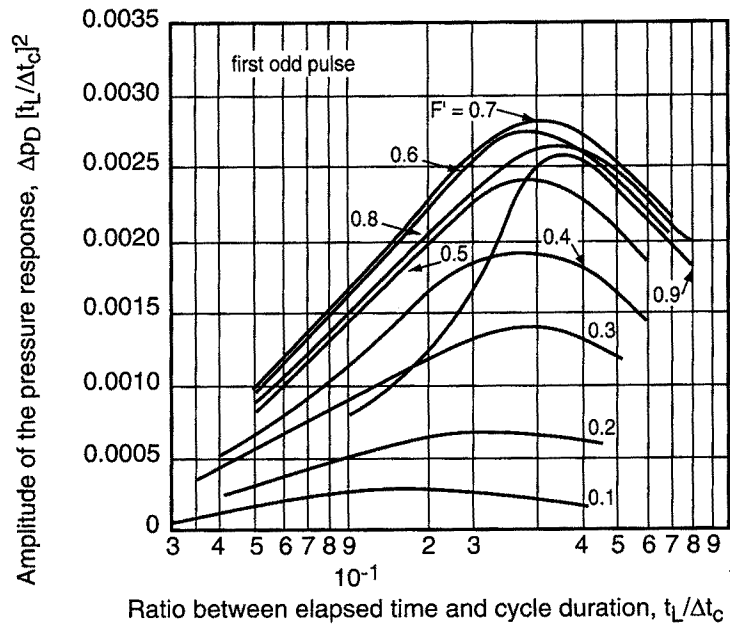


Fig. 23.4

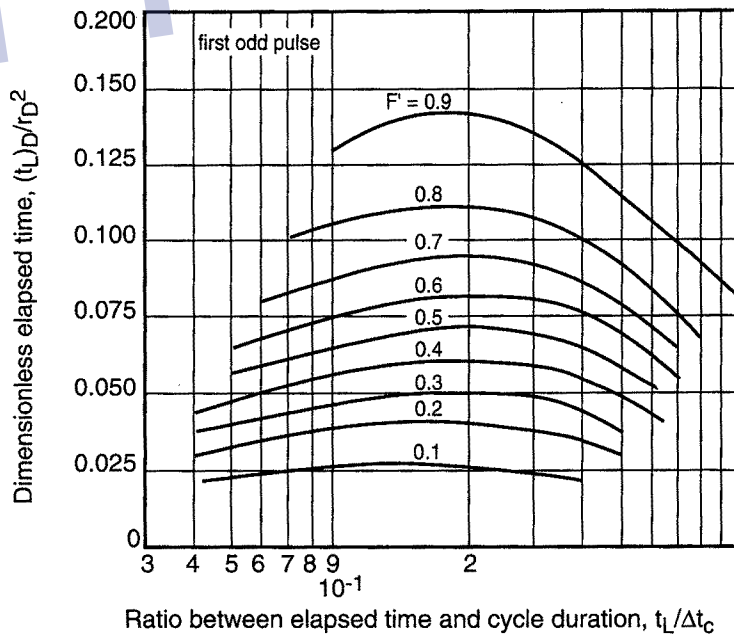


Fig. 23.5

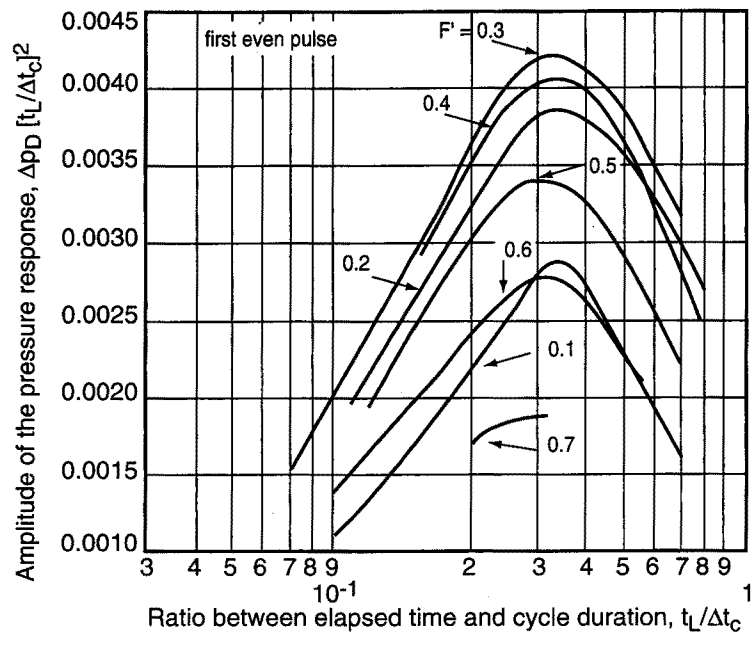


Fig. 23.6

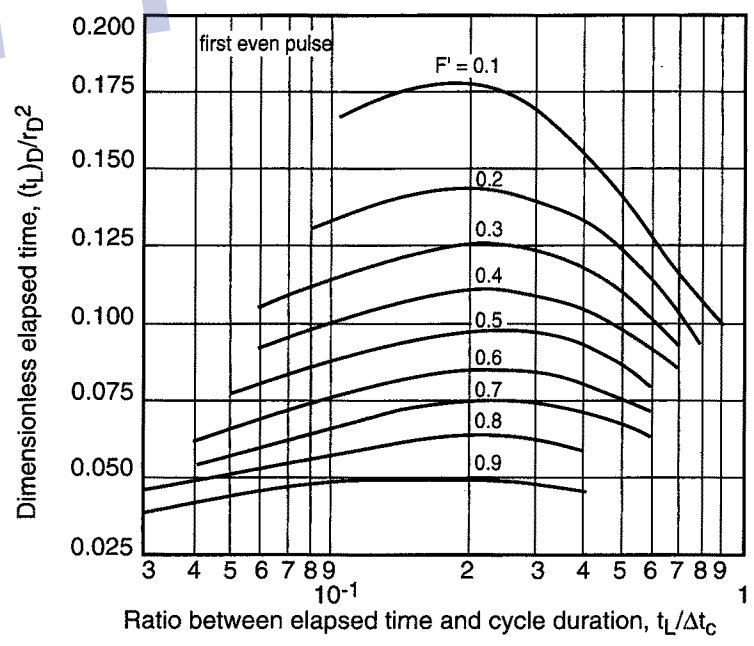


Fig. 23.7

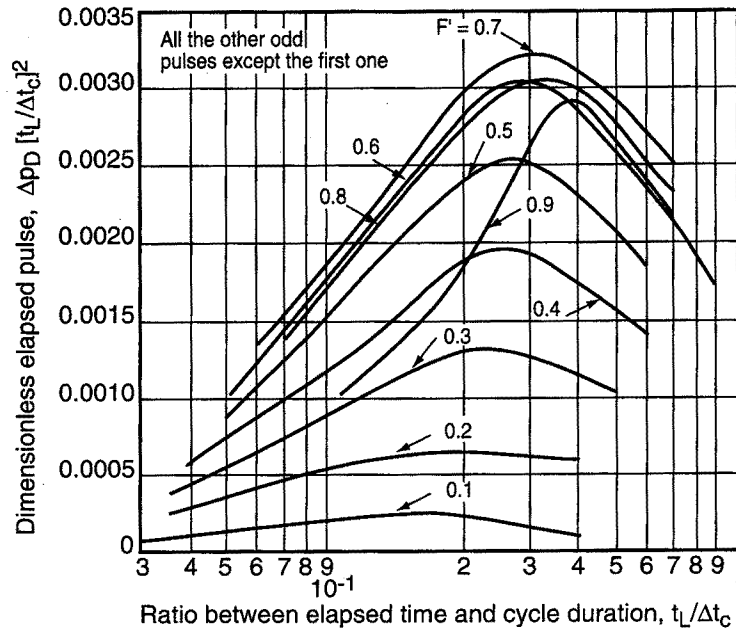


Fig. 23.8

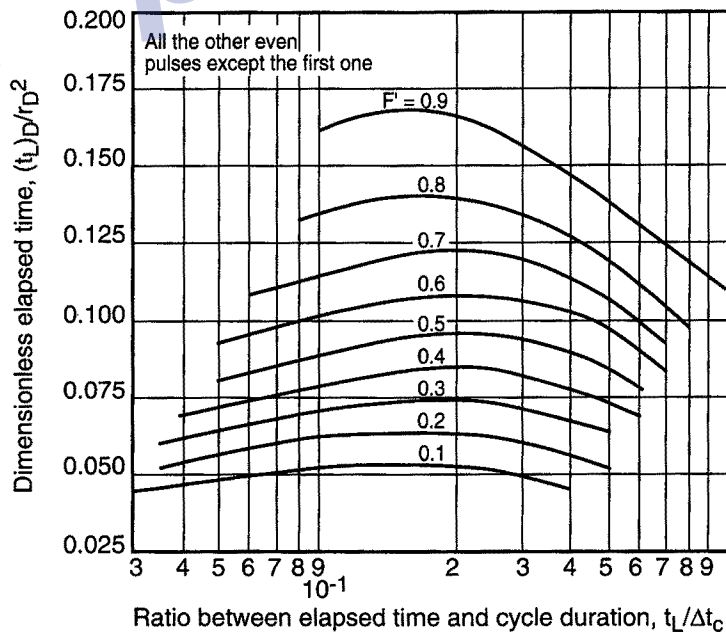


Fig. 23.9

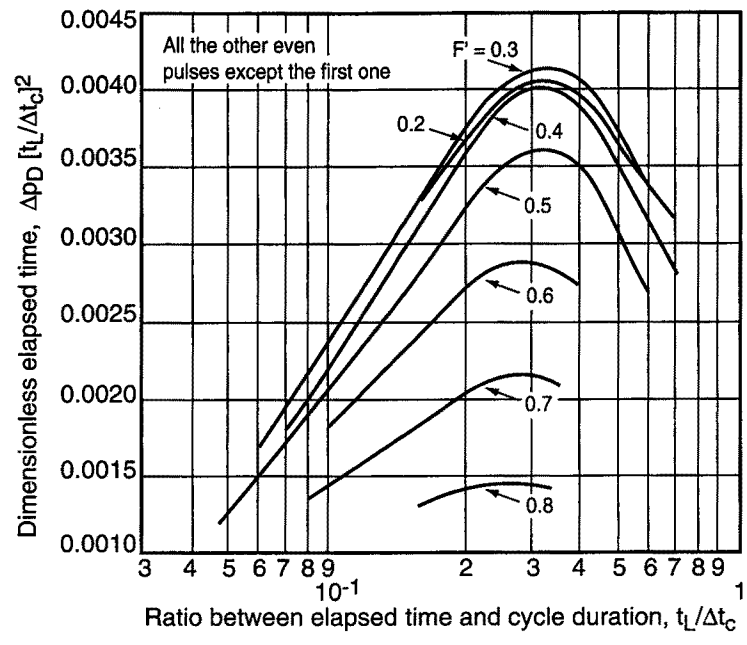


Fig. 23.10

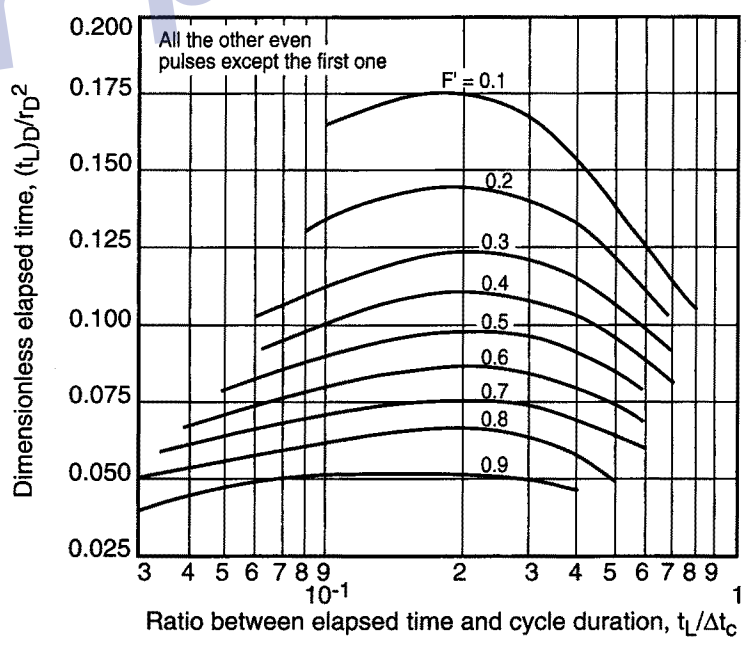


Fig. 23.11

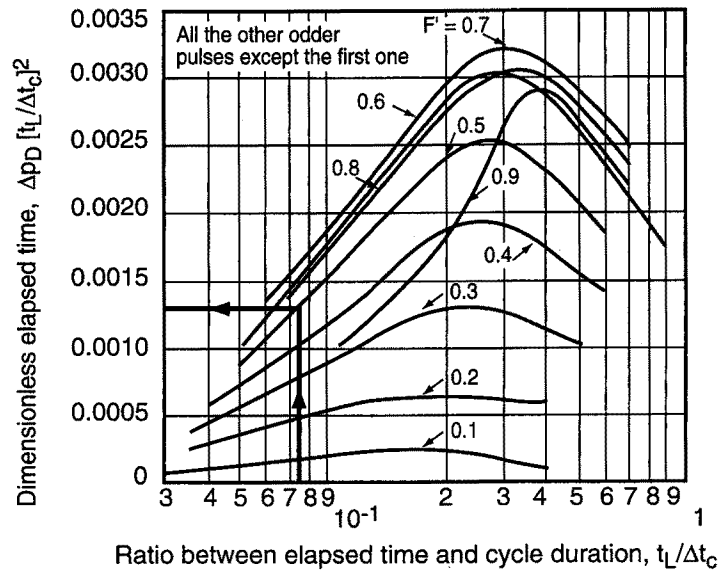


Fig. 23.12

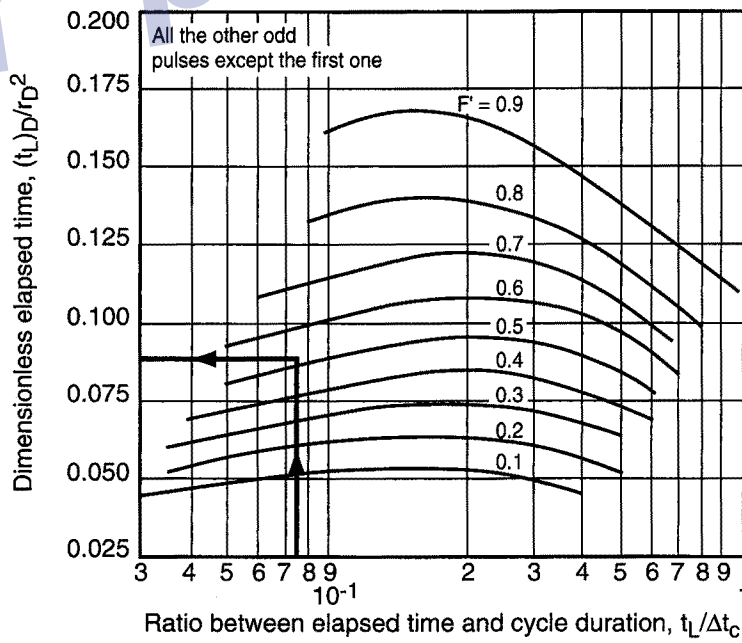


Fig. 23.13

Practical units

	Practical metric units	Practical US units
Length	m	ft
Permeability	mD	mD
Pressure	bars	psi
Temperature	°K	°R
Time	h	h
Viscosity	cP	cP
Liquid flow rate	m ³ /j	bbI/j
Gas flow rate	m ³ /j	cuft/j
Volume	m ³	cuft



References

- [1] DAVIAU F., *Interprétation des essais de puits : les méthodes nouvelles*, Éditions Technip, Paris, 1986.
- [2] CHAUMET P., *Écoulement monophasique des fluides dans les milieux poreux*, cours de production, ENSPM, tome III, Éditions Technip, Paris, 1965.
- [3] VAN POOLEN H.K., "Radius of drainage and stabilization time equations", *Oil and Gas Journal*, September 14, 1964, pp. 138-146.
- [4] LEE J., "Well testing", *SPE Textbook Series*, Vol. 1.
- [5] VAN EVERDINGEN A.F., "The skin effect and its influence on the productive capacity of a well", *Trans.*, AIME, 1953, **198**, pp. 171-176.
- [6] HORNER D.R., "Pressure build up in wells", *Proc. Third World Pet. Congr.*, E.J. Brill, Leiden, 1951, **II**, p. 503.
- [7] AGARWAL R.G., "A new method to account for producing time effects when draw type curves are used to analyse pressure build-up and other test data", *SPE 9289*, 1980.
- [8] MATTHEWS C.S., RUSSEL D.G., "Pressure build-up and flow tests in wells", *Monograph Volume 1 of the Henry L. Doherty Series*.
- [9] BOURDET D., WHITTLE T.M., DOUGLAS A.A., PIRARD V.M., "A new set of type curves simplifies well test analysis", *World Oil*, May 1983.
- [10] LARSEN L., HOVDAN M., "Analysing well test data from linear reservoirs by conventional methods", *SPE 16 777*, Dallas, 27-30 Sept. 1987.

REFERENCES

- [11] PRASAD R.K., "Pressure transient analysis in the presence of two intersecting boundaries", *SPE 4560*, Las Vegas, Oct. 1973.
- [12] EARLOUGHER R.C., "Advances in well test analysis", *Monograph Volume 5 of the Henry L. Doherty Series*.
- [13] RAMEY H.J. Jr., COBB W.M., "A general build up theory for a well in a closed drainage area", *JPT*, Dec. 1971, pp. 1493-1505.
- [14] WARREN J.E., ROOT P.J., "The behavior of naturally fractured reservoirs", *SPEJ*, Sept. 1963, pp. 245-255.
- [15] DIETZ D.N., "Determination of average reservoir pressure from build up survey", *JPT*, Aug. 1965, pp. 955-959.
- [16] EARLOUGHER R.C., RAMEY H.J., MILLER F.G., MUELLER T.D., "Pressure distribution in rectangular reservoirs", *JPT*, Feb. 1968, pp. 199-208.
- [17] SWANN O.A. (DE), "Analytic solutions for determining naturally fractured reservoir properties by well testing", *Trans., AIME*, 1976.
- [18] BOURDET D., GRINGARTEN A.G., "Determination of fissure volume and block size in fractured reservoirs by type curve analysis", *SPE 9293*, 1980.
- [19] BOURDET D., AYOUB J.A., WHITTLE T.M., PIRARD Y.M., KNIAZEFF V., "Interpreting well tests in fractured reservoirs", *World Oil*, Oct. 1983.
- [20] CINCO-LEY H., SAMANIEGO F., "The pressure transient behavior for naturally fractured reservoirs with multiple block size", *SPE 14 168*, Las Vegas, Sept. 1985.
- [21] REISS L.H., *Reservoir engineering en milieu fissuré*, Éditions Technip, 1980.
- [22] BARENBLATT G.I., ZELTOV J.P., KOCINA J.N., "Notions fondamentales de la théorie d'écoulement des liquides homogènes dans les milieux fissurés", *Priklad. Mat. i. Mekh. OTN*, **24**, 5, pp. 858-864, 1960.
- [23] RAWLINS E.L., SCHELLHARDT M.A., "Backpressure data on natural gas well and their application to production practices", *US Bureau of Mines*, Monograph 7, 1936.
- [24] Houpeurt A., "On the flow of gases in porous media", *Revue de l'Institut Français du Pétrole*, **XIV**, (11), pp. 1468-1684, 1959.
- [25] KATZ D.L., *Handbook of natural gas engineering*, McGraw-Hill, 1959.

REFERENCES

- [26] CORNELSON D.W., "Analytical prediction of natural gas reservoir recovery factors", *J. Can. Pet. Tech.*, **13**, (4), pp. 17-24, 1974.
- [27] BOURDET D., ALAGOA A., AYOUB J.A., PIRARD Y.M., "New type curves aid analysis of fissured zone well tests", *World Oil*, April 1984.
- [28] GRINGARTEN A.C., RAMEY H.J., RAGHAVAN R., "Pressure analysis for fractured wells", *SPE 4051*, San Antonio, Oct. 1972.
- [29] GRINGARTEN A.C., RAMEY H.J., "Unsteady-state pressure distribution created by a well with a single horizontal fracture, partial penetration or restricted entry", *SPEJ*, Aug. 1974, pp. 413-425.
- [30] CINCO-LEY H., SAMANIEGO F., DOMINGUEZ N., Transient pressure behavior for a well with a finite conductivity vertical fracture, *SPE 6014*, New Orleans, Oct. 1976.
- [31] CINCO-LEY H., SAMANIEGO F., "Effect of wellbore storage and damage on the transient pressure behavior of vertically fractured wells", *SPE 6452*, Denver, Oct. 1977.
- [32] CINCO-LEY H., SAMANIEGO F., "Transient pressure analysis for fractured wells", *JPT*, Sept. 1981, pp. 1749-1766.
- [33] CINCO-LEY H., SAMANIEGO F., "Transient pressure analysis: finite conductivity fracture case versus damaged fracture case", *SPE 10 189*, San Antonio, Oct. 1981.
- [34] BRITT L.K., BENETT G.O., "Determination of fracture conductivity in moderate permeability reservoirs using bilinear flow concepts". *SPE 14 165*, Las Vegas, Sept. 1985.
- [35] CINCO-LEY H., SAMANIEGO F., "Transient pressure analysis for fractured wells", *SPE 7490*, Houston, Oct. 1978.
- [36] AGARWAL R.G., AL-HUSSAINY R., RAMAY H.J. Jr., "An investigation of wellbore storage and skin effect in unsteady liquid flow – I. Analytical treatment", *SPEJ*, Sept. 1970, 279-290.
- [37] DAVIAU F., MOURONVAL G., BOURDAROT G., CURUTCHET P., "Pressure analysis for horizontal wells", *SPEFE*, Dec. 1988, pp. 716-724.
- [38] MONTIGNY O. (DE), COMBE J., "Hole benefits, reservoir types key to profit", *OGJ*, Apr. 11, 1988, pp. 50-56.

REFERENCES

- [39] PERRINE R.L., Analysis of pressure build-up curves, *Drilling and Prod. Prac. API*, Dallas, 1956, pp. 482-509.
- [40] BOE A., SKJAEVELAND S.M., WHITSON C.H., «Two phase pressure test analysis», *SPE 10 224*, San Antonio, 1981.
- [41] AL-KHALIFAH A.J.A., AZIZ K., HORNE R.H., "A new approach to multiphase well test analysis", *SPE 16 743*, Dallas, Sept. 1987.
- [42] RAGHAVAN R., "Well test analysis for multiphase flow", *SPEFE*, Dec. 1989, pp. 585-594.
- [43] VOGEL J.V., "Inflow performance relationships for solution-gas drive wells", *JPT*, Jan. 1968, p. 83-92, *Trans.*, AIME 243.
- [44] STANDING M.B., "Concerning the calculation of inflow performance of wells producing gas drive reservoirs", *JPT*, Sept. 1971, pp. 1141-1142.
- [45] THEIS C.V., "The relationship between the lowering of piezometric surface and rate and duration of discharge of wells using ground-water storage", *Trans. AGU*, II, p. 519, 1935.
- [46] ARDITTY P.C., "Response of a closed well-reservoir system to stress induced by earth tides", *SPE 7484*, Houston, Oct. 1978.
- [47] BOURDET D., GRINGARTEN A.C., "Determination of fissure volume and block size in fractured reservoirs by type-curve analysis", *SPE 9293*, Dallas, Sept. 1980.
- [48] DERUYCK B.G., BOURDET D.P., DAPRAT G., RAMEY H.J., "Interpretation of interference tests in reservoirs with double porosity behavior. Theory and field examples", *SPE 11 025*, New Orleans, Sept. 1982.
- [49] JARGON J.R., "Effect of wellbore storage and wellbore damage at the active well on interference test analysis", *SPE Reprint Series No. 14*, pp. 131-138.
- [50] OGBE D.O., BRIGHAM W.E., "A model for interference testing with wellbore storage and skin effects at both wells", *SPE 13 253*, Houston, Sept. 1984.
- [51] CHAPOTIN D., LOMER J.F., PUTZ A., "The Châteaurenard (France) industrial microemulsion pilot design and performance", *SPE/DOE 14 955*, Tulsa, Apr. 1986.
- [52] JOHNSON C.R., GREENKORN R.A., WOODS E.G., "Pulse-testing: a new method for describing reservoir flow properties between wells", *JPT*, Dec. 1966, pp. 1599-1604, *Trans.*, AIME 237.

REFERENCES

- [53] MILLER G.B., SEEDS R.W.S., SHIRA H.W., "A new surface recording, downhole pressure gauge", *SPE 4125*, San Antonio, Oct. 1972.
- [54] RAMEY H.J., "Interference analysis for anisotropic formations. A case history", *JPT*, Oct. 1975, pp. 1290-1298, *Trans.*, AIME 259.
- [55] BRIGHAM W.E., Planning and analysis of pulse tests, *JPT*, May 1970, pp. 618-624. *Trans.*, AIME 249.
- [56] KAMAL, MEDHAT, BRIGHAM W.E., "Pulse testing response for unequal pulse and shut-in periods", *SPEJ*, Oct. 1975, pp. 399-410, *Trans.*, AIME 259.
- [57] CINCO H., MILLER F.G., RAMEY H.J., "Unsteady-state pressure distribution created by a directionally drilled well", *JPT*, Nov. 1975, pp. 1392-1400.
- [58] BOURDET D., "Pressure behavior or layered reservoirs with crossflow", *SPE 13 628*, Bakersfield, March 1985.
- [59] GAO CHENG-TAI, "Single-phase fluid flow in a stratified porous medium with crossflow", *SPEJ*, Feb. 1984, pp. 97-106.
- [60] EHLIG-ECONOMIDES C.A., JOSEPH J.A., "A new test for determination of individual layer properties in a multilayered reservoir", *SPE 14 167*, Las Vegas, Sept. 1985.



Index

A

Absolute open flow potential test, 263.
 Active well, 293-295, 298, 303-305, 307, 313-316, 319.
 Acidized wells, 70.
 Agarwal, 67, 76-77, 170, 222.
 Agarwal's equivalent time, 76.
 AOF, 263, 266, 268, 272-274, 280.
 Aquifer, 117, 193.
 Average pressure, 57, 110, 123, 129, 131-135, 140-142, 203, 267, 287.

B

Back pressure test, 263-264, 266, 268, 272, 274-275, 277, 280.
 Bilinear flow, 217-218, 221, 226.
 Bottomhole flow rate, 27, 33.
 Boundary conditions, 25-26.
 Bounded channel, 106, 111.
 Bourdet D., 182.
 Brigham, 37, 306, 315-316.
 Buildup, 51, 54, 64, 66, 75-76, 244.

C

Capacity contrast, 151-152, 155, 159, 169, 183, 185, 302.

Channel, 93, 103-106, 108-112, 199.
 Chen, 37.
 Closed reservoir, 93, 123-140.
 Coefficient of deviation from Darcy's law, 226, 257.
 Compressibility, 20-25, 28, 33-34, 150-152, 179-180, 242, 248, 253-254.
 Compressibility of gas, 253-254.
 Compressibility factor, 253.
 Compressible capacity, 22, 24, 179.
 Compressible zone, 26, 28, 30, 40, 44, 93, 97-98, 101, 104, 106, 117-119, 123, 131, 195-197, 199, 219, 234-236, 242.
 Communication between two wells, 306.
 Constant pressure boundary, 93, 117-118, 121, 132.
 Conventional methods, 47-49, 77, 79, 203, 221, 231.
 Cubic matrix blocs, 147-148.

D

Damage, 41, 43, 163, 217.
 Damaged well, 70.

INDEX

- Darcy's law, 20-21, 23-24, 26-27, 40-42, 44, 119, 217, 226, 235, 254, 257, 263, 271, 274-275, 278.
- Daviau F., 26, 67-68, 77, 163, 228, 238, 306.
- Deliverability straight line, 268-269, 273, 276-277, 279.
- Derivative, 48-49, 77, 79-82, 84-85, 88-90, 93, 100-101, 104, 108, 110-112, 114-115, 121, 129, 131-132, 154-157, 159, 161, 163, 175, 179, 185-188, 199, 203-204, 207, 222-223, 226-227, 239-240, 246-248.
- Deviation from Darcy's law, 44, 217, 226, 235, 254, 257, 263, 271, 274.
- Diagnosis, 48-49, 82.
- Dietz method, 135, 140.
- Diffusion equation, 23-24, 28, 254-256, 259.
- Dimensionless equation, 52.
- Double porosity model, 183.
- Double-slope straight line, 99-100, 107-108, 199.
- Drainage area of the well, 123-125, 128-129, 131-135, 141-142, 233, 238, 263, 265, 267, 271.
- Drawdown, 51-52, 54, 56, 66, 75-77, 264-269, 271-275, 277, 280, 285.
- Drawdown test, 51-52, 54.
- E**
- Earlougher, 67, 124.
- Eccentricity of the well, 105.
- Effective angle of slant, 211.
- Effective radius, 39, 41-42-68, 156, 220-221.
- Equation of state, 23-24, 253-254.
- Equivalent compressibility, 23-24, 254.
- Equivalent one-phase fluid, 283.
- Equivalent radius, 197.
- Equivalent spherical source, 199.
- Equivalent time, 63, 76.
- Even-numbered pulse, 316.
- Exchange term, 183-184.
- Exponential integral, 25.
- Extrapolated pressure, 57, 60, 63, 100, 110, 114, 134, 203, 238, 246, 303.
- F**
- Falloff, 243-244.
- Fault, 30, 93, 95, 97-101, 104, 107, 111, 119-120, 123, 199, 307-308.
- Filtration rate, 21, 24.
- Fissures, 41.
- Flow profile, 27.
- Fractures, 41, 147-155, 159, 162-163, 167, 169-170, 175, 178-179, 206-207, 213, 216, 219, 228, 302-303.
- Fracture half-length, 218, 221-222.
- Fracture permeability, 152.
- Fracture porosity, 150-151.
- Fractured reservoirs, 147-180, 206.
- G**
- Gas cap, 30, 117.
- Gas wells, 44, 217, 225, 253-280.
- Geological skin, 44.
- Geometrical skin, 219-221, 237-238.
- Global reservoir capacity, 151, 169.
- Gravel pack, 42-43.
- Gravitational forces, 23.
- Gringarten, 67-68, 84, 163, 222, 228, 299.
- H**
- Horizontal fractures, 213.
- Horizontal permeability anisotropy, 293.
- Horizontal wells, 43, 210, 233-240.

INDEX

Horner, 54-55, 59, 62-64, 100, 133, 140.
 Houpeurt method, 265-266, 271-272, 274.
 Hydraulic diffusivity, 24, 52, 238, 248, 314.
 Hydraulic fracturing, 43-44, 213, 216, 223.

I

Impermeable shoulder beds, 233.
 Inclined wells, 43.
 Index, 141-144, 287.
 Infinite homogeneous reservoir, 25, 47, 51, 67-69, 77, 87.
 Initial pressure, 25, 28, 100, 110, 114, 119, 238.
 Infinite skin, 39.
 Infinitesimal skin, 39.
 Injection radius, 242, 245-246, 248-249.
 Injection skin, 44, 245.
 Injection wells, 135, 213, 241-250, 307, 310-311.
 Interferences, 19, 66, 293-295, 298-299, 302-311, 313-315.
 Intersecting linear boundaries, 93.
 Intersection point, 98.
 Isochronal test, 263-266, 269-275, 277-278.

J

Jargon, 305.
 Jones, 29.

K

Kamal and Brigham charts, 316.
 Kamal and Brigham method, 315-316

L

Lee, 29.
 Linear boundary, 95.
 Linear flow, 104-105, 107, 110-111, 115, 214, 217-219, 221, 226-227, 231, 240.
 Linear flow in the fracture, 214, 217, 226.
 Logarithmic approximation, 52, 98, 119, 299.

M

Match matrix blocs, 147-148.
 Match point, 70, 222, 298.
 Material balance, 24, 134, 142, 246, 254-255.
 Matrix-fracture exchange, 153, 155.
 Matrix, 147-153, 155-157, 159, 161-163, 167, 169, 182, 207, 248, 299, 302.
 Matrix permeability, 152-153, 178-180.
 Matrix porosity, 150, 182.
 MBH method, 100, 110, 114, 135.
 McKinley, 67.
 MDH method, 58, 75, 170.
 Method of images, 96, 106, 117.
 Mobility, 20, 24, 30, 44, 117, 241, 245, 248-250, 283, 285-286.
 Mobility ratio, 245, 249-250.
 Modified isochronal test, 263, 265.
 Multiphase flow, 281-289.
 Multirate testing, 32.
 Muskat, 29.

N

Naturally eruptive wells, 34.
 No flow, 30, 95-97, 100, 103-104, 106, 111, 123, 131, 135.

INDEX

O

Observation well, 293-295, 303, 307, 313-314, 316, 319.
 Odd-numbered pulse, 316.
 Open-flow potential, 263, 266, 268, 271, 274, 277, 280, 288.

P

Partial penetration, 193, 195.
 Partial perforation, 195, 200, 206-207
 Partial perforation skin, 200.
 Perforations, 43, 193, 196, 199-200, 203-206.
 Permeability, 28, 39-41, 43, 77, 88, 152-154, 159, 162-163, 167, 169, 175, 178-184, 195-198, 200, 204-207, 210-211, 216, 222-223, 225, 228, 235, 238, 242, 248-249, 264, 281-282, 286, 288, 306, 308-310, 314, 319.
 Permeability anisotropy, 196, 198, 200, 204-206, 210-211, 235, 238, 293, 308.
 Permeability tensor, 309.
 Perrine method, 281-282, 285-286.
 Plugging, 143, 206, 235.
 Poettman, 29.
 Pore volume, 22.
 Pore volume drained, 124, 128.
 Pressure buildup, 31-32, 35, 51, 54, 57-58, 61, 66, 75, 109, 132, 187, 244, 259, 278, 280.
 Principal directions, 309.
 Productivity index, 141-144, 287.
 Pseudopressure, 253, 255-257, 259, 266, 268-271.
 Pseudoradial flow, 210, 219, 221-222, 226, 231, 234-236, 238-239.
 Pseudosteady-state flow, 30, 128-129, 132, 135, 141-143, 266-269, 271.

Pseudosteady-state model, 156, 159, 162-163, 167, 178-179.
 Pulse test, 313-316, 319.
 Pumping wells, 35.

Q

Quadratic term, 257.

R

Radial flow, 21, 25-26, 51, 55, 79-80, 85, 104, 109, 128, 175, 185, 187-188, 195-196, 199, 203-207, 210.
 Radial vertical flow, 235-236, 239-240.
 Radius of investigation, 28-30.
 Ramey, 37, 140.
 Real PI, 143.
 Recorded flow rates, 49.
 Relative conductivity, 216, 220, 222-224.
 Reservoir capacity, 319.
 RFT, 152, 162, 206-207.

S

Semi-square root straight line, 108.
 Semi-log straight line, 53, 56, 59-60, 77, 85, 89, 97, 99-100, 104-106, 110, 113-114, 118-120, 126, 133-135, 140, 154-155, 157, 161, 175, 187-188, 203, 235-238, 243-246, 259-262, 286, 299.
 Shape factor, 124, 128, 140.
 Skin, 37, 39-44, 52-53, 56, 59, 63, 68, 69, 75, 77, 83, 86-89, 119, 135, 143-144, 156, 162-163, 165-166, 168-170, 178-179, 182-184, 187-188, 190, 197, 200, 205, 206, 210-211, 220-221, 223, 225, 227-228, 235, 237, 243-246, 248-250, 254,

INDEX

- 257-258, 263-264, 275-276, 278-280, 282, 286, 295, 298, 305-306.
- Skin around the fracture**, 222-223, 225-228, 231.
- Skin of slant**, 210-211.
- Slab matrix blocs**, 147-149, 170, 178.
- Slanted wells**, 209-211.
- Smoothing algorithm**, 88.
- Spherical flow**, 187, 196-199, 203-205.
- Spherical permeability**, 197-198.
- Standard conditions**, 37, 259.
- Steady-state flow**, 30.
- Stimulation**, 143.
- Superposition function**, 61-63, 85, 89, 104, 109-110, 131, 171, 198, 275, 277, 303, 315.
- Superposition**, 31, 60.
- T**
- Theis curve**, 294-296, 298, 302, 304-305.
- Theoretical PI**, 143.
- Tides**, 66, 294.
- Time lag**, 316, 319.
- Total compressibility**, 22, 150-151, 180, 242, 248, 284.
- Transmissivity**, 183-185, 188.
- Transmissivity contrast**, 183-185, 188.
- Transient flow**, 30, 128, 142-143, 155, 266-267, 269-270, 272-273, 275.
- Transient model**, 155-157, 159, 162-163, 167, 170, 175.
- Two-layer reservoirs**, 181-190.
- Type curves**, 37, 47-49, 67-68, 70, 75-77, 79-80, 82, 84-85, 89, 93, 100, 110, 114, 121, 129, 154, 159, 163, 167, 169-171, 221-222, 226, 228, 231, 239, 246, 299, 303, 306.
- V**
- Vertical flow**, 182, 187, 188, 235-236, 239-240.
- Vertical fractures**, 213.
- Vertical permeability**, 182-184, 195, 205, 207, 235, 238.
- Vogel's equation**, 287-288.
- W**
- Warren and Root**, 147-148, 153, 155, 162.
- Water drive**, 30.
- Wellbore storage**, 33-38, 49, 51-53, 55-56, 59-60, 62, 68, 70, 74, 77, 80, 84-85, 88-89, 97, 104, 111, 118, 151, 154-155, 157, 159, 161-162, 168-171, 175, 184, 187, 195-196, 203-206, 210, 217, 218, 222-223, 226, 228, 231-233, 236, 239, 242, 246, 248-249, 265-266, 295, 298, 303, 305-306.
- Wellbore storage effect**, 34-38, 53, 55-56, 59-60, 70, 77, 80, 84-85, 89, 97, 104, 111, 118, 155, 159, 161-162, 170-171, 175, 187, 195-196, 203-205, 210, 217-218, 223, 226, 228, 231, 233, 236, 239, 242, 246, 249, 265-266, 295, 298, 303, 305.
- Wellhead flow rate**, 27.



ACHEVÉ D'IMPRIMER
EN SEPTEMBRE 1998
PAR L'INSTITUT FRANÇAIS DU PÉTROLE
N° d'éditeur : 988
N° d'imprimeur : 113
Dépôt légal septembre 1998
IMPRIMÉ EN FRANCE



pdfelement

G. BOURDAROT

WELL TESTING: INTERPRETATION METHODS

Useful as both a text and a reference, this volume will greatly help practicing engineers and technicians to interpret well testing. It places emphasis on the most suitable interpretation methods for each case dealt with: traditional methods, standard type graphs, computer assisted graph generation, interpretation with the help of derivatives. The text presents all equations necessary for the interpretation while avoiding lengthy mathematical developments. Finally, the large number of references allows to trace the solutions back to their sources.

The scope and field of application of these methods are developed, with many practical examples and a large number of illustrations. The book shows how an interpretation of well testing varies according to the type of reservoir limits (faults, channels, secant faults, constant pressure limits, closed reservoirs) and the well reservoir configurations (partial penetration wells, inclined wells, artificially fractured wells, horizontal wells, injection wells). It also treats the case of more complex reservoirs (fissured reservoirs, two-layered reservoirs). The methods to be used when the fluid contained in a well is a gas or a polyphasic fluid are described in detail. Lastly, it describes interference and pulse tests, involving several wells at a time.



9 782710 807384

ISBN 2-7108-0738-6